1995

Chemistry Of Antiwear Films By X-ray Absorption Spectroscopy

Zhanfeng Yin

National Library of Canada
Acquisitions and Bibliographic Services Branch
395 Wellington Street
Ottawa, Ontario
K1A 0N4

Bibliothèque nationale du Canada
Direction des acquisitions et des services bibliographiques
395, rue Wellington
Ottawa (Ontario)
K1A 0N4

Your file Votre référence

Our file Notre référence

NOTICE

The quality of this microform is heavily dependent upon the quality of the original thesis submitted for microfilming. Every effort has been made to ensure the highest quality of reproduction possible.

If pages are missing, contact the university which granted the degree.

Some pages may have indistinct print especially if the original pages were typed with a poor typewriter ribbon or if the university sent us an inferior photocopy.

Reproduction in full or in part of this microform is governed by the Canadian Copyright Act, R.S.C. 1970, c. C-30, and subsequent amendments.

AVIS

La qualité de cette microforme dépend grandement de la qualité de la thèse soumise au microfilmage. Nous avons tout fait pour assurer une qualité supérieure de reproduction.

S'il manque des pages, veuillez communiquer avec l'université qui a conféré le grade.

La qualité d'impression de certaines pages peut laisser à désirer, surtout si les pages originales ont été dactylographiées à l'aide d'un ruban usé ou si l'université nous a fait parvenir une photocopie de qualité inférieure.

La reproduction, même partielle, de cette microforme est soumise à la Loi canadienne sur le droit d'auteur, SRC 1970, c. C-30, et ses amendements subséquents.

Canada

CHEMISTRY OF ANTIWEAR FILMS BY X-RAY ABSORPTION SPECTROSCOPY

by

Zhanfeng Yin

Department of Chemistry

Submitted in partial fulfilment

of the requirements for the degree of

Doctor of Philosophy

Faculty of Graduate Studies

The University of Western Ontario

London, Ontario

August 1995

ISBN 0-612-03502-6

Canada

Name ZHANFENG YIN

Dissertation Abstracts International is arranged by broad, general subject categories. Please select the one subject which most nearly describes the content of your dissertation. Enter the corresponding four-digit code in the spaces provided.

Material Science

SUBJECT TERM

0794

SUBJECT CODE

U·M·I

Subject Categories

THE HUMANITIES AND SOCIAL SCIENCES

COMMUNICATIONS AND THE ARTS

Architecture .0729
Art History .0377
Cinema .0900
Dance .0378
Fine Arts .0357
Information Science .0723
Journalism .0391
Library Science .0399
Mass Communications .0708
Music .0413
Speech Communication .0459
Theater .0465

EDUCATION

General .0515
Administration .0514
Adult and Continuing .0516
Agricultural .0517
Art .0273
Bilingual and Multicultural .0282
Business .0688
Community College .0275
Curriculum and Instruction .0727
Early Childhood .0518
Elementary .0524
Finance .0277
Guidance and Counseling .0519
Health .0680
Higher .0745
History of .0520
Home Economics .0278
Industrial .0521
Language and Literature .0279
Mathematics .0280
Music .0522
Philosophy of .0998
Physical .0523
Psychology .0525
Reading .0535
Religious .0527
Sciences .0714
Secondary .0533
Social Sciences .0534
Sociology of .0340
Special .0529
Teacher Training .0530
Technology .0710
Tests and Measurements .0288
Vocational .0747

LANGUAGE, LITERATURE AND LINGUISTICS

Language
- General .0679
- Ancient .0289
- Linguistics .0290
- Modern .0291

Literature
- General .0401
- Classical .0294
- Comparative .0295
- Medieval .0297
- Modern .0298
- African .0316
- American .0591
- Asian .0305
- Canadian (English) .0352
- Canadian (French) .0355
- English .0593
- Germanic .0311
- Latin American .0312
- Middle Eastern .0315
- Romance .0313
- Slavic and East European .0314

PHILOSOPHY, RELIGION AND THEOLOGY

Philosophy .0422
Religion
- General .0318
- Biblical Studies .0321
- Clergy .0319
- History of .0320
- Philosophy of .0322

Theology .0469

SOCIAL SCIENCES

American Studies .0323
Anthropology
- Archaeology .0324
- Cultural .0326
- Physical .0327

Business Administration
- General .0310
- Accounting .0272
- Banking .0770
- Management .0454
- Marketing .0338

Canadian Studies .0385
Economics
- General .0501
- Agricultural .0503
- Commerce-Business .0505
- Finance .0508
- History .0509
- Labor .0510
- Theory .0511

Folklore .0358
Geography .0366
Gerontology .0351
History
- General .0578
- Ancient .0579
- Medieval .0581
- Modern .0582
- Black .0328
- African .0331
- Asia, Australia and Oceania .0332
- Canadian .0334
- European .0335
- Latin American .0336
- Middle Eastern .0333
- United States .0337

History of Science .0585
Law .0398
Political Science
- General .0615
- International Law and Relations .0616
- Public Administration .0617

Recreation .0814
Social Work .0452
Sociology
- General .0626
- Criminology and Penology .0627
- Demography .0938
- Ethnic and Racial Studies .0631
- Individual and Family Studies .0628
- Industrial and Labor Relations .0629
- Public and Social Welfare .0630
- Social Structure and Development .0700
- Theory and Methods .0344

Transportation .0709
Urban and Regional Planning .0999
Women's Studies .0453

THE SCIENCES AND ENGINEERING

BIOLOGICAL SCIENCES

Agriculture
- General .0473
- Agronomy .0285
- Animal Culture and Nutrition .0475
- Animal Pathology .0476
- Food Science and Technology .0359
- Forestry and Wildlife .0478
- Plant Culture .0479
- Plant Pathology .0480
- Plant Physiology .0817
- Range Management .0777
- Wood Technology .0746

Biology
- General .0306
- Anatomy .0287
- Biostatistics .0308
- Botany .0309
- Cell .0379
- Ecology .0329
- Entomology .0353
- Genetics .0369
- Limnology .0793
- Microbiology .0410
- Molecular .0307
- Neuroscience .0317
- Oceanography .0416
- Physiology .0433
- Radiation .0821
- Veterinary Science .0778
- Zoology .0472

Biophysics
- General .0786
- Medical .0760

EARTH SCIENCES

Biogeochemistry .0425
Geochemistry .0996
Geodesy .0370
Geology .0372
Geophysics .0373
Hydrology .0388
Mineralogy .0411
Paleobotany .0345
Paleoecology .0426
Paleontology .0418
Paleozoology .0985
Palynology .0427
Physical Geography .0368
Physical Oceanography .0415

HEALTH AND ENVIRONMENTAL SCIENCES

Environmental Sciences .0768
Health Sciences
- General .0566
- Audiology .0300
- Chemotherapy .0992
- Dentistry .0567
- Education .0350
- Hospital Management .0769
- Human Development .0758
- Immunology .0982
- Medicine and Surgery .0564
- Mental Health .0347
- Nursing .0569
- Nutrition .0570
- Obstetrics and Gynecology .0380
- Occupational Health and Therapy .0354
- Ophthalmology .0381
- Pathology .0571
- Pharmacology .0419
- Pharmacy .0572
- Physical Therapy .0382
- Public Health .0573
- Radiology .0574
- Recreation .0575
- Speech Pathology .0460
- Toxicology .0383

Home Economics .0386

PHYSICAL SCIENCES

Pure Sciences

Chemistry
- General .0485
- Agricultural .0749
- Analytical .0486
- Biochemistry .0487
- Inorganic .0488
- Nuclear .0738
- Organic .0490
- Pharmaceutical .0491
- Physical .0494
- Polymer .0495
- Radiation .0754

Mathematics .0405
Physics
- General .0605
- Acoustics .0986
- Astronomy and Astrophysics .0606
- Atmospheric Science .0608
- Atomic .0748
- Electronics and Electricity .0607
- Elementary Particles and High Energy .0798
- Fluid and Plasma .0759
- Molecular .0609
- Nuclear .0610
- Optics .0752
- Radiation .0756
- Solid State .0611

Statistics .0463

Applied Sciences

Applied Mechanics .0346
Computer Science .0984
Engineering
- General .0537
- Aerospace .0538
- Agricultural .0539
- Automotive .0540
- Biomedical .0541
- Chemical .0542
- Civil .0543
- Electronics and Electrical .0544
- Heat and Thermodynamics .0348
- Hydraulic .0545
- Industrial .0546
- Marine .0547
- Materials Science .0794
- Mechanical .0548
- Metallurgy .0743
- Mining .0551
- Nuclear .0552
- Packaging .0549
- Petroleum .0765
- Sanitary and Municipal .0554
- System Science .0790

Geotechnology .0428
Operations Research .0796
Plastics Technology .0795
Textile Technology .0994

PSYCHOLOGY

General .0621
Behavioral .0384
Clinical .0622
Developmental .0620
Experimental .0623
Industrial .0624
Personality .0625
Physiological .0989
Psychobiology .0349
Psychometrics .0632
Social .0451

ABSTRACT

The antiwear and antioxidant additives, zinc dialkyldithiophosphates (ZDDPs), are an essential ingredient in engine oil formulations, and have been in use for many years. These additives function by forming antiwear films on surfaces in sliding contact, and thus reduce friction and wear. Among the surface techniques employed, X-ray absorption spectroscopy (including EXAFS and XANES) has been mainly used because of its high resolution, low detection limit and non-destructive characteristics.

This is the first time that P and S L-edge XANES spectroscopy has been used to analyze antiwear films and thermal films. About two hundred antiwear films and thermally prepared films have been measured by XANES spectroscopy. It has been found that longer rubbing time, higher concentration of ZDDP, moderate temperature and higher load help to form long chain phosphates. Sulphur species in most of the cases is sulphide. The presence of sulphate in very short rubbing time or high temperature films is likely from sulphur in base oil.

The chemical composition of additives also affects their behaviour. Secondary ZDDP tends to form long chain polyphosphate while primary ZDDP and aryl ZDDP, in most of the cases, form short chain polyphosphate. The chemical state of sulphur in the same film resembles ZnS or alkyl sulphide. It seems that Zn acts as an antioxidant for sulphur and also catalyses the polymerization of phosphates. These properties are more significant for secondary ZDDP than for primary ZDDP. The presence of detergents and dispersant reduce the amount of unreacted ZDDP on the rubbing surface. The addition of the detergent and dispersant may change the polymerization of phosphate in the antiwear films. The S signals are much weaker than P signals and sulphur is in the reduced sulphide form.

Depth profiling results from XPS showed that the antiwear film formed in 30 minutes is shorter than that formed in 12 hours. The measurements of wear scar widths are general consistent with the XANES study and the results of other researchers. It seems that after film formation in the first a few minutes, further rubbing doesn't increase wear significantly.

ACKNOWLEDGMENTS

I would like to thank my research supervisor, G.Michael Bancroft, for providing me with the opportunity to pursue this research project and for his enthusiasm, encouragement and understanding, which made my life in Western much easier.

I am deeply grateful to Masoud Kasrai for his technical help in XAS measurements and extensive discussions during my research works. Many thanks are due to Kim Tan, Bingxing Yang and Xinghong Feng at the Canadian Synchrotron Radiation Facility (CSRF) for their professional assistance during my stays in the CSRF.

This project is financially supported by Ontario Centre for Material Research (OCMR) and Imperial Oil (ESSO). I appreciate their support. I would like to thank Kim Fyfe and Kevin Kerrigen from ESSO for their technical assistance. I would like to acknowledge Pierre Willermet, Roc Carter III, Arup Gangopadhyay, Erin Clausing and David Dailey at Ford Dearborn for the preparation of some samples and helpful discussions.

I thank Peter Norton, John Sheasby, Wan K. Wan and Hongqi Li for valuable discussions on tribology; Bruce Campbell of the Physics workshop and John Forth of the Earth Science Department for steel sample preparation; Jinguang Chen of the Exxon Chemical Company for giving me the opportunity of using the U1 beamline.

My work greatly benefited from the friendship and help from the members of the department and fellow graduate students: T.K. Sham, John Tse, Yuyang Wu, Jianzhang Xiong, Detong Jiang, Qiwei Zhu, John Bozek, Roger Brunner, Jeff Cutler, Leighton Coatsworth, Marina Fuller, Ziqi Gui, Yongfeng Hu, Jim Johnson, Stephen Knipe, Dan Legrand, Dien Li, Xiaorong Li, Zhifeng Liu, Leone Maddox, Jay Mycroft, Jamie Price, Mike Scaini and Doug Southerland.

Special thanks must go to my dear wife, Zhuomei, for her love, caring and encouragement during the last five years. Thanks also go to my parents, brothers and sister, who have been extremely supportive throughout my career. To my family, this thesis is dedicated.

TABLE OF CONTENTS

LIST OF TABLES

LIST OF FIGURES

CHAPTER 1

INTRODUCTION

1.1 Lubricant additives and tribological films

1.1.1 General

Lubricants and lubrication techniques are indispensable in the automobile industry. Owing to the special operating conditions, characterized by high temperature, loads and speeds, lubricants have to cover extreme requirements. Among the lubricant oils consumed today, about forty percent of them are engine oils. Natural hydrocarbon oils alone can not provide an adequate lubricating performance for modern engines. Many properties of modern lubrication oils are achieved by the addition of chemicals, which are known as additives. Some of these additives affect the physical properties of the base oils while others have chemical effects. The additives can improve oxidation resistance, wear properties, corrosion resistance, viscosity, etc. They can also give properties to the oils which they did not possess initially, such as detergency and dispersancy. Individual additives are used at concentration levels ranging from several parts per million to values great than 10 volume percent[1]. Different additives can assist each other, resulting in synergistic effects or they can lead to antagonistic effects. Many modern additives have more than one function (multi-purpose additives) and thus reduce the possibility of additives interfering with each other. Today, all the engine oil functions can usually be represented by only a few separate additives.

1.1.2 Types of additives

1.1.2.1 Antiwear (AW) additives

In order to reduce the wear during the metallic contact on the rubbing surface, AW additives are added to base oil. AW additives encompass several classes of chemicals. The most important and most effective AW additive for controlling or

eliminating wear in valve train systems are zinc dialkyldithiophosphates (ZDDPs). Other important AW additives are organic phosphorus compounds such as tricresyl phosphate, dilauryl phosphate and compounds containing sulphur, sulfurized terpenes or combinations of sulphur and oxygen sulfurized fats and fat derivatives.

ZDDP has been widely used in lubricating oils for over forty years[2]. Although other factors may contribute to the antiwear activity of ZDDP, it is generally agreed that its primary function is to form wear resistant films on rubbing surfaces. The films are generally of two types: EP (extreme pressures) films (e.g. iron sulfides) formed at high local temperatures under extreme contact conditions, and AW (antiwear) films formed under moderate contact conditions. In most of the cases, the films discussed in this thesis are AW films. The nature of the films formed from ZDDP has long been a matter of debate. Assorted phosphate structures, sulfides, sulfates, organic, inorganic and organo-metallic polymers have been proposed. Widely varying data for film composition have been presented, but there is a little agreement as to their chemical nature.

The mechanism of ZDDP performance is still controversial. However, it is accepted that ZDDP is decomposed in oil to form different compounds and these compounds are responsible for the AW function. During friction, a protective film is formed on rubbing surfaces that provide the desirable AW property. Two mechanisms have been forwarded for the film formation. First, ZDDP adsorbs on the metal surfaces and then undergoes decomposition to form the films owing to the rubbing process[3,4,5,6,7]. Second, ZDDP decomposes in the lubricant oil in the engine and then the decomposition products react with the sliding surfaces to form the protective layer[8,9,10,11,12,13]. Several factors that may influence the decomposition process have been investigated. In general, these factors are thermal degradation[9,10,14,15], hydrolysis[11,12], oxidation by hydroperoxide[16,17], peroxy radicals[18,19] and oxygen in air[20,21].

1.1.2.2 Oxidation Inhibitors

Oxidation is the major process of engine oil deterioration[22]. The mechanism of this process involves free radical reactions which are catalyzed by metals and accelerated by heat. In engine oils composed of hydrocarbons, free radicals react with oxygen to form peroxy free radicals and hydroperoxides. The latter undergo further reactions to

form alcohols, ketones, aldehydes, carboxylic acids, and other oxygen containing compounds. As the oxidation process proceeds, the oxygenated compounds polymerize to form viscous materials which, at a particular point, become oil-insoluble. Consequently, the oxidation process generates viscous soluble materials which thicken the oil, and insoluble materials which form deposits. It has also been noticed that free radicals are formed faster than they are used, and the rate of oxidation increases. Meanwhile, nitrogen oxides formed in the combustion process are oxidizing agents and can result in unique oxidation products, which include nitrate esters and other nitrocompounds[23]. Some of the oxygenated compounds are active, polar materials, e.g. acids, that accelerate corrosion and rusting.

To retard and reduce the oxidation product formation in oil from hydrocarbons, oxidation inhibitors are used. They work by reducing organic peroxide concentrations. The reduction of organic peroxides inhibits the oxidation process (oxidation chain); and thus, minimizes the formation of acids, resins, polymers, varnish and sludge.

The oxidation inhibitors are normally ZDDPs, phenol derivatives, metal dithiocarbamates, aromatic amines, sulfurized fats and hydrocarbons, phospho-sulfurized fats and olefins, metal salicylates and many other compounds[24].

1.1.2.3 Detergents

The main functions of these oil-soluble detergents are: 1) To keep oil insoluble combustion products in suspension (e.g. soot, coke, salt particles) which can amount to 10 mass% in the case of diesel oils; 2) To neutralize the acidic by-products of the combustion process and thereby reduce corrosive wear; 3) To neutralize the acidic products of lubricant oxidation; 4) To act as a "detergent" to keep engine clean of deposits. Actually the function of detergents is not to clean the dirty metallic surface but to avoid the formation of deposits on the surface.

A number of different surfactant types have been used to produce lubricant detergents. Common examples include: sulfonates, phenates, sulfurized phenates, carboxylates, salicylates, phosphates and phosphinates. The metals most commonly employed are calcium, magnesium and barium. Chemistry, manufacturing, application and action mechanism of detergent additives have been extensively described in

literature[25,26,27,28,29].

1.1.2.4 Dispersants

Dispersant retard sludge formation and prevent flocculation and coagulation of colloidal particles. They are ash-free organic compounds characterized by a nitrogen or oxygen containing polar group attached to a high molecular weight hydrocarbon chain which solubilizes the additive in hydrocarbon base stocks. The most common used dispersants include: copolymers (polymethacrylates, styrenemaleinic ester copolymers, etc.), substituted succinamides, polyamine succinamides, polyhydroxy succinic esters and polybutene hydroxy benzyl polyamine.

Dispersants have a strong affinity for dirt particles and surround themselves with oil soluble molecules which keep the sludge from agglomerating and depositing in the engine. Many papers dealing with dispersants also relate to the detergent additive[26, 28,29,30]. The reason is that dispersants and detergents each perform both dispersancy and detergency functions and differ in their relative ability to function in the bulk of the lubricant or at the engine surface.

1.1.2.5 Other additives

Other additives widely used are: viscosity index improvers, pour point depressants, corrosion inhibitors, rust inhibitors, foam inhibitors, friction modifying additives and extreme pressure additives. Detailed descriptions of these additives and their functions have been reported in detail[2,22].

1.2 Surface analytical techniques in tribology studies

Metallic dialkyl and diaryldithiophosphates (MDDPs), particularly ZDDPs, as described previously, have combined lubrication-related properties such as antiwear, antioxidant, detergent, extreme pressure (load carrying capacities), etc. Since the introduction of ZDDPs, several studies have been focussed on its physical and chemical properties, thermal decomposition process, tribology behaviour, interaction with other additives and finally its performance mechanism. Among these, antiwear films that were generated by simulating engine working conditions (temperature, pressure in metal

interface, friction speed, etc.), have been extensively studied. These films were formed by using different type of friction machines (Cameron-Plint, four ball, cam and tappet, etc.) for different analytical purposes. Earlier studies were mainly focused on the tribology performance or antiwear efficiency of the additives. Friction coefficients and wear scars were used to assess the antiwear performance. With the advent of surface techniques, more investigations concerning the chemical characteristics of the additives and their films related to the antiwear behaviour and mechanism have been published.

Valuable information regarding the chemistry of the film using surface analytical techniques is available in the literature[11,12,13,31-39]. A number of investigations have been focused on the chemical nature of the films, but there is little agreement as to their chemical compositions. The difficulties in characterizing the film are due to the fact that films are extremely thin (a few hundred angstroms thick), and the conventional analytical methods are not sensitive enough to allow chemical speciation. In most of the cases, ZDDPs are the main additives added to the base oil. Other studies, such as adsorption and thermal decomposition have also been investigated. A number of different physical techniques have been utilized in the past to analyze the composition of the protective films. Among surface techniques used, electron probe micro analysis (EPMA) and X-ray fluorescence (XRF) spectroscopy are element sensitive. Sheasby et al.[31] used EPMA in conjunction with SEM-EDX to analyze the antiwear boundary lubrication films formed by several ZDDP additives in mineral oil in a reciprocating wear tester. The films were found to contain primarily Zn, S, P, O, corresponding to the elements found in the ZDDP additive. Using the XRF technique, Rounds[13] examined the decomposition of different types of ZDDP at different temperatures. He found that the coatings on the ball surface after thermal decomposition are mainly composed of Zn, S and P.

However, for a complete understanding of the antiwear mechanism, it is necessary to know the chemical species as well as the elements that are present in the films. The application of two widely used surface techniques, X-ray photoelectron spectroscopy (XPS) and Auger electron spectroscopy (AES), promoted this research to a new stage. From XPS and AES in conjunction with Ar^+ sputtering, elemental compositions, valence information and depth distributions can be obtained. Bird and Galvin, using XPS[32], reported that the film consisted of Zn, P, S, O and Fe. From binding energies they

concluded that P should be in the form of a phosphate and sulphur in the form of a sulphide. Spedding and Watkins[11,12], using XPS, arrived at the same conclusion for the P and S chemical states. They also found that zinc was associated with phosphates, but Zn and P were not associated with sulphur. Jahanmir[13] assumed the formation of zinc phosphate and iron sulphide. Glaeser and co-workers[33] reported a thin layer of phosphate on the topmost surface and a chemisorbed iron sulphide layer close to the metal substrate. Their results also suggested that iron oxide is necessary as an intermediate step in forming a protective film during the ZDDP surface action.

More recently, Willermet et al.[34,35] have studied films generated from engine oils containing overbased detergents, in a cam and tappet friction apparatus, using reflectance-absorbance infrared, XPS and AES spectroscopies. They reported that the films were inorganic amorphous phosphates, which were mainly orthophosphate and pyrophosphate associated with Zn and Mg (from the overbased detergents). Willermet et al.[36] have also studied films formed from base stock solutions of a secondary ZDDP (s-ZDDP) and a mixture of s-ZDDP and detergent and dispersant. They found that the films formed from the ZDDP were composed of longer chain phosphates with Zn as the cation. However, in the presence of the detergent-dispersant packages, only short chain phosphates were observed. In addition, the Ca cation from the overbased detergent replaced up to about 50% of the Zn cation in the phosphate films. Films were low in sulphur, with sulphur being present mostly as a sulphide. Zinc and iron EXAFS analysis of antiwear debris induced by friction using ZDDP have been investigated by Martin and his coworkers[37]. Using Fourier transforms of EXAFS spectra of several model compounds as fingerprints, they found iron was bonded to oxygen instead of sulphur and phosphorus. They predicted that the films were amorphous, inorganic long chain polyphosphates with Fe as the cation. Bell et al.[38,39] applied TOF-SIMS and XPS to analyze films derived from ZDDP solutions in a Camero-Plint machine (at 175 °C). Their data indicated an O/P ratio of 5/2, consistent with a long chain polyphosphate.

1.3. X-ray absorption spectroscopy (XAS)

1.3.1 General Introduction

The last decade has witnessed a growing awareness of the importance and utility of advanced structural characterization techniques in aiding our understanding, definition and optimisation of advanced material systems and processes. X-ray based .echniques are most useful in that they are non-destructive and can provide essential information concerning bulk and surface micro-structure over a wide range of atomic correlation length scales.

The interaction of X-rays with matter occurs by two processes: diffraction and absorption. Since 1912[40] diffraction has been the classical technique for determining crystal structures in various areas of science. At typical X-ray energies, absorption occurs when an X-ray photon is absorbed by a core electron in an atom. The absorption varies monotonically, but it exhibits a sharp increase at some specific energy, called the absorption edge. The fine features near the jump correspond to the energy required to excite electron at a core level to unoccupied levels in the atom.

Fricke[41] and Hertz[42] first observed that there are structures above the edge. These early measurements were only of structures very near the edge, and they were first explained by Kossel[43]. Later measurements[44,45] showed that the structure continued well beyond the edge, which was not explained by Kossel's theory. Kronig[46] was the first to attempt an explanation, and he relied explicitly on the long-range order of the material by considering the scattering of the photoelectron from the periodic lattice. This theory was quite successful in qualitatively explaining many observations. Kronig also began developing a short-range order theory, which is the basis of the modern theory. In this theory the fine structure is explained by modulations in the final state of the photoelectron that are caused by backscattering from the surrounding atoms. The inner shell photoionization process can be described as a two-step process. In the first step the photon creates a core-hole-electron pair (Figure 1.3.1 (a)), and in the seco.:d step the recombination process of the core-hole and electron takes place. There are many channels for the recombination. These channels, as shown in Figure 1.3.1, produce the emission of photons and electrons. The first one is the fluorescence process (Figure 1.3.1 b). An electron in a higher orbital drops in to the hole, and the excess energy is released as X-rays. The second process is Auger decay which involves lower binding energy electrons (Figure 1.3.1 c). An electron fills the lower empty orbital, while

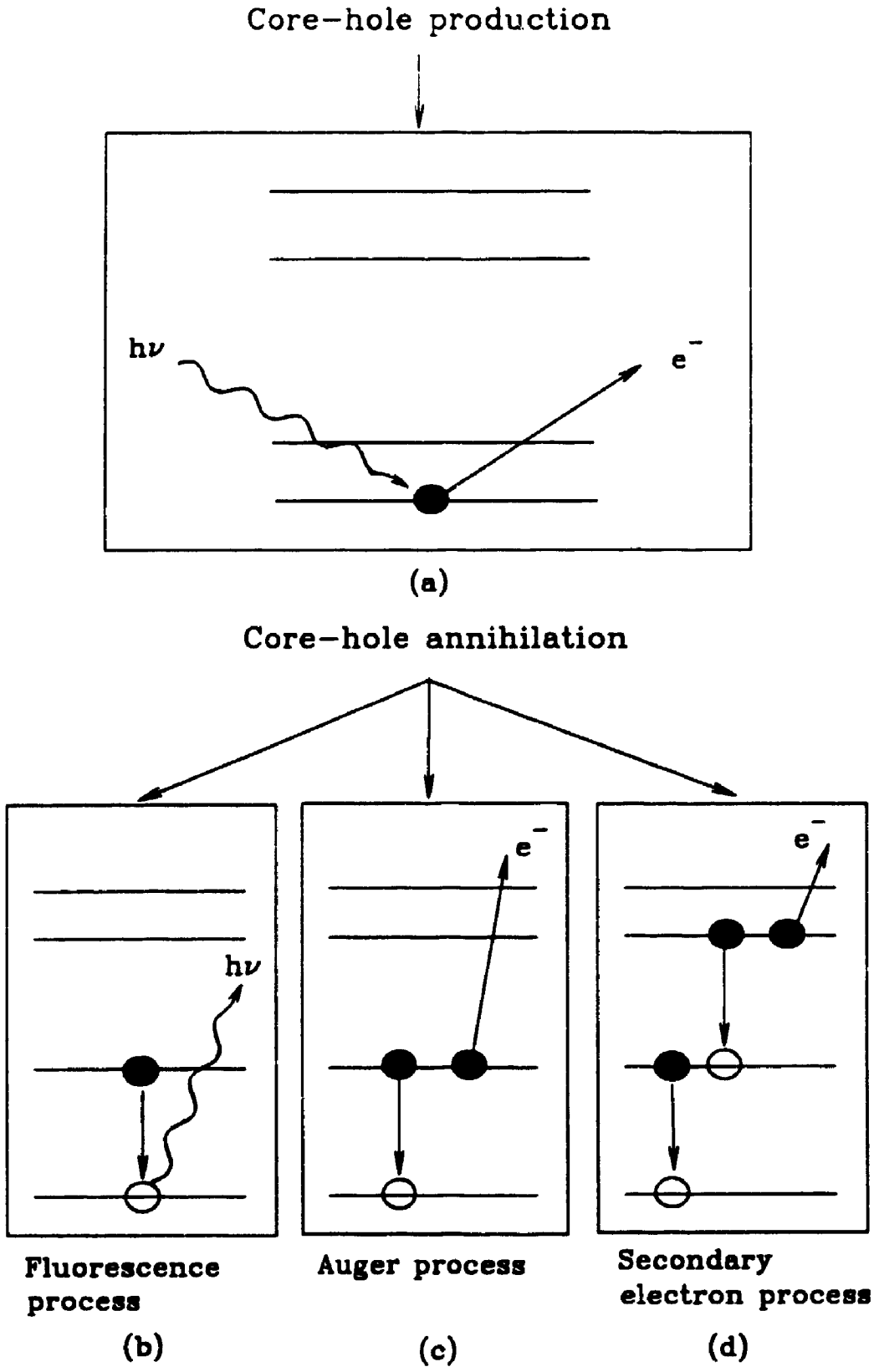

Figure 1.3.1 A schematic view of the inner shell photoionization process

another electron is ejected from the higher level. The third process is a cascade process, or secondary electron emission (Figure 1.3.1 d). Suppose an electron in an n level is ejected by X-ray photon. An Auger process takes place invoving the n+1 level with two new holes left. Another Auger decay process then occurs in the n+2 level. Auger emission and x-ray fluorescence are competing processes. Their relative strengths depend on the atomic number of the absorber. In light elements, Auger emission is more probable, while for heavy elements fluorescence becomes more likely. For the same element, florescence is more likely for K-shell holes than for L-shell holes. XAS spectra can be recorded measuring the absorption, fluorescence, Auger electrons or secondary electrons. For thin films on a thick substrate (such as antiwear films on steel), absorption cannot be measured, and one of the other three techniques is used. These techniques give results which are proportional to the absorption[47].

1.3.2 Synchrotron radiation

Synchrotron radiation is produced when charged particles are accelerated to relativistic (ca. GeV) energies[48] in an electron storage ring, where the particles move at velocity close to the velocity of light. The advantages of synchrotron radiation as compared to other radiation sources are: (a) a very intense and sharply collimated beam; (b) a broad spectral range from far infra-red down to hard X-ray region; (c) a tunable photon energy; (d) a highly polarized beam in the plane of the circular motion; (e) a time structure with a very short pulse.

Within this perspective, X-ray absorption spectroscopy using synchrotron radiation is finding increasing applications as it offers a technique capable of probing the local structural order around selected atomic species in materials. In addition, the intensity and penetrability afforded by the use of hard x-rays means that real chemical systems can be examined *in-situ* without their removal from operating conditions as well as obviating the need for UHV environments.

Interest in XAS experiments was accelerated greatly by the development of synchrotron radiation sources. Before 1970, it required a week or more to obtain high quality data using laboratory sources. This was changed with the advent of synchrotron radiation sources where the intense continuum of x-ray allowed similar quality data to

be obtained in approximately 10 minutes.

1.3.3 XANES

A typical P K-edge X-ray absorption spectrum of a sodium pyrophosphate is shown in Figure 1.3.2. The features observed ~5 eV below, to 40-50 eV above, the ionization threshold, as shown in Figure 1.3.2, are usually called XANES (X-ray absorption near edge structure). At the energy close to the absorption edge, scattering involves three or more atom groups causing multiple scattering, which is much stronger than pair scattering involved in EXAFS. This means that the XANES spectrum contains information on the local symmetry in addition to the pair correlation. The XANES spectrum provide a distinctive spectral "fingerprint" which enable different chemical states to be distinguished with confidence.

The features in the XANES spectra due to the multiple scattering resonances (MSR) are similar for each type of molecular symmetry. The energy positions of the MSR peaks are strongly dependent on interatomic distance. The contraction (expansion) of interatomic distance shifts the energies of the resonance to high (low) energies. It can be stated that the XANES in condensed matter can be predicted by the multiple scattering resonances within a small atomic cluster of neighbour atoms similar to the MSR in molecules[49].

Some general conclusions have been derived from a large set of experiments on XANES multiple scattering features:

1. The continuum XANES features are mainly due to the local symmetry of neighbouring atoms, with a major role of the electronic structure of the system. XANES is very sensitive to small atomic displacements and it is very difficult to find two identical spectra, even of very similar compounds.

2. In XANES, the geometrical distribution of atoms, that is bond angles and relative atomic positions in the environment of the absorbing atom, is of importance.

3. The main physical effect determining the XANES of condensed systems is photoelectron multiple scattering. Therefore, the XANES peaks have the same physical origin as the multiple scattering resonances or shape resonances in molecules.

4. The lowest energy XANES features can usually be described by core →

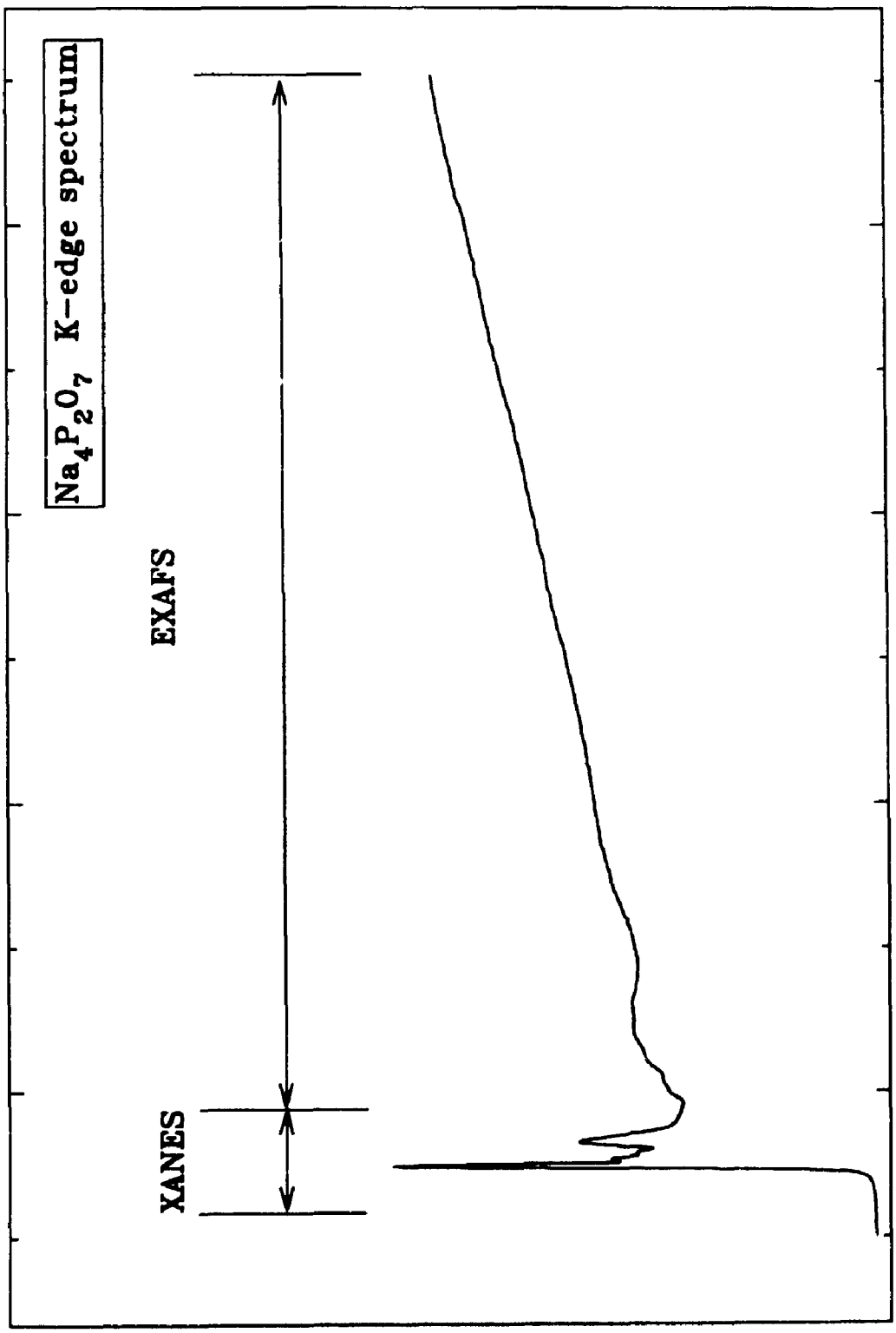

Figure 1.3.2 P K-edge spectrum of $Na_4P_2O_7$ in both XANES and EXAFS regions

antibonding traansitions in a molecule or cluster.

In conclusion the XANES can be used to determine the local geometrical structures by using model compounds as comparison, and thus reveal induced structural changes.

1.3.4 EXAFS

As shown in the Figure 1.3.2, the structure observed more than 40-50 eV beyond the edge, the EXAFS (Extended X-ray Absorption Fine Structure), is due to interference between the outgoing photoelectron wave and the wave as backscattered from the neighbouring atoms. These interference effects are determined by the distance, the chemical type and the number of atoms around the absorbing atom. The EXAFS formula is generally defined as

$$\chi(k) = \sum_{j=1}^{N} N_j F_j(k) / (kr_j^2) \exp(-2\sigma_j^2 k^2) \exp(-2r_j/\lambda) \sin[2kr_j + \Phi_j(k)]$$

Detailed explanation of the formula and its application will be addressed in chapter 3. Since only elastically scattered electrons can interfere, and the elastic mean free path of electrons is short, the analysis of EXAFS structure provides information on the local atomic structure around the absorbing atom. As the EXAFS oscillations in the absorption cross-section can be decomposed into a Fourier series of sinusoidal functions, one for each neighbour shell of neighbour atoms, a Fourier transform of the spectra reveals the radial distribution function (RDF) of atomic sites with respect to the absorbing atom. Although single scattering is often sufficient to describe the EXAFS oscillations, there are specific cases where some multiple scattering events need to be included in the interpretation of the experimental spectra.

In order to describe dynamic properties of surfaces, it is necessary to know accurately the atomic structural coordinates of the first one or two layers at the surface. Since 1977, studies[50,51] of surfaces using EXAFS have provided structural information with a precision of 0.03 Å, which was better than the accuracy achieved using most other

surface structure probes. Analysis of EXAFS spectra can be carried out using standard procedures[52,53,54] that will be introduced later.

1.4 The significance and arrangement of this thesis

This is the first time that the P L-edge and S L-edge XANES spectroscopies have been applied to analyze systematically the tribological films. A number of model compounds have been measured for the K-edge of P, S and O, and the L-edge of P, S and Fe. The XANES spectra of these model compounds, especially L-edge spectra can be used as fingerprints to study the chemical nature of those elements in the films. About two hundred thermally prepared films and tribochemical films generated with a Cameron-Plint friction machine have been investigated. Different chemical and physical parameters have been considered. A semi-quantitative method to evaluate the phosphate chain length in the films has been established. Based on the results, a possible mechanism for antiwear film formation has been proposed.

This thesis consists of seven chapters. This first chapter is a brief introduction of previous studies in tribochemistry and X-ray absorption spectroscopy including XANES and EXAFS. The second chapter is an overview of experimental procedures and instrumentation. Two detection methods, fluorescence yield (FY) and electron yield (EY) have been used to obtain x-ray absorption spectra. In chapter 3, the XANES spectra of all model compounds are shown and discussed. A series of phosphates with different chain lengths have been measured, and a semi-quantitative method has been established to analyze the phosphate structures in unknown systems. The physical and chemical parameters affecting the film formation and/or composition are discussed in chapter 4 and chapter 5, respectively. Chapter 6 presents the chemical analysis of thermally prepared films from the antiwear/antioxidant agent ZDDP. Chapter 7, is devoted to general discussion and conclusions.

1.5 References

1. *SAE Handbook: Fuels and Lubricants*. Warrendale, Pa.: Society of Automotive Engineers 1987, p. 23.01-23.17

2. Klamman, D. ed., "*Lubricants and Related Products*", Chapter 9: Additives, Weinheim, Deerfield Beach, Fla., Verlag Chemie, 1984

3. Dacre, B., and Bovington, C.H., *ASLE Trans.*, 1981, 24, 546

4. Dacre, B., and Bovington, C.H., *ASLE Trans.*, 1983, 26, 333

5. Schumacher, R., Gegner, E., Schmidt, A., Mathieu, H.J. and Landolt, D., *Tribology International*, 1980, 13, 311

6. Bovington, C.H. and Dacre., B., *ASLE Trans.*, 1984, 27, 252

7. Baumgarten, E., *Erdöl und Kohle-Erdgas Petrochem*, 1972, 25, 577

8. Rowe, C.N. and Dickert Jr., J.J., *ASLE Trans.*, 1967, 10, 85

9. Rounds, F.G., *ASLE Trans.*, 1975, 18, 79

10. Coy, R.C., and Jones, R.B., *ASLE Trans.*, 1981, 24, 77

11. Spedding, H and Watkins, R.C., *Tribol. Int.*, 1982, 15, 9

12. Watkins, R.C., *Tribol. Int.*, 1982, 15, 13

13. Jahanmir, S., *J. Tribology*, 1987, 109, 577

14. Harrison, P.G., Brown, P. *Wear*, 1991, 148, 123

15. Dicket, J.J., Rowe, C.N. *J. Org. Chem.*, 1967, 32, 647

16. Paddy, J.A., Lee, N.C.J., Waters, D.N., Troft, W. *Tribology Trans.*, 1990, 33, 15

17. Ohkatsu, Y., Kikkawa, K., Osa, T. *Bull. Chem. Soc. Jpn.*, 1978, 51, 3606

18. Howard, J.A., Ohkatsu, Y., Chener, J.H.B., Ingold, K.U. *Can. J. Chem.*, 1973, 51, 1543

19. Willermet, P.A., Kandah, S.K. *ASLE Trans.*, 1984, 27, 67

20. Willermet, P.A., Kandah, S.K. *Lubrication Science*, 1993, 5, 129

21. Begelinger, A., deGee, A.W.J., Salomon, G. *ASLE Trans.*, 1980, 23, 23

22. W.J. Bartz "*Engine oils and automotive lubrication*", Ed. Marcel Dekker, New York, 1993

23. Coates, J.P. Setti, L.C. *ASLE Trans.* 1986, 29, 394

24. Krocek, S., Mahoney, L.R., Johnson, M.D., Siegl, O.W. *SAE technical Paper Series Paper* No. 810014. Warrendale, Pa., SAE 1981

25. (a) Jensen, R.K., Korcek, S., Mahoney, L.R., Zimbo, M. *J. Am. Chem. Soc.*, 1979, 101, 7574 (b) Jensen, R.K., Kircek, S., Mahoney, L.R., Zimbo, M. *J. Am. Chem. Soc.*, 1981, 103, 1742

26. Hamilton, E.J., Korcek, S., Mahoney, L.R., Zimbo, M., *Int. J. Chem. Kinet.*, 1980, 12, 577

27. Titov, A.I. *Tetrahedron*, 1963, 19, 557

28. Albright, L.F. "Nitration" in *Encyclopedia of Chemical Technology*, 1981, 15, 841

29. Adachi, H., Basco, N. *Int. J. Chem. Kinet.*, 1982, 14, 1242

30. Atkinson, R., Aschman, S.M., Carter, P.L., Winer, A.M., Pitts, J.N. *Phys. Chem.*, 1982, 86, 4563

31. Sheasby, J.S., Cauphlin, T.A., Blahey, A.G., Laycock, K.F. *Tribology International*, 1990, 23, 301

32. Bird, R.J., Galvin, G.D. *Wear*, 1976, 37, 143

33. Glaeser, W.A., Baer,D., Engelhardt, M. *Wear*, 1993, 162-164, 132

34. Willermet, P.A., Pieprzak, J.M., Diley, D.P., Carter III, R.O., Lindsay, N., Haack, L.P., deVries, J.E. *ASME Transactions*, 1991, 113, 38

35. Willermet, P.A., Carter III, R.O., Boulos, E.N. *Tribology International*, 1992, 25, 371

36. Willermet, P.A., Dailey, D.P., Carter III, R.O., Schmitz, P.J., Zhu, W., Bell, J.C., Park, D. Submitted to *Tribology International*

37. Martin, J.M., Belin,M., Mansot, J.L., Dexpert, H, Lagarde, P. *ASLE Trans.*, 1986, 29, 523

38. Bell, J.C., Delargy, K.M., Seeney, A.M. *Proceeding of the 18th Leeds-Lyon Symposium on Tribology*, Lyon, France, September 1991, Elsevier, Amsterdam, Holland (1992)

39. Bell, J.C., Delargy, K.M. *6th International Congress on Tribology "Eurotrib 93"*, Budapest, Hungary, August 30 to September 2, (1993)

40. Bragg, W.L., *Proc. Cambridge Philos. Soc.*, 1912, 17, 43

41. Fricke, H., *Phys. Rev.*, 1920, 16, 202

42. Hertz, G., *Phys. Z.*, 1920, 21, 630; *Z. Phys.*, 1920, 3, 19

43. Kossel, W., *Z. Phys.*, 1920, 1, 119; 1920, 2,470

44. Ray, B.B., *Z. Phys.*, 1929, 55, 119

45. Kievet, B. and Lindsay, G.A., *Phys. Rev.*, 1930, 36, 648

46. Kronig, R. de L., *Z. Phys.*, 1931, 70, 317

47. Stöhr, J. *NEXAFS spectroscopy*, Chapter 5, Principles, Techniques, and Instrumentation of NEXAFS, Springer-Verlag, New York, 1992

48. Margaritondo, G. *Introduction to Synchrotron Radiation*, Oxford University Press, 1988

49. Bianconi, A., In: *X-Ray Absorption: Principles, Applications, Techniques of EXAFS, SEXAFS and XANES,* Ed. Koningsberger, D. C. and Prins, R., 1988, p573

50. Citrin, P.M., Eisenberger, P., Hewitt, R.C. *Phys. Rev. Lett.*, 1978, 41, 309

51. Citrin, P.M., Eisenberger, P., Hewitt, R.C. *Phys. Rev. Lett.*, 1980, 45, 1948

52. Hastings, In "*EXAFS Spectroscopy*", Ed. Teo, B.K., Joy, D.C., Plenum, New York, 1981, p171

53. Hayers, T.M., Boyce, J.B. *Solid State Physics Vol. 37*, Academic Press, New York, 1982, p173

54. Stern, E.A., Heald, S.M., In "*Handbook on Synchrotron Radiation*", Ed. Koch, E.E., Vol. 1, 1983, North Holland, 1983

CHAPTER 2

EXPERIMENTAL

2.1 Materials and additives

All model compounds are commercial products, and are used without further purification. The chemical structures of certain model compounds are depicted in Table 2.1.1.

Five synthesized additives and other commercial additives were supplied by ESSO Petroleum Canada. The composition of these additives are listed in Table 2.1.2. The commercial additives were supplied in mineral oil in a concentrated solution (~ 75 mass%), which were diluted to give the required concentrations. The synthesized ZDDPs are in neutral form which was confirmed by the melting point of the compound. The commercial ZDDPs used in this study are a mixture of neutral and basic forms[1]. The general formula of the ZDDP in the neutral form is shown in Table 2.1.1, where R is an alkyl or aryl group, as listed in the Table 2.1.2.

The base oil used to generate thermal films and antiwear films contains 0.17 mass % elemental sulphur. The steel coupon and pin used in this thesis is A2 tool steel, with 1% C, 1% Mo and 5% Cr.

2.2 Thermal decomposition and thermally prepared films

Thermally deposited films were made in oil. A steel coupon was immersed in oil containing the desired additive in a beaker. The beaker was heated in an oil bath at 50 ^{0}C, 100 ^{0}C, 150 ^{0}C and 200 ^{0}C for 1 to 6 hours. After heating, the coupon was allowed to cool down, dried in an air jet and then stored in a desiccator. No apparent change in the oil was observed when it was heated below 200 ^{0}C. But when the temperature reached 200 ^{0}C, a buff-coloured precipitate was formed quickly. The precipitate was filtered and washed with hexane followed with a small amount of acetone, then dried in a desiccator for further analysis.

Decomposition of a pure additive was examined in an oven. It is a synthetic

Table 2.1.1 Chemical structures of some model compounds

Samples	Structures
ZDDP Zinc [dialkyldithiophosphate]$_2$	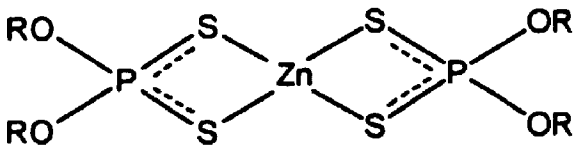
KDDP Potasium dialkyldithiophosphate	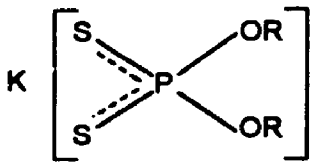
DPPM Diphenyl phosphino methane	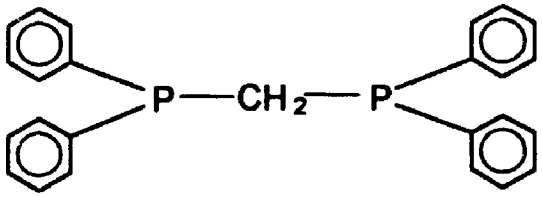
TPCD Tricyclohexylphosphine carbon disulphide	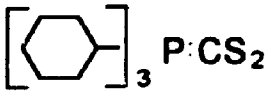
PO_4^{3-} Orthophosphate	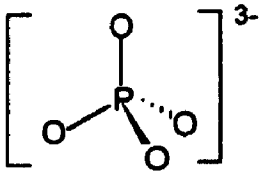
$P_2O_7^{4-}$ Pyrophosphate	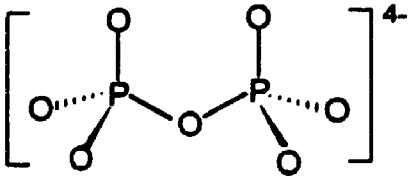
$P_3O_9^{3-}$ Metaphosphate	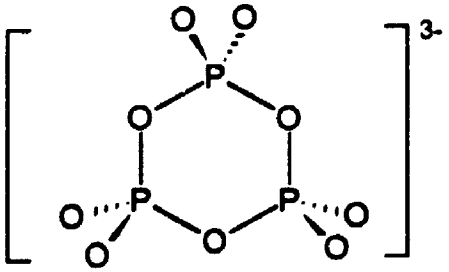

Table 2.1.2 The compositions of commercial additives

Additives	Compositions
Synthesized	
IP-ZDDP	Zinc [diisopropyl dithiophosphate]$_2$
IP-DDP	[Diisopropyl dithiophosphate]$_2$
NB-ZDDP	Zinc [di-n-butyl dithiophosphate]$_2$
NB-DDP	[Di-n-butyl dithiophosphate]$_2$
AR-DDP	[Diaryl dithiophosphate]$_2$
Commercial	
ZDDP-1	Secondary ZDDP: 85% sec-butyl, 15% n-octyl
ZDDP-2	Secondary ZDDP: 30% iso-propyl, 70% sec-butyl
ZDDP-3	Primary ZDDP: 65% iso-butyl, 35% iso-pentyl
ZDDP-4	Primary ZDDP: Iso-octyl
ZDDP-5	Aryl ZDDP
Detergent-1	Calcium sulphonate, neutral 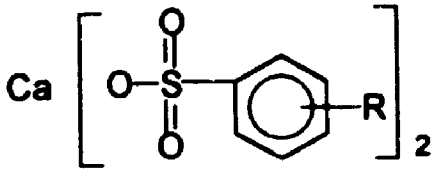
Detergent-2	Calcium phenate, 170 TBN* 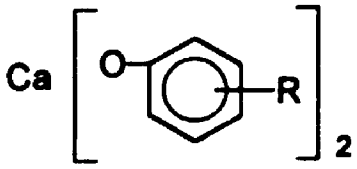
Dispersant	Polyisobutylene succinic anhydride polyamide 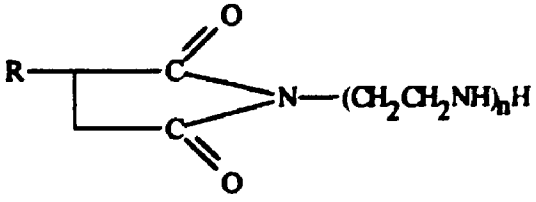

* TBN: Total base number, mg KOH/g

isopropyl ZDDP (IP-ZDDP). The elemental analysis result shows: C, 29.31% (calculated 30.05%); H, 5.80% (5.84%); P, 12.75% (12.92%); S, 26.25% (26.73%). It confirms that it is in neutral form. A small amount of IP-ZDDP was placed in a test tube and heated for 45 minutes at 135 ^{0}C and 185 ^{0}C, respectively. The residue was used for later measurements without purification.

2.3 Antiwear film generation

The antiwear films were generated on steel coupons. The steel specimen was sanded with 400 grade and 600 grade sand paper then cleaned in an ultrasonic bath for 30 minutes using light hydrocarbon solvent. The specimen was then placed in the Cameron-Plint reciprocating wear rig (at ESSO Research, Sarnia), in a bath of test oil at regulated temperature. The cylindrical pin was loaded against the coupon under an applied load as shown in Figure 2.3.1, and the reciprocating speed of the cylinder against the liner was increased slowly to the desired speed. The speed was maintained for a certain period of time depending on the experiments. Then the rig was stopped. The

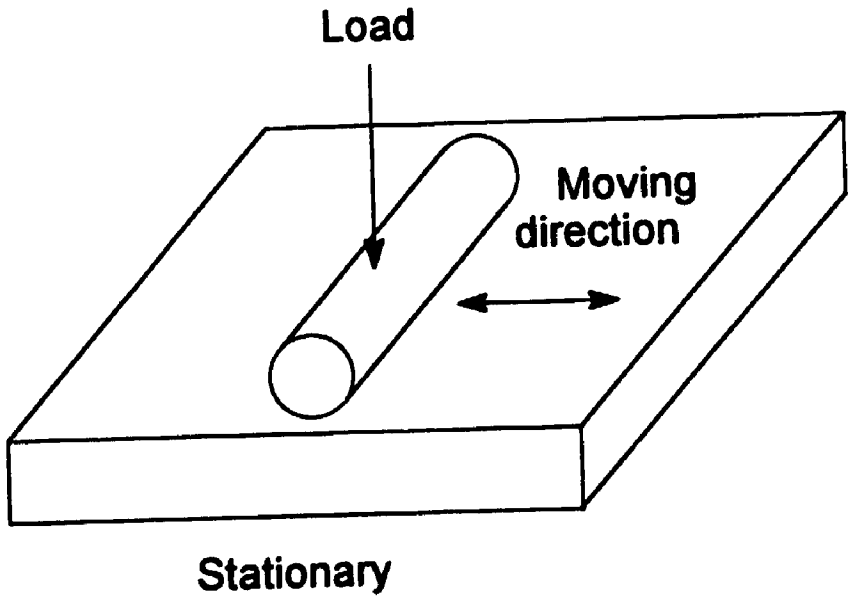

Figure 2.3.1 A block diagram of the Cameron-Plint friction machine used for film generation

specimen was removed, dried with the air jet, and stored in a desiccator.

The commonly used test variables are:

Temperature	100 °C
Speed	25 Hz
Load	225 N (Newton)
Stroke	5-7 mm
Rubbing time	30 minutes

These parameters selected are believed to be close to engine working condition.

2.4 XAS measurements

2.4.1 Instrumentation

Phosphorus and sulphur X-ray absorption spectra were collected at the Canadian Synchrotron Radiation Facility (CSRF)[2] situated at the 1 GeV Aladdin storage ring, University of Wisconsin, Madison. The operating electron energy of the storage ring is 0.8-1.0 GeV, and operating currents are 60-180 mA at 0.8 GeV and 40-80 mA at 1 GeV, respectively. For the K-edge, the double crystal monochromator (DCM) beamline, which covers the energy region of 1500-4000 eV, was used. For the L-edge spectra, the Grasshopper beamline, in which the X-ray beam is monochromatized by an 1800 g/mm grating and covers the photon region of 70-900 eV, was used. A schematic view of these beam lines is shown in Figure 2.4.1 and a close look of the Grasshopper beam line is shown in Figure 2.4.2. The photon resolutions at the DCM and Grasshopper are 1.0 and 0.2 eV respectively at the phosphorus and sulphur K- and L-edge energy regions. The energy scale for the DCM was calibrated setting the strong absorption line (white line) of elemental sulphur at 2472.0 eV, and that of the Grasshopper was calibrated with reference to the lowest pre-edge peak of elemental sulphur at 162.7 eV. These values are not absolute values, but are close to the binding energy of S 1s and S 2p levels, respectively. The P L-edge has been calibrated using the lowest pre-edge peak of $Na_3P_3O_9$ at 135.5 eV. The relative energy scale was reproducible within $\pm$ 0.05 eV.

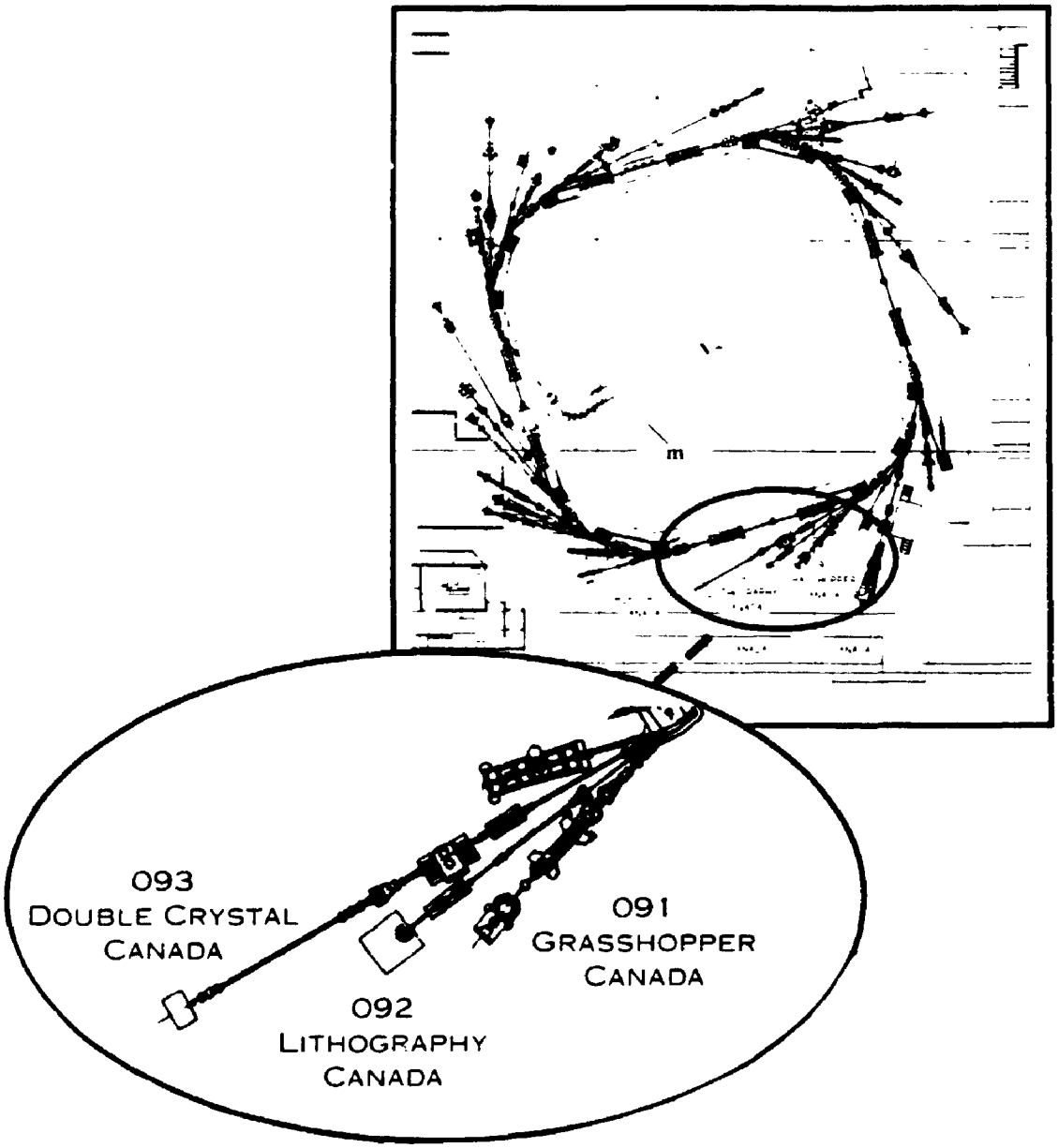

Figure 2.4.1 A schematic view of the Aladdin storage ring in Madison, Wisconsin (top) and three beamlines of the CSRF (bottom)

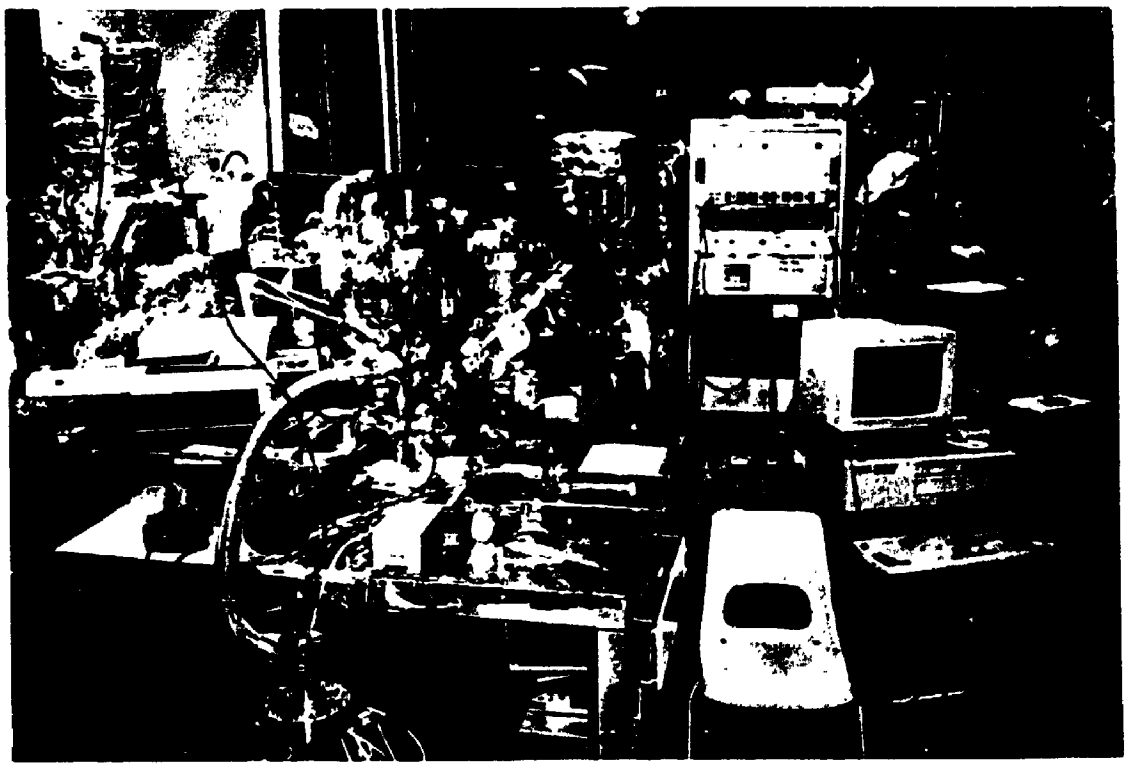

Figure 2.4.2 A picture of the Canadian Grasshopper beamline

A single scan gave good signal-to-noise ratio for both L- and K-edge spectra. However, in most cases, at least three scans were digitally combined and after normalization, a background was removed.

Oxygen and iron spectra were obtained at the U1 beam line of the National Synchrotron Light Source, Brookhaven National Laboratory. Details concerning the optics on the beam line have been described elsewhere[3,4]. The operating energy is 0.745-0.8 GeV and the maximum current is 1.0 A. The X-ray beam is monochromatized by a 1200 g/mm grating and covers the energy of 275-1000 eV. The absolute energy calibration of the incident photon beam was performed by measuring the XANES spectrum of gas-phase O_2.

2.4.2 Detection methods

2.4.2.1 General introduction

Total electron yield (TEY)[5,6] and conventional (transmission)[7,8] detection methods have been used to investigate the L-edge x-ray absorption near edge structure of low-Z elements, in a variety of systems, in the last decade. While the conventional method can only be applied to gas systems or very thin films, the TEY can be successfully used for all solid samples. On the other hand, the Fluorescence method, has been the choice of detection technique for K-edge X-ray absorption measurements in the soft (> 1000 eV)[4] and hard X-ray regions (> 5000 eV)[9].

X-ray fluorescence yield (FY) detection for low-Z elements in the L-edge region, however, has two additional problems. First, the fluorescence photon energies are < 200 eV for Cl, S, P, Si, etc. Second, the fluorescence yield is at least four orders of magnitude smaller than the Auger yield[10], and thus the background of the detector must be relatively low in order to even detect the low fluorescence yield. Very recently, Rosenberg et al.[11] have shown that, using a set of microchannel plates (MCPs), it is possible to measure the fluorescence yield for the L-edge of Al (< 70 eV). The same design with some minor modifications to improve the sensitivities, was used to measure FY spectra at the P and S K- and L-edges. The system consists of two MCPs (40-mm diameter, Galileo, MCP-40) with two electrically isolated Cu grids mounted in the front

of the channel plates, and a copper plate in the back as a collector. The detector was used both for TEY and FY measurements. For TEY, the grids were grounded and the front of the first MCP was set to 130 V and the rear to 1300 V. The electrons emitted from the rear channel plate were detected at the collector, and biased to 2100 V using a battery box. The current from the battery was directly measured with a current amplifier (Keithly Model 427). For FY measurements, the front of the MCP was set to -1450 V (to ensure that no electrons impinged on the MCP) and the rear to -150 V. The collector was set at ground potential. The larger MCPs enabled us to measure the FY in the analog mode. Applying a positive voltage to the grids in the FY measurements had no noticeable effects on the current, indicating that no positive ions were detected under the condition of the measurement. The current for most samples for TEY detection was in the range 20-80 nA while that of FY was 30-70 pA. The dark current of the detector, with no beam, in the fluorescence mode was < 0.1 pA. TEY was also measured by directly monitoring the current from the sample. It was found that this mode of TEY measurement gives better quality spectra, and thus most spectra presented in this thesis were recorded in the current TEY mode.

Figure 2.4.3 shows the reproducibility of the XAS measurement. Both peak positions and intensities are reproducible in these spectra taken by FY, and in the other spectra taken by total electron yield (TEY) and partial electron yield (PEY).

2.4.2.2 Comparison of FY against TEY/ PEY

The main difference between FY and EY (TEY/PEY) methods is the fact that the EY method is basically a surface or near surface technique whereas the FY method is a bulk one. The EY method is sensitive only to the top few surface layers because of the limited escape depth of electrons. On the other hand, the FY method can detect species up to a few thousands angstroms deep into the bulk structure due to the much deeper escape depth of energetic photons[12,13].

At the U1 beam line, the O K-edge and Fe L-edge fluorescence yield near edge spectra were measured using a differentially pumped UHV-compatible proportional counter filled with 200 Torr of P-90 (90% methane, 10% argon) as the counter gas, as described elsewhere[3]. In brief, the photons from the sample were intercepted by the

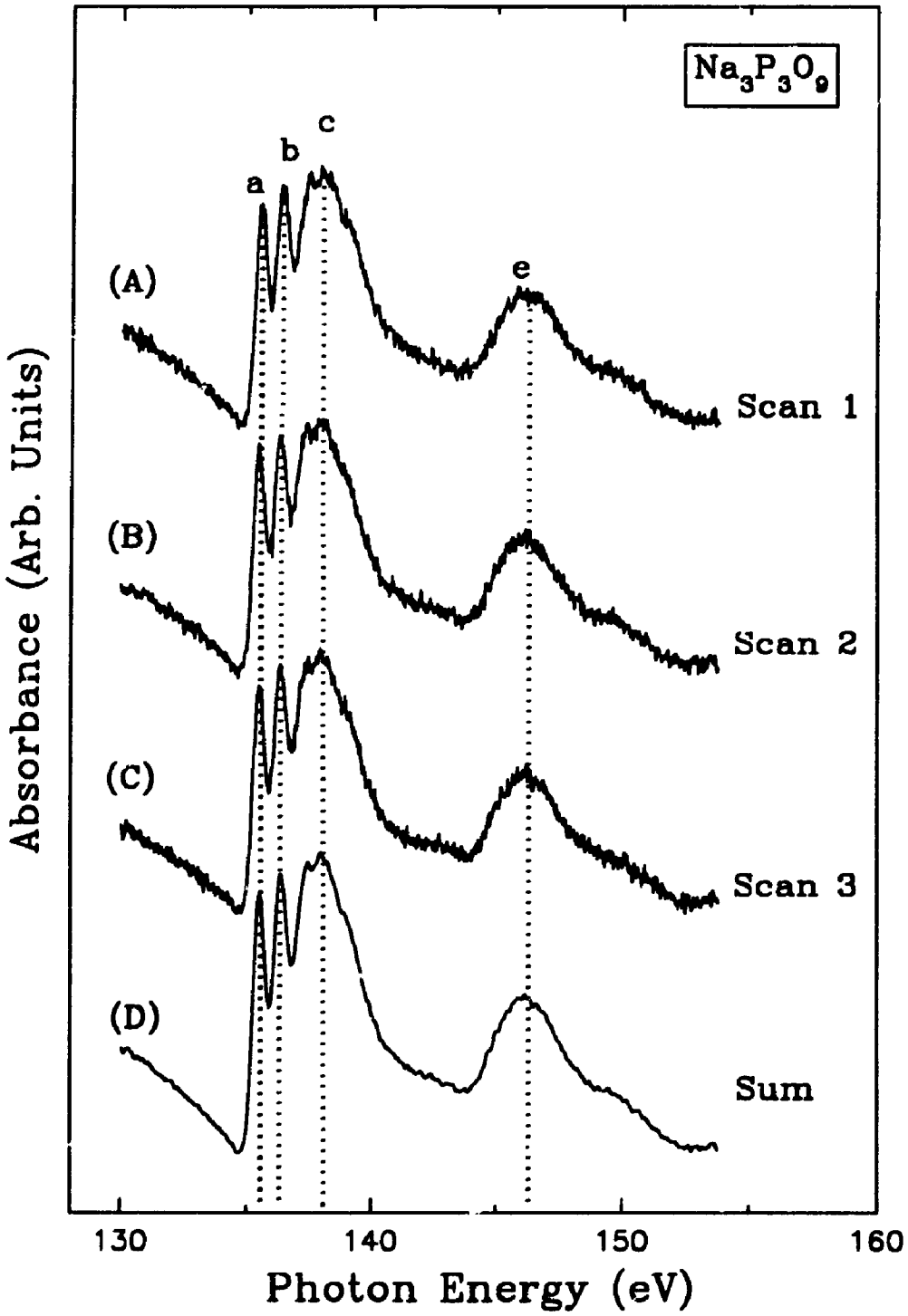

Figure 2.4.3 Comparison of spectra from different scans and the sum of three scans in FY mode

proportional counter at a fixed solid angle and absorbed by the counter gas, creating electron-ion pairs in the proportional counter. The charged particles were accelerated by the high electric field of the proportional counter anode and the charge was multiplied by impact ionization of the counter gas. The resulting pulse of electrons was then collected at the anode and amplified by a charge sensitive amplifier[3]. The electron yield XANES spectra were recorded by a channeltron located near the sample surface. In order to make this measurement more surface sensitive, the entrance of the channeltron was biased by -100 eV to repel the low-energy secondary electrons. The partial electron yield (PEY) was recorded simultaneously with the FY measurement. Examples of S and P XANES spectra measured in TEY and FY yields modes are presented below.

Figure 2.4.4 and 2.4.5 show the S L-edge XANES spectra of Pyrite (FeS_2) in the crystal and powder forms, respectively. A pyrite sample was carefully polished to remove any contamination and introduced into the measuring chamber with a minimum exposure to air. In Figure 2.4.4, the S L-edge spectrum measured in the TEY mode is compared with the FY mode. It is obvious that the spectral features are better resolved in the FY mode. For example, peak *b* in the TEY spectrum is not well resolved.

It is well known that sulphur in pyrite is readily oxidized to sulphate when the sample is exposed to air for a short period of time[14,15]. Figure 2.4.5 illustrates S L-edge spectra for a powdered pyrite which had been exposed to air for a long time. The general features of the FY spectrum of the powder in the figure is identical with the FY spectrum of the crystal (Figure 2.4.5 A) except for peak *e* and *g* which are only present in the powder spectra. Inspecting the TEY spectrum in Figure 2.4.5 (B), It is noticed that these two peaks are much stronger compared to the FY spectrum (Figure 2.4.5 A). Peaks *e* and *g* originate from a sulphate layer[6]. These spectra clearly show the surface and bulk sensitivity of TEY and FY, respectively.

In Figure 2.4.6, the P L-edge XANES spectra of two phosphate model compounds measured in TEY and FY modes are presented. As is apparent in the figure, the spectral patterns are very similar for both compounds, but the peaks are somewhat better resolved in the FY mode. Also the peak position of peaks *a*, *b* and *c* in the FY spectra have been shifted slightly to lower energy, while peak d is shifted in the opposite direction by 0.2-0.5 eV. As has been shown before, these small shifts are

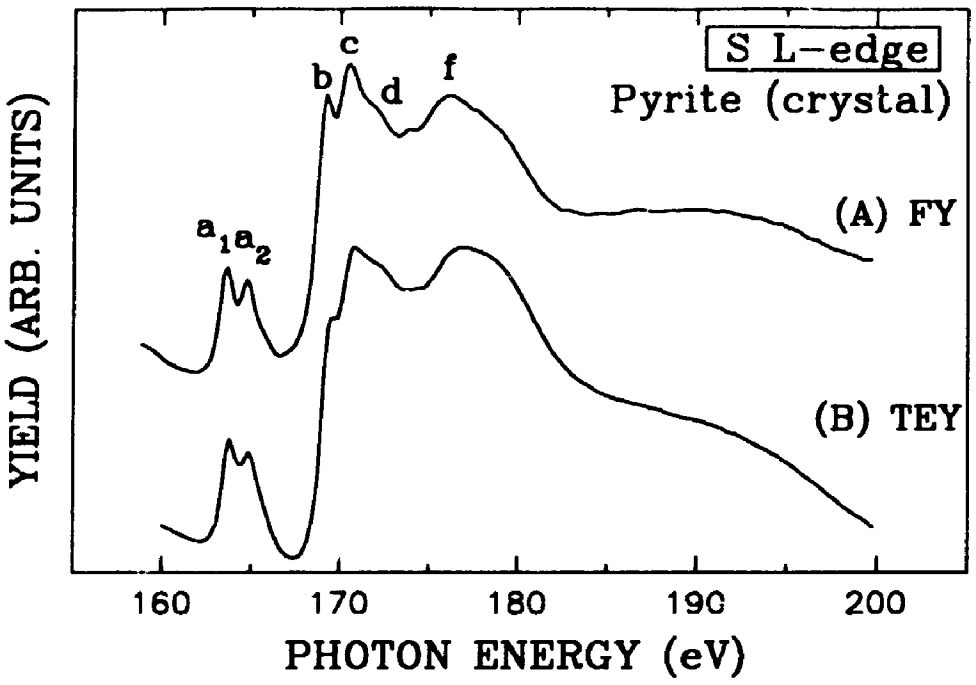

Figure 2.4.4 S L-edge XANES spectra of crystalline pyrite in FY and TEY modes

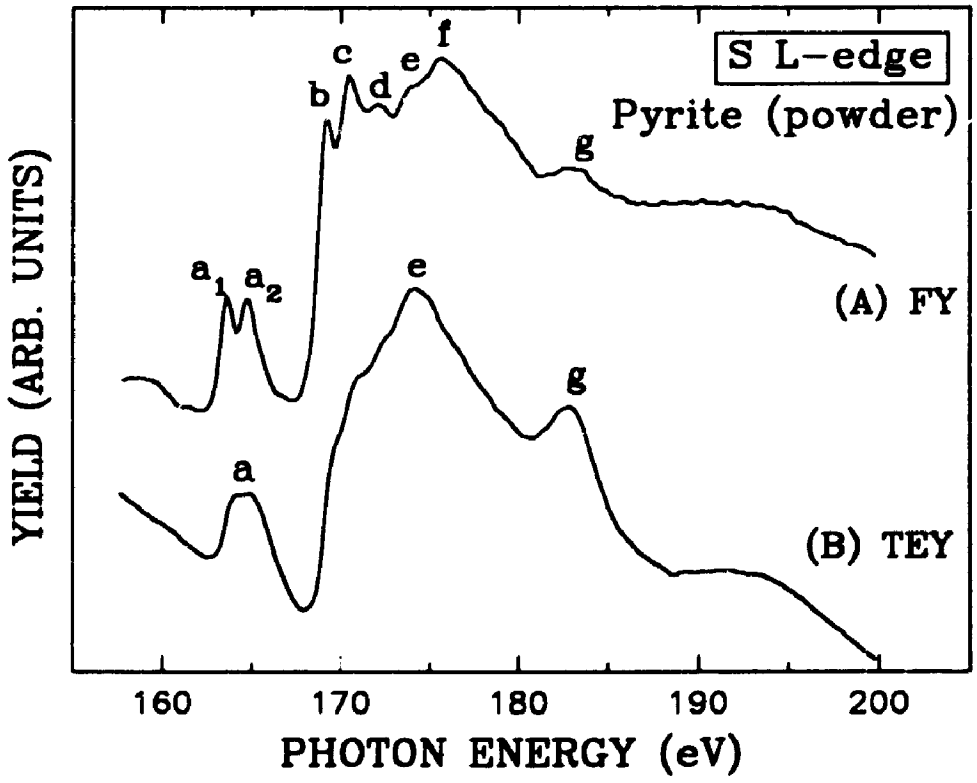

Figure 2.4.5 S L-edge XANES spectra of powdered pyrite in FY and TEY modes

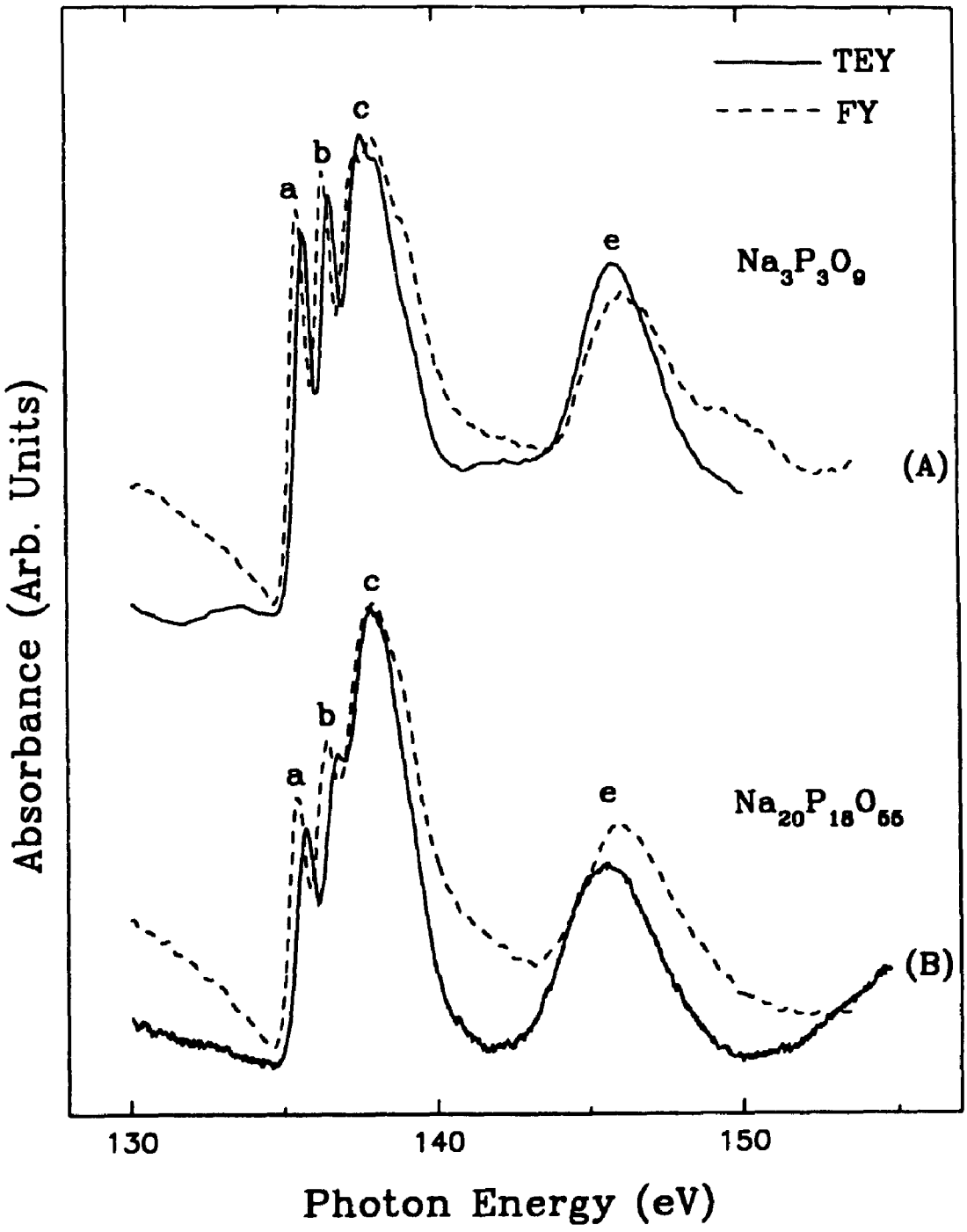

Figure 2.4.6 P L-edge XANES spectra of two polyphosphates in TEY and FY modes

due to surface effects[16]. The important observation here is that in contrast to powdered pyrite, when bulk and surface compositions are the same as for pyrite crystals, TEY and FY measurements provide very similar results. But when the composition of the surface and the bulk is different, as in the case of the powdered pyrite, the two techniques can provide very useful complementary information.

2.4.3 Data analysis

XANES and EXAFS spectra were analyzed using a BAN program[17], which can be used to divide I_0, remove the background, and construct new spectra from model compounds in different combinations.

For quantitative estimation, the intensity of the spectra of model compounds was normalized to the intensity of the highest peak in films. Then, the spectra of the model compounds were compared with those of the films. In order to determine the area under the peak in the films, a least squares fitting procedure was used. The details have been described elsewhere[18].

2.5 Other measurements for characterization

X-ray photoelectron spectroscopy (XPS) analysis and depth profiling were performed at Surface Science Western using a modified Science Laboratories SSX-100 X-ray Photoelectron Spectrometer with a monochromatized Al Kα X-ray (1486.6 eV) and base pressure of 5×10^{-9} torr in the analytical chamber. The spectrometer work function was adjusted to give a value of 83.90 ± 0.05 eV for the Au $4f_{7/2}$ peak of metallic gold. Energy resolution of spectra was approximately 0.05 eV with a nominal reproducibility of ±0.1 eV. All the binding energies were referenced to carbon at 285.0 eV. X-rays were focused to a 600 μ spot size; and a pass energy, into the electron analyzer, of 150 eV was used. In high resolution the pass energy of 25 eV was used. An Argon ion gun was used to depth profile, with Ar ions of 4.0 KeV energy and 2×2 mm^2 raster. Taking SiO_2 as reference, the etching rate was about 100 Å/min. The time interval for Ar^+ etching was chosen as 10 seconds in the first several etchings to obtain more detailed chemical information. Then the interval was adjusted to a longer time (20 or 30 seconds) because most of the film had been removed in that time.

Wear scar widths were taken by using Zeiss Axioplan optical microscope. Ten points along the scar were measured and average values were compared.

2.6 References

1. Burn, A.J., Joyner, R.W., Meehan, P., Parker, K.M.A. *J. Chem. Soc., Chem. Commun*, 1986, 982

2. Bancroft, G.M. *Canadian Chem. News*, 1992, 44, 15

3. (a) Fischer, D.A., Colbert, J., Gland, J.L. *Rev. Sci. Instrum.*, 1989, 60, 1596; (b)Parlar, D.H., Fischer, D.A., Colbert, J. and Gland, J.L., *Surf. Sci. Lett.*, 1990, 236, L372

4. Stöhr, J., Kollin, E.B., Fischer, D.A., Hastings, J.B., Zaera, F., Sette, F. *Phys. Rev. Lett.*, 1985, 30, 1468

5. a) Kasrai, M., Fleet, M.E., Sham, T.K., Bancroft, G.M., Tan, K.H., Brown, J.R. *Solid St. Commum.*, 1988, 68, 507; b) Kasrai, M., Fleet, M.E., Bancroft, G.M., Tan, K.H., Chen, J.M. *Phys. Rev. B* , 1991, 43, 1763

6. a) Kasrai, M., Brown, J.R. Bancroft, G.M., Tan, K.H., Chen, J.M. *Fuel* 1990, 69, 411; b) Brown, J.R. Kasrai, M. Bancroft, G.M., Tan, K.H., Chen, J.M. *Fuel* 1992, 71, 649.

7. a) Bozek, J.D., Tan K.H., Bancroft, G.M. *Chem. Phys. Letters*, 1987, 138, 33; b) Addison, B.M., Tan K.H., Bancroft, G.M., *Chem. Phys. Letters*, 1986, 129, 468.

8. Liu, Z.F., Cutler, J.N., Bancroft, G.M., Tan, K.H., Cavell, R.G., Tse, J.S., *Chem. Phys.* 1992, 168, 133.

9. Jaklevic, J., Kirby, J.A., Klein, M.P., Robertson, A.S., Brown, G.S., Eisenberger, P. *Solid State Commun.* 1977, 23, 680

10. Krause, M.O., *J. Phys. Chem. Ref. Data*, 1979, 8, 307

11. Rosenberg, R.A., Simons, J.K., Frigo, S.P., Tan K.H., Chen, J.M. *Rev. Sci. Instrum.*, 1992, 63, 2193

12. Chen, J.G., De Vries, B.D., Lewandowski, J.T., Hall, R.B. *Catal. Lett.*, 1994, 23, 25

13. Veigele, W.M.J. *At. Data Tables*, 1973, 5, 51

14. Buckley, A.N., Woods, R. *Appl. Surface Sci.*, 1987, 27, 437

15. Thorpe, A.N., Senftle, F.E., Alexander, C., Dulong, F.T., LaCount R.B., Friedman, S. *Fuel*, 1987, 66, 147

16. Kasrai, M., Yin, Z., Bancroft G.M., Tan, *K.H. J. Vac. Sci. Technol.* A, 1993, 11, 2694

17. Tyliszczak, T., McMaster University, unpublished program.

18. Huffman, G.P., Mitra, S., Huggins, F.E., Shah, N., Vaidya S., Lu, F. *Energy & Fuel*, 1991, 5, 574

CHAPTER 3

XAS SPECTRA OF MODEL COMPOUNDS

XANES spectroscopy is a very powerful technique for chemical characterization of complex matrices[1,2,3,4]. The spectra are very sensitive to small changes in the chemical environment of the absorbing atom. In order to identify the chemical nature of the atoms such as P, S, O and Fe in antiwear films, it is essential to compare the spectra of films for different model compounds in which the local chemical environments of those atoms are known.

3.1 P K- and L-edge spectra

The P K-edge XANES spectra of several model compounds are shown in Figure 3.1.1 and their peak positions are presented in Table 3.1.1. In the Figure, the P K-edge XANES spectra of the antiwear agent ZDDP (spectrum B) is plotted along with the spectra of two phosphates and other two model compounds. The strong peak *a* is due to the transition of electrons from the P 1s orbital to p-like empty antibonding orbitals below or within the conduction band. The same peak is observed for other model compounds. The only major difference is that the peak *a* shifts to the lower energy (for DPPM, spectrum A) or higher energies (for phosphates, spectrum D and E) compared with that of ZDDP. The peak *a* position of KDDP (spectrum C) is close to that of ZDDP because of the similar local environment. In DPPM, since P is in oxidation state of -3, the *a* peak position is lower than that in ZDDP or phosphates where P is in oxidation state of +5. In ZDDP and KDDP, the central phosphorus is coordinated to two oxygen and two sulphur atoms; whereas in the phosphates, the phosphorus is bonded to four oxygen atoms. Since the electronegativity of oxygen is larger than sulphur, the residual positive charge on P in phosphates is expected to be higher than P in ZDDP and KDDP. Thus the binding energy of P 1s will be relatively higher, which is reflected in the shifts observed in the XANES spectra. Peak *a* in the phosphate spectra is accompanied by some, so-called, post-edge broad features[5], which most likely correspond

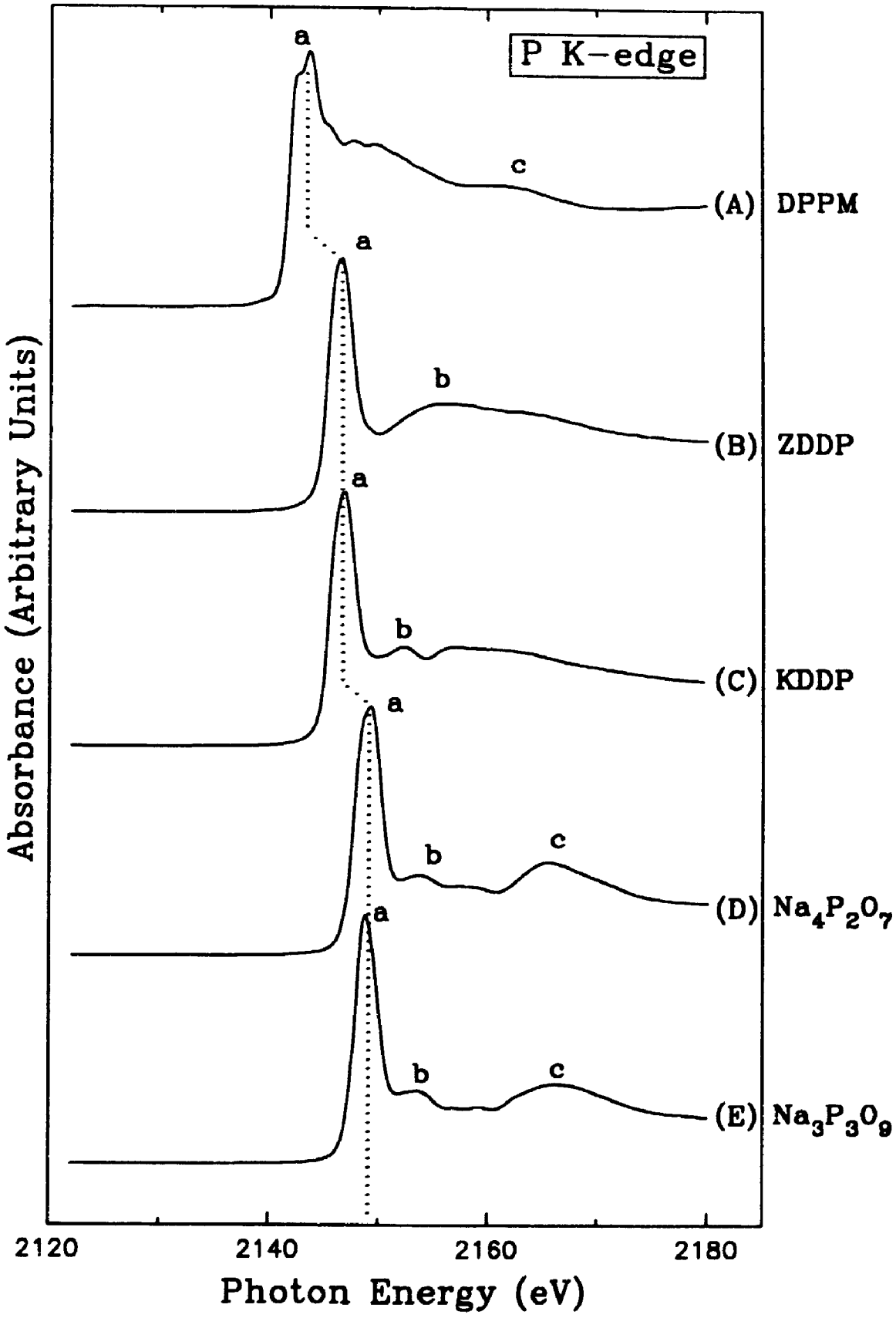

Figure 3.1.1 P K-edge XANES spectra of model compounds

Table 3.1.1 Peak positions of P K- and L-edge XANES spectra of some model compounds (± 0.1 eV)

Samples	K-edge			L-edge				
	a	b	c	a	b	c	d	e
DPPM	2143.2		2162.3	131.0	132.0	133.4	134.2	141.6(x)
ZDDP	2146.8	2156.1	-	133.9	134.8	135.5	143.2	-
KDDP	2146.6	2152.3		134.1	135.0	135.7	-	-
Na_3PO_3S	-	-	-	133.8 134.6(a')	135.4	136.3	137.8	144.5
$Na_4P_2O_7$	2149.2	2153.8	2165.6	134.9	136.0	138.3	-	145.9
$Na_3P_3O_9$	2148.8	2153.5	2166.3	135.5	136.4	137.5	138.0	146.4
$CaHPO_4$				135.9	-	137.7	140.8	146.3
NaH_2PO_4				135.6	136.8	138.4	-	145.9
$FePO_4$				135.7	136.6	138.7	-	146.4
Na_3PO_4				134.6	135.4	138.9	-	146.4
$Zn_3(PO_4)_2$				134.5	135.4	138.1	140.6	146.2
$Fe_4(P_2O_7)_3$				135.3	136.3	138.1	-	145.9
$Na_4P_2O_7$				134.9	135.8	138.2	-	146.2
$Zn_2P_2O_7$				135.4	136.3	138.6	-	146.2

to shape resonances or multiple scattering[6]. Although the features differ slightly from pyrophosphate to metaphosphate (spectra D to E), the differences are not significant enough to be used as fingerprints.

The P L-edge XANES spectra of some model compounds are depicted in Figure 3.1.2 and their peak positions are listed in the Table 3.1.1 too. The four compounds used here are the same as those used in the K-edge spectra. The only difference is that the KDDP, which gives a very similar spectrum as ZDDP (spectrum B), is replaced by Na_3PO_3S (spectrum C). The same shift of the edge jumps to high energy has been observed from DPPM (spectrum A) to the phosphates (spectra D and E) as discussed in the K-edge spectra and the same explanation applies here. Similar chemical shifts are generally observed for all core levels in the case of XPS spectra[7], indicating that the binding energy of the P 2p levels has shifted to higher energies. In contrast to XPS, which gives a broad 2p doublet spectrum with no fine features, XANES spectra are rich in structural detail. Phosphorus in DDPM is bonded to three carbon atoms; whereas P in ZDDP is bonded to two oxygen and two sulphur atoms and P in Na_3PO_3S is bonded to three oxygen and one sulphur. It is evident from Figure 3.1.2 that their spectra differ in the number of peaks as well as relative peak intensities. The L-edge XANES method shows particular value in differentiating phosphorus compounds of the same oxidation state. Pyrophosphate (D), and metaphosphate (E) both contain phosphorus in the +5 oxidation state and bonded to four oxygens, but their local symmetries are different. These differences are reflected very strongly in their spectra; peaks *a* and *b* are much more intense for $Na_3P_3O_9$. The XANES spectrum of ZDDP (spectrum B) has a triplet feature. This is due to the transition of electrons from P 2p core levels to the empty antibonding orbitals below or within the conduction band[8]. Peaks *a* and *b* are separated by ~ 0.9 eV which is the spin-orbit splitting of the 2p level. One other important difference between the ZDDP spectrum and the phosphates is the fact that peak *e* is missing in the spectrum of ZDDP. Peak *e* which is sometimes referred to as a shape resonance peak, appears whenever the central atom is coordinated to 3 or more strong electronegative atoms such as oxygen[8]. Thus the appearance of this peak in the spectra of the films will identify a phosphate; and the fine structures *a* and *b* on the shoulder of strong peak *c* will indicate the local symmetry and the structure of the phosphate. It

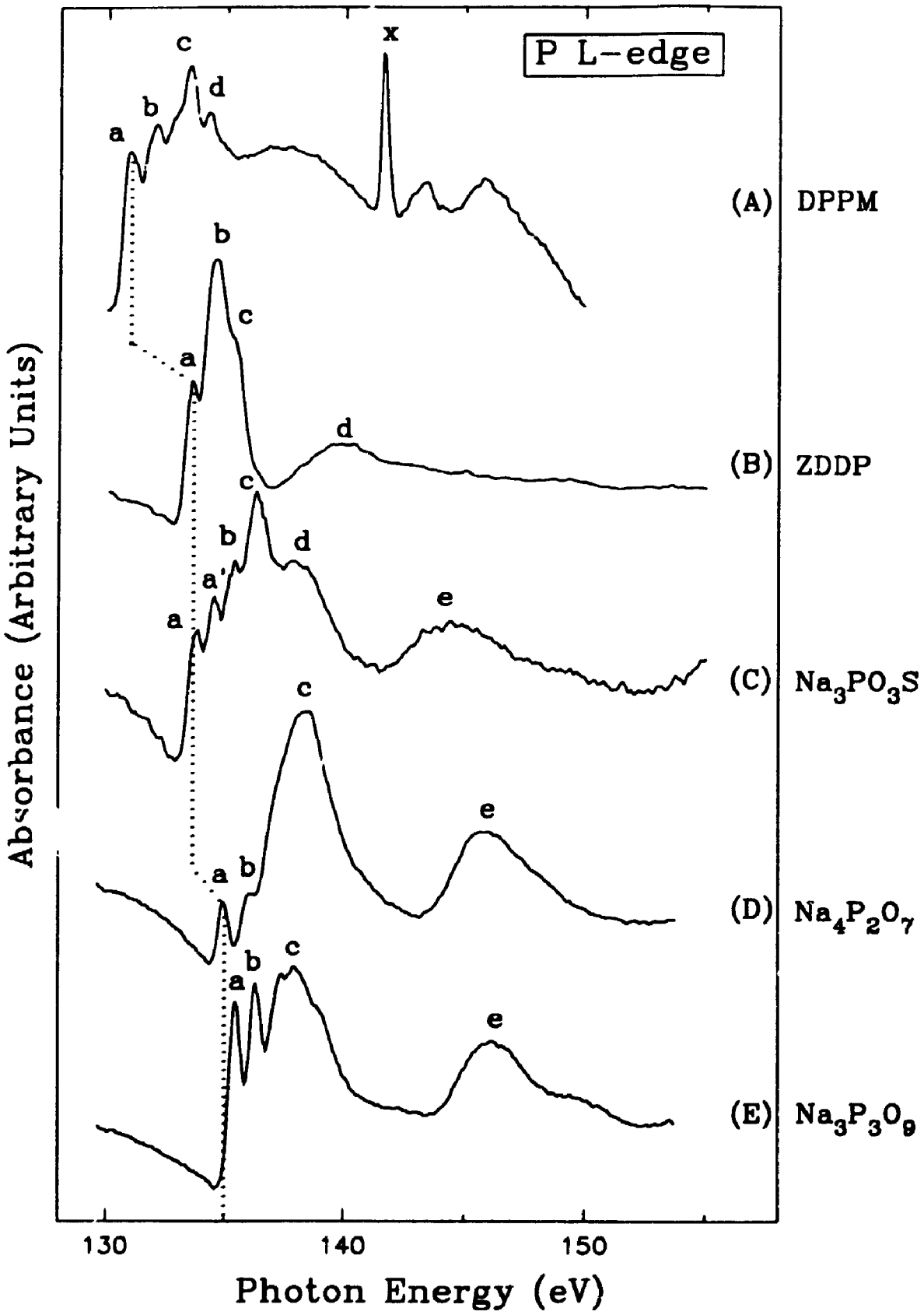

Figure 3.1.2 P L-edge XANES spectra of model compounds

should be pointed out that peak *x* in DDPM is the second order harmonic of a C 1s transition at 283.2 eV. Thus, because of the much better chemical sensitivity of the P L-edge over the K-edge, only the P L-edge XANES spectra of the model compounds will be used to fingerprint the unknown phosphate species in the tribochemical films.

As listed in the Table 3.1.1, other phosphates with different cations were also measured. Their spectra are demonstrated in Figure 3.1.3 and 3.1.4 respectively. In Figure 3.1.3 five orthophosphate spectra are plotted. When Ca is used as cation (spectrum A) the P L-edge spectrum is significantly different from other spectra in peak *c* position shift and a shoulder *d* present. Peak positions of NaH_2PO_4 (spectrum B) are similar to those of $FePO_4$ (spectrum C), but the relative intensities of peak *a* and *b* are higher in (B). In spectra (D) and (E), the intensities of peaks *a* and *b* are similar to each other but shifted 1.0 eV to lower energy from (B) and (C). However, the pyrophosphate spectra shown in Figure 3.1.4 seems not to be affected so much by different cations. With the peak positions of $Na_4P_2O_7$ (spectrum B) shifted to lower energy 0.4-0.5 eV, the general shape and relative intensities of these spectra are very similar.

3.1.1. Peak assignment of P L-edge spectra

In Si and S L-edge X-ray absorption spectroscopic studies[8,9], the lowest spin-orbit doublet (*a* and *b*) has been assigned to the $2p_{3/2,\ 1/2} \rightarrow a_1^*$ transitions. In P L-edge, peak *b* is separated by 0.8-0.9 eV from *a*, which indicates that peak (b) is the spin-orbit counterpart of peak (a); the spin-orbit separation is 0.86 eV[10]. But the relative intensities of *a* and *b* are not what are generally found in XPS studies. This observation is not uncommon in photoabsorption spectroscopy[11,12], as has been discussed by Schwarz[13]. This assignment is also in agreement with the systematic study of the tetrahedral oxides and oxyanions of the third-row elements[8]. It has been shown that for SiO_2, PO_4^{3-}, SO_4^{2-} and ClO_4^-, the first peak (doublet) in the L-edge spectra is due to the transition of the 2p electron to the a_1^* molecular orbital. The change in intensity of the doublet (peaks *a* and *b*) in Fig. 3.1.2 (D), (E) is likely due to the distortion of the phosphate tetrahedra.

The assignment of peak *c* is still controversial. Previously it has been assigned to the electron transition to a mixed valence band[9]. People seldom considered it as a p-

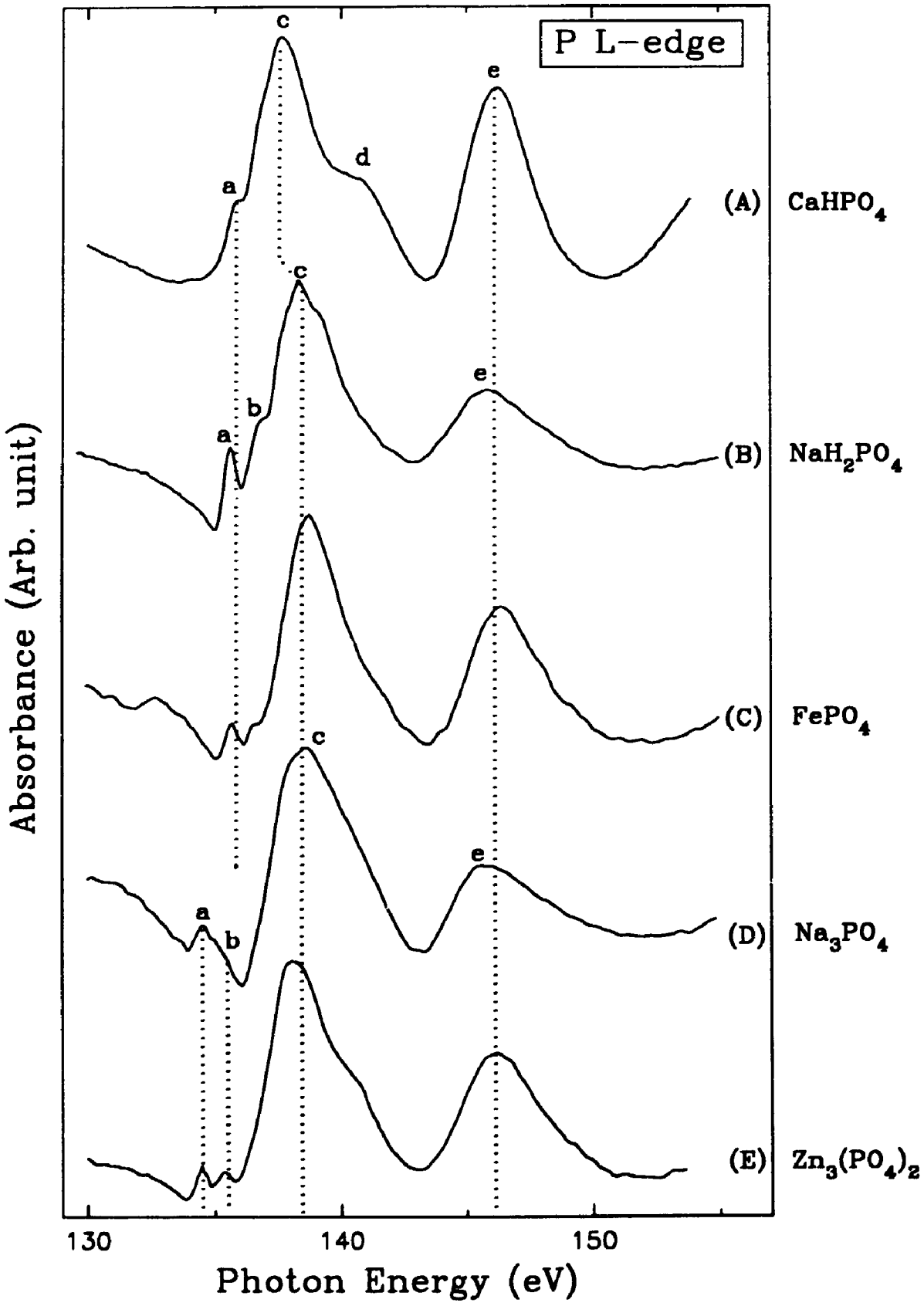

Figure 3.1.3 P L-edge XANES spectra of different ortho-phosphates

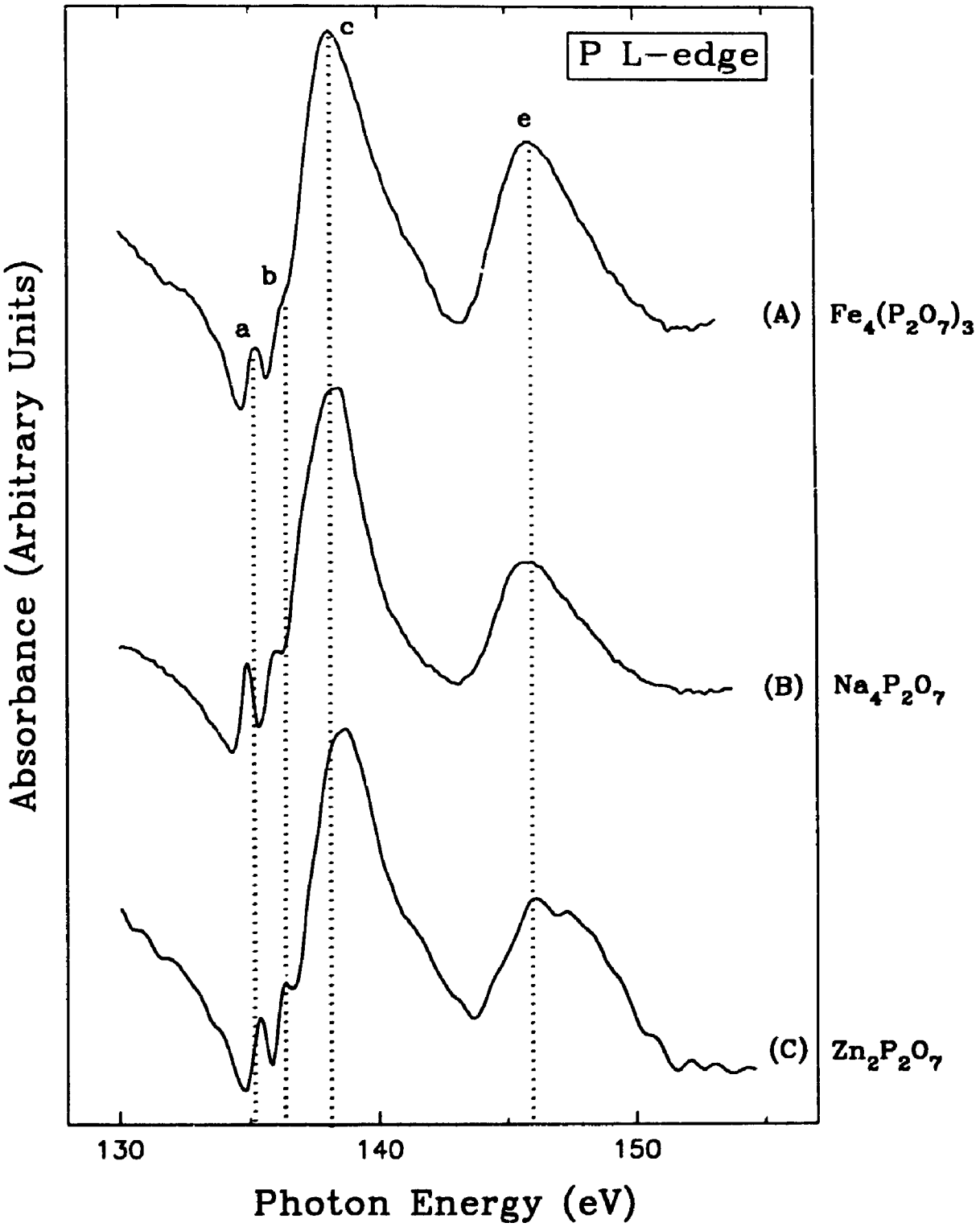

Figure 3.1.4 P L-edge XANES spectra of different pyro-phosphates

like transition because it is forbidden. However, recently Hansen et al.[14] have shown that this peak for SiO_2 is due to the transition to a p-like t_2* orbital. This arises because of significant mixing of p and d atomic orbitals. The assignment is also in agreement with Dehmer's results[15].

Peak *e* is usually assigned to a d-like shape resonances[8,14,15]. From spectra (D) to (E) in Figure 3.1.2, and P L-edge spectra of all sodium phosphates and sodium phosphate glasses which will be discussed later, it is noticed that this peak is always present at the same energy position for all sodium phosphates, whether crystalline or glassy. However, when oxygen is replaced by other elements with lower electronegativity (such as S), the peak is shifted to lower energies[16]. For example, as shown in Figure 3.1.2 and Table 3.1.1, peak *e* in Na_3PO_3S is at lower energy than that of phosphates by one electron volt.

3.1.2 Polyphosphate glasses and P L-edge XANES spectroscopy

In order to better understand the effects of local environment and symmetry on phosphorous, which is believed to be a major component of the antiwear films, the spectra of a series of linear polyphosphate glasses have also been studied[17] and their spectra will be used to fingerprint the antiwear films. The glasses were purchased from the Sigma company and were used without purification. The average chain lengths of polyphosphates reported by the company were determined by end group titration[18].

In 1950, Van Wazer and Holst found that the branching or cross linked phosphates are relatively less stable than linear or cyclic structures[19]. This conclusion is called the Antibranching Rule and originally stems from X-ray and pH titration data. This has also been supported by hydrolytic degradation experiments[20,21,22,23] and thermodynamic analysis[24]. Thus according to the Antibranching Rule, the phosphate glasses that have been obtained commercially for this study have long chain structures. Because of the mutual repulsion exerted by the negative phosphate charges, ring structures are not as favourable[25]. Phosphate glass is a very special and interesting material in which the units are arranged one dimensionally in space, but are irregularly oriented. The general formula of chain phosphates can be expressed as $M_{n+2}P_nO_{3n+1}$, where n is the number of phosphorus and M is a univalent metal. The average chain

length or average degree of polymerization $\bar{n}$ of these anions is given by the following equation[26]:

$$\bar{n} = \frac{2}{R-1} \qquad (1)$$

where R is the molecular ratio of univalent cation to phosphorus in a given phosphate. It has been demonstrated in both amorphous and crystalline systems that the M_2O:P_2O_5 ratio of a system is a dominant controlling factor. For any single molecule, the ratio precisely dictates the chain length[25]. Figure 3.1.5 shows that as n (proportional to chain length) increases, 1/R (= P/M) ratio increases. The increase is very sharp up to n ≈ 20 and then it levels off and approaches unity.

In order to further investigate the relationship between the P L-edge XANES spectra and polyphosphate properties, the spectra of a series of phosphates and polyphosphate glasses with different chain lengths have been measured. Their spectra are shown in Figures 3.1.6 and 3.1.7. Except for sodium orthophosphate (Na_3PO_4), sodium pyrophosphate ($Na_4P_2O_7$), and pentasodium tripolyphosphate ($Na_5P_3O_{10}$) which are in crystalline forms, the rest of the phosphates are glasses. All phosphates shown in the figures are sodium salts, which makes their spectra comparable. Spectrum (A) of orthophosphate is the only one in which peaks *a* and *b* are well resolved from peak *c* due to larger separation between the doublet and peak *c* (see Table 3.1.2). Spectra (D) to (H) are phosphate glasses with the number of phosphorus in the chain varying from 5 to 91. As can be noticed, peak *a* shifts to high energy from orthophosphate (n = 1) to Glass-5 (n = 5).

Most strikingly, from Figure 3.1.6 and 3.1.7, the relative intensities of peaks *a* and *b* are very sensitive to the number of P in the linear polyphosphate glasses. In order to obtain accurate peak positions, peak widths and peak intensities for polyphosphate glasses, all the spectra were fitted to Gaussian lines using a least squares fitting programme[27]. As illustrated by Figure 3.1.8, the spectra of phosphates have been fitted to several Gaussian peaks representing the transition of P 2p electrons to the antibonding orbitals. An arctangent step function representing the transition of ejected photoelectrons to the continuum has also been fitted to the spectrum. A number of conditions and

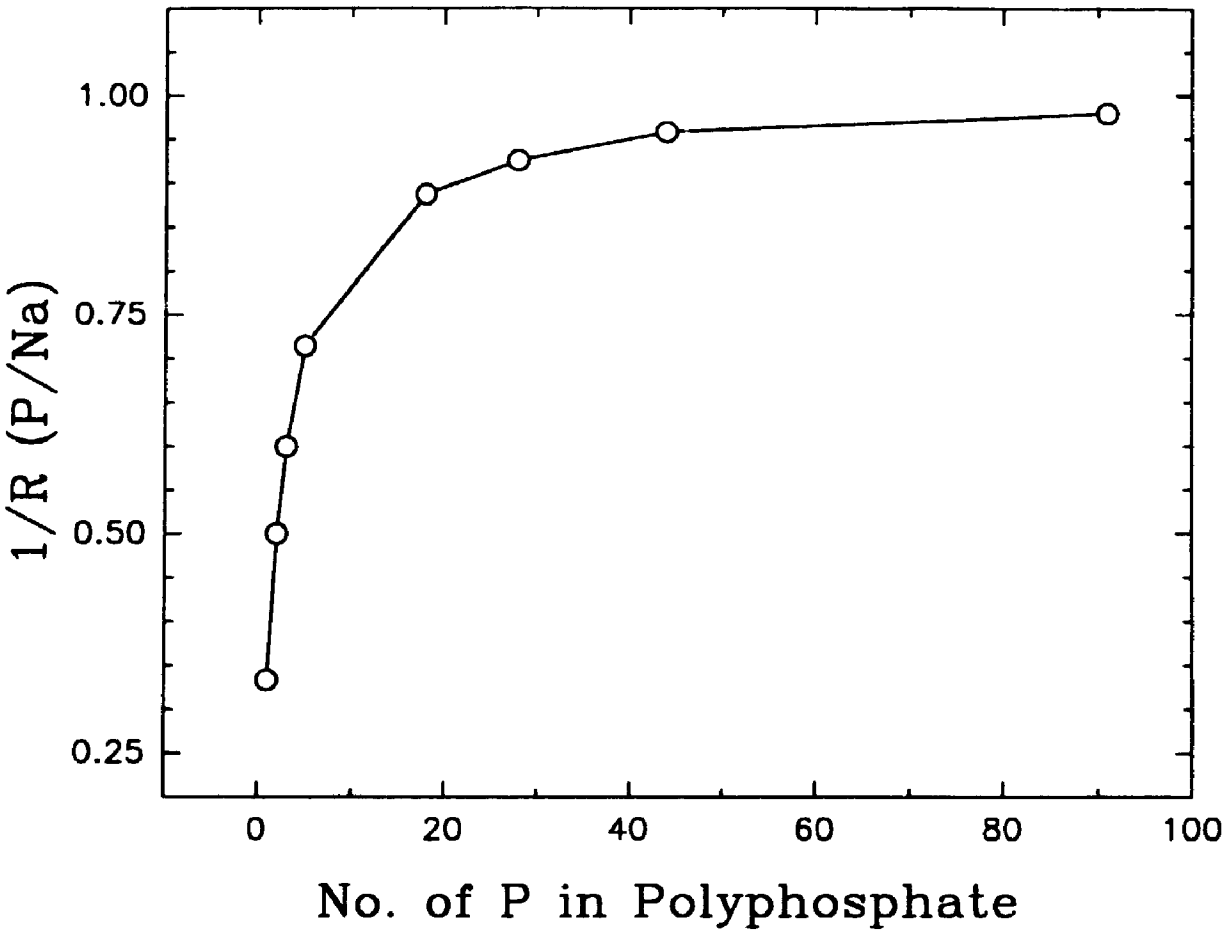

Figure 3.1.5 Number of P in polyphosphates (chain length) versus the ratio of P to Na

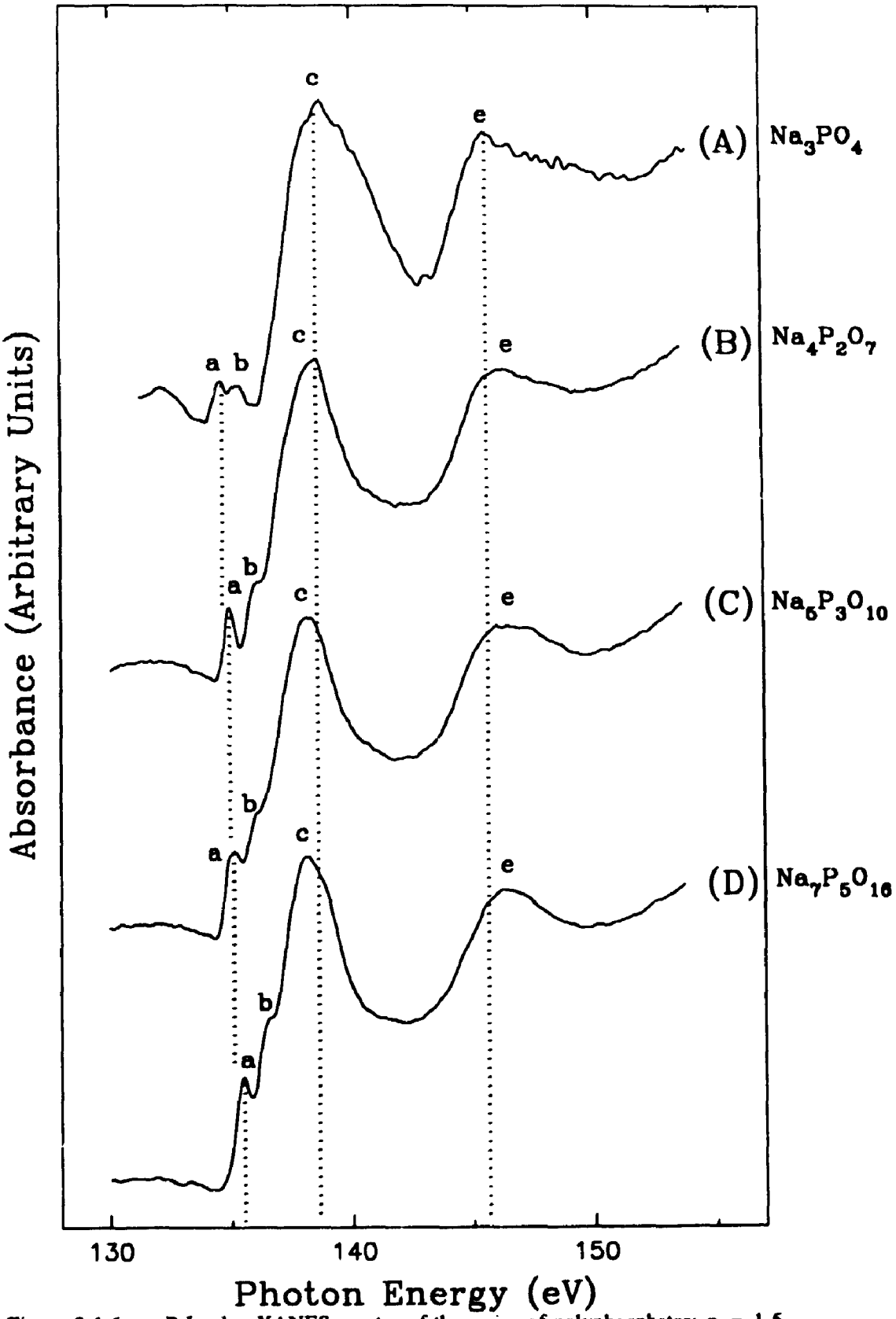

Figure 3.1.6 P L-edge XANES spectra of the series of polyphosphates: n = 1-5

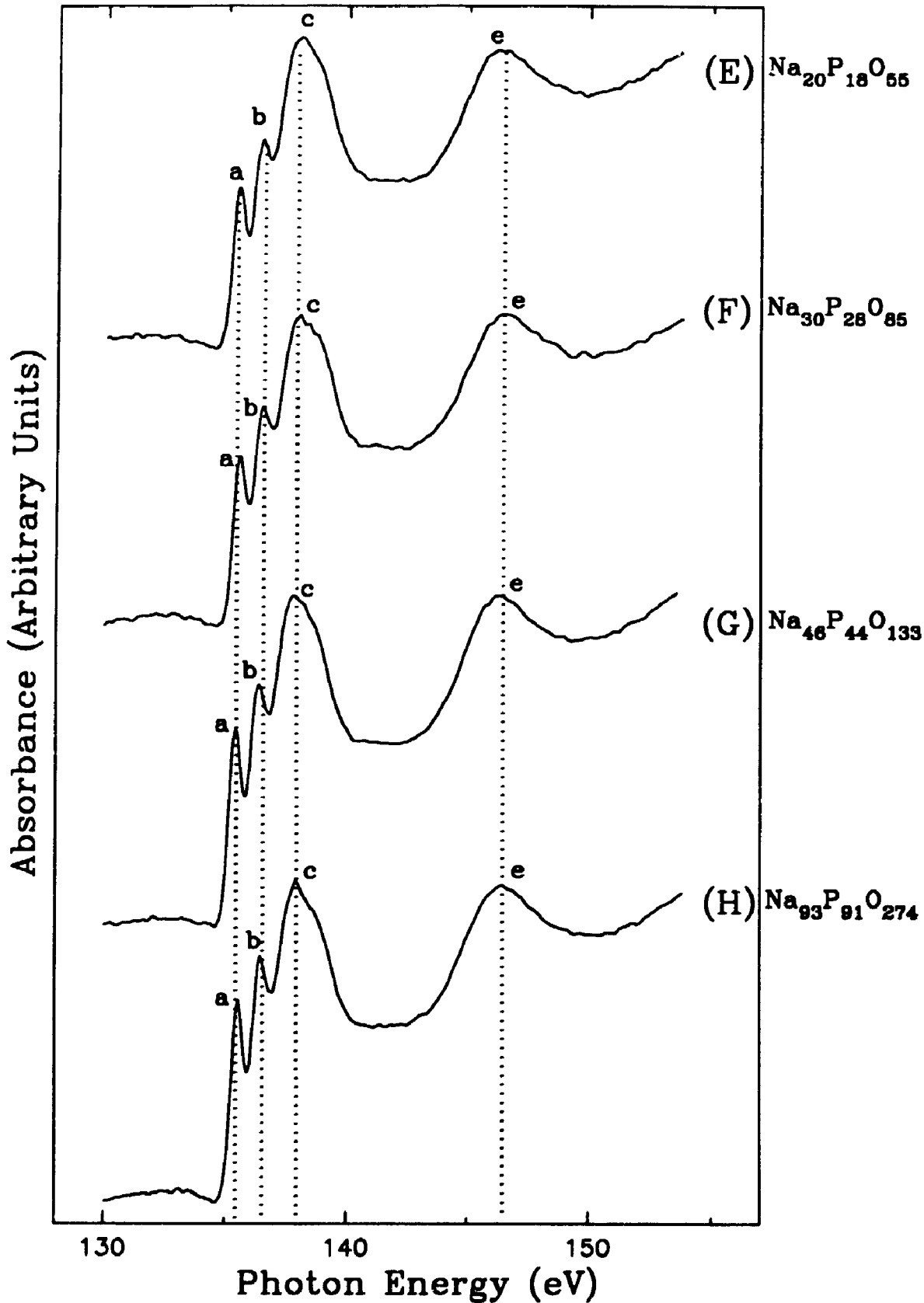

Figure 3.1.7 P L-edge XANES spectra of the series of polyphosphates: n = 18-91

Table 3.1.2 Peak positions, widths and intensities of phosphates from least squares fitting

Samples	Peak Positions (± 0.07 eV)				Peak widths (± 0.01eV)				Intensities*(± 6%)	
	a	b	c	e	a	b	c	e	a	b
Na_3PO_4	134.55	135.35	138.94	146.43	0.57	0.57	3.50	4.29	0.029	0.017
$Na_4P_2O_7$	134.93	135.83	138.20	146.37	0.45	0.45	2.85	3.74	0.040	0.031
$Na_5P_3O_7$	135.13	135.96	137.92	146.43	0.56	0.56	3.14	3.71	0.050	0.031
$Na_7P_5O_{16}$	135.43	136.33	138.02	146.40	0.62	0.62	2.87	3.48	0.079	0.067
$Na_{20}P_{18}O_{55}$	135.45	136.31	137.94	146.36	0.58	0.58	2.78	3.25	0.134	0.110
$Na_{30}P_{28}O_{85}$	135.46	136.33	137.97	146.36	0.61	0.61	2.78	3.30	0.151	0.139
$Na_{46}P_{44}O_{133}$	135.42	136.30	137.77	146.36	0.58	0.58	2.83	3.23	0.154	0.128
$Na_{93}P_{91}O_{274}$	135.51	136.38	137.85	146.44	0.58	0.58	2.82	3.38	0.163	0.136

* The intensities are ratioed to peak (c).

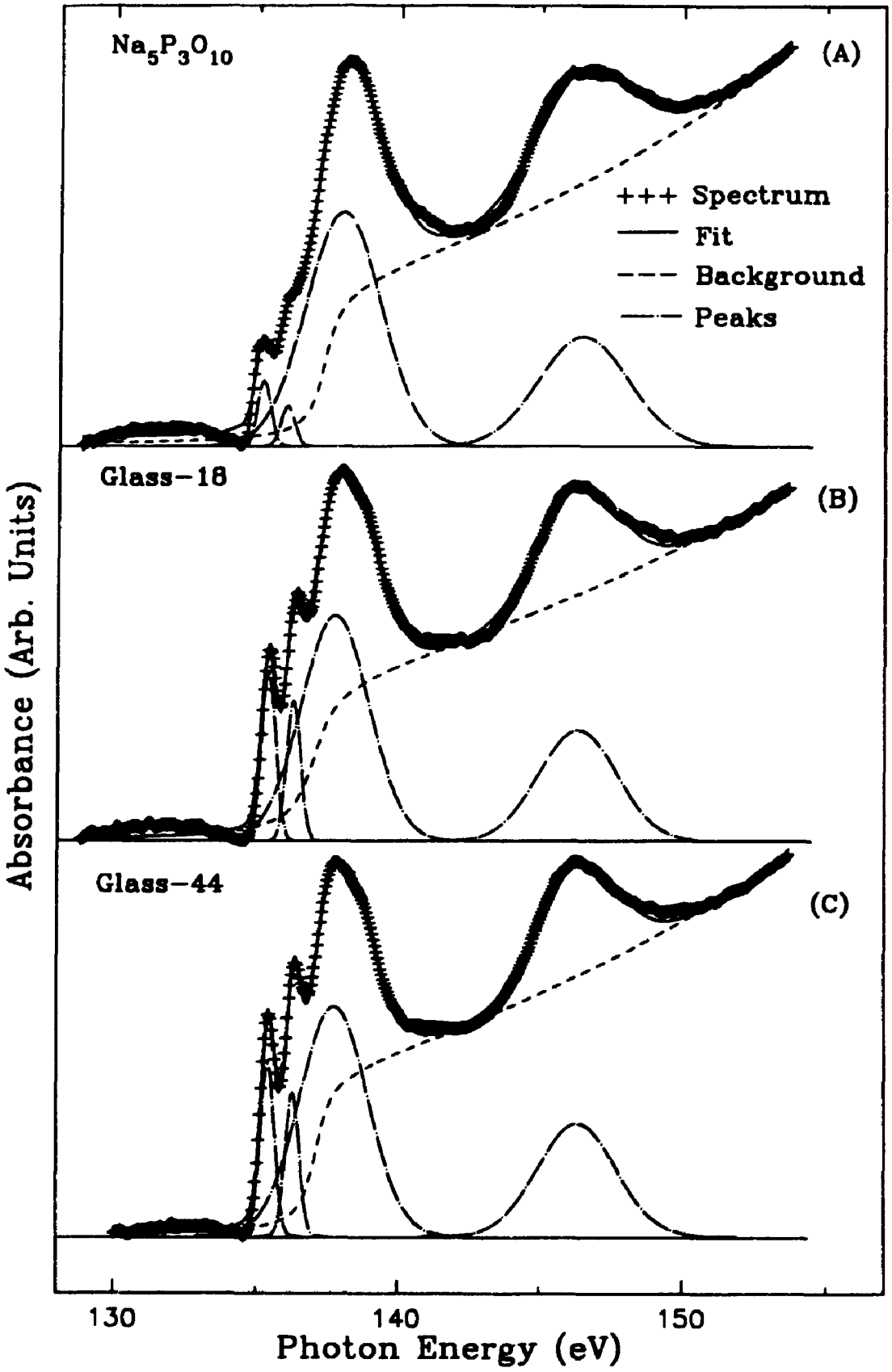

Figure 3.1.8 The least-squares fitting of polyphosphate spectra

constraints were introduced to obtain meaningful fits. First, the position of the arctangent step function was aligned just before peak *c*. This position is preceded by excitonic states (peaks *a* and *b*) which are observed in certain solids and generally lie below the bottom of the conduction band (continuum)[28]. Second, the peak widths of peaks *a* and *b* (the spin-orbit doublet) were constrained to be equal. All peak heights and peak positions were allowed to vary. Except for peaks *a* and *b*, the widths of the other peaks were allowed to vary.

Three XANES spectra of polyphosphate, fitted as described above, are shown in Figure 3.1.8 (A)-(C). All peak positions, peak widths, relative intensities (normalized to peak *c*) are summarized in Table 3.1.2. Figure 3.1.9 shows the positions of peaks *a* and *b* as a function of n. From Figure 3.1.9 and Table 3.1.2 it is found that the peak *a* position shifts to high energy when chain length increases from PO_4^{3-} (n = 1), to $P_5O_{16}^{7-}$ (n = 5). There is no obvious increase in energy above n = 5. The same trend has been found in XPS studies of sodium phosphate glasses[29,30]. This is expected, since the difference between XPS and XANES is in the final state of the ejected electron from the 2p core level. Because changes in screening affects the inner-shells more than the unoccupied levels, shifts observed in XANES and XPS are generally similar. However, the XPS peak widths are at least 1.5 eV compared to the 0.6 eV observed in XANES spectra. In XPS it has been found that the P 2p, 2s and O 1s binding energies are proportional to chain length[28]. This has been attributed to the fact that as the chain length increases, more bridging oxygen forms, and thus the electron density around P is reduced, which makes the core electrons more tightly bound. Also from Table 3.1.2, it is found that the peak position of peak *e* in all the spectra remains constant at 146.4 eV.

The chain length versus the relative area of peak *a* is plotted in Figure 3.1.10 (a). In order to compare the peak areas, the peak intensities of peak *a* has been ratioed to peak *c*. It is obvious from Figure 3.1.10 (a), that the ratio *a:c* increases sharply from PO_4^{3-} (n = 1) to $P_{18}O_{55}^{17-}$ (n = 18), then levels off relatively for higher chain polyphosphates. It has also been found that the relative height of peak *a* is proportional to the chain length, which is demonstrated in Figure 3.1.10 (a). The interesting thing is that when Zn replaces Na as cation in the polyphosphates, the relative height of peak

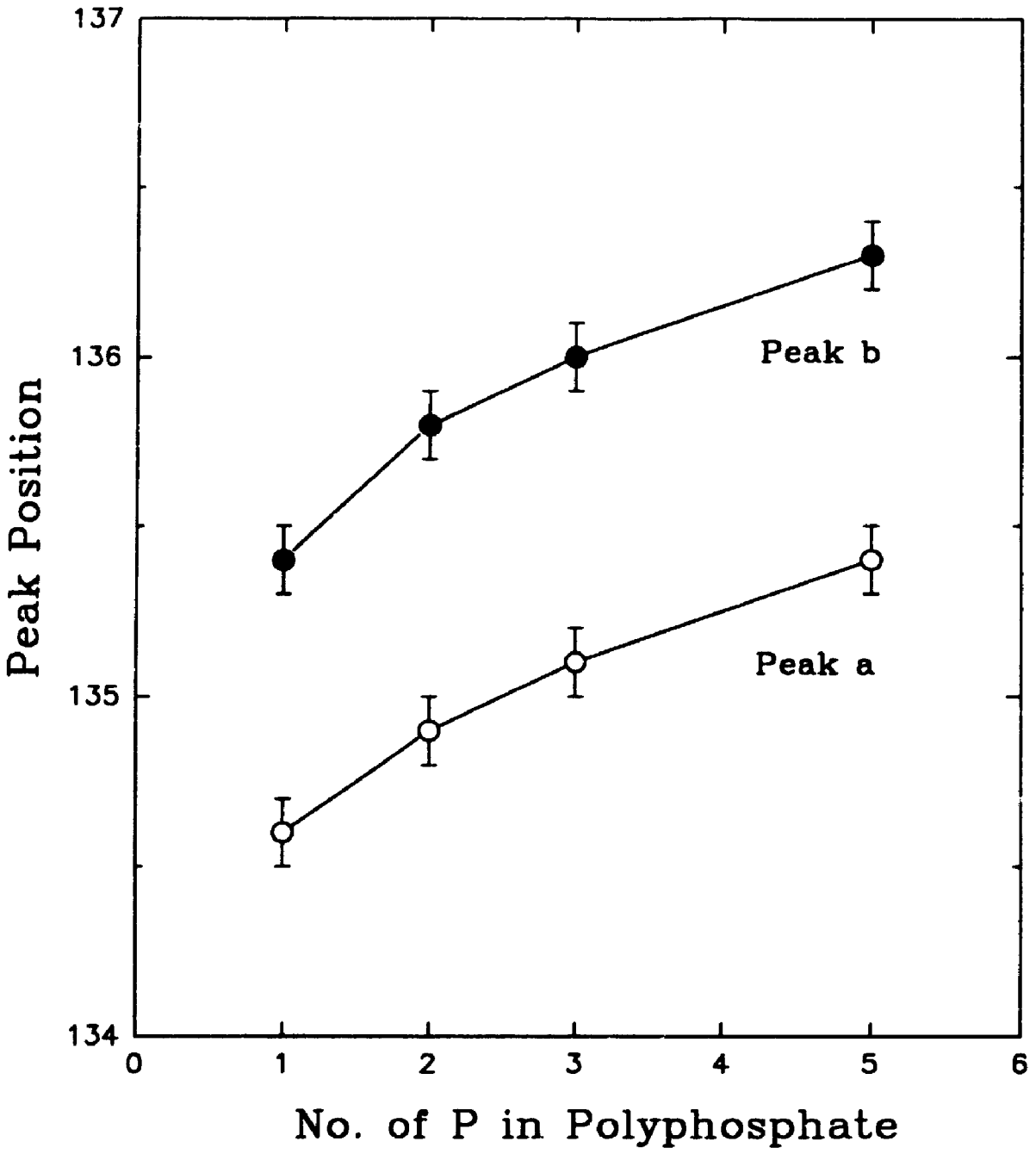

Figure 3.1.9 A plot of the pre-edge doublet peak positions against the number of P in polyphosphates (chain length)

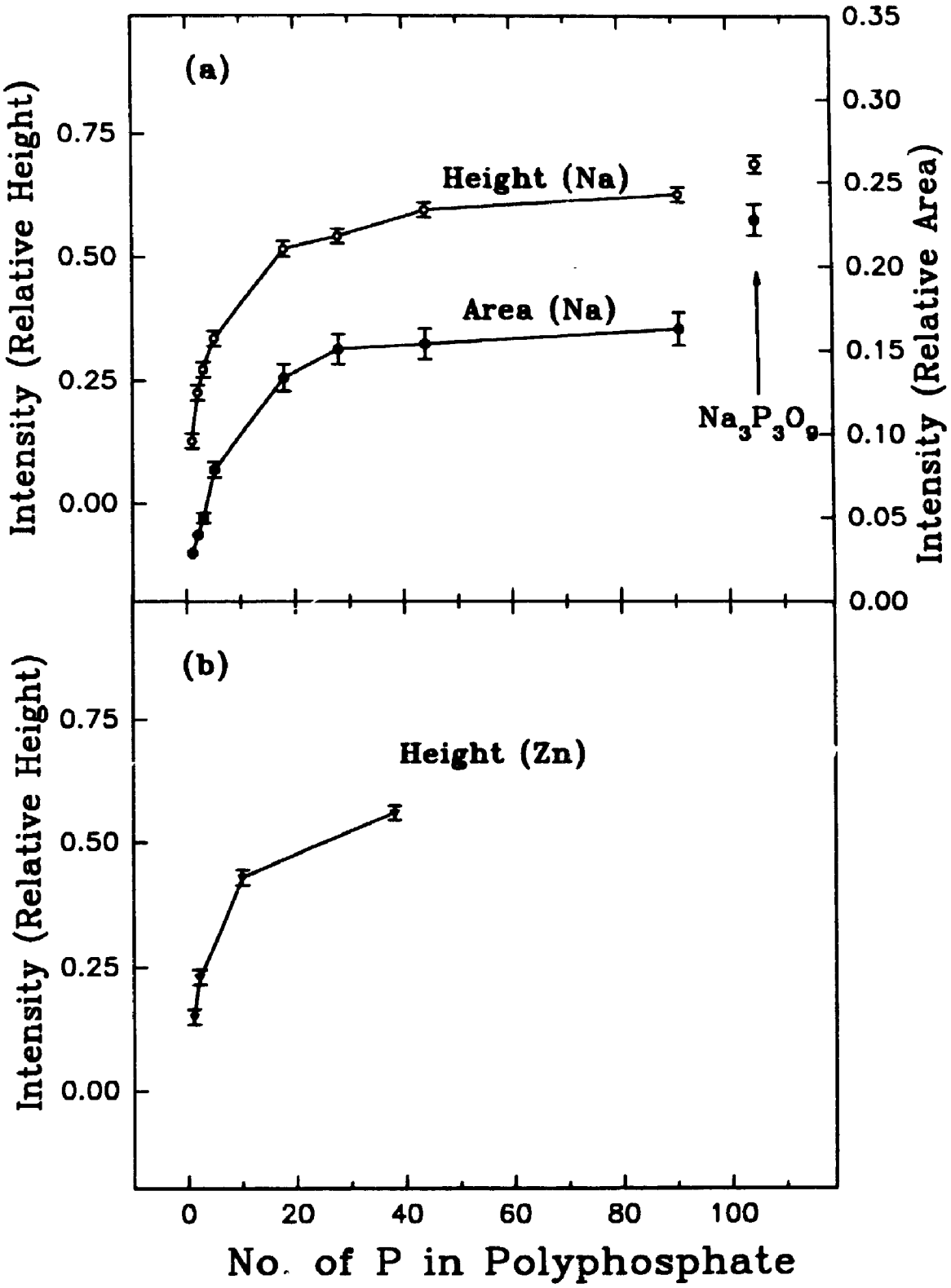

Figure 3.1.10 Number of P in Polyphosphates (chain length) as a function of relative area and relative heights of peak *a*

a shows the same trend as Na polyphosphates, which is shown in Figure 3.1.10 (b). It is also noticed that the plots in Figure 3.1.10 (a) and (b) are very similar to what is found in Figure 3.1.5.

Now, using Table 3.1.2 and Figure 3.1.10 it is possible to directly determine the number of P in polyphosphate glasses. The relative error for area measurement was estimated at about six percent from the standard deviation from duplicate spectra. As noticed in the figure, up to n = 18, the change in the peak area with number of phosphorus atoms is large, and as a result chain length can be determined with good accuracy. Above n = 18, the change is rather subtle, and thus the result will be less accurate. This intensity measurement is much more sensitive than the use of chemical shifts shown in Figure 3.1.9. There, the change in the peak position versus the chain length is small and can only be used up to n = 5. This technique is also much more sensitive than XPS, because the peak widths in the XPS spectra are much larger than those in the XANES spectra (1.5 eV vs. 0.6 eV). However, it should be pointed out that film polyphosphates constitute a range of polyphosphates with variable chain length. Therefore from this method, it is possible to obtain an average chain length in an unknown phosphate system. The major advantage of this method is that it can be applied to thin films and surfaces where other techniques such as titration and liquid chromatography cannot be utilized. Also, FY and TEY can give the chain length in both surface and bulk. This is the first time that P L-edge XANES is used quantitatively to solve such a complex problem. This will have very important application in systems such as surface films and it will be used in this study to fingerprint polyphosphates in the antiwear films.

3.1.3 P K-edge EXAFS spectra of polyphosphates

Since the spectral pattern in the K-edge XANES of phosphate glasses does not change substantially, the information gained can not be used to fingerprint the phosphate chain length. However, the analysis of K-edge spectra in the range of 50-1000 eV above the ionization threshold, or EXAFS region, can be used to estimate the bond distance and the coordination number around the absorbing atom.

Figure 3.1.11 shows a typical X-ray absorption spectrum recorded to ~ 600 eV

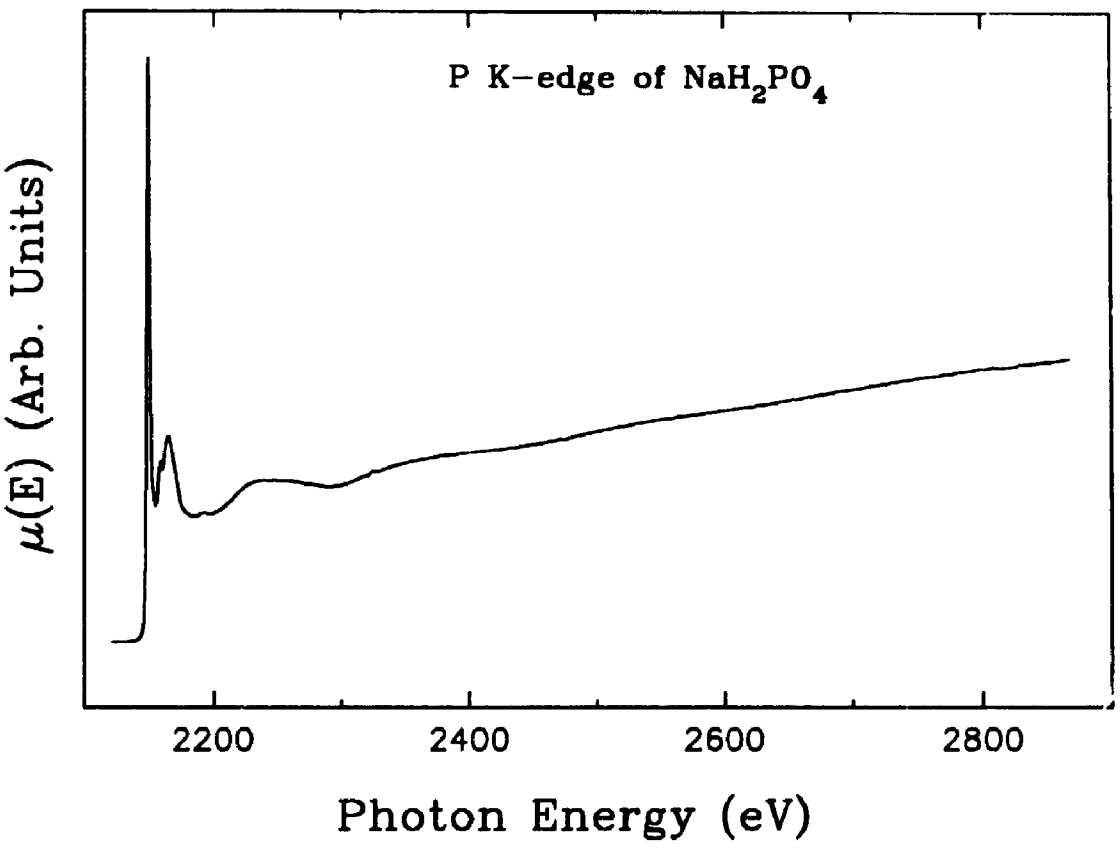

Figure 3.1.11 P K-edge spectrum of NaH_2PO_4

above the P K-edge for NaH_2PO_4. A standard procedure has been used to extract the bond distance and coordination number from the experimental X-ray absorption spectra[31,32]. The EXAFS interference function is defined by

$$\chi(k)=[\mu(E)-\mu_0(E)]/\mu_0(E) \qquad (2)$$

where E and k are the X-ray photon energy and the wavenumber of the photoelectron ejected by the X-ray photon, respectively. The coefficient $\mu(E)$ refers to absorption by an atom in the material of interest, while $\mu_0(E)$ refers to absorption by an atom in the free state, both of which are a function of k. In order to relate $\chi(k)$ to structural parameters, it is necessary to convert E into the photoelectron wavevector k by the relationship

$$k = [2m/\hbar^2(E - E_0)]^{1/2} \qquad (3)$$

where m is the mass of the electron; $\hbar$ is Planck's constant divided by 2π; E_0 is the threshold energy of the absorption edge. In our experiment, E_0 was determined from the inflection point at the absorption threshold. The transformation of $\chi(E)$ into $\chi(k)$ in k space gives rise to

$$\chi(k)=\sum_{j=1}^{N} N_j F_j(k)/(kr_j^2)\exp(-2\sigma_j^2k^2)\exp(-2r_j/\lambda)\sin[2kr_j+\Phi_j(k)] \qquad (4)$$

where $F_j(k)$ is the backscattering amplitude from each of the N_j neighbouring atom of type j; σ_j is the Debye-Waller factor which accounts for thermal vibration and possible statistical disorder, viz., distribution of distances; r_j is the mean internuclear distance between the central (absorbing) atom and atoms in the jth neighbour shell; λ is the mean free path of the photoelectron due to the finite core hole lifetime and interactions with the valence electrons; $\phi_j(k)$ is the scattering phase shift due to both the centre and backscattering atom.

In practice, the $\chi(k)$ of phosphates were extracted from the raw absorption data

(Figure 3.1.11) in the following steps. First, the raw data was truncated above the edge to exclude the XANES region and a pre-edge background is removed. A computer program[33] was used to convert the photoelectron energy scale to k-space using the above equation. At this stage, $\chi(k)$ was multiplied by k^3 to enhance features at high k values. Second, EXAFS $k^3\chi(k)$ was obtained by subtracting post-edge background function $\mu_0(k)$. This background was approximately the smooth part of $\mu(k)$ and generated by fitting $\mu(k)$ to a multi-section polynomial spline function of 3-4 sections. Finally the data were normalized by the edge jump obtained by extrapolation of a straight line fit above the edge.

The $k^3\chi(k)$ versus k is plotted for orthophosphate and polyphosphate glasses in Figure 3.1.12 (A, B, C). As is noticed from the spectra, the amplitude and positions for the three spectra are very similar. This indicates that the coordination number and bond distances for the three samples should be very similar. In order to obtain a more quantitative picture, the $k^3\chi(k)$ was Fourier transformed in R-space. The magnitude of the corresponding Fourier transform (FT) of the P EXAFS are shown in Figure 3.1.12 (D, E, F). This gives a qualitative picture of the local structure around P. Since the transform is made without including the phase shift, all of the peaks in F(R) are shifted closer to the origin. Further data analysis are needed in order to obtain quantitative structural information (such as the P-O bond length, R) about the local environment of the absorbing atom.

In general, the parameters (distance R, coordination number N and relative mean square disorder σ_j^2) relevant to a particular structure model can be deduced from the Fourier filtered experimental EXAFS. This is achieved by reverse Fourier transform (RFT). The RFT (shell by shell) permits a well defined phase and amplitude function to be determined for each shell distinguishable in the F(R) function. In order to obtain the structural parameters from the phase and amplitude function, the scattering phase shift and amplitude scale need to be corrected and calibrated respectively. Thus, model phase or amplitudes, either calculated or derived experimentally, are needed. In this paper, two calculated tables called FEFF[34] and McKale[35] have been used. The phase shift and amplitude of NaH_2PO_4 was used as an experimental model for glass analysis.

The main peak (see Figure 3.1.12 D) around 1.2 Å in the Fourier transform is

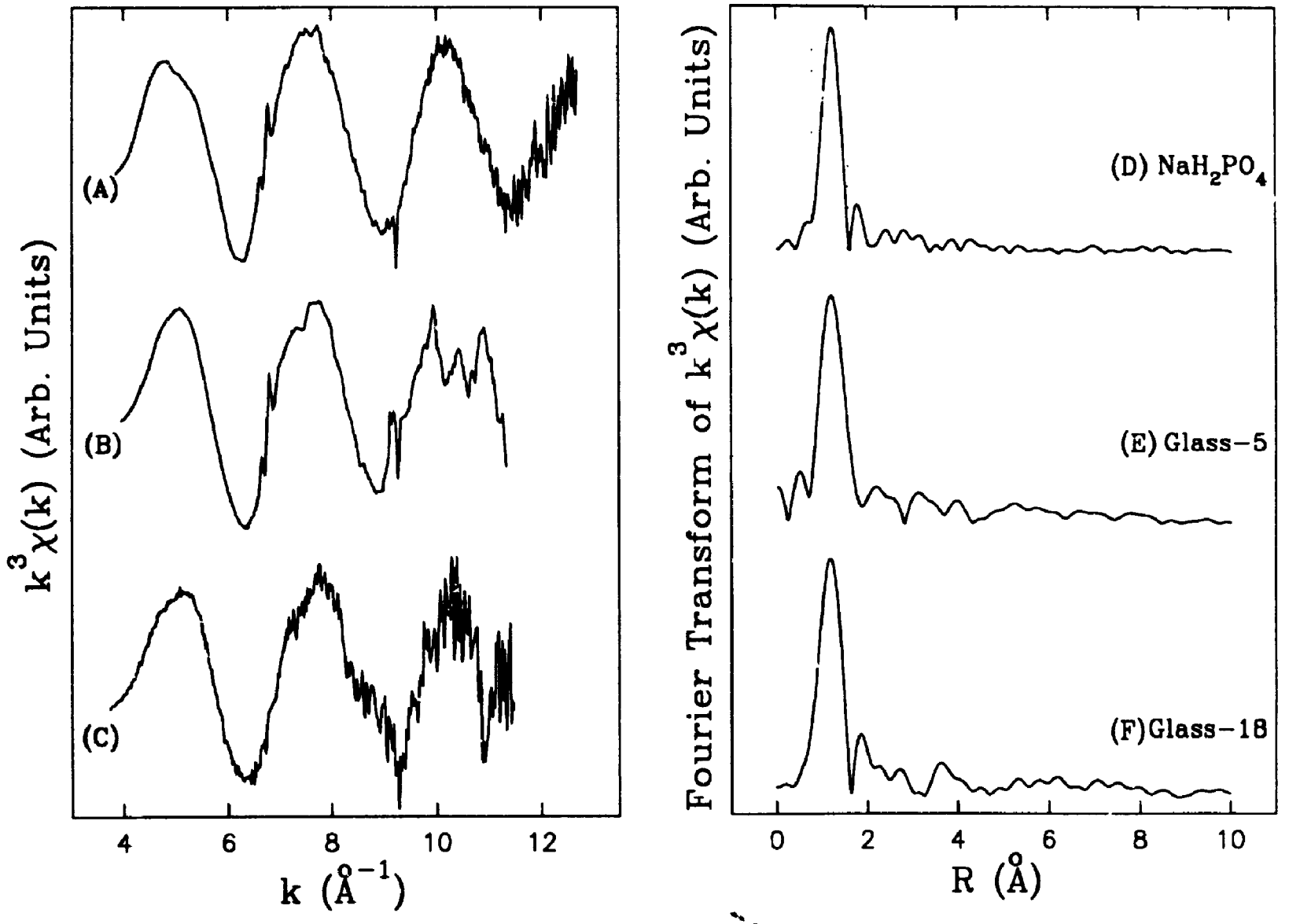

Figure 3.1.12 EXAFS spectra (left) and their Fourier transform spectra (right) of three phosphates: (A) and (D) NaH_2PO_4; (B) and (E) $Na_7P_5O_{16}$; (C) and (F) $Na_{20}P_{18}O_{55}$

assigned to the first P-O coordination shell. Several small peaks in the higher distance are likely due to high frequency noise. A symmetric Hanning window was chosen for reverse Fourier transform (Figure 3.1.12 D, dotted line). Then utilizing the calculated (FEFF and McKale) phase shift and amplitude function, the P-O distance R and coordination number N have been determined. These results are summarized in Table 3.1.3. The P-O bond distance of NaH_2PO_4 derived from EXAFS, using FEFF or using McKale, is very close to the diffraction data of 1.56 Å[36]. As is expected from the structure of the compound, the coordination number N is essentially 4 (3.9 and 3.6 respectively from FEFF and McKale). Having measured the phase shift and amplitude for a known structure, we can use them for the analysis of the polyphosphate glasses.

Two glass samples, $Na_7P_5O_{16}$ (glass-5) and $Na_{20}P_{18}O_{55}$ (glass-18), have been analyzed using the same procedure described for sodium dihydrogen orthophosphate. Their k^3 weighted P K-edge EXAFS are shown in Figure 3.1.12, (B) and (C), and the magnitude of their Fourier transforms are shown in (E) and (F). Again, a single coordination shell is observed for these glasses in the Fourier transform plots around 1.2 Å. The weak peaks should have the same origin (probably noise) as those of the model compound. Comparing R and N of the glasses with those of NaH_2PO_4 in Table 3.1.3, it is noticed that the chemical environment of P in these two glasses looks very similar to that of NaH_2PO_4. Again P in the glasses is coordinated to four oxygen atoms, and the average P-O bond distance is about 1.55 Å. The bond distances and coordination numbers extracted from EXAFS results accounts for an average value. As the chain length increases in polyphosphates, the number of bridging P-O bonds also increase. The bridging P-O distance is 1.60 Å[37] which is longer than the terminal P-O. Since the error in EXAFS measurements is expected to be 0.02 Å, the small changes in the bond distances can not be easily detected in the EXAFS. Thus we are not able to deduce the chain length of the polyphosphate glasses from the EXAFS data using the P-O bond distance and coordination number.

3.1.4 Conclusions

From the above discussion, the following conclusions can be drawn:

1. Both the P K-edge and L-edge XANES are very sensitive to the electron

Table 3.1.3 EXAFS data analysis

Compounds	P-O Bond Distance (Å)			Coordination Number			Diffraction Data of P-O
	Feff	McKale	Exp.*	Feff	McKale	Exp.	
NaH_2PO_4	1.55	1.54		3.9	3.6		1.56**
Glass-5 ($Na_7P_5O_{16}$)	1.55	1.54	1.54	3.6	3.3	4.8	
Glass-18 ($Na_{20}P_{18}O_{55}$)	1.55	1.53	1.55	3.7	3.3	5.0	

* The phase shift and amplitude of NaH_2PO_4 were used for the glasses;
** Diffraction data from KH_2PO_4.

charge density around the absorbing atom. The P K- and L-edges shift to higher energy as the core level becomes less screened by the ligand surrounding the absorbing atom. The fine features in the spectra have been assigned to electronic transitions from the P core levels to appropriate antibonding orbitals below and above the edge.

2. While the P K-edge XANES can provide limited structural information, the P L-edge is very sensitive to the small local structural changes caused by bridging P-O bonds in polyphosphates.

3. Using the ratio of intensities from the P L-edge XANES spectra of the polyphosphates, it was possible to construct a calibration curve for chain length determination. It was found that the chain length was proportional to the intensity of the first sharp peaks in the XANES spectra of the polyphosphates. This calibration plot will be very useful for determining the phosphate chain length in thin films and biological molecules where other techniques can not be applied. An important objective of XANES spectroscopy is to provide non-destructive and quantitative results, in complex systems. This is the first time the P L-edge XANES is applied quantitatively to solve such a complex problem.

4. Bond distances and coordination numbers obtained by analyzing the EXAFS region of the absorption spectra, indicated that the small changes in the bond distance, going from Ortho- to polyphosphates, cannot be easily detected by the EXAFS analysis.

3.2 Sulphur K- and L-edge spectra of model compounds

S K-edge and L-edge spectra of some model compounds are shown in Figure 3.2.1 and 3.2.2 respectively, and their peak positions are listed in Table 3.2.1. Similar to the P K-edge spectra, as the oxidation state of sulphur increases from -2 in TPCD (spectrum A) to +6 in sulphate (spectra E and F), peak *a* in the S K-edge spectra shifts by ~ 12 eV to the high energy side of the spectrum. Again it is noticed that the information from the S K-edge is not detailed enough to be used as fingerprint to analyze unknown samples with S in the same oxidation state.

Inspecting Table 3.2.1 and the L-edge spectra in Figure 3.2.2, a similar shift for the main peaks was observed. Because of better resolution, the S L-edge XANES spectra of the model compounds are more informative than the corresponding K-edge and

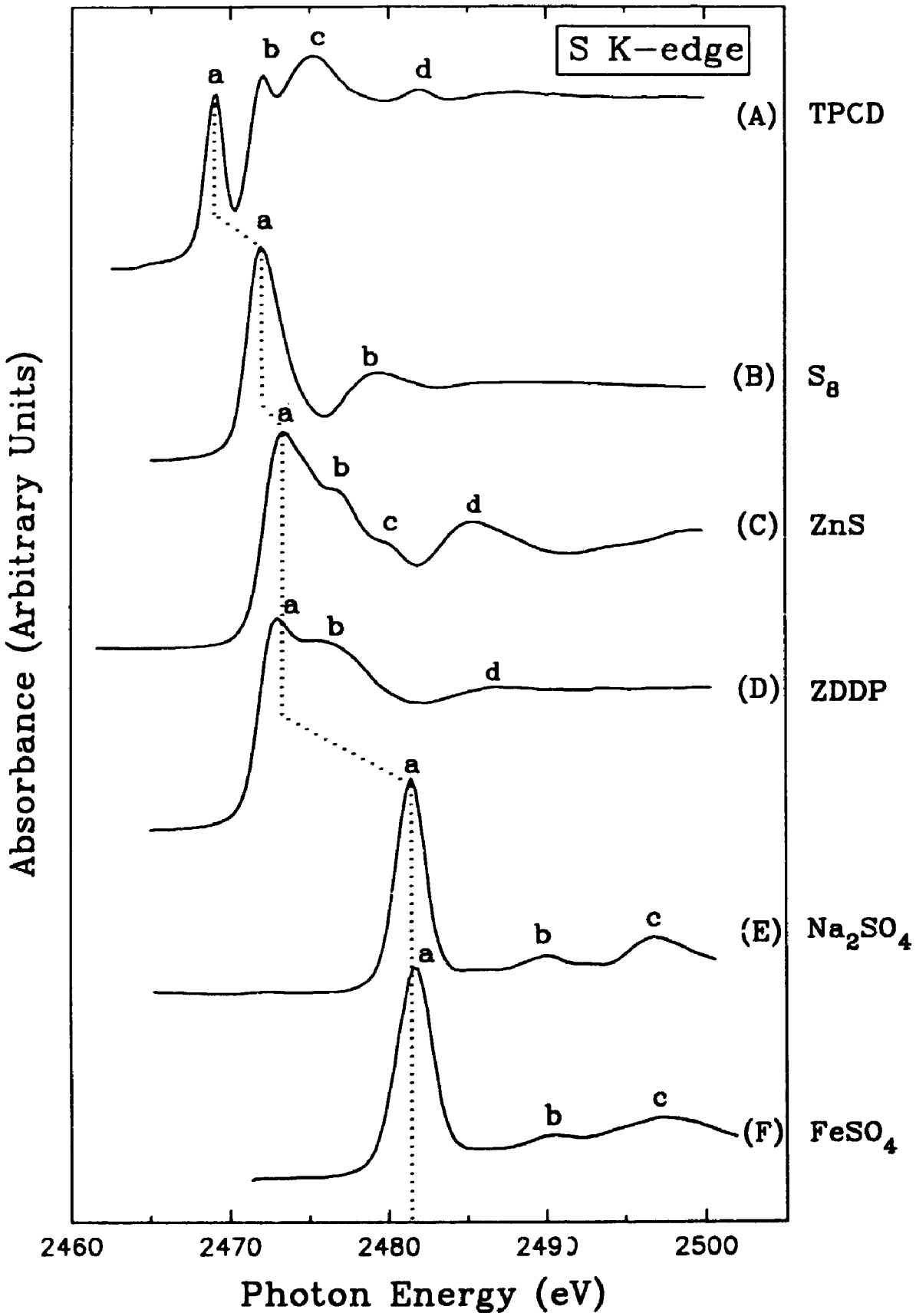

Figure 3.2.1 S K-edge XANES spectra of model compounds

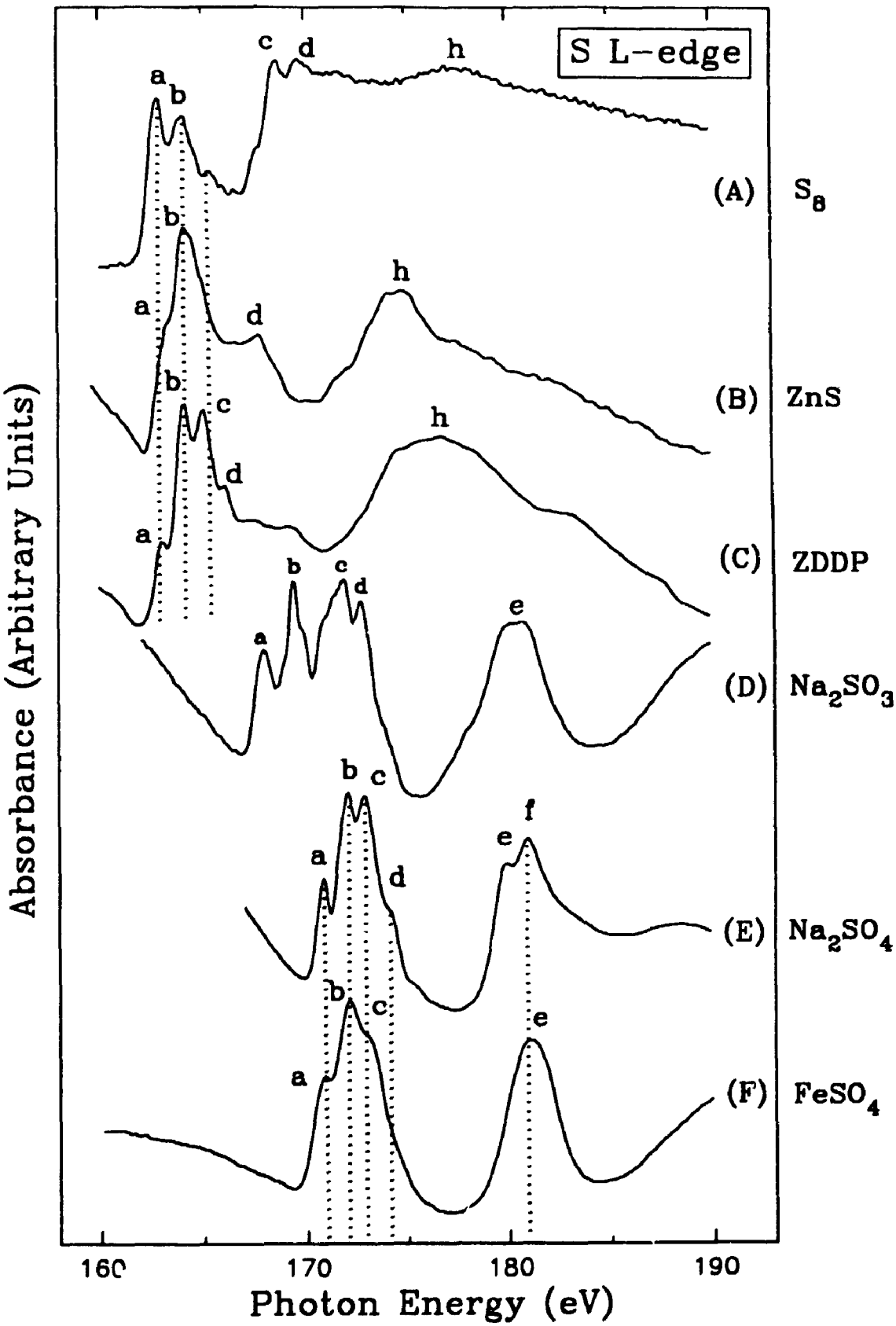

Figure 3.2.2 S L-edge XANES spectra of model compounds

Table 3.2.1 Peak positions of S K- and L-edge XANES spectra of some model compounds (± 0.1 eV)

Samples	K-edge				L-edge						
	a	b	c	d	a	b	c	d	e	f	h
TPCD	2469.0	2472.1	2475.2	2481.9							
Element sulfur	2472.0	2479.4	-	-	162.6	163.8	168.5	169.5	-	-	177.3
ZnS	2473.4	2476.8	2479.9	2485.3	163.3	164.1	-	167.7	-	-	174.9
ZDDP	2473.0	2475.6	-	2486.8	163.0	164.0	164.9	166.0	-	-	176.2
Na_2SO_3					168.0	169.5	171.9	172.8	180.3	-	-
Na_2SO_4	2481.3	2490.0	2496.8	-	170.8	172.0	172.9	174.2	179.9	181.0	-
$FeSO_4$	2481.7	2490.6	2497.4	-	170.9	172.1	173.1	-	181.1	-	-

better suited as reference spectra. For example, the strong shape resonance peak *e* plus other fine features in the sulphite (spectrum D) and sulphate spectra (E, F) are clear indications of the local symmetry and the oxidation state of sulphur. ZDDP (spectrum C) can be clearly distinguished from elemental sulphur (A), ZnS (B), sulphite (D) and sulphates (E and F). In addition, sodium and iron sulphates (E and F) give distinctive spectra. However, it should be pointed out that the very broad peak *h* in ZDDP, ZnS and element sulphur spectra has a different origin and should not be mistaken for peak *e* in sulphite and sulphate. This peak is most likely associated with multiple scattering features[5,6]. Thus S L-edge XANES will be used for fingerprinting the nature of sulphur forms in the films.

3.3 O K-edge spectra of model compounds

O K-edge spectra of some model compounds are depicted in Figure 3.3.1. The peak positions of these spectra are listed in Table 3.3.1. It is obvious that the general shape of iron oxide spectra (spectra A, B) is different from those of phosphates (spectra C, D, F-J) and ZDDP (E). The striking differences are the strong intensity of peak *a* and extra peak *d* compared to other compounds. Amongst the phosphate spectra, iron phosphate spectra are different. In spectra (C) and (D), peak *a* aligns very well with that of Fe_3O_4 (B). Thus peak *a* probably has the same origin as in the oxides and is related to Fe-O bonding. There is no noticeable difference between sodium pyrophosphate (spectrum I) and zinc pyrophosphate (G), which is similar to what is found in P L-edge spectra as discussed in section 3.1. In sodium phosphates, peak *b* is usually assigned to PO_4 tetrahedra. But in two linear sodium polyphosphate (I) and (J), an extra peak *c* indicates a new transition which can be related to the bridging oxygen[28,38]. The same phenomenon has been observed in XPS study for zinc polyphosphate glasses[39,40]. The energy separation between peak *b* and *c* is about 1.5 eV in XPS studies while it is 1.4 eV as listed in Table 3.3.1. It is noticed that peak *c* in NaH_2PO_4 (spectrum H), which should have a different origin from other phosphates because of the absence of bridging oxygen. It is probably due to the contribution from O-H bonding[41]. In a study of the O K-edge XANES spectra of 3d transition metal

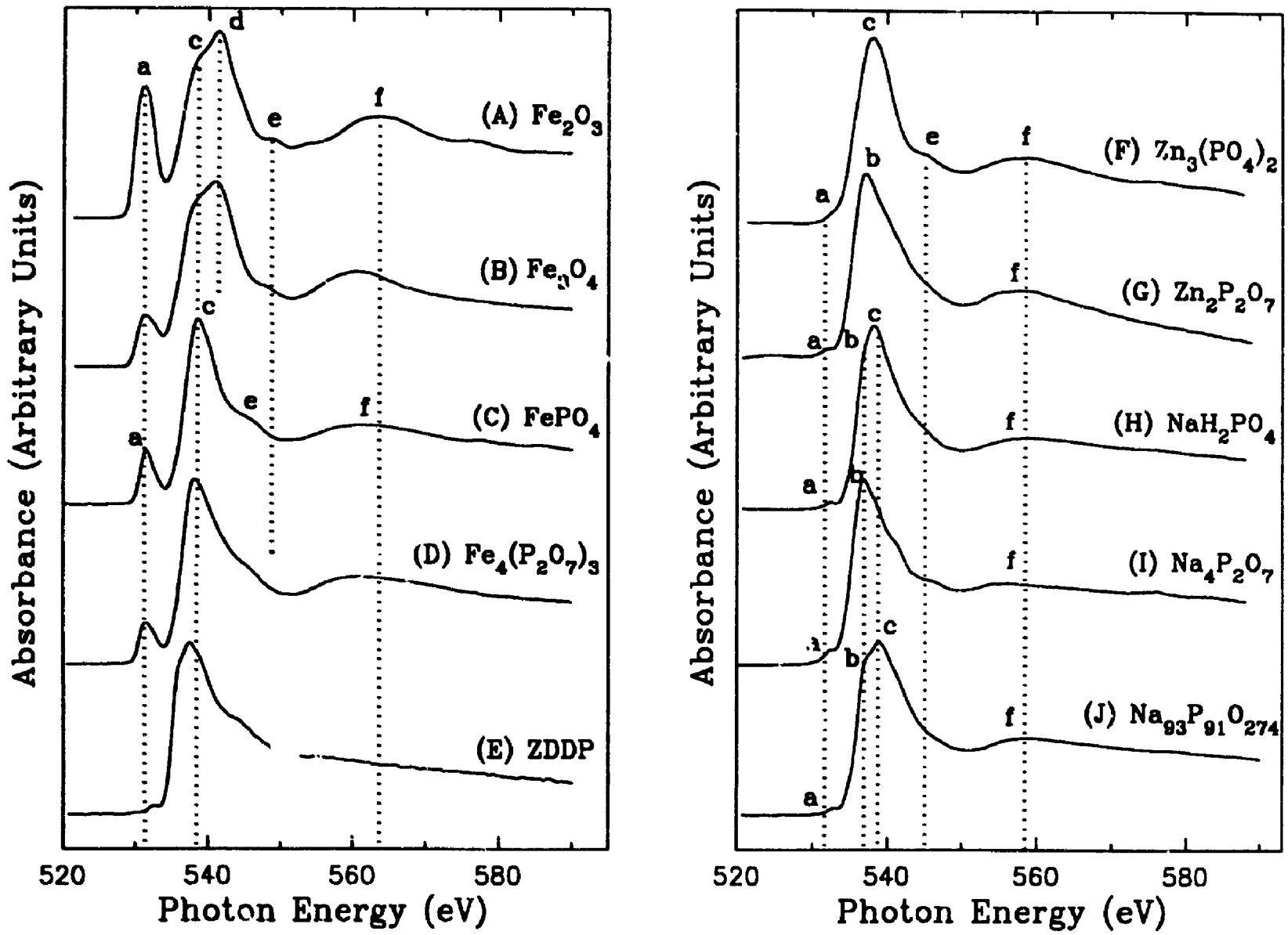

Figure 3.3.1) K-edge XANES spectra of model compounds

Table 3.3.1 Peak positions of O K-edge XANES spectra of model compounds (± 0.1 eV)

Samples	a	b	c	d	e
Fe_2O_3	531.2	538.8	541.3	548.7	562.5
Fe_3O_4	531.3	538.2	540.8	547.3	560.0
NaH_2PO_4	532.7	538.6	-	-	560.2
$Na_4P_2O_7$	532.8	537.4	-	541.5	557.0
$Na_{93}P_{91}O_{274}$	532.9	537.5	538.9	-	558.5
$FePO_4$	531.7	538.6	-	545.2	560.5
$Fe_4(P_2O_7)_3$	531.5	538.2	-	545.3	560.2
$Zn_3(PO_4)_2$	-	538.7	-	545.9	559.0
$Zn_2P_2O_7$	-	537.8	-	-	559.5
Isobutyl ZDDP	532.7	537.5	-	-	-

oxides[42], Grunes and coworkers assigned peak *a* to the O 1s electron transition to the $3e_g$ (Fe 3d + O 2pσ) orbitals of iron oxide. And peak d, which is absent in all phosphates, was assigned to the O 1s electron transition to the 3 a_{1g} (Fe 4s + O 2pσ) orbital. Since peak *a* has also been found in phosphates, the main contribution of the $3e_g$ orbital may come from Fe 3d orbitals.

3.4 Fe L-edge spectra of model compounds

Figure 3.4.1 shows Fe L-edge spectra of some model compounds, and Table 3.4.1 lists the peak positions of the spectra. Both peaks a and b shifted from Fe (0) to Fe (III) about +1.7 eV. The reason is that when Fe oxidation state increases, the valence electron density decreases. Thus the inner-shell electrons (such as the Fe 2p electrons) are less screened which results in them being more tightly bound and thus having a higher chemical shift. Peak *a* is similar to the assignment of that for O K-edge. It is related to the excitation of Fe 2p electron to the $3e_g$ orbitals. And peak *b* is the spin-orbital counterpart of peak *a*. The energy separation of these two peaks is about 13 eV. The chemical sensitivity of these spectra is poor. Thus, the spectra of Fe_2O_3, $FePO_4$ and $Fe_4(P_2O_7)_3$ are not noticeably different. As a result, Fe L-edge spectra of the antiwear films are not reported in the AW film analysis.

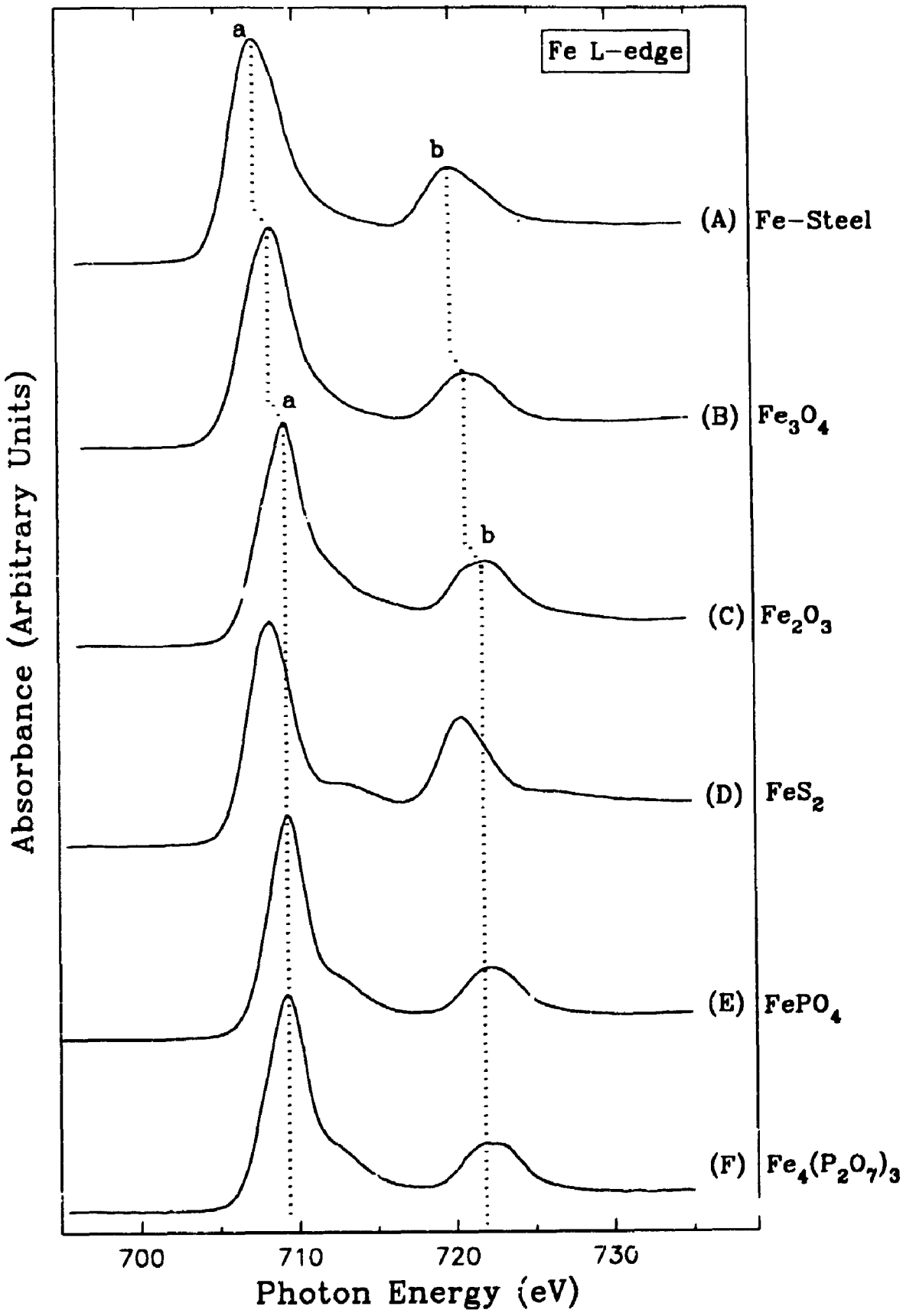

Figure 3.4.1 Fe L-edge XANES spectra of model compounds

Table 3.4.1 Peak positions of Fe L-edge XANES spectra of model compounds (± 0.1 eV)

Samples	a	b
Fe (steel)	707.5	720.0
Fe_3O_4	708.4	720.1
Fe_2O_3	709.2	721.8
FeS_2	708.2	720.5
$FePO_4$	709.3	722.3
$Fe_4(P_2O_7)_3$	709.3	722.2

3.5 References

1. Kasrai, M., Brown, J.R., Bancroft, G.M., Tan, K.H., Chen, J.M. *Fuel*, 1990, 69, 411

2. Brown, J.R., Kasrai, M., Bancroft, G.M., Tan, K.H., Chen, J.M. *Fuel* 1992, 71, 649

3. Chen, J.G., Fischer, D.A., Hardenbergh, J.H., Hall, R.B. *Surface Science*, 1992, 279, 13

4. Chen, J.G., De Vries, B.D., Lewandowski, J.T., Hall, R.B. Catalysis Lett., 1994, 23, 25

5. Kasrai, M., Fleet, M.E., Bancroft, G.M., Tan, K.H., Chen, J.M. *Phys. Rev. B*, 1991, 43, 1763.

6. Bodeur, S., Nenner I., Millie, P. *Phys. Rev. A*, 1986, 34, 2986

7. Lindberg, B.J., Hamrin, K., Johansson, G., Gelius, U., Fahlman, A., Nordling, C. Siegbahn. K. *Physica Scripta*, 1970, 1, 286

8. Sutherland, D.G.J., Kasrai, M., Bancroft, G.M., Liu, Z.F., Tan, K.H., *Phys. Rev. B*, 1993, 48, 14989

9. Ferrett, T.A., Piancastelli, M.N., Lindle, D.W., Heimann, P.A., Shirley, D.A. *Phys. Rev. A*, 1988, 38, 701

10. Cavell, R.G., Tan, K.H. *Chem. Phys. Lett.*, 1992, 197, 161

11. Tse, J.S., Liu, Z.F., Bozek J.D., Bancroft, G.M. *Phys. Rev.* A, 1989, 34, 2986

12. Bozek, J.D., Bancroft G.M., Tan, K.H. *Chem. Phys.*, 1990, 145, 131

13. (a)Schwarz W.H.E., and Buenker, R.J. *Chem. Phys.*, 1976, 13, 153 (b) Schwarz, W.H.E. *ibid*, 1975, 11, 217

14. Hansen, P.L., Brydson R., McComb, D.W. *Microsc. Microanal. Microstruct.*, 1992, 3, 213

15. Dehmer, J.L. *J. Chem. Phys.* 1972, 56, 4496

16. Yin, Z., Kasrai, M., Bancroft, G.M., Laycock K.F., Tan, K.H. *Tribol. Int.*, 1993, 26, 383

17. Yin, Z., Kasrai, M., Bancroft, G.M., Tan, K.H., Feng, X. *Phys. Rev. B*, 1995, 51, 742

18. Griffith, E.J., *J. Am. Chem. Soc.*, 1957, 79, 509

19. Van Wazer, J.R., Holst, K.A. *J. Am. Chem. Soc.*, 1950, 72, 639

20. Strauss, U.P., Smith E.H., Wineman, P.L. *J. Am. Chem. Soc.*, 1953, 75, 3935

21. Pfanstiel, R., Iler, R.K. *ibid*, 1952, 74, 6062

22. Strauss, U.P., Treitler, T.L. *ibid*, 1955, 77, 1473

23. Strauss, U.P., Treitler, T.L. *ibid*, 1956, 78, 3553

24. Van Wazer, J.R.. *Phosphorus and Its Compounds, Vol. 1: Chemistry*, (Interscience Publishers, New York, 1958) p. 439

25. Van Wazer, J.R. *J. Am. Chem. Soc.*, 1950, 72, 644

26. Gutsov, I., in *The Structure of Glasses*, Vol. 7, Ed., E.A. Po.ai-Kishits, (Co.:sultants Bureau, New York, 1966) p.154

27. Huffman, G.P., Mitra, S., Huggins, F.E., Shah, N., Vaidya, S., Lu, F. *Energy & Fuel*, 1991, 5, 574

28. Stöhr, J. *NEXAFS spectroscopy*, Spinger Series in Surface Science (Springer-Verlag, New York, 1992), Vol. 25

29. Gresch, R., Müller-Warmuth, W., Dutz, H. *J. Non-crystalline Solids*, 1979, 34, 127

30. Fluck, E., Weber, D. *Pure and Applied Chem.*, 1975, 44, 373

31. Lytle, F.W., Sayers D.E., Stern, E.A. *Phys. Rev. B.*, 1975, 11, 4825

32. Lee, P.A., Citrin, P.H., Eisenberger, P., Kinkaid, B.M. *Rev. Mod. Phys.*, 1981, 53, 769

33. Tyliszczak, T. (McMaster University), BAN program, Unpublished

34. Rehr, J.J., de Leon, J., Zabinsky, S.I., Albers, R.C. *J. Am. Chem. Soc.*, 1991, 113, 5135

35. McKale, A.G., Veal, B.W., Paulikas, A.P., Chan, S.-K., Knapp, G.S. *J. Am. Chem. Soc.*, 1988, 110, 3763

36. Frazer, B.C., Pepinsky, R. *Acta Crystal.*, 1953, 6, 273

37. Cruickshank, D.W.J. *Acta Crystal.*, 1964, 17, 6672

38. Brückner, R., Chun, H., -U., Goretzki, H., Sammet, M. *J. Non-Cryst. Solids*, 1980, 42, 49

39. Onyiriuka, E.C. *J. Non-Crystl. Solids*, 1993, 163, 268

40. Kasrai, M., Fuller, M., Scaini, M., Yin, Z., Brunner, R.W., Bancroft, G.M., Fleet, M.E., Fyfe, K., Tan, K.H. *Proceedings of Leeds Tribology Symposium*, 1994

41. McIntyre, N.S., Zetaruk, D.G., Analytical. Chem., 1977, 49, 1521

42. Grunes, L.A., Leapman, R.D., Wilker, C.N . Hoffmann, R., Kunz, A.B. Phys. Rev. B, 1982, 25, 7157

CHAPTER 4

THE EFFECTS OF PHYSICAL PARAMETERS ON ANTIWEAR FILMS

4.1 Introduction

In this chapter, the parameters related to the physical environment will be discussed. It has been found that the AW performance of ZDDPs and the chemical nature of AW films depend on several physical parameters such as rubbing time, concentration of ZDDP, temperature, load, surface roughness, etc. Some of the physical parameters have been investigated previously by other investigators. The kinetic properties of ZDDP have been studied by Paddy et al[1]. They found that S and P species on the surface changed with time. Other researchers[2,3,4] have reported from adsorption tests that the film became thicker with time, which implied that the film accumulated on the metal surface. In a wear experiment, Habeeb and Stover[5] showed that the wear rate increased in the first 20 hours then leveled off. Similar results have been found by So and Lin[6]. Palacios' investigation[7] has shown that both the film thickness and friction coefficient increases with rubbing time and then levels off.

Plaza[8] studied the adsorption of ZDDP on iron and iron oxide powder and found that adsorption of ZDDP increased with increasing ZDDP concentration. Studies by Willermet and coworkers[9,10] have shown that antiwear performance of ZDDP depends on the ZDDP concentration. Coy and Jones[11] found that the rate of decomposition of a given ZDDP increased with increasing concentration. Bovington and Dacre[12,13] reported that the surface coverage by the additive increased with increasing concentration.

Thermal decomposition has been accepted as the main mechanism of AW film formation. As a result, the temperature effect has been investigated extensively. Dickert and Rowe[14] reported from their adsorption experiments that ZDDP started to decompose below 150 ^{0}C and the decomposition rate of IP-ZDDP increased with temperature. Similar results have been reported by other researchers[2,11,12]. Palacios[15] has concluded that the film thickness and AW performance are affected by temperature. The higher the

temperature, the thicker the film formed and the worse the AW performance. Several groups[16,17] have came to a similar conclusion. Furthermore, some investigators[2,18,19,20,21,22] found that the ratio of Zn:S:P in the surface films, varied with temperature.

The effect of load has been studied by Palacios[7]. He found that the surface film thickness increased with load up to 600 N and then decreased. He also reported that surface composition changed with increasing load. When the load increased, the concentration of S was increased and that of P was decreased. Glaeser and partners[23] came to a similar conclusion from their in *situ* wear experiments in combination with scanning Auger spectroscopy. They also concluded that the surface composition was altered with increasing load. From a wear test made by Rounds[24], the wear rate was found to be proportional to the load. Similar results have been reported by Jahanmir[20] and Sheasby et al[17]. They found that both wear scar width and friction coefficient increased with increasing load.

Effects of other parameters have been reported by other groups. So and coworkers[6,25] reported the effects of roughness and sliding speed on the film formation. The rougher surface required a longer time to form a protective film. At higher sliding speed, the film forms quicker. Sheasby[17] reported that the wear scar width increased with increasing rubbing speed.

4.2 Results and discussions

In this thesis, the effect of rubbing time, ZDDP concentration, temperature, load and surface roughness have been investigated separately while keeping all the other variables constant.

4.2.1 Effects of rubbing time

4.2.1.1 P L-edge XANES spectra

Films were generated from commercial ZDDP-1 (mostly s-butyl) at rubbing times of 5 minutes, 30 minutes, 6 hours and 12 hours. Also a film was made in two stages: The film which was generated in 30 minutes was further rubbed in base oil (in the absence of any additive) for 5.5 hours. Figure 4.2.1 shows the P L-edge spectra of these

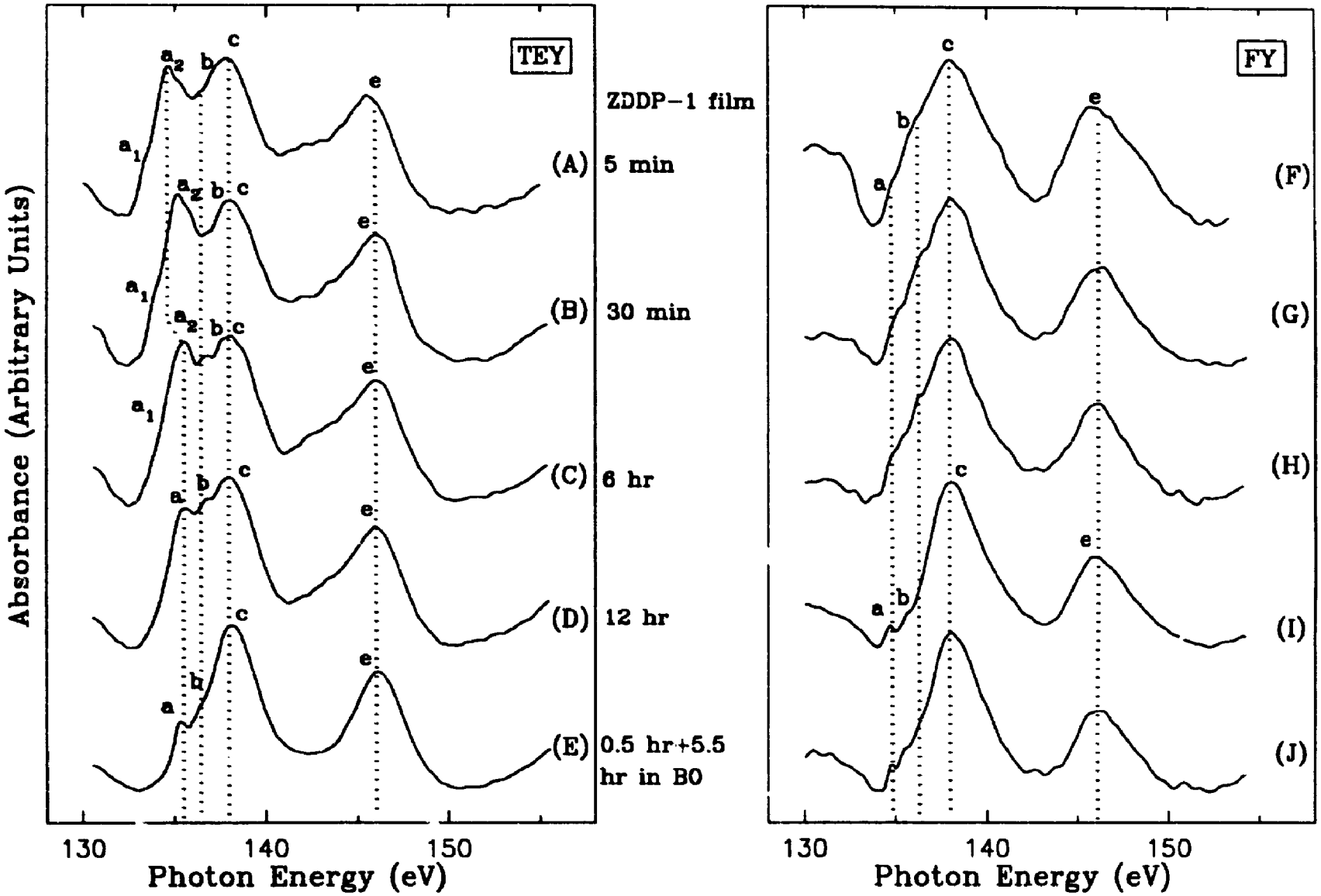

Figure 4.2.1 P L-edge XANES spectra of ZDDP-1 films generated in diff ent rubbing times measured by TEY mode (left) and FY mode (right)

films measured in total electron yield (TEY) mode (left) and fluorescence yield (FY) mode (right). The peak positions of these spectra are listed in Table 4.2.1. The TEY spectra (left) will be considered first.

Comparing (A), (B), (C) and (D) in Figure 4.2.1, it is noticed that when the rubbing time was increased from 5 minutes to 12 hours, a stronger peak a_2 accompanied by a shoulder a_1, gradually vanishes and is replaced by peak a. The relative intensity of peak a_2 is similar in the 5 minute film (spectrum A) and the 30 minute film (spectrum B), but it is reduced and is shifted to higher energy in the 6 hour film (spectrum C). However, peak positions and relative intensities of peaks c and e in all the spectra remain the same and are similar to model polyphosphates in section 3.1. This observation suggests that since only phosphates exhibit peaks c and e films made at a shorter time than 12 hours may have components other than phosphates. For example it was shown in Chapter 3 that pure ZDDP does not exhibit peak e.

From Table 4.2.1 the peak positions of peaks a_1 and a_2 are very close to peaks a and b in those of ZDDP (Table 3.1.1). In order to examine the possibility of ZDDP being an impurity in these films, synthetic spectra were generated[26]. Assuming spectrum (D) represents a "pure" polyphosphate film, the spectrum of ZDDP was digitally combined with this spectrum to construct a synthetic spectrum. Then the resultant spectrum was compared with that of the film. The proportion of the spectrum of each component was varied until a close fit between the synthetic spectrum and the actual film spectrum was achieved. The synthetic spectra are compared with the experimental spectra in Figure 4.2.2. Spectrum (A) (solid line) is produced by removing 5% of the ZDDP spectrum from the spectrum of film generated in 12 hours (dashed line). It is found that removing $\sim \pm 5\%$, dose not have much effect on the features of the spectrum. In spectra (B)-(E) the proportion of ZDDP is increased from 10% to 35% and the resultant spectra are compared with spectrum (B) in Figure 4.2.1. It is very clear that synthetic spectrum (E in Figure 4.2.2) matches the experimental spectrum (B in Figure 4.2.1). These findings strongly suggest that the major impurity in the film comes from unreacted ZDDP. In the same manner the amount of ZDDP in the film made in 6 hours (C in Figure 4.2.1) was found to be 25%. Films (A) and (B) in Figure 4.2.1 both had about 35% ZDDP content.

Table 4.2.1 P L-edge spectral positions of AW films formed in different rubbing times (± 0.1 eV)

ZDDP-1 Films	a_1	a_2	a	b	c	e
TEY:						
5 min.	133.5	134.7	-	136.4	137.9	145.5
30 min.	133.8	135.2	-	136.7	138.0	146.0
6 hr.	134.0	135.5	-	136.7	138.0	146.0
12 hr.	-	-	135.6	136.7	138.0	146.0
30 min.+ 5.5 hr. in base oil	-	-	135.4	136.4	138.2	146.1
FY:						
5 min.			134.8	135.8	138.0	146.0
30 min.			135.1	136.4	138.0	146.1
6 hr.			134.9	136.2	138.1	146.0
12 hr.			134.8	135.6	138.1	146.1
30 min.+ 5.5 hr. in base oil			134.7	135.7	138.0	146.1

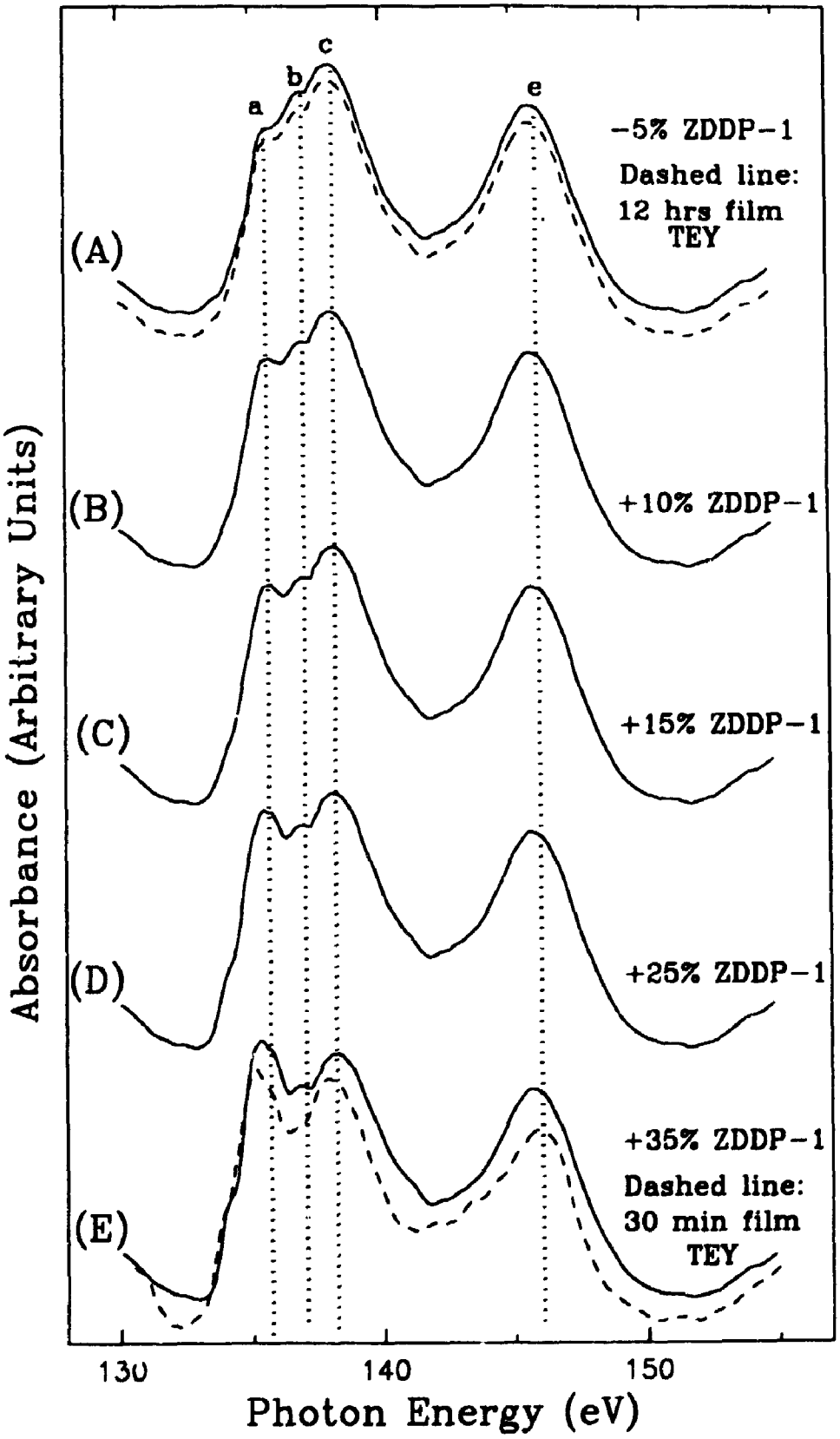

Figure 4.2.2 Digitally composed P L-edge XANES spectra with different concentrations of ZDDP

Spectrum (E) in Figure 4.2.1 was made in two stages. As is noticed, the spectrum is quite different from other spectra in the figure. The total rubbing time of this sample (0.5 + 5.5 = 6 h) was the same as that of (C), but peaks a_1 and a_2 are not observed for this film. Using the intensity calibration curve (Figure 3.1.10), the phosphate chain length corresponding to this film was found to be about 8 ± 1. Comparing spectra (E) with (D), it is noticed that the intensities of peaks *a* and *b* are much stronger in (D) and thus the chain length must be longer. Using the calibration curve it is found that the ratio of peaks *a/c* is greater than what is expected for any linear polyphosphate studied. It corresponds closely to the metaphosphate which has a cyclic structure (Chapter 3). It should be pointed out that attempts were made to generate the synthetic spectrum corresponding to spectrum (D) using spectrum (E) and the ZDDP spectrum, with no success. The fine structures could not be reproduced. Thus it was concluded that the higher intensity of peak *a* in spectrum (D) is indeed due to higher polyphosphate chain length and not to a ZDDP impurity.

On the right of Figure 4.2.1 are the spectra recorded in fluorescence yield (FY) mode. In contrast to TEY detection which probe ~ 50 Å depth of the film, FY detection mode probes >500 Å in the P and S L-edge region. This is the only non-destructive method one can apply to obtain information about the chemical species on the surface and in the bulk of the film. The details of the two techniques have been described in Chapter 2. It was shown that absorption spectra measured for the model polyphosphates in TEY and FY modes were very similar indicating that surface and bulk species are the same in those model compounds. Thus any differences observed here must be related to the differences between the chemistry of polyphosphate on the surface and in the bulk, and not due to the detection modes.

Examining spectra (F)-(H), it is immediately clear that the intensities of peaks *a* and *b* in the FY spectra are much weaker than the corresponding TEY spectra (A-C). This suggests that the polyphosphate chain length is much shorter in the bulk than on the surface. But the broad shoulder at low energy indicates that the spectra still contains some signals from ZDDP, long chain polyphosphate and possibly from partially decomposed ZDDP. These signals most likely come from the top section of the film. Alternatively ZDDP can be trapped in the wear tracks in the first few second of rubbing

when the wear rate is high. The ZDDP trapped in these regions are decomposed with further rubbing as was seen in the TEY measurements.

Spectra (I) and (J) in Figure 4.2.1 are very interesting. These two spectra in all aspects are very similar and consist of short chain polyphosphates. In order to better understand them, they are compared with Zn and Fe phosphates spectra in Figure 4.2.3. The resemblance of the spectra of the films with zinc and iron ortho or pyrophosphate is remarkable. However, careful examination indicates that the spectral pattern of the 12 h film is closer to iron phosphate (spectrum B) in Figure 4.2.3, and the two-stage film closely corresponds to iron pyrophosphate (spectrum E). The presence of peak *c'* in spectrum (A) is not clearly noticed in the film spectra. However, peak *c* of the film spectra is generally broader than those of iron phosphate. On the other hand, peaks *a* and *b* shift to lower energy position. This suggests that there is probably a mixture of zinc and iron phosphates. The assignment for the cations here is tentative as the differences between the spectra of different metal phosphates is marginal. The presence of iron phosphate in films has been shown using Fe and Zn K-edge absorption spectroscopy[27]. Willermet et al.[9] also found that in overbased additives, Zn could be replaced by Ca from calcium sulphonate detergent. The overall conclusion of the findings here is that film generated from the commercial s-butyl ZDDP is composed of polyphosphates on the surface and short chain polyphosphates, probably iron and zinc phosphate, in the bulk.

4.2.1.2 S L-edge XANES spectra

It was found that the sulphur signal of the films in most cases was much weaker than the phosphorus signal, indicating that film is depleted in sulphur. Sulphur most likely is replaced by oxygen. This has been reported by other researchers[9,28] and will be discussed in Chapter 5. Since FY for low Z element is very much weaker than TEY, absorption measurements in FY for S L-edge XANES were very noisy. Therefore only TEY spectra are reported for S L-edge XANES.

Figure 4.2.4 shows the S L-edge XANES spectra of the films formed in different rubbing times along with spectra of three model compounds ZnS, $FeSO_4$ and ZDDP. The peak positions of these films and model compounds are listed in Table 4.2.2. The

PM-1 3½"x4" PHOTOGRAPHIC MICROCOPY TARGET
NBS 1010a ANSI/ISO #2 EQUIVALENT

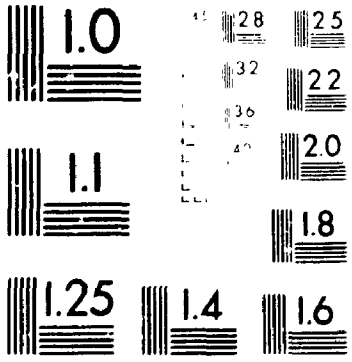

PRECISION[SM] RESOLUTION TARGETS

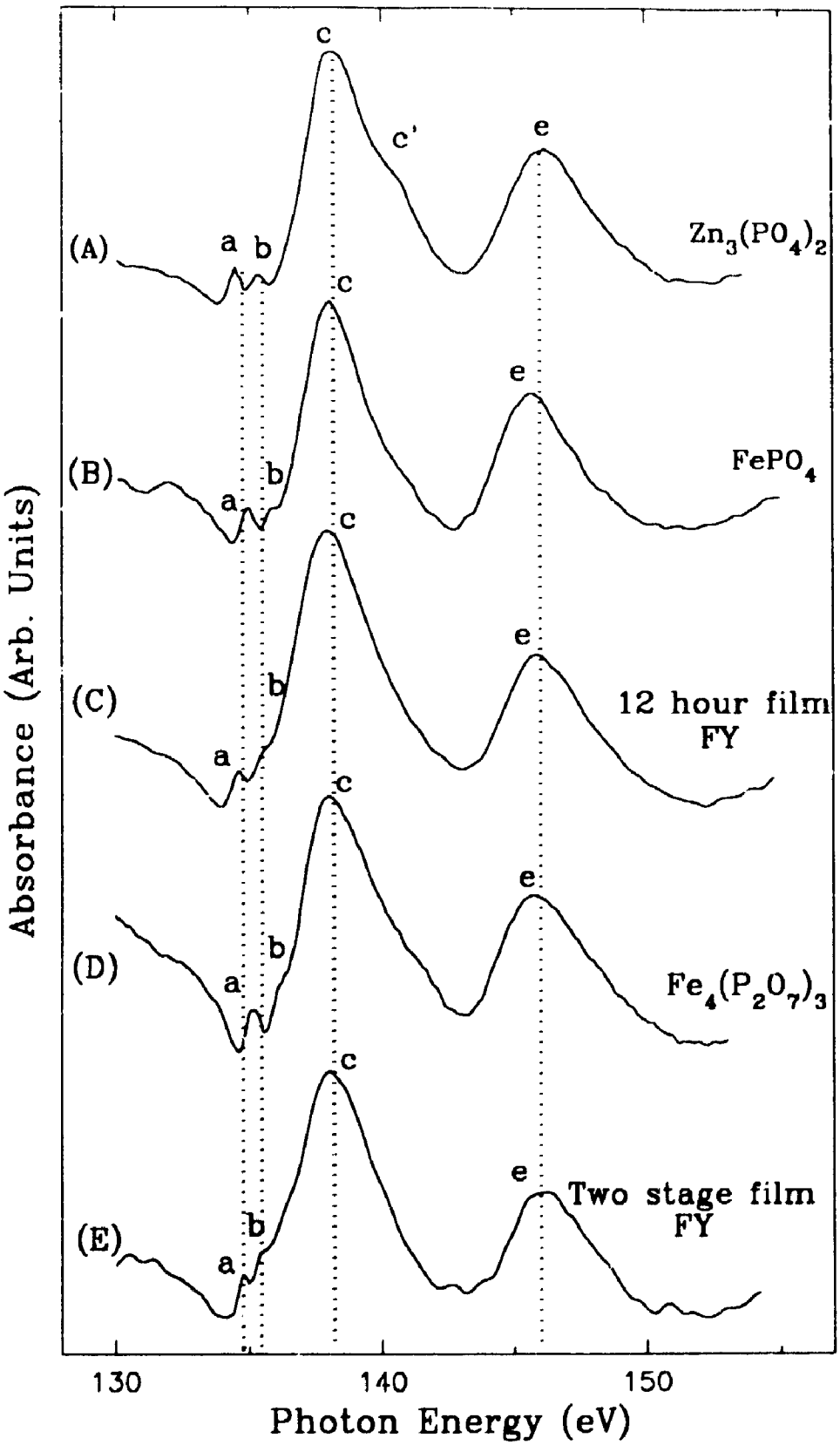

Figure 4.2.3 Comparison of antiwear films with model compounds

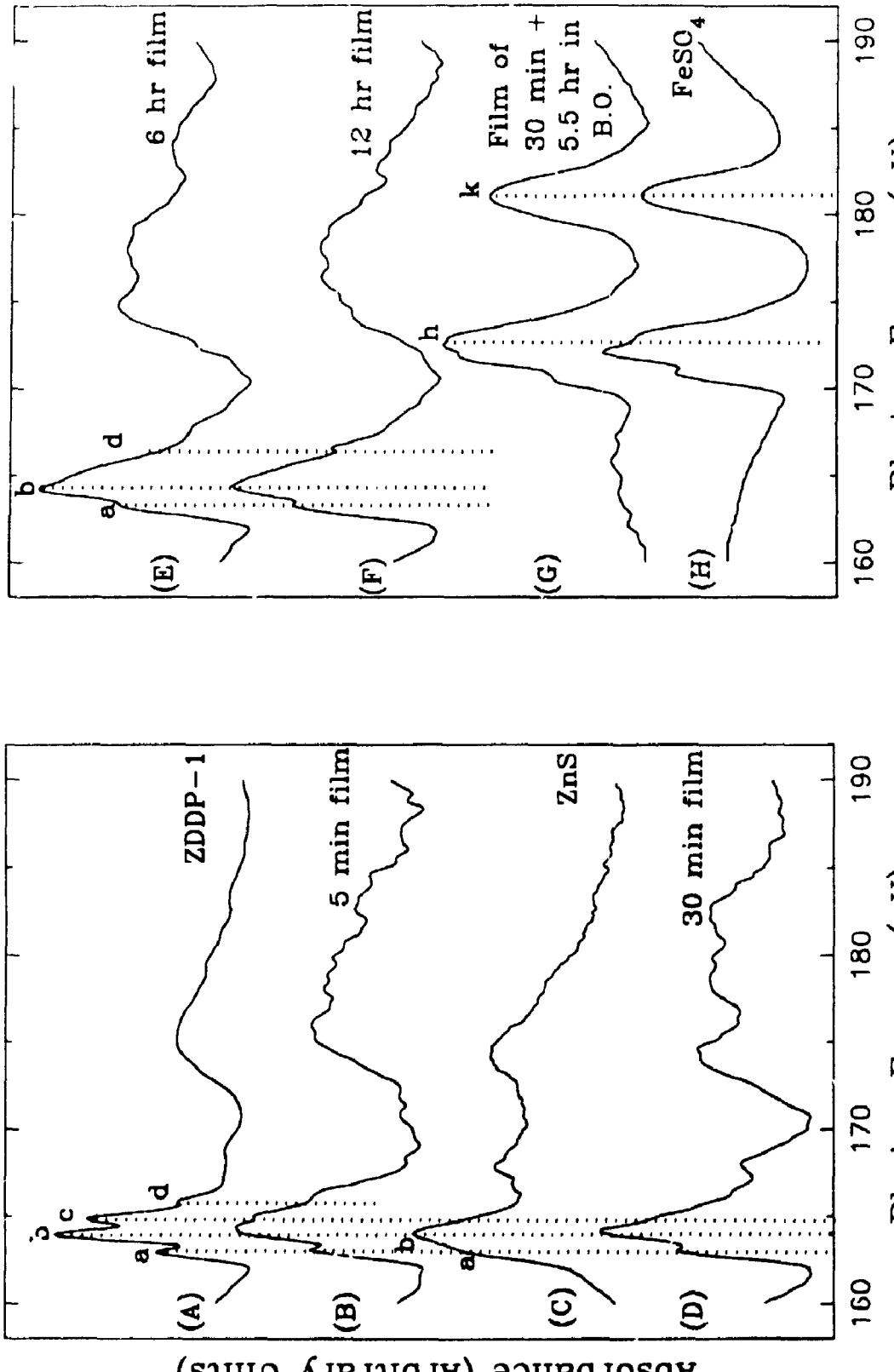

Figure 4.2.4 S L-edge XANES spectra of the films formed in different rubbing times compared with model compounds

Table 4.2.2 S L-edge spectral positions of AW films formed under different rubbing conditions (± 0.1 eV)

ZDDP-1 Films	a	b	c	d	h	k
Time:						
5 min.	163.0	164.1	164.8	165.9		
30 min.	163.0	164.1	164.9			
6 hr.	163.1	164.2	164.6	165.5		
12 hr.	163.2	164.2	164.8	165.8		
30 min.+ 5.5 hr. in base oil					172.5	181.0
Temperature:						
100 ^{0}C	163.0	164.1	164.9			
150 ^{0}C	163.5	164.3	165.3	166.1	175.0	180.6
200 ^{0}C	164.5	165.4			173.1	180.9
Low frequency:						
100 ^{0}C					172.5	180.0
200 ^{0}C		164.5			172.4	180.4

spectrum of ZDDP (A) shows four well resolved peaks *a*, *b*, *c* and *d* which can be used to trace the presence of unreacted ZDDP in the film. The spectrum of the 5 minute film (B) has the same features as ZDDP but the peaks are not as well resolved. This is a further proof for the existence of unreacted ZDDP in the film, as was shown in the P L-edge XANES spectra (Figure 4.2.1). For the 30 minute film (spectrum D) and the 6 hour film (spectrum E), peaks *a*, *b*, *c*, and *d* become less resolved and their features become similar to the spectrum of ZnS (spectrum C). However, the spectral features of the 12 hour film (spectrum F) indicate that other sulphur entities are contributing to the S spectrum. Alkyl sulphide have features similar to this spectrum[26].

Spectrum (G) corresponding to the two-stage film is quite different from the rest of the spectra. It has shifted to high energy and is very similar to the spectrum of $FeSO_4$ (spectrum H). This observation indicates that in the absence of ZDDP, the sulphur species has undergone oxidation to form sulphate. In thermally prepared films, it has been found that the base oil contains a certain amount of elemental sulphur that can be oxidized to sulphate (Chapter 6). Therefore, the sulphate formed on the metal surface is most likely from the base oil. It has been shown in the past that the relative intensity of peak *e* (Figure 4.2.1) in the P L-edge XANES is related to the kind of electronegative atoms (S or O) bonded to the P atom[29]. Thus, if sulphur was bonded to P in the film, a change would have been expected in the relative peak intensity of peak *e* in the TEY spectra going from (D) to (E), and in the FY spectra going from (I) to (J) (see Fig. 4.2.1). Since no change is observed, it is a good indication that S-P bonds in ZDDP are broken in the process of phosphate formation, and the presence of thiophosphates is unlikely.

In summary, ZDDP is first adsorbed on the surface and as rubbing proceeds, it decomposes to form the AW film. When most of the ZDDP is decomposed, the film contains long chain polyphosphates with Zn or Fe as cations. Before that, the film is composed of both polyphosphates and unreacted ZDDPs, which has also been suggested by other investigators[30]. After a long time rubbing, the AW film will get thicker to form two layers. On the top layer, there is a long chain polyphosphate and in the bulk there is a short chain phosphate. This layer structure of AW film has also been suggested by Bell et al[31]. S species in the film is mainly sulphide, but it can be oxidized to sulphate

if the system is short of zinc supply. The cation counterpart of sulphide is likely the Zn or an alkyl group, or a combination of both.

4.2.2 Effects of ZDDP concentration

The effects of concentration for film formation, using ZDDP-1 at four different concentrations, have been examined. It should be pointed out that the concentration used here is the weight of concentrated oil (~ 75 wt. % of ZDDP) in the final base oil solution. The P L-edge XANES spectra of films generated at the different concentrations are compared in Figure 4.2.5. The peak positions are listed in Table 4.2.3. It is quite obvious from the spectra that the intensity of peak a_2 increases with increasing ZDDP concentration. As was shown before, the intensity of this peak is partly attributable to the unreacted ZDDP. The highest intensity of peak a_2 is in spectrum (A) which corresponds to the highest concentration of ZDDP in the oil. In order to estimate the composition of film (A), a synthetic spectrum was constructed as shown in Figure 4.2.5 (dashed line). This spectrum was produced, combining 25% of the ZDDP spectrum, 60% of the 12 h film spectrum (spectrum D in Fig. 4.2.1) and 15% of spectrum (D) in Figure 4.2.5. In this combination, it is assumed that film contains ZDDP, long chain and short chain polyphosphates. As is obvious from Figure 4.2.5, the synthetic spectrum matches the experimental spectrum extremely well.

The ZDDP signal decreases significantly when the concentration of ZDDP is lowered from 2.0 wt.% to 0.25 wt.% (Figure 4.2.5). At 0.5 wt% concentration (spectrum C), the spectrum can be simply constructed using a combination of short and long chain polyphosphates, with the proportion of 80% and 20%, respectively. The results is shown in spectrum (C) of Figure 4.2.5 (dashed line). Spectrum (D) corresponds to the 0.25 wt.% film, which is similar to a short chain polyphosphate. Thus, it can be concluded that when ZDDP concentration is low only short chain polyphosphates are formed. But when the concentration is high, short and long chain polyphosphates as well as ZDDP constitute the film.

As mentioned in the introduction, the ZDDP concentration affects the thermal decomposition rate of the ZDDP and its AW performance. On the rubbing surface, the concentration of ZDDP has to be in a certain range in order to provide a sufficient

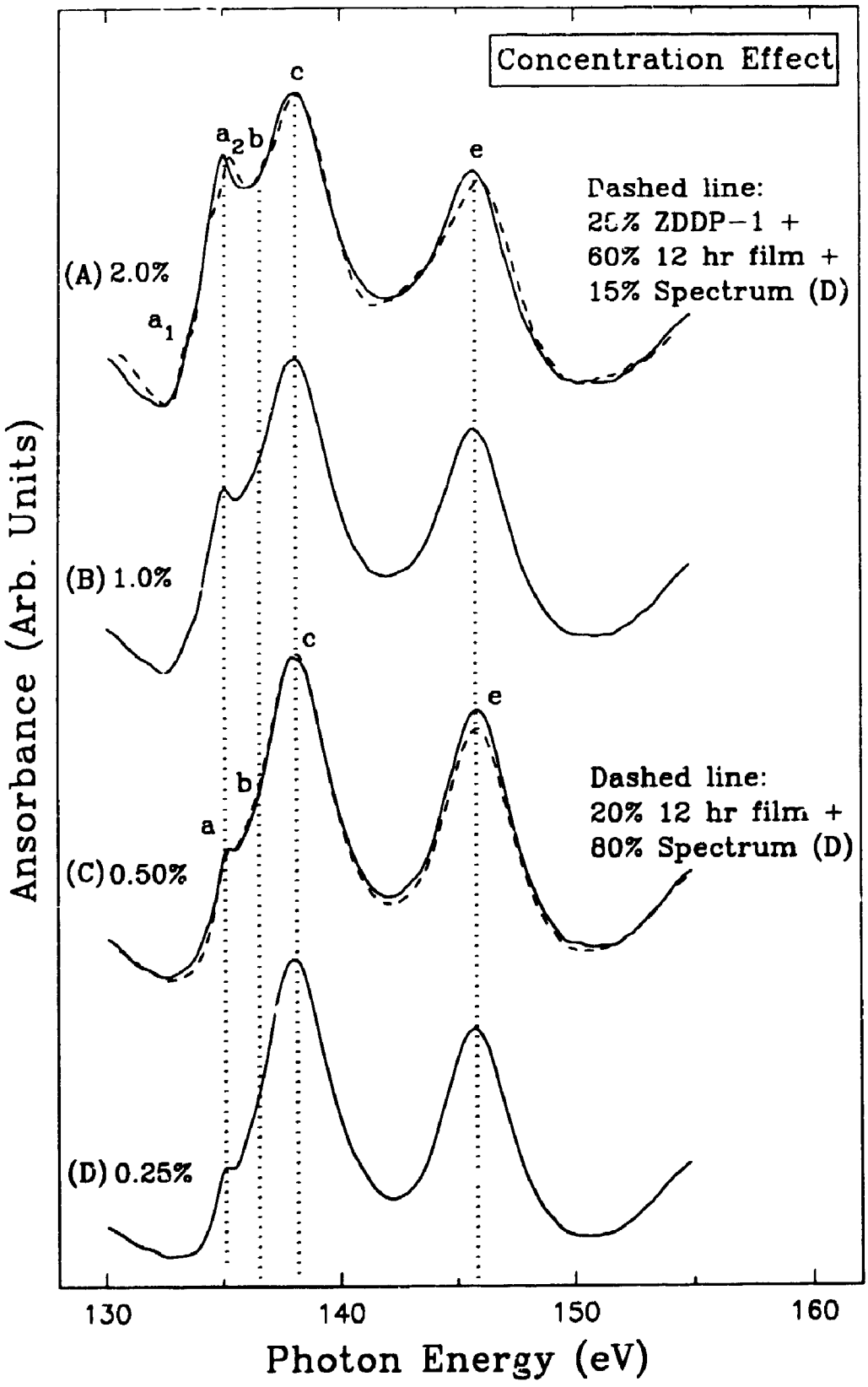

Figure 4.2.5 P L-edge spectra of the films formed in different ZDDP concentrations

Table 4.2.3 P L-edge spectral positions of AW films formed under different rubbing conditions (± 0.1 eV)

ZDDP-1 Films	a_1	a_2	a	b	c	e
Concentration:						
0.25 wt.%	-	-	135.2	-	138.0	145.8
0.50 wt.%	-	-	135.2	-	138.0	145.8
1.0 wt.%	-	-	135.1	136.2	138.1	145.8
2.0 wt.%	133.9	135.1	-	-	138.0	145.7
Temperature:						
100 °C	133.8	135.2	-	136.7	138.0	146.0
150 °C	-	-	135.7	136.9	138.2	146.0
200 °C	-	-	135.8	136.8	138.3	146.0
Low frequency (5 Hz):						
100 °C	134.9	-	-	-	138.1	144.8
200 °C	-	-	135.8	136.8	138.2	145.5
Load:						
40 N	135.4	-	-	-	138.6	145.9
220 N	133.8	135.2	-	136.7	138.0	146.0
400 N	-	-	135.8	136.9	138.3	146.0
Roughness:						
polished, 30 min.	-	-	135.8	136.8	138.1	145.8
Unpolished, 30 min.	-	135.6	-	137.0	138.3	145.8
polished, 6 hr.	-	-	135.8	136.8	138.1	145.8
Unpolished, 6 hr.	-	135.7	-	136.9	138.1	145.9

quantity of ZDDP to reach the saturated state. In commercial application, the concentration of ZDDP is usually ~ 1 wt.%, which has also been reported as optimum concentration for the AW regime[16]. When the concentration is low, the coverage of ZDDP or its decomposition products on metal surface is also low which affects the polymerization of phosphate. Other researches revealed that ZDDP concentration affects the AW performance. Willermet and Kandah's studies[9,10] showed a direct relationship between antiwear performance and ZDDP concentration. The wear on the steel surface monotonically decreased with increasing ZDDP concentration. They also suggested that the formation of polyphosphate was favoured as the concentration of ZDDP increased.

Chao et al.[16] reported that increasing the concentration of ZDDP tended to promote faster and thicker film formation. With increasing concentration, wear and friction decreased. Experimental results shown here are in good agreement with the above findings. At higher concentration, since the adsorption rate is higher, formation of long chain polyphosphate is promoted. But at lower concentration when the adsorption is less, only short chain polyphosphate is formed. Comparing their conclusion with results presented here, it seems that long chain polyphosphates provide better AW function than short chain phosphates.

However, there may be a drawback for increasing the ZDDP concentration. As was shown, the higher the concentration, the stronger the ZDDP signal, which is observed in the films; and the undecomposed ZDDP probably does not provide the AW properties. On the other hand, Willermet et al.[32] have found that at low concentration of ZDDP, the wear rate is even higher than using base oil alone. This finding is later supported by Plaza's studies[33] in which he found that the high wear rates at low ZDDP concentration were associated with corrosive wear.

4.2.3 Temperature effects

So far in this study, all the films have been generated in an oil bath at 100 °C. In order to study the temperature effect, films were generated at 150 °C and 200 °C, respectively. The P L-edge spectra of these films are compared with the film formed at 100 °C in Figure 4.2.6, and their peak positions are documented in Table 4.2.3. The first striking difference between the 100 °C film (spectrum A) and films made at high

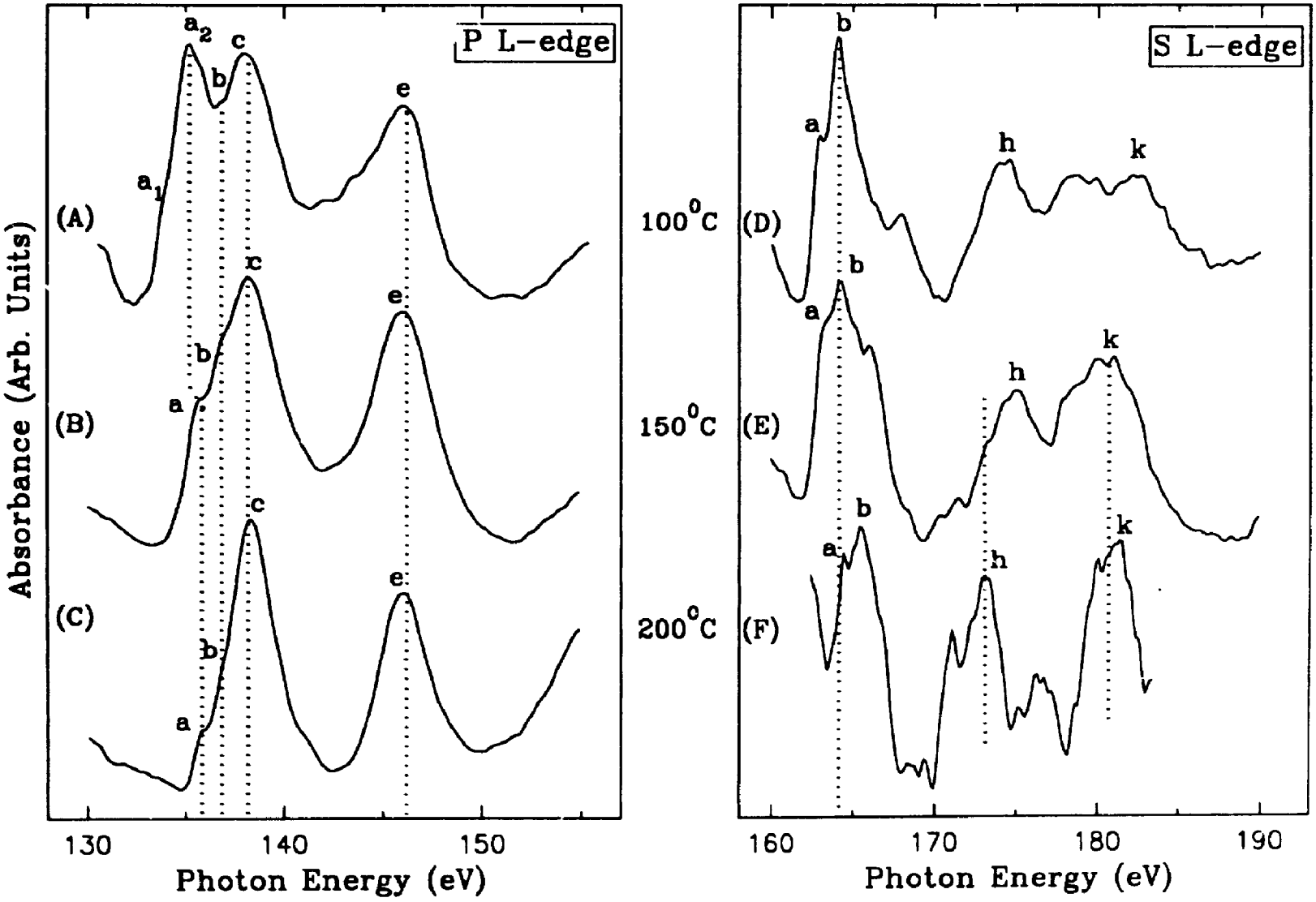

Figure 4.2.6 P and S L-edge spectra of the films formed at different temperatures

temperature (spectra B and C) is the absence of shoulder a_1 and peak a_2 in spectra (B) and (C). As discussed previously, peaks a_1 and a_2 originates from ZDDP. The absence of these features suggests that, as is expected, ZDDP decomposes much faster at higher temperature. Another difference is the relative intensities of peaks *a* and *b* in spectra (B) and (C). It is obvious that polyphosphate chain length in spectrum (B) is longer than that in spectrum (C), but shorter than in the 100 ^{0}C film. As was shown above, the spectrum of the 100 ^{0}C film could be simulated by digitally combining the spectra of 12 hour film (long chain phosphates or cyclic phosphates) and ZDDP (see Fig. 4.2.1).

On the right of Figure 4.2.6, the S L-edge spectra of films generated at different temperatures are shown. Spectrum (D), corresponding to the film formed at 100 ^{0}C, is similar to the spectrum of ZnS as shown in Figure 4.2.4. There is no clear sulphate signal present. When the temperature increases to 200 ^{0}C (spectrum F), apart from the sulphide signal (peaks *a* and *b*), peaks *h* and *k* become more prominent. The peak positions of *h* and *k* align well with those of $FeSO_4$ shown in Figure 4.2.4 (H). At intermediate temperature, 150 ^{0}C, the spectrum (E) is different from the 100 ^{0}C film (spectrum D) and 200 ^{0}C film (spectrum F). This spectrum seems to be a mixture of spectra (D) and (F).

Another sets of experiments were conducted at reduced frequency. Two films were generated with rubbing frequency of 5 Hz (usually 25 Hz) for one minute (usually 30 min.) at 100 ^{0}C and 200 ^{0}C, respectively. The P (left) and S (right) L-edge spectra of the films are demonstrated in Figure 4.2.7. The raw spectra indicate the relative intensities of P and S signals. Their peak positions are also listed in Table 4.2.3. At 100 ^{0}C (spectrum A), a poor signal/noise ratio indicates that the signal is very weak. Comparing it with spectrum (B) and other spectra, it implies that the film formed under this condition is very thin. The general shape of the P L-edge spectrum is similar to the spectrum of the 5 minutes (25 Hz) film (Figure 4.2.1 A). It contains signals from both ZDDP and polyphosphates. No adsorption could be detected by the XANES measurement at this temperature (Chapter 6). Therefore the formation of phosphates must be initiated by the rubbing process. The ZDDP dissolved in oil may be trapped on the surface by the initial rubbing which can undergo decomposition due to the rise of temperature initiated by the rubbing. The interesting finding is that in the S L-edge, only

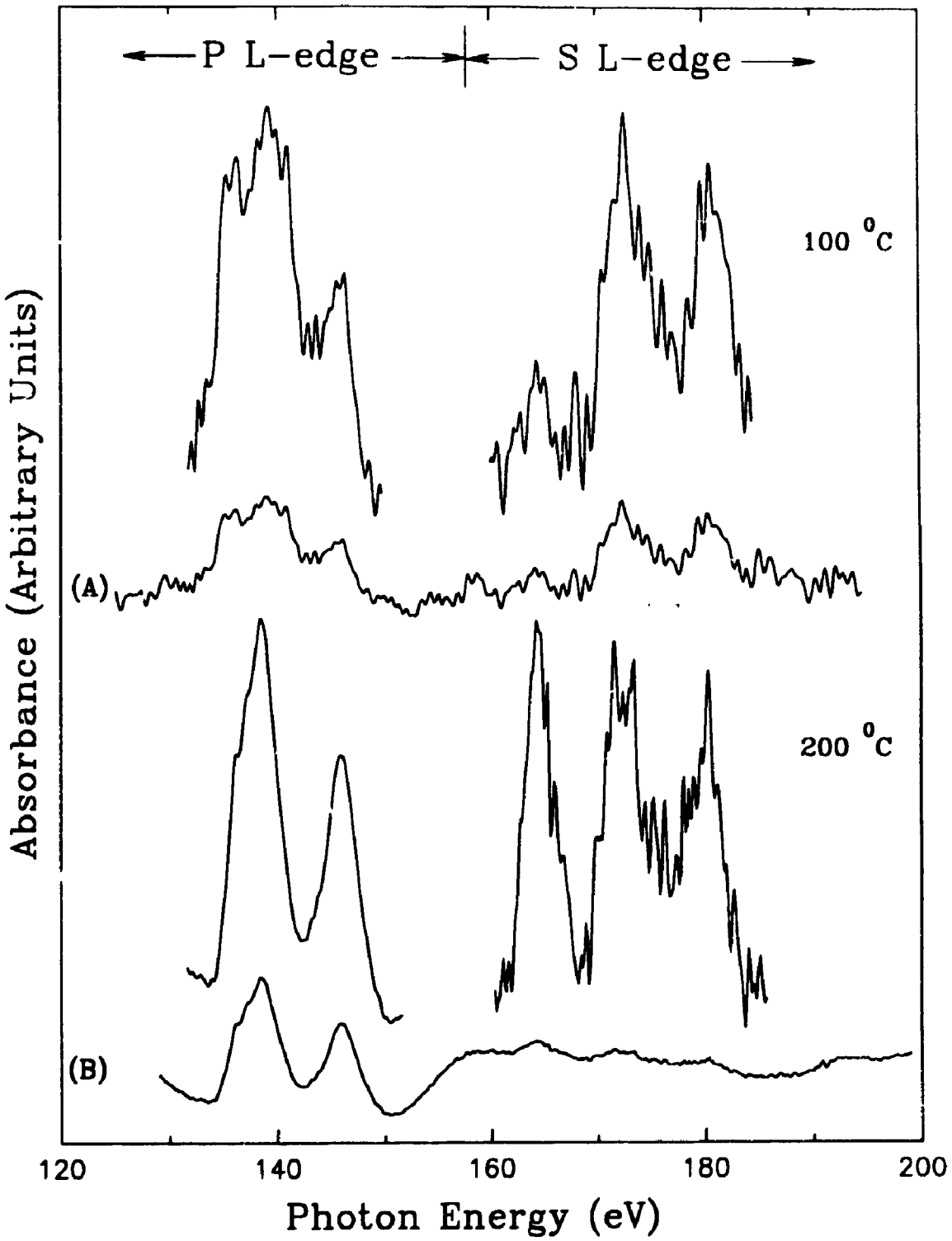

Figure 4.2.7 P and S L-edge spectra of the films formed in 1 minute and 5 Hz

the sulphate signal is detected instead of sulphide. It implies that S, which is likely from the base oil as discussed before, is oxidized to sulphate at initial stage of rubbing. After long time rubbing, sulphate may migrate to solution[19].

When the same experiment was carried at 200 ^{0}C, spectrum (B) in Figure 4.2.7, the P L-edge signal is much stronger. The high intensity of peaks *a* and *b* indicates the presence of a long chain polyphosphate. It is not surprising that no ZDDP signal can be detected because the ZDDP-1 is easily decomposed at this temperature. With more rubbing, the phosphate chain length may be reduced further as in the 30 minute film (spectrum C in Figure 4.2.6). As can be seen from Figure 4.2.7 (B), the S L-edge signal is much weaker than that of the P signal. But from the expanded scale it is clear that there are two species of S, sulphide and sulphate. A similar result has been found in longer rubbing time (such as 30 minutes, 25 Hz) films (spectrum F, Figure 4.2.6).

The O K-edge of the above films were measured in the PEY and FY mode. The results are shown in Figure 4.2.8. Spectra (A) and (B) correspond to PEY and FY of 200 ^{0}C films, respectively. In general, peaks *a*, *b* and *d* are similar to the Zn phosphate model compound as demonstrated in Chapter 3. It should be pointed out that peaks *e* and *f* originate from the Cr L-edge signal present in the steel substrate (see Chapter 2). Peaks *e* and *f* in PEY (A) are much weaker than those in FY (B) because the former provides the surface information ($<$ 10 Å) while the latter probes the bulk ($>$ 2000 Å). At 100 ^{0}C, the PEY spectrum (C) and FY spectrum (E) are similar to those of steel blank (spectra D and F). The relatively weaker peaks *e* and *f* in the films indicate the presence of a thin film formed on the substrate which is in agreement with P L-edge spectra (Figure 4.2.7). The oxygen signal in this film most likely originates from a mixture of iron oxide and iron polyphosphates.

It is generally agreed that thermal decomposition is one of the most important properties of ZDDP which constitute the main AW film formation mechanism. It has been accepted that the ZDDP decomposition rate is proportional to temperature. However, very high temperature may be detrimental to the AW effectiveness of ZDDP. Chao and coworkers[16] studied AW films formation at different temperature ranging from 20 ^{0}C to 200 ^{0}C. First, they found that the film thickness increased with increasing temperature, which is in agreement with Palacios' investigation[15]. But they found that

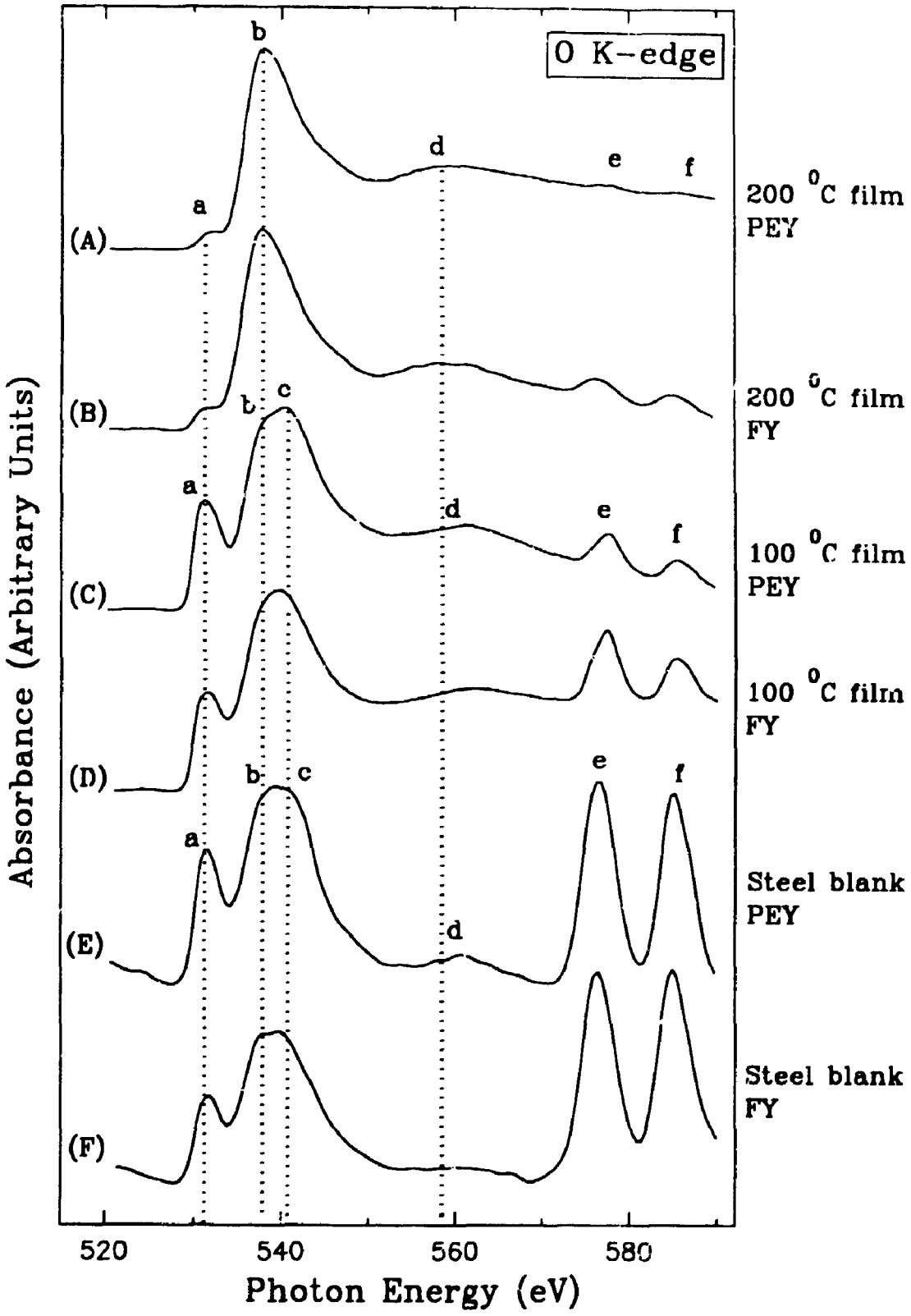

Figure 4.2.8 O K-edge spectra of the films formed in 1 minute and 5 Hz

the thick film formed at high temperature provided worse AW performance than the thin film formed at lower temperature. Second, they reported that the films formed at higher temperature are less durable than those formed at room temperature. This is probably due to either the reduced mechanical strength or structure changes of the thick film.

In general, results of this study are in agreement with Chao et al.'s studies. As shown above, high temperature helps to decompose ZDDP and establish the AW film. At lower temperature (100 ^{0}C, 150 ^{0}C), long chain phosphates are formed in the film, although there is signal due to the unreacted ZDDP in the 100 ^{0}C film. It was proposed before that long chain polyphosphate might provide better AW performance. At 200 ^{0}C, short chain phosphate was found in the film. The sulphur species in the films formed at 100 ^{0}C is sulphide, which is believed to protect the metal surface[34].

4.2.4 Effect of Loads

The effects of load were investigated by forming the films under different loads, 40, 225 and 400 N. Figure 4.2.9 shows the P L-edge XANES spectra of films generated under different loads for 6 hours. In all previous results, a 225 N load was used to generate the films. Thus, spectrum (B) is the same as spectrum (C) in Figure 4.2.1. It was shown that the film contained ~25% unreacted ZDDP. When the load decreases to 40 N (spectrum C), the ZDDP signal does not change a great deal, but peak *b* disappears in spectrum (C). This implies that when the load is lower, the polyphosphate chain length may be shorter. However, when the load increased to 400 N (spectrum A), the ZDDP signal disappears. From the relative intensities of peaks *a/c*, the average chain length for 400 N was estimated to be 18±2. S L-edge XANES (not shown) indicated that the sulphur signal decreased with increasing load. However, the sulphur form did not change with load and remained S^{2-}. With this limited data, it can be concluded that at higher loads (400 N) ZDDP decomposes more rapidly and as a result no unreacted ZDDP was detected. Under high load, the contact temperature will rise, which will have a similar effect to increasing the oil temperature. It is indeed noticed that the spectrum (A) in Figure 4.2.9 is similar to spectrum (B) in Figure 4.2.6. But the higher load may have some other effect such as deformation of the surface which may be found in the load higher than 400 N.

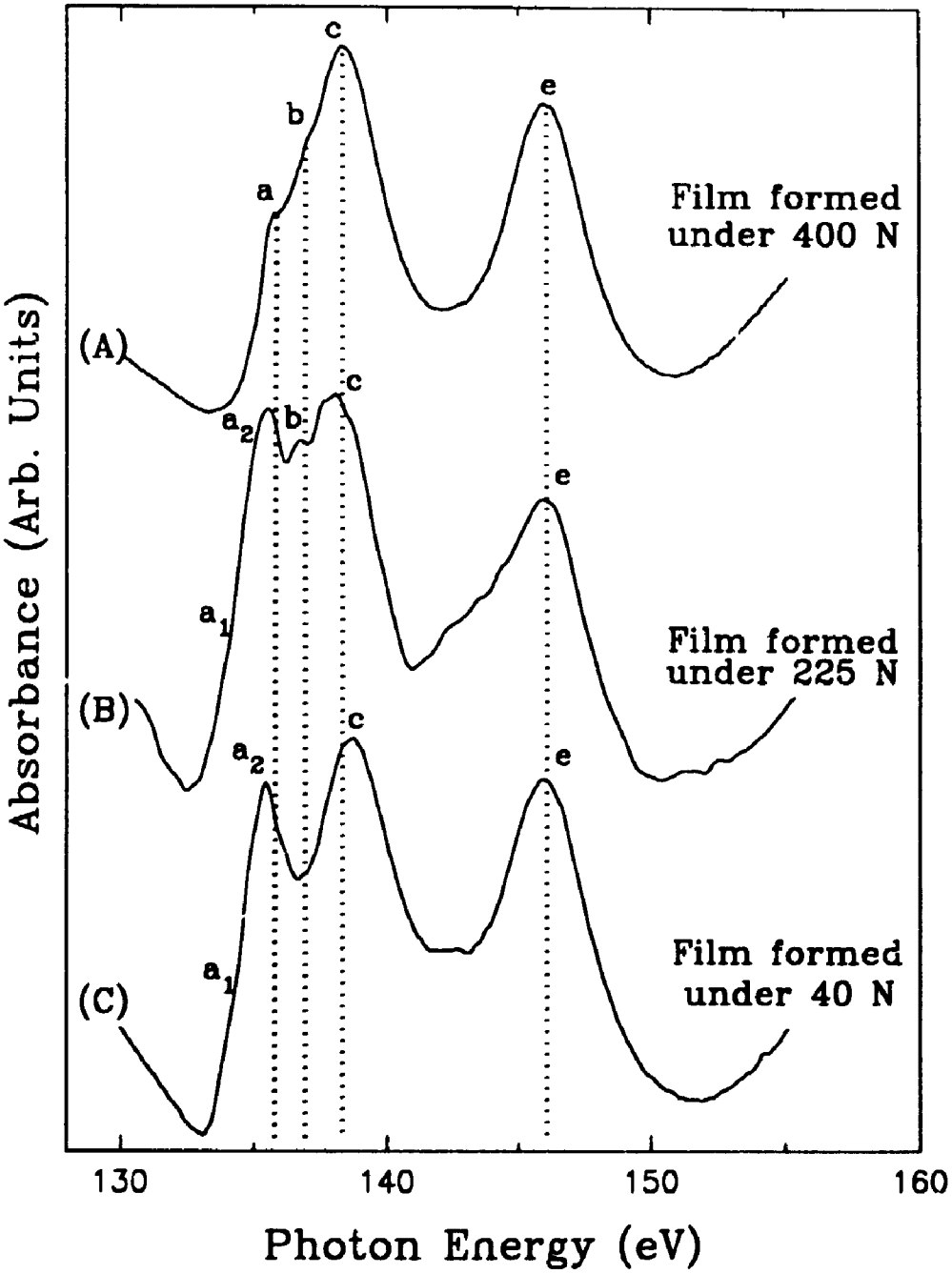

Figure 4.2.9 P L-edge spectra of the films formed under different loads

It can be concluded from the above results that the load applied to rubbing surface has two fundamental effects to the AW film formation. First, the rate of film formation is affected by load. The higher the load, the faster the formation rate. Second, the load may change the chain length of polyphosphates formed in the AW films. The chain length of phosphate in the films formed at higher load is higher than that at lower load. It should be pointed out that this conclusion is only valid at the range of loads used in this work. Several investigators[7,18,20,23,34] have reported that surface composition changes with different load, which is consistent with the results presented here. Some of them[20,23,34] reported that S species, especially sulphide was increased in the films with increasing load. Thus sulphide should hitherto be responsible for the AW effectiveness[34]. No significant change was observed in the S content of the film with different loads in this study. Therefore, this work shows that phosphates are still the most important component to the AW function.

4.2.5 Effects of surface roughness

The surface roughness of antiwear films and the steel substrate have been measured by atomic force microscopy (AFM). Two steel coupons with surface roughnesses of Ra = 10 (polished) and Ra = 289 nm (unpolished), were used to prepare the films. The P L-edge XANES spectra of films generated using those coupons are presented in Figure 4.2.10. Two rubbing times of 30 minutes and 6 hours were used. In Figure 4.2.1, it was shown that when the rubbing time was relatively short, the ZDDP signals could be detected in the film. However, as can be seen from Figure 4.2.10, spectrum (B) and (D) for polished surfaces, are very similar, although they correspond to two different rubbing times. Even the spectrum of the 12 hour film generated on the polished surface (not shown here) looks similar to spectra (B) and (D). This finding suggests that since there is a better contact between the rubbing surfaces in the polished surfaces, there is less chance of ZDDP being trapped and therefore the ZDDP signal cannot be seen here. Meanwhile the phosphate formed, at least on the surface, is a long chain polyphosphate. As observed before, the high intensities of peak *a* in the spectra of unpolished samples (A and C) suggest that the ZDDP component is present in these spectra, although the content of ZDDP in the film may differ from the previous test.

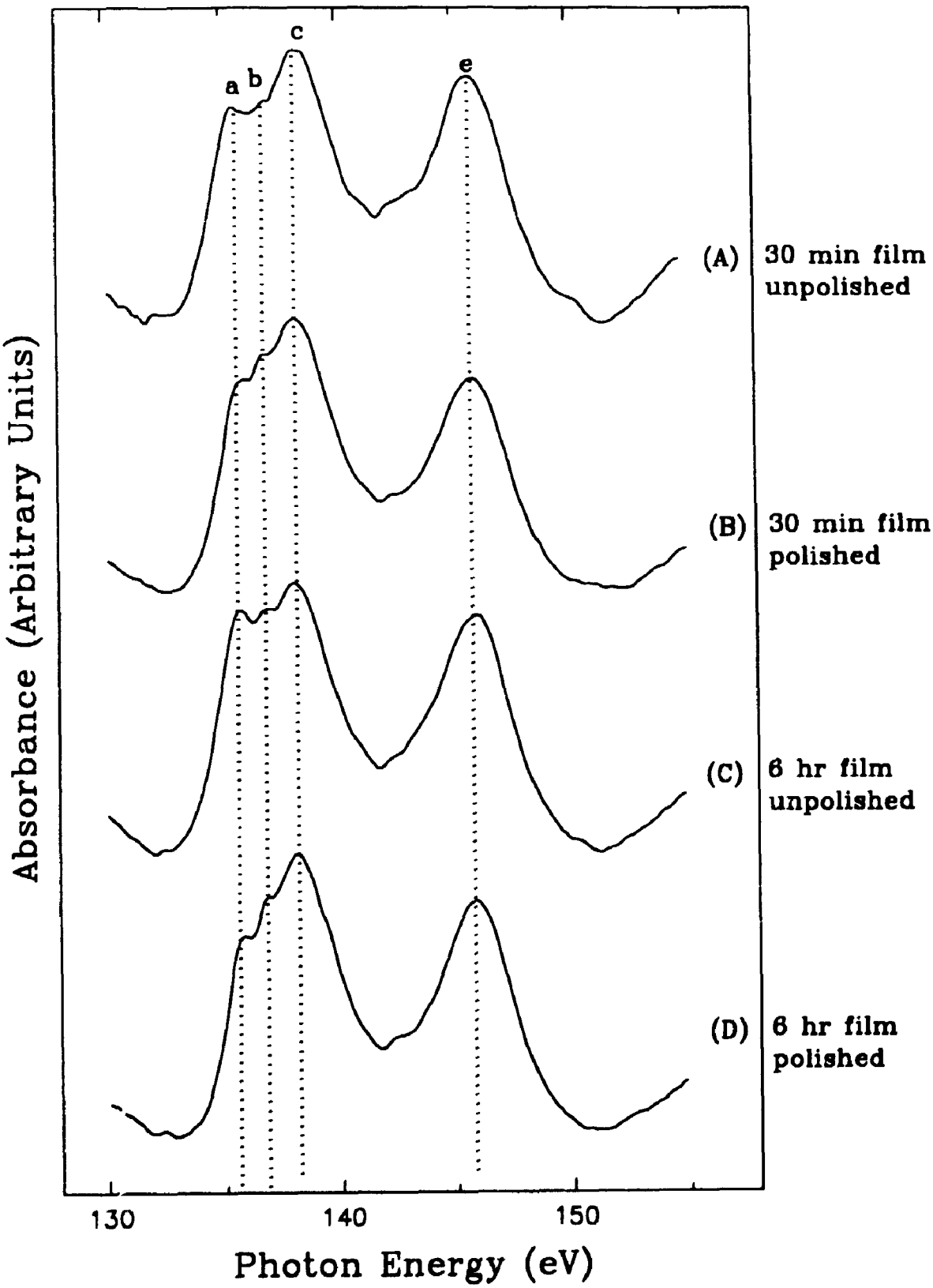

Figure 4.2.10 P L-edge spectra of the films formed on rough surface (A) and (C) and polished surface (B) and (D)

The S L-edge spectra (not shown) confirmed the above findings.

4.3 Conclusions

From the experimental results, the following conclusions can be drawn.

1. ZDDP decomposition to form AW films is a complex process. Many physical parameters affect this process. In general, the higher temperature, the higher concentration of ZDDP, the higher load and the smoother surface will accelerate the decomposition rate of ZDDP.

2. The composition of the films depends on the experimental parameters. Mixtures of phosphates and ZDDP were found in short rubbing times, high ZDDP concentration, low temperature, low load and rough surface. It is assumed that long chain polyphosphate on the surface provides better AW performance which is in accord with other wear and friction tests. It has been found that longer rubbing time, higher concentration of ZDDP, moderate temperature and higher load may help to form long chain phosphates. Short chain phosphates are always present in the bulk film. Sulphur species in most of the cases is sulphide. The presence of sulphate in very short rubbing time or high temperature films is likely from sulphur in the base oil.

4.4 References

1. Paddy, J.L., Lee, N.C.J., Waters, D.N., Trott, W. *Tribol. Trans.*, 1990, 33, 15

2. Barcroft, F.T., Bird, R.J., Hutton J.F., Park, D. *Wear*, 1982, 77, 355

3. Dacre, B., Bovington, C.H. *ASLE Trans.*, 1983, 26, 333

4. Dacre, B., Bovington, C.H., *ASLE Trans.*, 1981, 24, 546

5. Habeeb, J.J., Stover, W.H. *ASLE Trans.* 1987, 30, 419

6. So, H., Lin, Y.C. *Wear*, 1994, 177, 105

7. Palacios, J.M., *Tribology International*, 1986, 19, 36

8. Plaza, S. *ASLE Trans.*, 1987, 30, 233

9. Willermet, P.A., Kandah, S.K., Siegl W.O., Chase, R.E. *ASLE Trans.* 1983, 26, 523

10. Willermet, P.A., Kandah, S.K. *Lubrication Science*, 1993, 5, 129

11. Coy, R.C., Jones, R.B. *ASLE Trans.*, 1981, 24, 77

12. Bovington, C.H., Dacre, B. *ASLE Trans.*, 1984, 27, 252

13. Dacre, B., Bovington, C.H. *ASLE Trans.*, 1981, 24, 546

14. Dickert, J.J., Rowe, C.N. *J. Org. Chem.*, 1967, 32, 647

15. Palacios, J.M. *Wear*, 1987, 114, 41

16. Chao, S.-H., Ludema, K.C., Potter, G.E., DeKoven, B.M., Morgan, T.K., Kar., K.K. *Wear*, 1994, 177, 33

17. Sheasby, J.S., Cauphlin, T.A., Blahey, A.G., Laycock, K.F. *Tribology International*,1990, 23, 301

18. Bird, R.J., Galvin, G.D. *Wear*, 1976, 37, 143

19. Spedding, H., Watkins, R.C. *Tribol. Int.*, 1982, 15, 9

20. Jahanmir, S. *J. Tribology*, 1987, 109, 577

21. Harrison, P.G., Brown, P. *Wear*, 1991, 148, 123

22. Rhodes, K.L., Stair, P.C. *Tribol. Trans.*, 1993, 36, 27

23. Glaeser, W.A., Baer, D., Engelhardt, M. *Wear*, 1993, 162-164, 132

24. Rounds, F. *Tribol. Trans.*, 1993, 36, 297

25. So, H., Lin, Y.C., Huang, G.G.S., Chang, S.T., *Wear*, 1993, 166, 17

26. Brown, J.R., Kasrai, M., Bancroft, G.M., Tan K.H., Chen, J.M. *Fuel*, 1992, 71, 649

27. Martin, J.M., Belin, M., Mansot, J.L., Dexpert, H., Lagarde, P. *ASLE Trans.*, 1986, 29, 523

28. Molina, A. *ASLE Trans.*, 1987, 30, 479

29. Yin, Z., Kasrai, M., Bancroft, G.M., Laycock, K.F., Tan, K.H. *Tribol. Int.*, 1993, 26, 383

30. Hastie, G.P., Roberts, K.J., Adams, D., Fischer, D., Meitzner, G. *Jpn. J. Appl. Phys.*, Vol. 32 (1993) Suppl. 32-2, pp 407-409

31. Bell, J.C., Delarge, K.M., Seeney, A.M. *Proceedings of the 18th Leeds-Lyon Symposium on Tribology*, Sept. 3-6, 1991, Ed. Dowson, D. et al., Elsevier, New York, 1992

32. Willermet, P.A., Mahoney, L.R., Bishop, C.M. *ASLE Trans.*, 1980, 23, 225

33. Plaza, S., Kajdas, C. *Wear*, 1994, 176, 1

34. Sieber, I., Meyer, K., Kloss, H., Schöpke, A. *Wear*, 1983, 85, 43

CHAPTER 5

THE EFFECTS OF CHEMICAL PARAMETERS ON ANTIWEAR FILMS

5.1 Introduction

Both the antiwear film composition and the antiwear performance of ZDDP can be affected by many factors. In this chapter, some factors related to the chemical nature of the original additives, such as the composition of ZDDPs, and the mutual interaction between ZDDP and detergent or dispersant, will be discussed. The most commonly studied chemical parameter is the influence of alkyl groups in ZDDP. Previous studies are limited to decomposition of ZDDP at high temperature[1,2,3] or the effects of oxidizing agents[4,5,6,7]. Various investigations have shown that secondary ZDDP is much easier decomposed than primary ZDDP[1,8,9,10,11]; and aryl ZDDP is even more difficult to decompose than primary ZDDP[12]. Selective studies have been focused on the study of the AW films generated by primary ZDDP[13,14,15] and secondary ZDDP[16]. However, there is no systematic study to compare the effects of alkyl groups in ZDDPs. Meanwhile, the function of zinc in the AW system has not been recognized properly. A comparative study, which include the measurements of the AW films generated from ZDDPs and DDPs (without Zn), has been made in this chapter.

The ZDDP additive is used rarely as the sole additive in oil formulations. In the vast majority of cases, the finished oil contains one or more other additives to give other properties such as detergency, dispersancy and antirust to oil. The performance of ZDDP is strongly influenced by other additives such as detergents and dispersants. The interaction of ZDDP with detergent or dispersant has been investigated widely as evidenced by the number of references available in the literature. Three review articles have dealt extensively with this subject[17,18,19]. It is generally believed that the ZDDP is decomposed, and that its decomposition products adsorb on and/or react with the rubbing surface to form the protective antiwear surface layer. The rate of ZDDP decomposition can be retarded by additives such as detergents[20,21]. In addition, these other additives

could interfere with the ZDDP-derived antiwear species by co-adsorbing on the surface[18,22,23]. Complex formation between ZDDP and detergent or dispersant in the bulk oil has also been proposed as a reason for reduced antiwear performance[18,19,24,25]. In this chapter, the effects of a commercial secondary ZDDP (ZDDP-1) in combination with a calcium sulphonate (Neutral) detergent, a calcium phenate (basic) detergent and a polyisobutylene succinic anhydride polyamide dispersant have been examined.

5.2 Results and discussion

5.2.1 Effects of alkyl and aryl groups in ZDDP

In this section, several AW films generated from synthesized ZDDPs will be discussed. The composition of these additives are listed in Table 2.1.1 and 2.1.2. ZDDP was dissolved in base oil to give a concentration of ZDDP of ~1 wt.%. The parameters used for film formation are: temperature 100 ^{0}C, rubbing time 30 minutes, speed 25 Hz and contact pressure 225 N.

First, the P and S L-edge XANES spectra of AW films will be compared. The spectra of the films together with the spectrum of pure IP-ZDDP (Table 2.1.2) are plotted in Figure 5.2.1. P and S regions of the spectra are marked at the top of the figure. Examining the ZDDP spectrum (A), very sharp features both for P and S edges are observed. Qualitatively the relative intensities of the major P and S features are not that much different in the spectrum although the atomic ratio of P to S in ZDDP is 1:2. In contrast, for the films, the relative intensities of P and S signals are substantially different. From the relative intensities of P L-edge and S L-edge peaks, as demonstrated in Figure 5.2.1, it is found that the sulphur content of the films was much less than the phosphorus content. This is in agreement with thermal decomposition findings[26,27]. The depletion of S has been attributed to forming volatile materials[3,22,28,29], or migration of sulphur species to base oil[26]. Although the S signal is weak, it can be found from spectra (B), (C) and (D) that S is in a reduced form, sulphide. The chemical state of sulphur in films from IP-DDP and NB-DDP is different from the rest of the films (see below). Another important feature of these spectra is that the P and S chemical forms have changed in the films compared with ZDDP, and no significant amount of the original

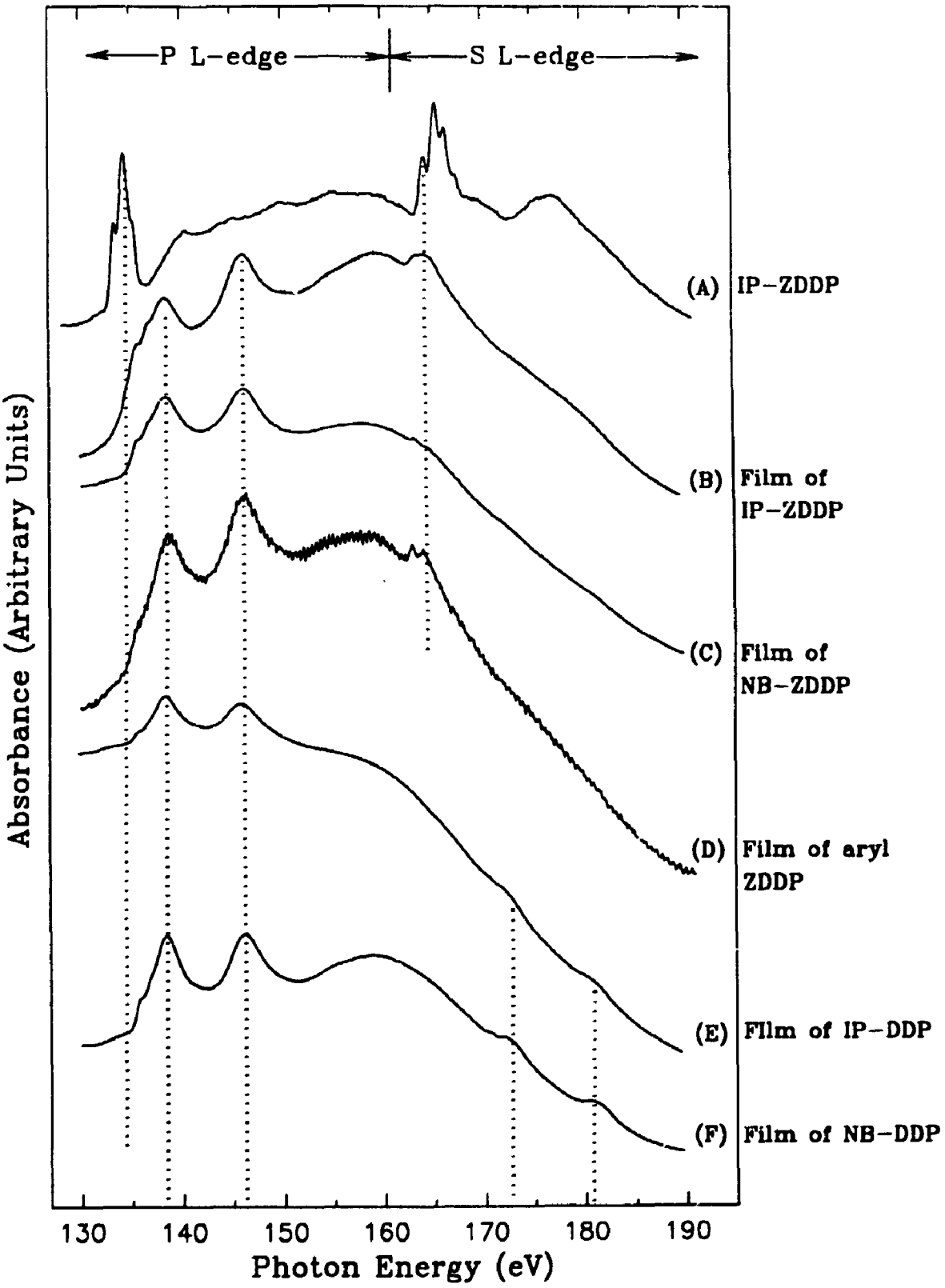

Figure 5.2.1 Comparison of P and S L-edge spectra of the films formed from different ZDDPs

compound is left in the film. This is a good indication that ZDDP, as has been suggested in the literature[8,26,30], decomposes to form the antiwear film. Zinc and iron can be the cations in the metal sulphide. The former is from the original ZDDP and the latter is from the substrate. After rubbing under high pressure, iron oxide on the steel surface or even metallic iron can react with ZDDP or its decomposition products to form the AW film.

Now, the P and S L-edge XANES spectra will be discussed in more detail. Figure 5.2.2 compares the P L-edge XANES spectra of ZDDP, the antiwear films formed from different ZDDPs, sodium thiophosphate and two phosphates in different structures. It should be pointed out that all pure ZDDPs measured in this thesis have very similar spectra. Therefore only one spectrum, the spectrum of IP-ZDDP will be shown in this chapter. Peak positions are summarized in Table 5.2.1. Comparison of the spectrum of IP-ZDDP (spectrum A) with AW films (spectrum B, E and G) confirms that the chemical composition of the antiwear film is not the same as that of the ZDDP.

The appearance of an intense peak *e* in spectra (B), (E) and (G) indicates that the chemical state of phosphorus in these films is in the form of a phosphate, since this feature is not observed in non-phosphate forms. The pre-edge features in the spectra of the films are not as well resolved as those of pure inorganic phosphates such as in spectra (C) and (F). This is not surprising since the films are unlikely to be pure. Examining the spectrum of thiophosphate (D) and also referring to Table 5.2.1, it is evident that when oxygen is replaced by sulphur in thiophosphate, the phosphorus spectrum has shifted to lower energy and peak *e* becomes much less intense. The fact that the spectra of the film does not show the low energy peaks *a* and *a'* of Na_3PO_3S, and also peak *e* of the film spectra shifts to higher energy ~ 1 eV, indicates that sulphur is no longer attached to phosphorus in the film. Inspecting the spectrum of the IP-ZDDP film (B), it appears that the phosphate structure in the film is similar to $Na_3P_3O_9$ (spectrum C), rather than short chain phosphates (spectra F). Attempts were made to simulate the film spectrum by linear combination[31] of the spectra of linear phosphate model compounds discussed in section 3.1, but no one linear phosphate compound simulates the films. As shown in Table 2.1.1, $Na_3P_3O_9$ is a cyclic polyphosphate. Although the peak positions of $Na_3P_3O_9$ are close to those of linear phosphates, $Na_3P_3O_9$ posses the highest intensities

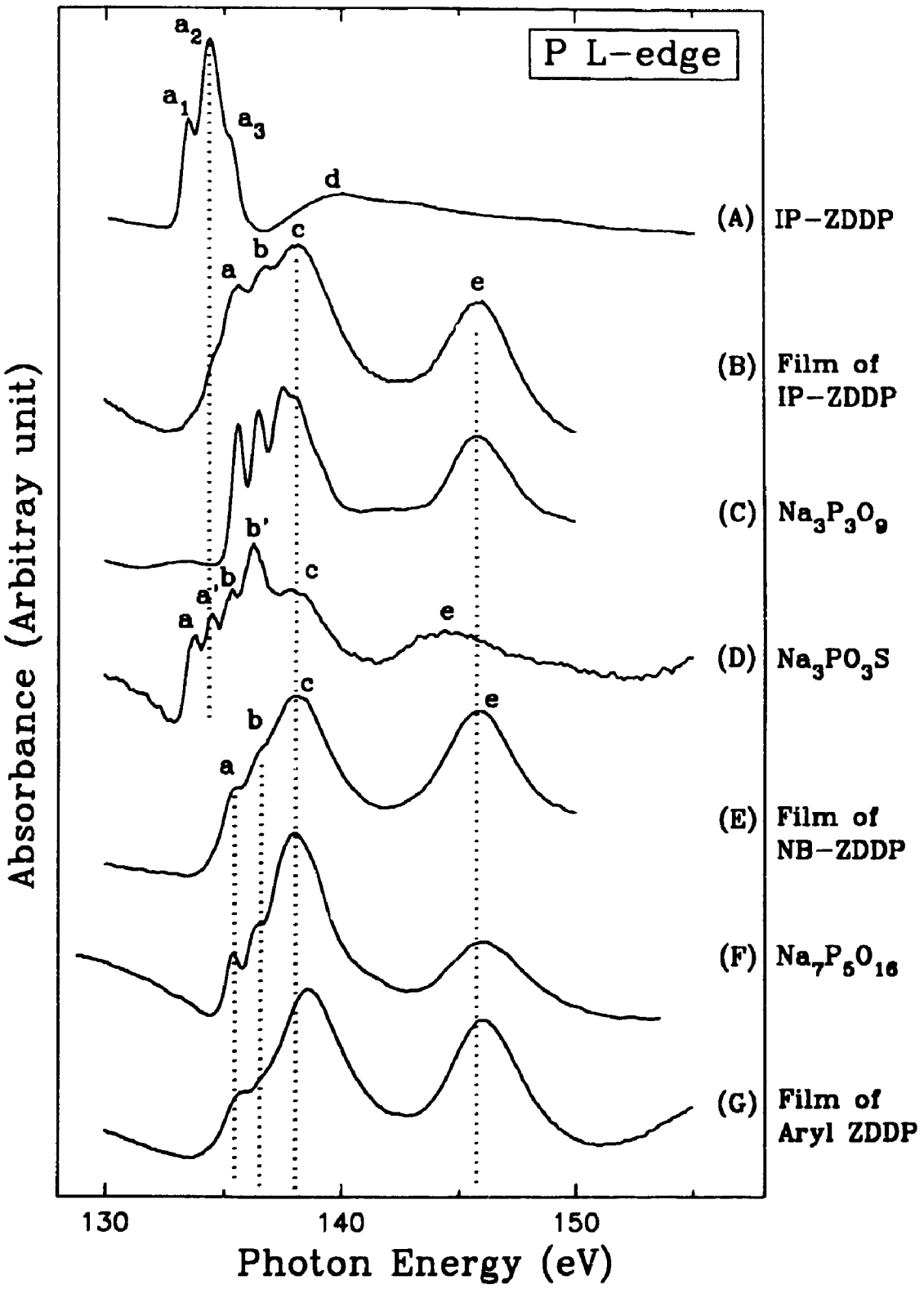

Figure 5.2.2 P L-edge spectra of the films formed from different ZDDPs

Table 5.2.1 Peak positions and intensities of phosphates and AW films

Samples	Peak Positions (± 0.07 eV)*				Heights** (±0.01)
	a	b	c	d	
Na_3PO_4	134.55	135.35	138.94	146.43	0.13
$Na_4P_2O_7$	134.93	135.83	138.20	146.37	0.23
$Na_5P_3O_7$	135.13	135.96	137.92	146.43	0.27
$Na_7P_5O_{16}$	135.43	136.33	138.02	146.40	0.34
$Na_{20}P_{18}O_{55}$	135.45	136.31	137.94	146.36	0.52
$Na_{30}P_{28}O_{85}$	135.46	136.33	137.97	146.36	0.54
$Na_{46}P_{44}O_{133}$	135.42	136.30	137.77	146.36	0.60
$Na_{93}P_{91}O_{274}$	135.51	136.38	137.85	146.44	0.63
$Na_3P_3O_9$	135.46	136.29	137.92	146.53	0.75
Film, IP-ZDDP	135.6	136.8	138.0	145.9	0.78
Film, NB-ZDDP	135.5	136.6	138.0	145.8	0.49
Film, aryl ZDDP	135.8	-	138.5	146.1	0.40
Film, IP-DDP	135.9	-	138.5	146.0	0.26
Film, NB-DDP	135.9	137.0	138.3	146.1	0.36
Film, ZDDP-1	135.2	-	138.0	146.0	-
Film, ZDDP-1 + DET-1, 0.5%	135.3	136.8	138.4	145.6	-
+ DET-1, 1.0%	135.5	-	138.1	145.9	-
+ DET-1, 2.0%	135.5	136.8	138.2	145.8	0.74
+ DET-2, 0.5%	135.4	136.5	137.7	145.8	0.63 (0.43)
+ DET-2, 1.0%	135.4	-	137.7	145.8	0.38 (0.36)
+ DET-2, 2.0%	135.4	136.4	137.8	145.8	0.34 (0.19)
+ DISP, 1.0%	135.5	136.6	137.9	145.7	0.59
+ DISP, 2.0%	135.4	-	138.1	145.8	0.43
+ DISP, 5.0%	135.3	136.5	138.0	145.8	0.45

* Peak position error for films is ±0.2 eV.
** The heights are ratioed to the height of peak (c).
*** Values from FY mode are in parenthesis.

of the pre edge doublets.

The least squares fitting program[32] used in section 3.1 has been employed to fit the spectra of these three films. The results are shown in Figure 5.2.3. Spectrum (A) of $Na_3P_3O_9$, was fitted to two pre edge peaks and two post edge peaks. Similarly, spectrum (B) of IP-ZDDP film was fitted to pre-edge and post-edge peaks. In this case there are two extra peaks at lower energy which are absent in spectrum (A) of $Na_3P_3O_9$. These features can also be seen in Figure 5.2.2 (B) as a shoulder of peak *a*. The shoulder position aligns well with ZDDP peaks a_1 and a_2. At the same time, the shoulder aligns with peaks *a* and *a'* in the thiophosphate spectrum (D of Figure 5.2.2). But as discussed above since peak *e* of thiophosphate does not align with that of the film, the contribution of thiophosphate should be very small. The peak widths of the spin-orbit doublets ($\sim$ 1 eV) in the film are broader than those of model compounds ($\sim$ 0.6 eV). These widths are probably due to the presence of other phosphates in AW films with variable chain length and different cations. It appears, therefore, that the phosphorus form in the film produced by IP-ZDDP, in most part, is close to a long chain linear or cyclic polyphosphate.

Comparing the spectrum of the surface film of NB-ZDDP (E in Figure 5.2.2) and (C in Figure 5.2.3) with the phosphate model compounds and also considering the peak positions from Table 5.2.1, it is clear that, from all aspects, the spectrum of the film is very similar to the spectrum of a shorter chain polyphosphate such as shown in section 3.1. Similarly, the P L-edge spectrum of aryl ZDDP film (G) is also similar to that of a shorter chain polyphosphate (F). The fitted spectra of these two films are also shown in Figure 5.2.3 (C) and (D). Since the line widths increases from model compounds ($\sim$ 0.6 eV) to the films ($\sim$ 1.0 eV), the accurate chain length cannot be determined from the relative area of the doublets. However, it has been found that the relative heights of the doublets follow the same trend as the relative area (Figure 3.1.10). Therefore it is possible to determine the chain length by measuring the relative height of peak *a*. The intensities listed in Table 5.2.1 are the heights of peak *a*. According to Figure 3.1.10 and Table 5.2.1, the chain lengths of phosphates in the film from NB-ZDDP is about 16 ± 2 and that of the aryl ZDDP is about 9 ± 1.

Figure 5.2.4 shows the S L-edge spectra of the films and a number of model

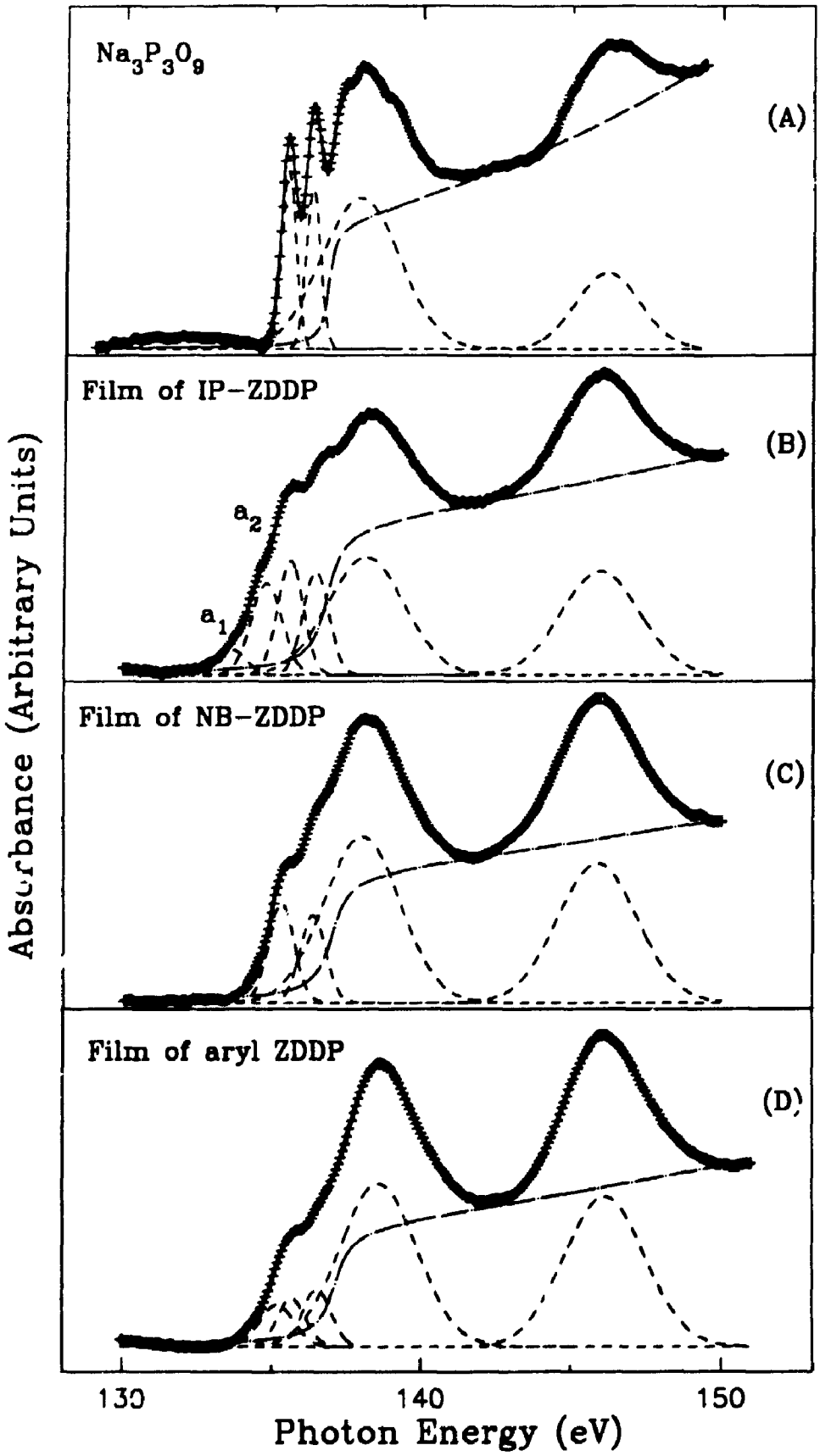

Figure 5.2.3 The least-squares fittings of P L-edge spectra of the films from different ZDDPs

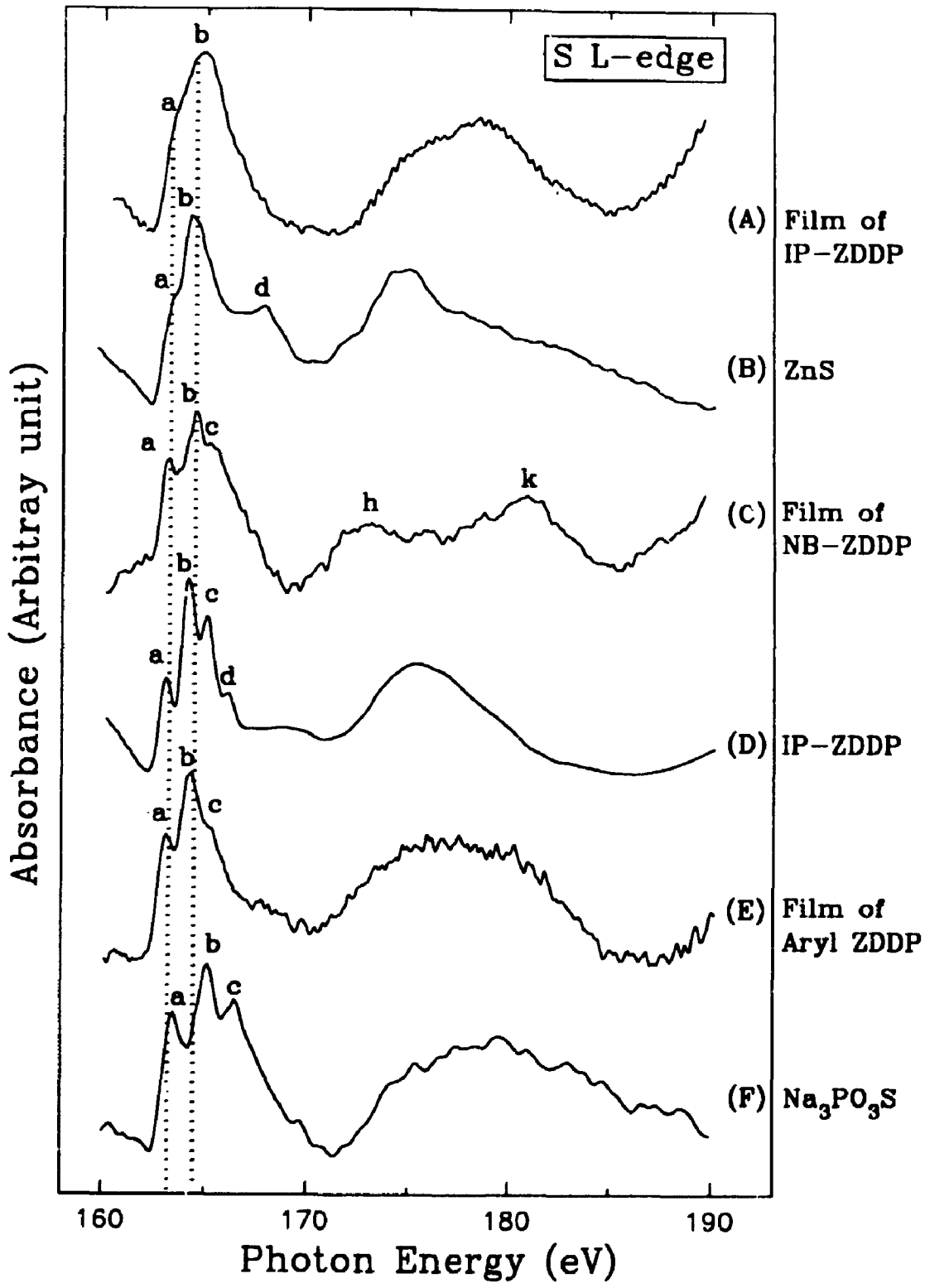

Figure 5.2.4 S L-edge spectra of the films formed from different ZDDPs

compounds as a reference, and Table 5.2.2 summarizes the corresponding peak positions. First, spectrum (A) in Figure 5.2.4, corresponding to the surface film of IP-ZDDP, is considered. Comparing the spectrum with the spectra of model compounds presented in the figure and also referring to the peak positions in Table 5.2.2, it appears that the closest spectrum is that of ZnS (spectrum B). The spectrum of FeS was also recorded (not shown) and found that the compound was extremely surface sensitive and underwent rapid oxidation. So the spectra in Figure 5.2.4 (A) cannot correspond to FeS. Using model compounds in section 3.2 as reference, it is obvious that features around 178 eV in spectrum (A) do not correspond to sulphate and are, most likely, post edge structures[33]. In conclusion, sulphur in the film from secondary ZDDP is in the form of a sulphide, and is most likely associated with zinc.

Inspecting Figure 5.2.4, the spectrum of the film produced by NB-ZDDP (C), on the other hand, is quite different from that of the film from IP-ZDDP. A triplet spectrum (*a-c*) is observed which is different from that of pure ZDDP (spectrum D). Indeed, the spectrum is not similar to metal sulphide, but it has a contribution from the pure ZDDP (spectrum D). It is also similar to what has been reported for alkyl and aryl sulphides[31]. Generally, all alkyl and aryl sulphides produce a triplet spectrum similar to spectrum (C). However, these compounds are very volatile and their presence in the film is doubtful. As is noted in Figure 5.2.1 (C), the sulphur signal is very weak and what is observed in Fig 5.2.5 (C) is most likely due to unreacted ZDDP. In contrast, the sulphur signal in the films of IP- and aryl ZDDP are stronger (Figure 5.2.1 B and D). It is observed that the peak positions of *h* and *k* in spectrum (C) is similar to those in $FeSO_4$. It is likely that a small amount of S has been oxidized to sulphate. The presence of sulphate in the films has been reported by other investigators[30,34,35]. From Figure 5.2.4 (F), the spectrum of thiophosphate has shifted to higher energy and it confirms the absence of thiophosphates in films. Again, there is a similarity between the spectra of films from aryl ZDDP and NB-ZDDP, as has been found in the P L-edge spectra. Examining spectra (C) and (E), it is noticed that their pre-edge triplets are very similar. The post-edge region, consisting of very broad features, are somewhat different. These features cannot be used effectively as fingerprints.

In a four ball friction machine, Sieber et al[13] investigated the AW film formed

Table 5.2.2 Peak positions of S L-edge spectra of model compounds and AW films (± 0.1 eV)

Samples	a	b	c	d	e	f	g	h	i	j	k
IP-ZDDP	163.0	164.1	164.9	165.9	175.0						
ZnS	163.3	164.1	-	167.7	174.9						
Na_3PO_3S	163.4	165.1	166.5	-	179.5						
Na_2SO_4						170.8	172.0	172.9	174.2	179.9	181.0
$FeSO_4$						170.9	172.1	173.1	-	-	181.1
$Fe_2(SO_4)_3$						171.3	172.7	173.4	-	-	181.6
Film, IP-ZDDP	163.6	164.8	-	-	-						
Film, NB-ZDDP	163.1	164.5	165.1	-	-	-	-	173.1	-	-	180.8
Film, aryl ZDDP	163.1	164.3	165.2	-	-						
Film, IP-DDP						170.8	-	172.3	-	-	181.3
Film, NB-DDP						171.0	172.2	172.9	-	-	181.6
Film, ZDDP-1 + DET-1,0.5%	163.1	164.1	165.1	165.9	-						
+ DET-1,1.0%	163.1	164.2	-	165.9	-						
+ DET-1,2.0%	163.1	164.1	165.3	-	-						

from a primary ZDDP (NB-ZDDP) in paraffin oil. They found that, under mixed friction conditions, the antiwear efficiency of ZDDP is due to the formation of phosphate, sulphide and oxide containing layers. Glaeser and coworkers[28] made an *in situ* wear experiment in which a scanning Auger spectrometer was employed. They reported that there were two surface layers on the steel surface. On the top are zinc phosphates, and on the bottom above the metal surface is iron sulphide or iron oxide. In an EXAFS analysis for AW films, Belin et al[36,37] reported the formation of highly amorphous inorganic polyphosphate glasses in friction particles. Similar results have been reported by other researchers[30,38]. In general, because of the limitation of the methods used, it has been impossible to determine the chain length of phosphates formed in the AW films. Recently, Bell et al[14,15] applied SIMS and XPS to analyze films derived from n-butyl ZDDP solution in a Cameron-Plint friction machine (at 175 ^{0}C). Based on the ratio of M_2O/P_2O_5, they concluded that there was a long chain polyphosphate in the AW film. Since their technique does not provide the exact chain length, direct comparison of their results to this work is not possible. Willermet et al[16], using reflectance-absorbance IR, XPS and Auger spectroscopies, studied films formed from secondary ZDDP in a cam-tappet friction machine. They found that the films contained both short and long chain polyphosphates with zinc as cations. Considering the variables in different experiments, their results, in general, are consistent with this work.

5.2.2 Effects of Zn in ZDDP

Two films were generated from different additives without Zn. One is from a secondary IP-DDP and another is from a primary NB-DDP. Both of them are the ligands of IP-ZDDP and NB-ZDDP, respectively. These ligands are also suggested to be one of the by-products of thermal decomposition of ZDDP in oil[8,26,39,40]. The relative intensities of S signals in films are significantly weaker than those of P signals (Figure 5.2.1). The structures and the chemical forms of P and S entities in the film will be discussed below. The P L-edge XANES spectra of the films along with the relevant reference spectra are plotted in Figure 5.2.5. For easy comparison, the spectra of three model compounds (spectra A, C and E) are presented along with the spectra of the films (spectra B and D). Spectrum (B) in Figure 5.2.5 belongs to the film generated from IP-

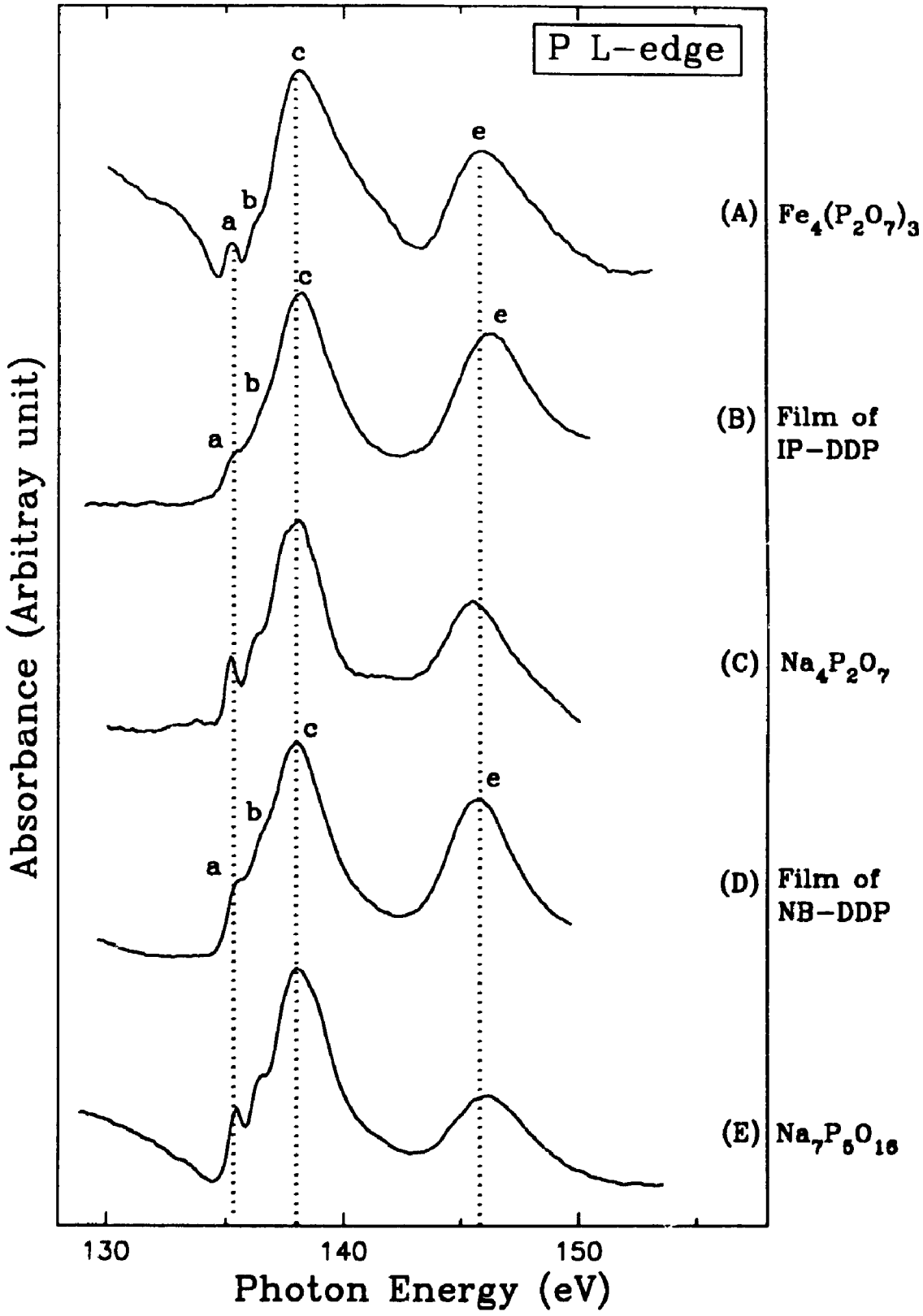

Figure 5.2.5 P L-edge spectra of the films formed from DDPs (no Zn)

DDP. In contrast to the film from IP-ZDDP, the absence of any intense fine structures on the shoulder of peak *c* indicates that the phosphate was not polymerized to any great extent when Zn was not present. As listed in Table 5.2.1, the relative intensity (height) of peak *a* in the spectrum corresponds to a polyphosphate with chain length of the order of 2-3. Since no zinc is present, iron is the only possible metal cation. Indeed, comparing the spectra of the film with that of $Fe_4(P_2O_7)_3$, an extremely good match was found. All the features in the two spectra align quite well. These findings suggest that zinc plays an important role in the film formation. It may help to form longer chain phosphates films. The spectrum of the film from NB-DDP (D) is similar to spectrum (B). From the relative heights of peak *a*, the chain length seems to be longer than that of IP-DDP (B) and close to that of $Na_7P_5O_{16}$.

The S L-edge XANES spectra of films and some reference spectra are presented in Figure 5.2.6 and the peak positions are listed in Table 5.2.2. The chemical form of sulphur in films generated in the absence of Zn is quite different from those when Zn is present. In Figure 5.2.6, the spectra of the two films are compared with those of sulphates. No sulphur signals corresponding to reduced forms of S were found. This means that sulphur species has been oxidized to sulphate in the AW films. A careful comparison of the two spectra of the films with those of sodium sulphate (A), iron (II) sulphate (C) and iron (III) sulphate (E) shows a great resemblance between sulphur forms in the films and iron (II) sulphate. Another role of Zn in antiwear agents becomes apparent. It can protect the steel surface from oxidation. Therefore it can be concluded that Zn has two important roles. First, when Zn is present, the phosphate in the film tends to polymerize more; and secondly, Zn acts as an antioxidant in protecting the sliding surfaces, probably by reacting with S to form ZnS, which may replace sulphate as main sulphur species on the surface.

5.2.3 Interaction of ZDDP-1 with calcium sulphonate

5.2.3.1. Effects of concentration

The effect of the calcium sulphonate detergent (DET-1, neutral) was investigated in combination with ZDDP-1. Generally, the purpose of the detergent additive in motor

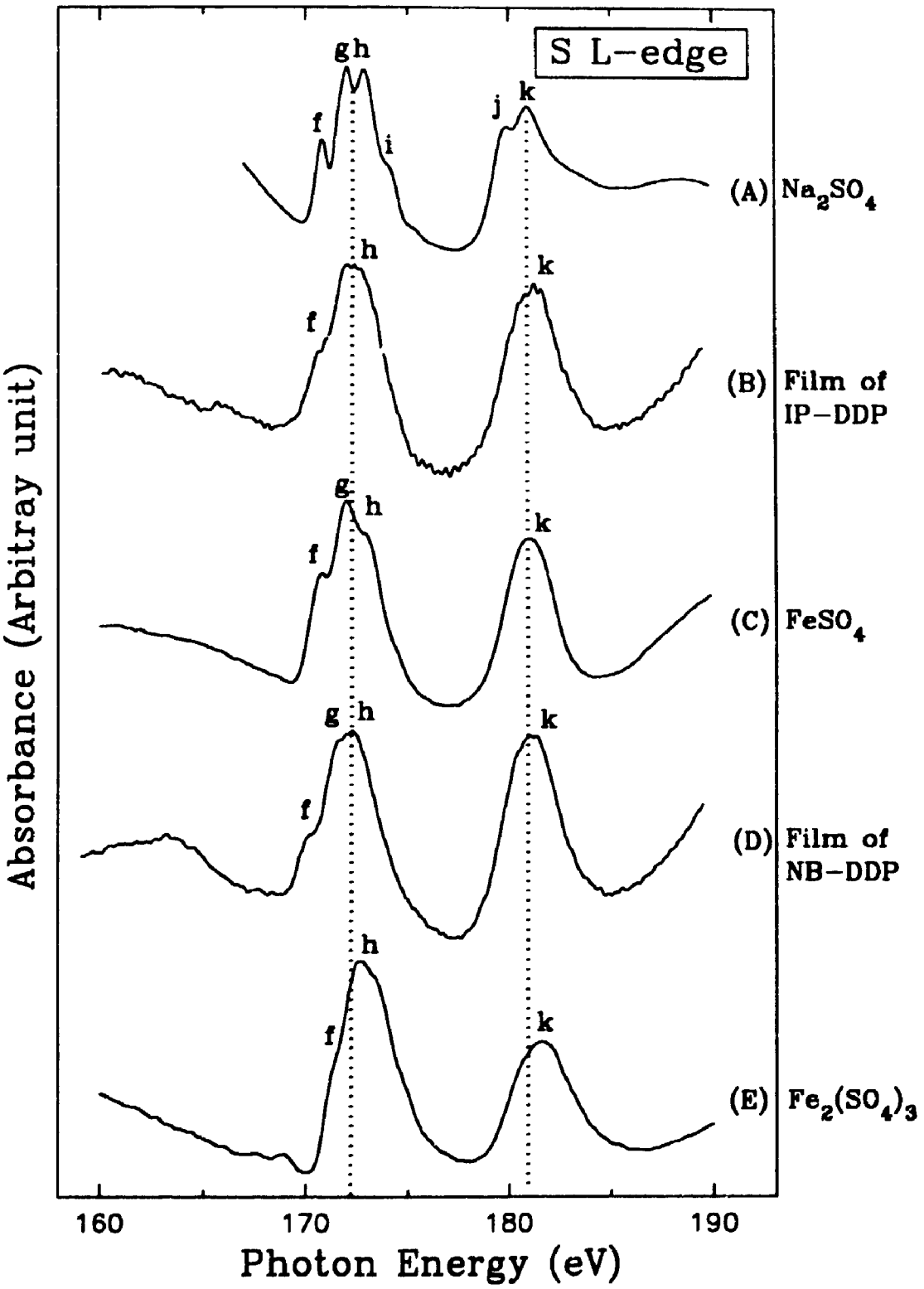

Figure 5.2.6 S L-edge spectra of the films formed from DDPs (no Zn)

oil, is to keep insoluble products, formed as result of combustion, in suspension. Different concentrations of calcium sulphonate (0 wt.%, 0.5 wt.%, 1 wt.% and 2 wt.% by weight) were used. The experimental parameters are the same as before. The P L-edge XANES spectra of the films formed from ZDDP-1 (1.2 wt.%) plus detergent in different concentrations are plotted in Figure 5.2.7. Spectrum (A) corresponds to the film generated using ZDDP-1 without DET-1. When the concentration of DET-1 increased to 0.5% (spectrum B), it has almost no effect to the phosphates in the film. With the further increasing of DET-1 concentration, peaks a_1 and a_2, which has been assigned to the ZDDP (Chapter 4), are decreased dramatically (spectra D and F). In the concentration of 2% (spectrum F), there is almost no ZDDP present. Its general shape is similar to the spectrum of a film formed in long rubbing time without detergent (Fig. 4.2.1). The relative height of peak *a* (0.74) in spectrum (F) is close to the spectrum of the cyclic phosphate (Table 5.2.1). The results imply that in order to modify the structure of surface films, the effective concentration of DET-1 in the system should be higher than 0.5 wt.%. For better formation of polyphosphate, 2 wt.% detergent seems to be the suitable choice. A linear combination procedure[31] has been used to estimate the amount of unreacted ZDDP-1 in the films. Using spectrum (F) and the spectrum of ZDDP-1, two synthetic spectra have been constructed, which are displayed in Figure 5.2.7 as dashed lines (C and E). It was found that in order to simulate spectrum (B), it was required to combine 35% ZDDP-1 spectrum and 65% spectra (F). In order to simulate spectrum (D) it was required to digitally combine 5% ZDDP-1 spectrum and 95% spectrum (F). These results clearly indicates that excess ZDDP is not adsorbed on the film when the concentration of detergent is high.

The S L-edge XANES spectra of the same set of films are shown in Figure 5.2.8. The peak positions and intensities are listed in Table 5.2.2 and Table 5.2.3 respectively. In general, the S L-edge XANES of the films are less informative than the P L-edge due to the strong overlap of pure ZDDP features with those of the degradation products. It is observed that sulphur is still in the reduced form and no sulphate is present. As indicated in Table 5.2.3, the P/S ratio increases as the concentration of the detergent increases from 0 to 2 wt.%. This indicates that addition of the detergent has caused the depletion of S in the film. It should be mentioned that peak *e*, present in the spectra of

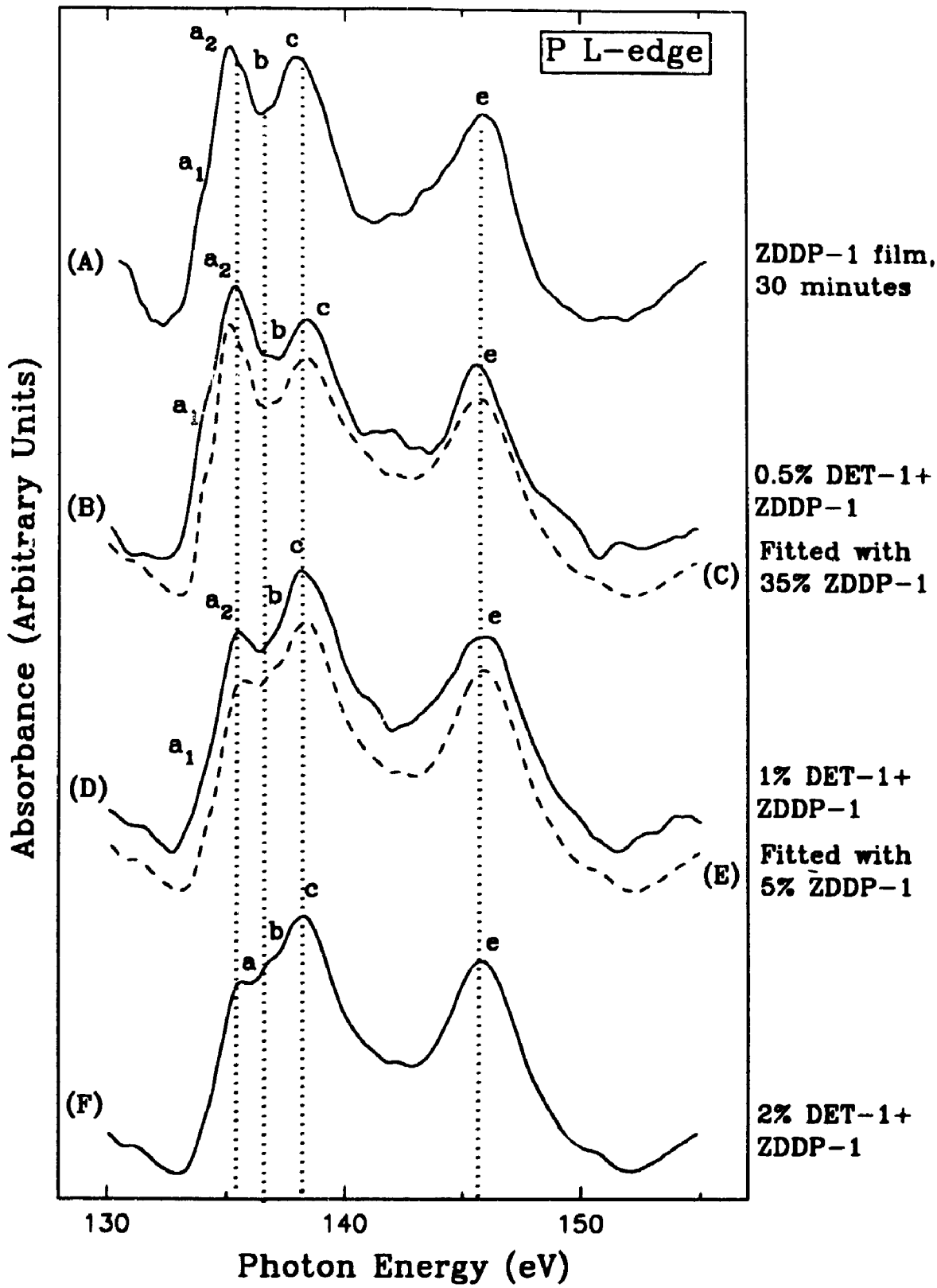

Figure 5.2.7 P L-edge spectra of the films formed from ZDDP-1 plus DET-1 in different concentrations

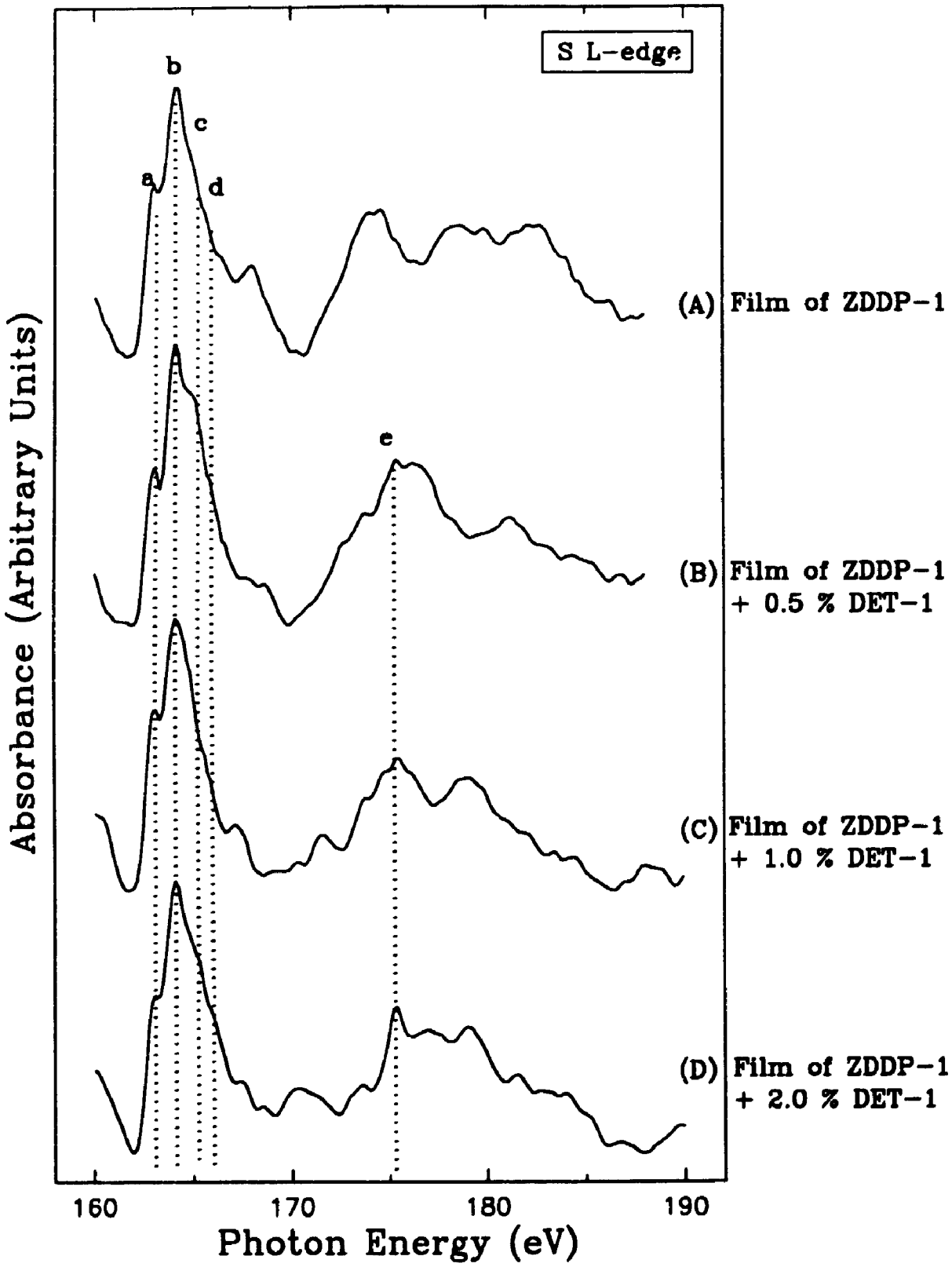

Figure 5.2.8 S L-edge spectra of the films formed from ZDDP-1 plus DET-1 in different concentrations

Table 5.2.3 Relative intensities of P and S XANES signal measured in TEY

Additives	P area (±5%)	S area (±10 %)	P/S (±10%)
ZDDP-1, 1.2 wt.%	2.90	1.70	1.7
+ DET-1, 0.5 wt.%	2.42	1.18	2.1
+ DET-1, 1.0 wt.%	0.59	0.18	3.3
+ DET-1, 2.0 wt.%	0.43	0.12	3.6
+ DISP, 1.0 wt.%	0.41	0.16	2.6
+ DISP, 2.0 wt.%	0.41	0.15	2.7
+ DISP, 5.0 wt.%	0.11	0.04	2.8

films from ZDDP-1 and calcium sulphonate detergent, is the second order harmonic of the Ca L-edge feature at ~350 eV. However, no sulphonate signal corresponding to sulphonates salts[41] were detected in Figure 5.2.8.

5.2.3.2 Cations in the AW films

In order to investigate the cations in the polyphosphate in films, XANES spectra at the calcium, iron and zinc L-edge, and oxygen K-edge have been recorded. Unfortunately, the line width at the zinc L-edge is too broad to be used for speciation. Also, the iron L-edge can only provide limited oxidation state information (see section 3.4). Therefore, at this stage, only the calcium L-edge and oxygen K-edge spectra will be used to analyze the compositions of AW films. Plotted in Figure 5.2.9 are Ca L-edge spectra of the film generated from ZDDP-1 (1.2 wt.%) plus DET-1 (2.0 wt.%) in both partial electron yield (PEY) and fluorescence yield (FY) modes. As described in Chapter 2, the PEY mode only probes the very top surface (< 10 Å) of the film. Peaks *a* (349.6 eV) and *b* (353.0 eV) are assigned to the Ca L-edge spin-orbit doublets. Weak peaks *c* and *d* in spectrum (A) which align well with spectrum (B) recorded in FY mode, originated from second order harmonics of the iron L-edge. Since PEY is very surface sensitive, peaks *c* and *d* of Fe are relatively weak. In contrast, FY probes up to a few thousand angstroms, and spectrum (B) is dominated by Fe with little or no Ca. These findings indicate that Ca originating from calcium sulphonate is associated with the surface film and probably is present as a phosphate counter cation.

O K-edge spectra of the films are shown in Figure 5.2.10. Spectrum (A) corresponds to zinc pyrophosphate. The general shape of the spectra of the films, both in PEY mode (B) and FY mode (C), resemble that of the model compound. The O K-edge spectra of zinc orthophosphate, pyrophosphate and metaphosphate glasses are found to be very similar, which means that phosphate chain length cannot be determined by the O K-edge spectrum. Therefore the phosphorus species in this film is not necessarily a pyrophosphate. However, XPS spectra have shown that the binding energy of bridging oxygen and non-bridging oxygen in polyphosphate have different binding energies[42]. Comparing with the oxide spectra in Chapter 3, the narrow peak *b* and missing peak *a* implied that no iron oxide or iron phosphate can be detected in the surface part of the

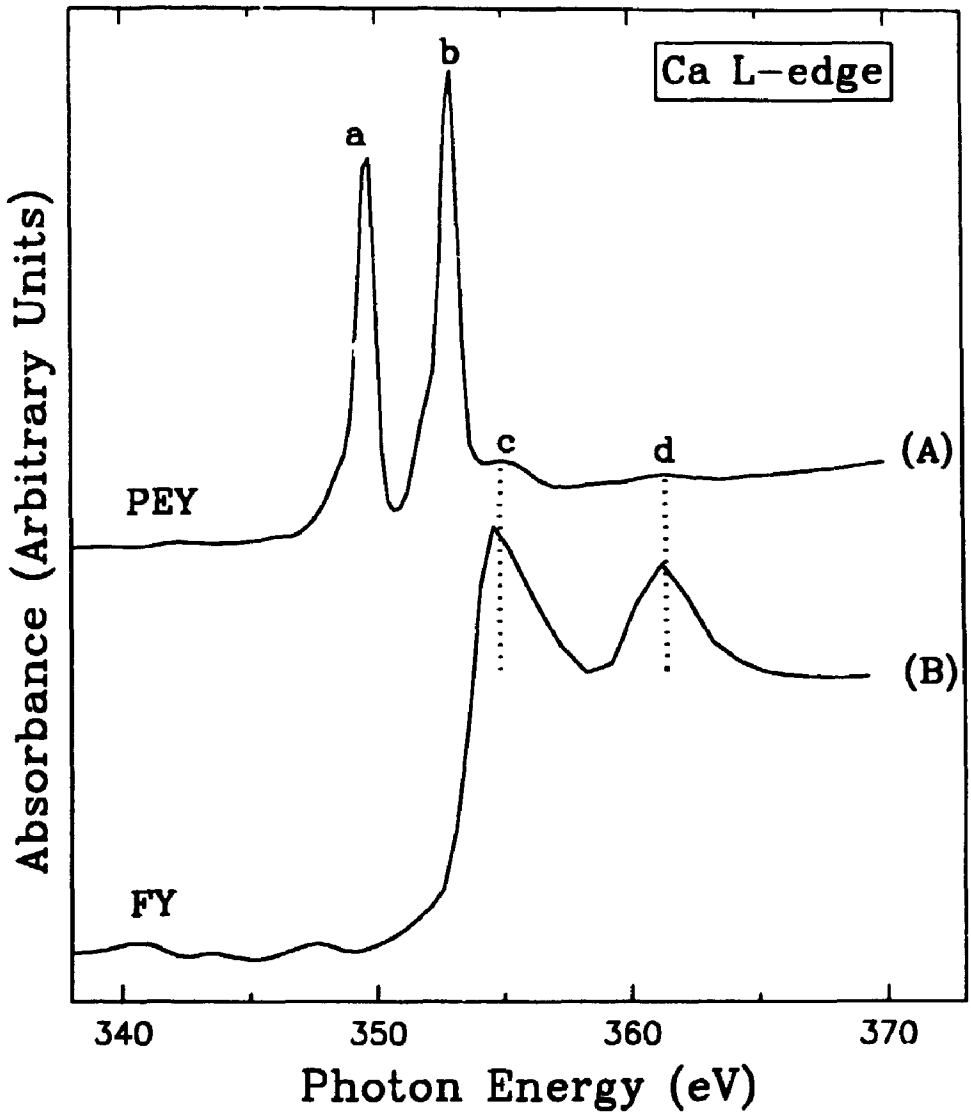

Figure 5.2.9 Ca L-edge spectra of the film formed from ZDDP-1 plus 2 wt.% DET-1 in both PEY and FY modes

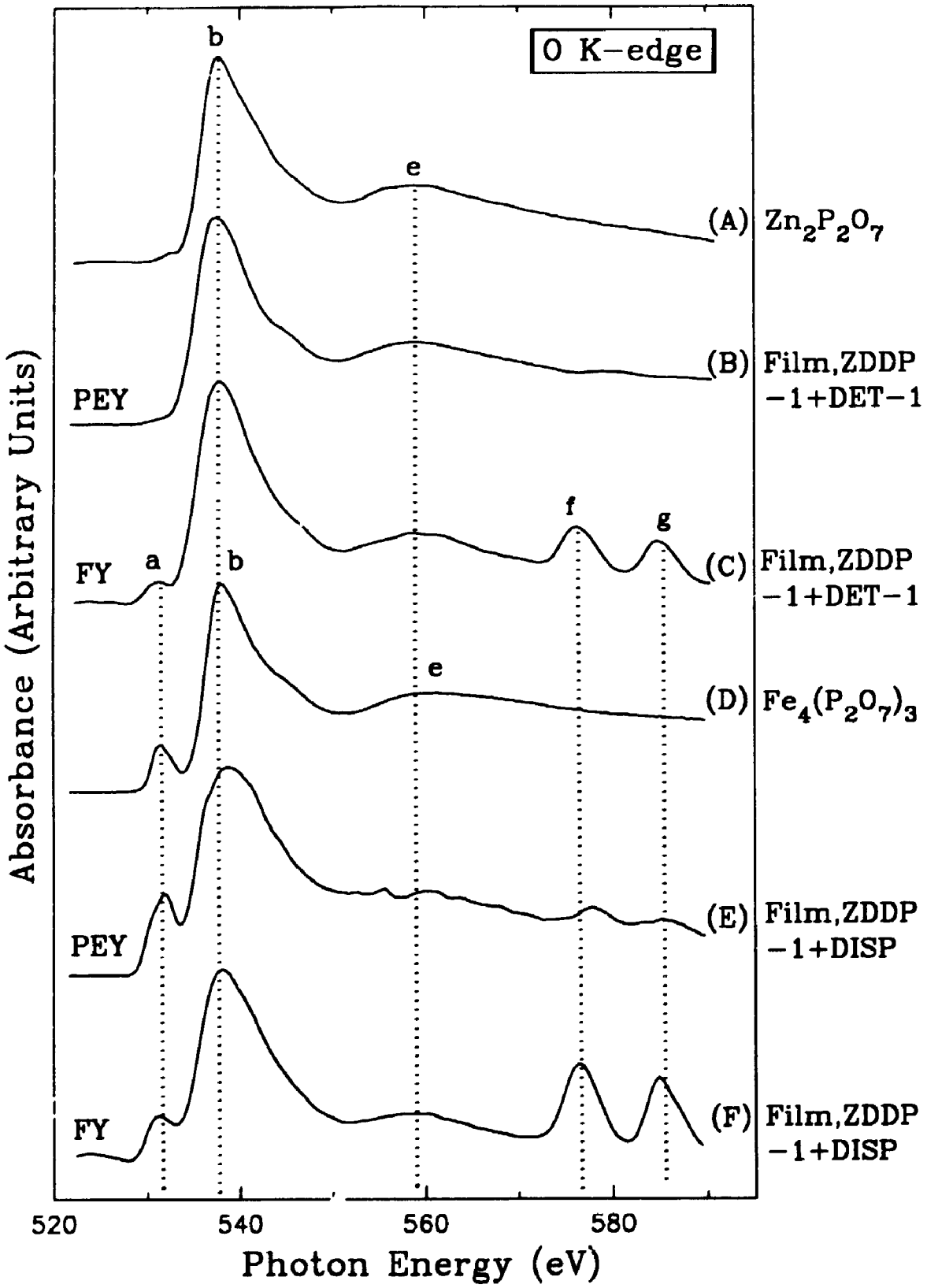

Figure 5.2.10 O K-edge spectra of the film formed from ZDDP-1 plus 2 wt. % DET-1 in both PEY and FY modes

film. However, the FY (C) spectrum shows peak *a* and indicates that Fe is indeed associated with the bulk film either as oxide or phosphate. It should be pointed out that peaks *f* and *g* at high energy region originate from the Cr L-edge, which is a component of the steel substrate (Chapter 2). Willermet and coworkers[43] found that when the film was generated from ZDDP alone, Zn^{2+} was the cation; but when ZDDP was mixed with Mg detergent, Mg partially replaced Zn in the film. Barcroft and Park's hot-wire adsorption studies[44] showed that when Ca sulphonate is added to ZDDP, a substantial amount of calcium was incorporated into the deposited layer. They have reported the presence of calcium and zinc pyrophosphate in the deposited layer, with Ca pyrophosphate dominating. In general, their work is in agreement with these results. Although the chemical environment of Ca remains unclear, these results show that the presence of Ca in the top layer of the film is certain.

The issue of interaction of ZDDP with sulphonate detergent is controversial. In the earlier studies, it was hitherto considered to be antagonistic[45,46]. This was because the sulphonate was believed to retard the decomposition of ZDDP which was presumably the rate-determining step of the antiwear action of ZDDP. However, recent work by Rounds[47] indicated that basic sulphonate detergent gave extremely good synergistic enhancement to the antiwear action of ZDDP. The explanation was that the sulphonate residue forms a paste-like structure with ZDDP on the contact surface, thus forming a firm antiwear layer. But he found that the neutral sulphonate detergent had essentially no effect on wear. The antiwear mechanism of ZDDP in the presence of calcium sulphonate detergent has been studied by Kapsa et al[19]. They found that the presence of calcium sulphonate, either basic or neutral, induced a wear rate increase. The comparison of neutral and over based detergent showed that the ZDDP/detergent antagonism seems to be emphasized by the presence of the overbasing agent. The Auger analysis results lead to a conclusion that the surface coating composition is slightly different from using ZDDP alone. This is probably due to the decrease of effective concentration of ZDDP caused by interaction of ZDDP with the neutral detergent. Willermet and coworkers[16] found that when detergent and dispersant were present along with ZDDP in the system, the polyphosphate chain length was reduced. The results of this thesis indicates that addition of calcium sulphonate detergent has little effect on the

polymerization of phosphate. Lower polymerization may be due to the addition of dispersant in Willermet's research, which is also supported by Inoue and Watanabe's studies[18]. They concluded that there was no interaction between detergents and ZDDP. However, they found a strong interaction between dispersant and ZDDP.

5.2.4 Interaction of ZDDP-1 with calcium phenate

The effects of basic calcium phenate detergent (DET-2) mixed with ZDDP-1 have been studied. The detergent additives are commonly introduced as neutral or basic salts. The basic salts are used to neutralize any acidic products formed from the degradation of base oil. Thus it prevents deposits to be formed on metal surfaces. The P L-edge spectra of the films from ZDDP-1 plus DET-2 in different concentration are demonstrated in Figure 5.2.11. Spectra (A) (0.5 wt.%), (B) (1.0 wt.%) and (C) (2.0 wt.%) were measured in TEY mode and spectra (D), (E) and (F) for the same samples were recorded in FY mode. From the shoulder of peak *a* it can be concluded that, even in the lowest concentration, 0.5 wt.% (A), there is no obvious ZDDP signal. The spectrum (A) in the figure is similar to spectrum (F) in Figure 5.2.7 and arises from a long chain linear polyphosphate or a cyclic phosphate. With increasing concentration, the relative intensities of the pre-edge doublets decrease. From Table 5.2.1 and using calibration curve in Figure 3.1.10, the chain length of phosphates in the films are estimated and they decrease from > 44 in (A) to 8 ± 1 in (B) and further to 5 ± 1 in (C).

This trend is followed in the FY mode. The intensities of peaks *a* and *b* in the FY measurements are noticeably smaller compared with the TEY measurements. This immediately tells us that the polyphosphate chain lengths are shorter in the FY spectra. The chain lengths in spectra (D), (E) and (F) are estimated at 12 ± 1, 7 ± 1 and ~1, respectively. Thus, the topmost surface measured by TEY contains relatively long chain polyphosphates and the bulk of films measured by FY contains mostly shorter chain phosphates. Since the FY signal is relatively strong, it indicates that the films formed with calcium phenate are relatively thick (several hundred angstrom).

The S L-edge XANES spectra measured in TEY (not shown) indicated that S for all concentrations was in the sulphide form. The S signal was too weak to be detected by FY mode, which indicates that sulphur species are only present on the topmost part

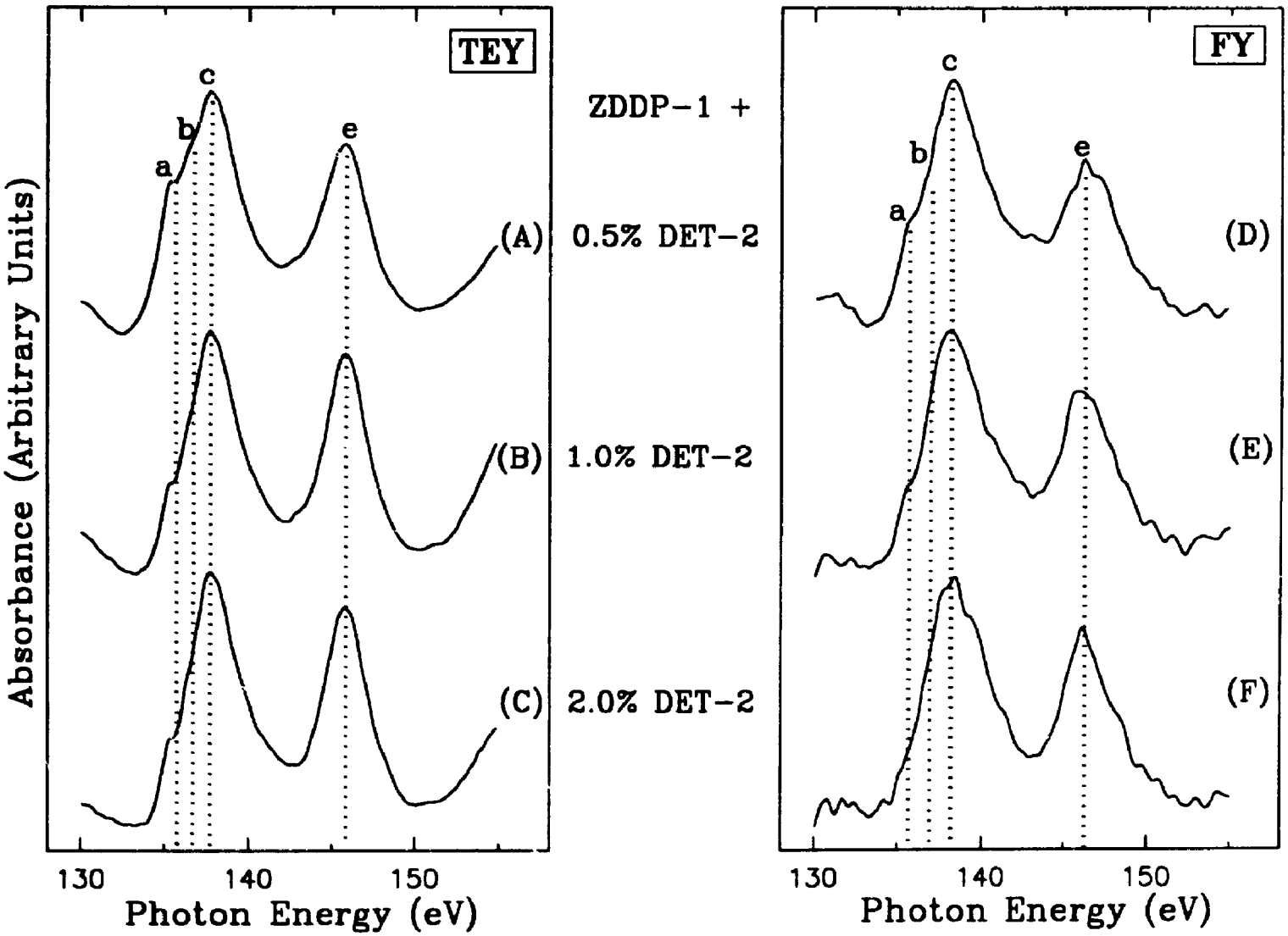

Figure 5.2.11 P L-edge spectra of the films formed from ZDDP-1 plus DET-2 in different concentrations measured in TEY mode (left) and FY mode (right)

of the film.

5.2.5 Interaction of ZDDP-1 with dispersant

Dispersants refer to those additives which disperse sludge formed in engines operated at relatively low temperatures. Common dispersant additives include N-substituted long chain alkenyl succinic derivatives of amines, a specific example being polyisobutylene succinic anhydride polyamide (DISP).

In this study, three concentrations of dispersant, varying from 1.0 wt.% to 5.0 wt.% were used to form films with ZDDP-1. The P L-edge spectra of these films are shown in Figure 5.2.12. The ZDDP-1 concentration for all experiments was 1.2 wt.% in oil. It is noticed from the spectra (A-C) that for all the concentrations used, no significant ZDDP signal can be detected. Thus with the addition of dispersant, as observed for DET-1 (at higher concentration) and DET-2, the dispersant has removed ZDDP from the film. Comparing spectra (A), (B) and (C) and using calibration curve in Figure 3.1.10, the chain lengths of polyphosphates in the films were estimated at $\sim 41 \pm 4$, $\sim 13 \pm 1$ and $\sim 13 \pm 1$, respectively. Since there is no further reduction from 2 wt.% to 5 wt.%, the effective concentration of dispersant to alter phosphate chain length in the system should be ~ 2 wt.%. Ramakumar et al[17] have studied the optimum concentration of dispersants to be used with ZDDP. The detergency characteristics of the dispersant increased with concentration, and levelled off after the concentration reached 4 wt.%. At the same time, the wear scar diameter (WSD) increased as the concentration increased to 4 wt.% but levelled off above 4 wt.%. These findings are similar to this work although the effective concentrations are different. When the concentration of DISP increases, polyphosphate chain length decreases and wear rate may increase.

The dispersant had a strong effect on the amount of phosphorus and sulphur detected in the film. As demonstrated in Table 5.2.3, both the P and the S signals are very weak compared with the case where ZDDP was used alone. However, the weak signal detected in the film confirmed that sulphur was in the reduced sulphide form. When spectra were recorded in the FY mode, neither S nor P signals could be detected at dispersant concentration of $>$ 1 wt.%. This result implies that AW films formed with dispersant present are much thinner than either films generated using ZDDP alone or

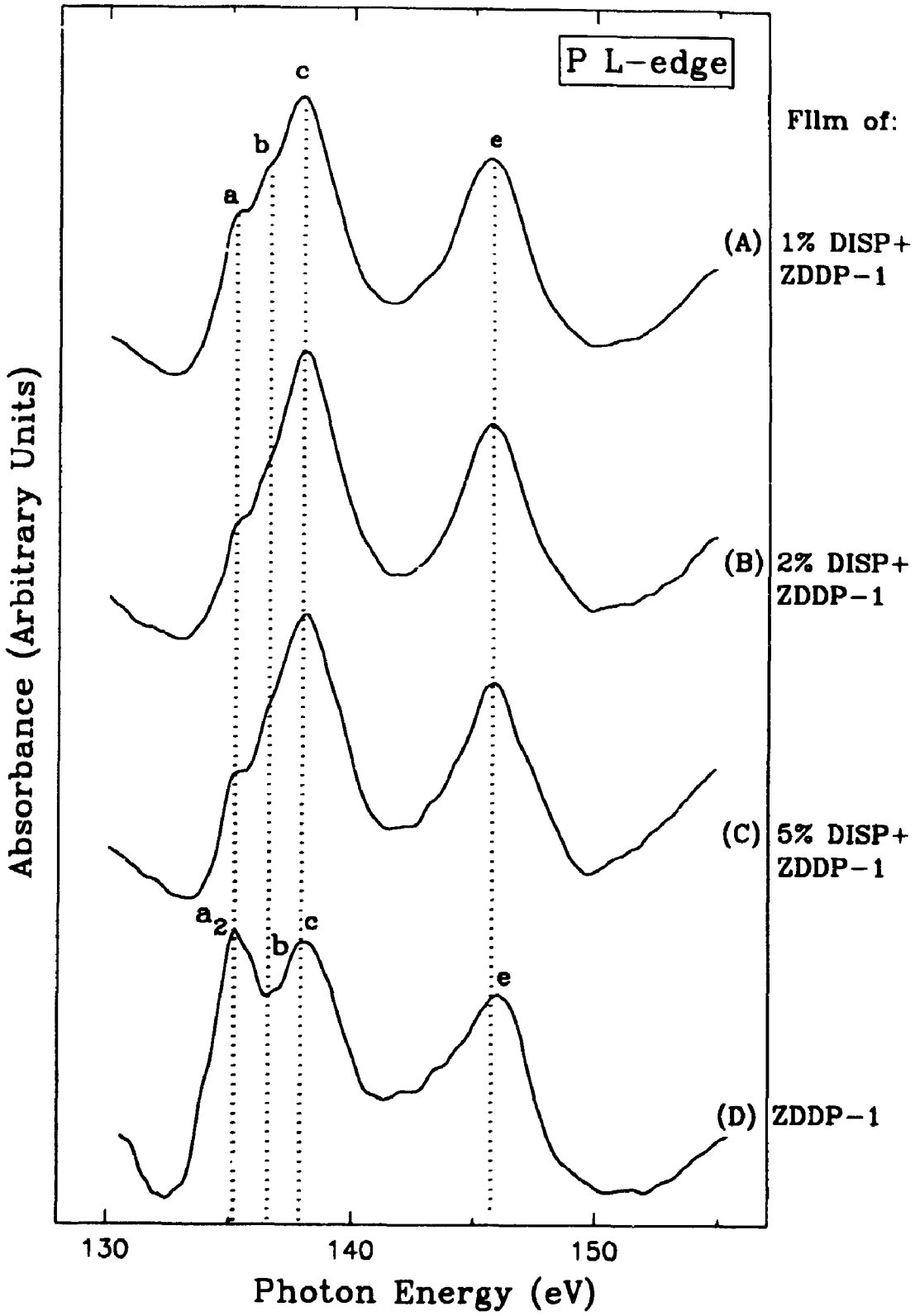

Figure 5.2.12 P L-edge spectra of the films formed from ZDDP-1 plus DISP in different concentrations

ZDDP plus detergents.

Comparing O K-edge spectra measured in PEY and FY (Figure 5.2.10, E and F), it is noticed that peaks *f* and *g* intensities are much weaker in the PEY spectrum. These peaks originate from the Cr L-edge spin-orbit splitting from Cr in the steel coupon, the substrate. Once again, this confirms that the film is relative thinner than the film formed using only ZDDP, which is consistent with the P and S L-edge analysis. The presence of iron in the AW film as a cation is in agreement with Martin et al.'s investigations[37]. In their EXAFS studies of wear debris, they found the formation of iron polyphosphate.

Similarly, a ZDDP-dispersant pair also enjoy a dual reputation in the existing literature. In a hot-wire experiment, Barcroft[44] found that the presence of a succinimide dispersant reduced the film formation rate and film thickness. This could be due to the interaction between ZDDP and dispersant, modifying the behaviour of the ZDDP, or merely a reflection of the dispersant competing effectively for adsorption sites on the metal surface. Several investigators[22,24,48] reported that ZDDP formed an association complex with an amino group of succinic type dispersant, and this complexation had been proved to be antagonistic to antiwear action. Rounds[47] has concluded that addition of dispersant destroys the synergism of ZDDP with sulphonate detergent. However, Forbes[49] have concluded that association of dispersants and ZDDP helps the adsorption of ZDDP on the surface and thus has improved the antiwear performance of the additives. Another investigation made by Harrison et al.[2] concluded that the formation of a chelating compound in ZDDP and dispersant system would decrease the adsorption rate of ZDDP on steel surface, making the engine oil last longer. Shirahama and Hirata[46] found that a combination of ZDDP and dispersant resulted in good antiwear performance regardless of the poor AW characteristics of the dispersant itself. Besides the complexation mechanism, Gallopoulos et al[48] proposed a reaction mechanism. They reported the reaction of ZDDP and dispersant, producing ionic phosphorodithioates that could be detected by IR spectroscopy.

5.3 Depth profiling and wear scar measurements

5.3.1 Depth profiling

In surface science, the composition distribution is much more meaningful than merely the average composition. In principle these "depth profiles", as well as the chemical composition as a function of depth, are obtained by any technique which allows a separation of the analytical information with respect to distance perpendicular to the solid surface[50]. The depth distribution of chemical composition can be obtained by bombarding the surface with energetic ions (> 100 eV). In general, noble gas ions (Ar^+) are used because disturbing chemical reactions should be avoided. Due to the successive sputtering of surface layers, deeper layers are exposed and can be readily analyzed by a surface-sensitive method such as XPS and AES. A perquisite for the measurement of depth profiles is a constant erosion rate within the analyzed area. In XPS and AES, this condition is easily achieved because the analyzed area is much smaller than the primary ion beam diameter. Several groups have measured AW film thickness using XPS[51,52,53,54] and AES[54,55,56,57,58,59,60,61] spectroscopies.

In order to estimate quantitatively the AW film thickness, selected films were examined with X-ray photoelectron spectroscopy (XPS). From the XPS data, Zn, S, P, C, O, and a small amount of Fe were present on the surface. The film then was Ar^+ sputtered at different intervals and the photoelectron spectra were recorded. In Figure 5.3.1 the atomic percentages of Zn, S, P, O and Fe of a ZDDP-1 film generated in 12 hours are plotted versus the sputtering time. As noticed from the figure, S and P have similar proportions. The Fe proportion is very small to begin with, but increases very rapidly as the sputtering proceeds. The initial high percentage of C is likely due to the surface contamination mainly from the base oil. With the Ar^+ sputtering (ion energy is 4 keV) in the first 10 seconds, the percentage of C dropped quickly, and thus the percentages of other elements monitored increased.

As a comparison, another AW film generated from ZDDP-1 in 30 minutes has also been measured. The depth profiling result is shown in Figure 5.3.2. In 12 hour film (Figure 5.3.1), it took 320 seconds sputtering to reach a 50% iron signal. In the 30 minute film, the time needed to reach the same level is only 30 seconds. It is confirmed that the AW film formed in longer time is thicker than that formed in short time, which is discussed in section 4.2.1. From this information and using SiO_2 as a reference it might be concluded that the average thickness of the film is a few hundred

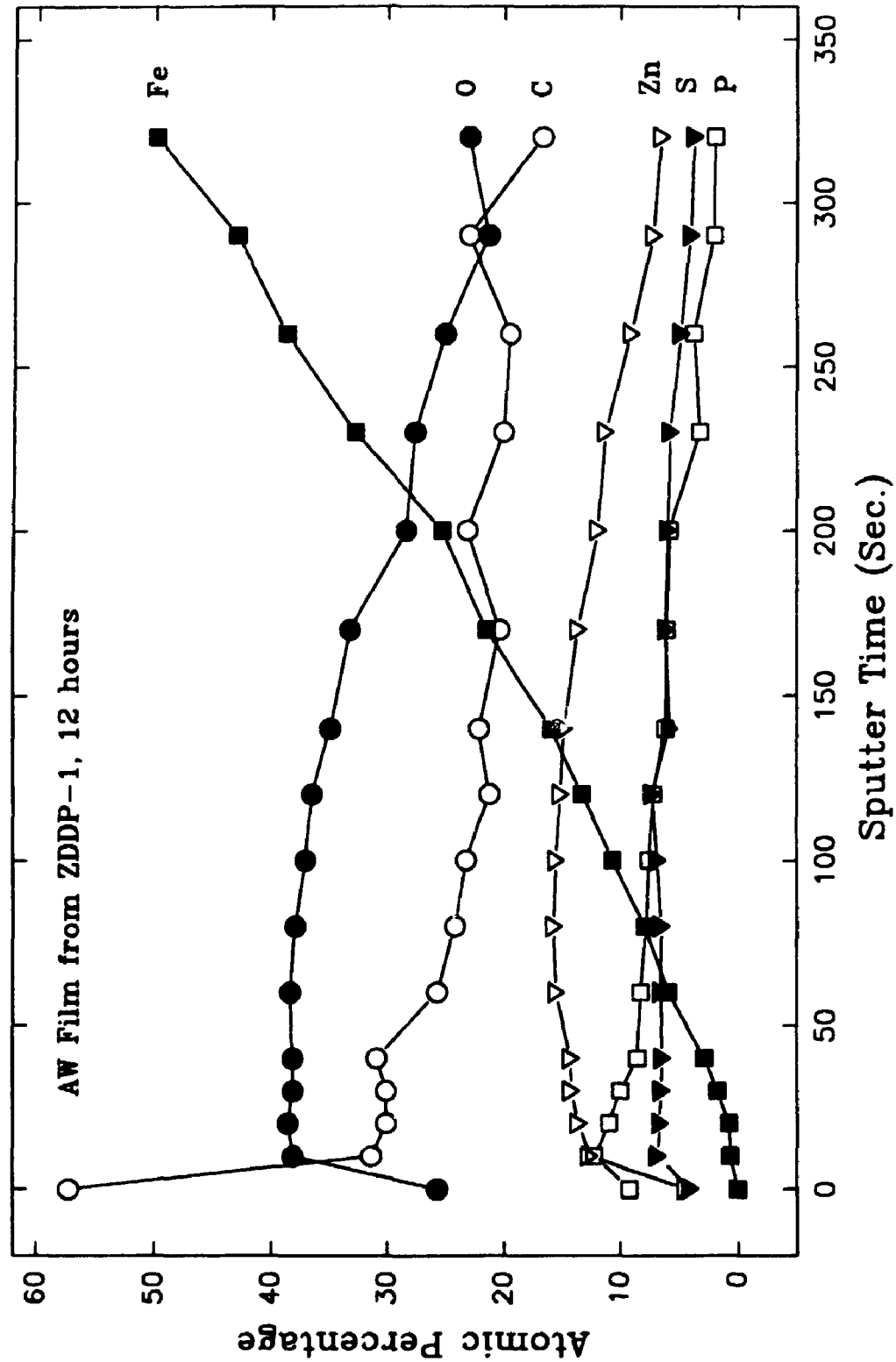

Figure 5.3.1 XPS depth profiling of ZDDP-1 film formed in 12 hours

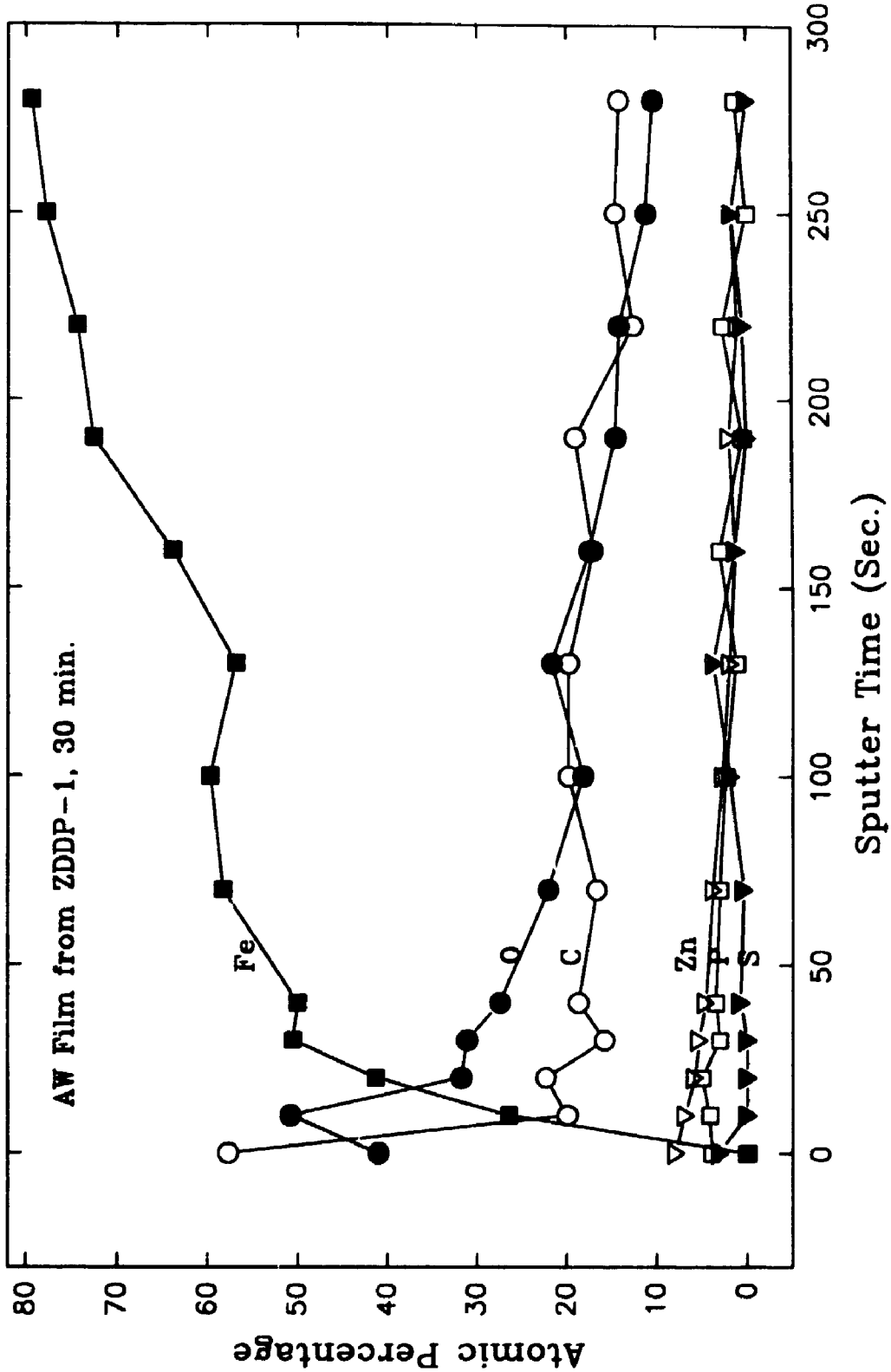

Figure 5.3.2 XPS depth profiling of ZDDP-1 film formed in 30 minutes

angstroms.

From the XPS results, atomic ratio of O/P and O/S are different from the original additives. In the additives, the O/P ratio is 2 and O/S ratio is 1, while in the films the oxygen content is significantly larger. It is another evidence that the films are derived from the decomposition products of the additive. The composition of the film varied with the composition of the original additives.

Unfortunately, due to the rough surface and inhomogeneity of the films, and also due to the limited sensitivity and resolution of the techniques, detailed layer analysis is impossible at this stage. It should be point out that since there was not a suitable reference material to quantify the sputtering rate, all depth profiling measurement cannot be very accurate. Further work is required to better quantify these results.

5.3.2 Wear scar measurements

All the spectroscopic measurements presented so far have been done on a steel coupon surface. The film area on the pin was too small for convenient XANES measurements. However, in a few cases, the film on the pin and the coupon were compared and found to give similar results. In order to find the relationship between the wear scar width and phosphate chain length, some of the wear scars on the pin have been measured using an optical microscope (Chapter 2). For the wear measurements, the pins were used, since the wear scars on the pins are smaller and more easily measured and compared.

Table 5.3.1 summarizes the results of wear scar width measurements. In the last column, the phosphate chain length from P L-edge XANES spectra of the coupons corresponding to the pins are listed. From sample (1) to sample (7), the time effect has been examined. It can be concluded that: 1. Most of the wear occurs in first five minutes before film formation; 2. The wear after twelve hours is not substantially larger than after 2 hours (with the exception of the 6 hour sample); 3. Phosphate formation is critical for antiwear performance; 4. The most interesting finding is in the film formed in the two stage film (section 4.2.1). It has been found that the phosphate in this film is a short chain phosphate. In most cases when the film was thick enough for FY measurements, it was found that the bulk consisted of short chain polyphosphate and only

Table 5.3.1 Wear scar widths and chain lengths of some AW films

Number	Film description*	Scar Width (±20 μm)	Chain Length**
1	ZDDP-1, 5 min	155	ZDDP
2	ZDDP-1, 2 hr.	148	V. Long
3	ZDDP-1, 6 hr.	254	Long
4	ZDDP-1, 0.5 + 5.5 hr.(BO)	182	Short
5	ZDDP-1, 12 hr.	144	V. Long
6	ZDDP-1, 12 hr.	174	V. Long
7	ZDDP-1, 12 hr.	163	V. Long
8	ZDDP-1 + DISP, 5 min	133	ZDDP
9	ZDDP-1 + DISP, 30 min	143	Short
10	ZDDP-1 + DISP, 6 hr.	260	Short
11	ZDDP-1 + DISP, 0.5+5.5 hr.(BO)	172	Short
12	ZDDP-1 + DISP, 12 hr.	336	Medium
13	ZDDP-1, Polished, 30 min.	108	V. Long
14	ZDDP-1, Polished, 12 hr.	96	Long
15	ZDDP-1, 40 N	50	ZDDP
16	ZDDP-1, 400 N	136	Long
17	ZDDP-2, 6 hr.	172	Long
18	ZDDP-4, 6 hr.	160	Short
19	ESSO Aryl-ZDDP, 6 hr.	989	Short

* If it is not indicated, the variables for film generation are: 100 °C, 25 Hz, 225 N, 30 minutes.

** Chain lengths of phosphates are estimated from P L-edge XANES spectra.

Short	≤ 3
Medium	4-10
Long	10-25
Very Long	> 25

the surface film was composed of long chain polyphosphate. This observation shows that when the film with long chain polyphosphate is rubbed in base oil, the top surface is either removed or converted to short chain polyphosphate. This process does not have any effect on the scar widths! This result shows that after the film has been formed initially, it can provide the AW function for a long time when there is no more ZDDP in the solution. The same trend has been found in the films from ZDDP-1 plus DISP. When the rubbing time increased from 5 minutes (8) to 12 hours (12), the wear scar widths increased from 133 to 336 μm. The wear after 12 hours with dispersant is larger than that without dispersant. However, the film formed in two stages (11) keeps a lower wear rate (172 μm). It seems that after the film is formed on the steel surface, clean oil without additives provides better AW effectiveness than the old oil. It is also interesting to note that the wear with the DISP is larger than that without DISP while the thickness of the film decreases and the chain length decreases with DISP. In a four ball machine test, Plaza[29] reported that when a secondary butyl ZDDP was used as additive, the wear scar diameter increased with rubbing time. But the increase was sharp in the first 30 minutes and levelled off afterward. Considering the initial contact area is much smaller in four ball experiment than that in Cameron-Plint test, the two results are generally consistent.

On the polished surface, sample (13) and (14) represent the films formed in 30 minutes and 12 hours, respectively. Their wear scar widths are very close (108 and 96 μm), which shows that the surface is protected better on a polished surface than on a rough surface although they all contain long chain phosphates. Much of the initial wear must be associated with wearing down the asperities on the rough surface.

The wear rate is also affected by the load applied on the surface during rubbing. Under 40 N (15), the wear scar width is only 50 μm, while under 400 N (16), the width is 136 μm. This result is in agreement with Rounds' studies[62,63]. The higher the load, the worse the wear.

From previous measurements[3,64,65,66], antiwear performance of different ZDDPs should be in the order of secondary ZDDP > primary ZDDP > aryl ZDDP. In this work, no difference has been found between the secondary ZDDP, ZDDP-2 (17) and the primary ZDDP, ZDDP-4 (18). The striking difference has been found between alkyl

ZDDPs and aryl ZDDP. When an aryl ZDDP was used as additive (19), the wear scar width (989 μm) is much wider than for other additives used. It indicates that aryl ZDDP provides much worse surface protection than alkyl ZDDP. This may be related to the slow decomposition of the aryl ZDDP and thus slow the formation of AW film. From the above results, it seems that short and long chain polyphosphates provide equally good AW films once a critical thickness of film is formed.

5.4 Conclusions

Employing L-edge XANES spectroscopy, the chemical states and the local environments of phosphorus and sulphur in antiwear films produced by antiwear agents have been investigated. Comparing the L-edge XANES spectra of the films with the spectra of model compounds with known structures, it has been possible to speciate the chemical nature of P and S in the antiwear films. Especially from the P L-edge, relative polyphosphate chain length can be estimated.

1. The chemical state of phosphorus in the film of secondary IP-ZDDP corresponds closely to that of metaphosphate, a polyphosphate with a cyclic structure or a very high chain length linear polyphosphate. The chemical state of sulphur in the same film is mostly in the reduced form and for the most part, resembles ZnS. The chemical nature of the film produced by primary ZDDP is different from the secondary ZDDP. The phosphorus state in the film is similar to a shorter chain polyphosphate rather than a cyclic phosphate or a long chain linear polyphosphate. The spectrum of the S L-edge corresponds closely to alkyl sulphide or ZnS.

2. The effect of Zn in the antiwear agent is very significant. The chemical nature of sulphur and phosphorus, in the films of IP-DDP and NB-DDP in the absence of Zn, is quite different from those with Zn. It seems that Zn acts as an antioxidant for sulphur and also promotes the polymerization of phosphates. These properties are more significant for secondary ZDDP than for primary ZDDP.

3. The interaction between ZDDP and calcium sulphonate detergent has been examined. The presence of detergent reduces the amount of unreacted ZDDP on the rubbing surface, either by decreasing the adsorption of ZDDP on the surface or catalyzing the decomposition of ZDDP on the surface. The addition of the detergent

does not apparently change the polymerization of phosphate in the antiwear films. The S signals are much weaker than P signals and sulphur is in the reduced sulphide form.

4. The interaction of DET-2 with ZDDP is different from DET-1. No ZDDP signal can be detected even at lower concentration 0.5 wt.%. However, the chain length of polyphosphate decreased with increasing concentration of DET-2. Different chain lengths measured from TEY and FY mode imply that the polymerization is altered from surface to bulk. Sulphur is again present as sulphide.

5. The addition of polyisobutylene succinic anhydride polyamide dispersant decreases the polymerization of phosphates in the films. When the concentration of the dispersant increased to higher than 1 wt.%, the films formed on the steel surface are too thin to be detected by FY mode. The sulphur signal is much weaker, but sulphur is most likely in the form of a sulphide again.

6. Depth profiling results from XPS showed that the AW film thickness is a few hundred angstroms, which is in agreement with other investigations. It is found that the 12 hour film is thicker than the 30 minute film.

7. The measurements of wear scar widths have been compared with the XANES study and the results of other researchers. Most of the wear comes from the initial rubbing (a few minutes). After the film is formed on the surface, further rubbing will not increase the wear rate significantly. More work is needed to better reveal the relation between chemical nature and antiwear effectiveness.

5.5 References

1. Jones, R.B., Coy, R.C. *ASLE Trans.*, 1981, 24, 91

2. Harrison, P.G., Brown P., McManus, J. *Wear*, 1992, 156, 345

3. Rowe, C.N., Dickert, J.J. Jr. *ASLE Trans.*, 1967, 10, 85

4. Willermet, P.A., Kandah, S.K. *Lubrication Science*, 1993, 5, 129

5. Paddy, J.L., Lee, N.C.J., Waters, D.N., Trott, W. *Tribol. Trans.*, 1990, 33, 15

6. Bridgewater, A.J., Dever, J.R., Sexton, M.D., *J. Chem. Soc.* Perkin II, 1980, 1006

7. Howard, J.A., Ohkatsu, Y., Chenier, J.H.B., Ingold, K.U. *Can. J. Chem.*, 1973, 51, 1543

8. Coy, R.C., Jones, R.B. *ASLE Trans.*,1981, 24, 77

9. Barcroft, F.T., Bird, R.J., Hutton, J.F., Park, D. *Wear*, 1982, 355, 384

10. Plaza, S. *ASLE Trans.*, 1987, 30, 233

11. So, H., Lin, Y.C., Huang, G.G.S., Chang, T.S.T. *Wear*, 1993, 166, 17

12. Gergel, W.C., presented at the *International Symposium, Technical Organic Additives and Environment*, Interlakes, Switzerland, 1984

13. Sieber, I., Meyer, K., Kloss, H., *Wear*, 1983, 85, 43

14. Bell, J.C., Delargy, K.M., Seeney, A.M. *Proceeding of the 18th Leeds-Lyon Symposium on Tribology*, Lyon, France, September 1991, Elsevier, Amsterdam, Holland, 1992

15. Bell, J.C., Delargy, K.M. *6th International Congress on Tribology "Eurotrib 93"*, Budapest, Hungary, August 30 to September 2, 1993

16. Willermet, P.A., Dailey, D.P., Carter III, R.O., Schmitz, D.J., Zhu, W., Bell, J.C., Park, D. To be submitted to *Tribology International*

17. Ramakumar, S.S.V., Rao, A.M., Srivastava, S.P. *Wear*, 1992, 156, 101

18. Inoue, K., Watanabe, H. *ASLE Trans.*, 1983, 26, 189

19. Kapsa, Ph., Martin, J.M., Blanc C., Georges, J.M. *ASME Trans.*, 1981, 103, 486

20. Rounds, F.G. *ASLE Trans.* 1975, 18, 79

21. Dickert, J.J. Jr., Rowe, C.N., *J. Org. Chem.*, 1967, 32, 647

22. Rounds, F.G., Proc. *5th Int. Colloq. on Additive for Lubricants and Operation Fluids*, Esslingen, Germany, 1986, p4.8-1

23. Silver, H.B., *Tribol. Int.*, 1978, 11, 185

24. Shiomi, M., Tomizawa, H., Kuribayashi, T., Tokashiki, M. *Proc. 5th Int. Colloq. on Additive for Lubricants and Operation Fluids*, Esslingen, Germany, 1986, p3.7-1

25. Rounds, F.G., *ASLE Trans.*, 1981, 24, 434

26. Spedding, H., Watkins, R.C. *Tribol. Int. 1982*, 15, 9

27. Molina, A. *ASLE Trans.* 1987, 30, 479

28. Glaeser, W.A., Baer, D., Engelhardt, M. *Wear*, 1993, 162, 132

29. Plaza, S., Kajdas, C. *Wear*, 1994, 176, 1

30. Bird, R.J. and Galvin, G.D. *Wear*, 1976, 37, 143

31. Brown, J.R., Kasrai, M., Bancroft, G.M., Tan, K.H., Chen, J.M. *Fuel*, 1992, 71, 649

32. Huffman, G.P., Mitra, S., Huggins, F.E., Shah, N., Vaidya, S., Lu., F. *Energy and Fuel*, 1991, 5, 574

33. Kasrai, M., Fleet, M.E., Bancroft, G.M., Tan, K.H., Chen, J.M. *Phys. Rev. B*, 1991, 43, 1763

34. Rhodes, K.L., Stair, P.C. *J. Vac. Sci. Technol. A*, 1988, 6, 971

35. Rhodes, K.L., Stair, P.C. *Tribol. Trans.*, 1993, 36, 27

36. Belin, M., Martin, J.M., Mansot, J.L., *Tribol. Trans.*, 1989, 32, 410

37. Martin, J.M., Belin, M., Mansot, J.L., Dexpert, H., Lagarde, P. *ASLE Trans.*, 1986, 29, 523

38. Cao, L.L., Sun, Y.M. Zheng, L.Q. *Wear*, 1990, 140, 345

39. Jahanmir, S.J., *J. Tribol.*, 1987, 109, 577

40. Willermet, P.A., Kandah, S.K., ASLE Trans., 1984, 27, 67

41. Kasrai, M., Brown, J.R., Bancroft, G.M., Yin, Z., Tan, K.H. Submitted to *Int. J. Coal Geology*

42. Kasrai, M., Yin, Z., Bancroft, G.M., Laycock, K.F., Tan, K.H., Feng, X.H. *Proceeding of the European Academy of Surface Technology*, p.79-85, 1994, Eugen G. Leuze Verlag, Saulgag/Württ.

43. Willermet, P.A., Dailey, D.P., Carter III, R.O., Schmitz, P.J., Zhu, W. To be submitted to *Tribology International*

44. Barcroft, F.T., Park, D. *Wear*, 1986, 108, 213

45. Rounds, F.G. *ASLE Trans.*, 1978, 21, 91

46. Shirahama S., Hirata, M. *Proc. 5th. Int. Colloq. on Additive for lubricants and Operational Fluids*, Esslingen, Germany, 1986

47. Rounds, F.G. *Lubr. Eng.*, 1989, 45, 761

48. Gallopoulos, N.E., Murphy, C.K. *ASLE Trans.*, 1991, 14, 1

49. Forbes, E.S., *J. Colloid Interface Sci.*, 1971, 33, 629

50. Benninghoven, A. *Thin solid film*, 1976, 39, 3

51. Chao, S.-H., Ludema, K.C., Potter, G.E., DeKoven, B.M., Morgan, T.A., Kar, K.K., *Wear*, 1994, 177, 33

52. Rhodes, K.L., Stair, P.C. *Tribol. Trans.*, 1993, 36, 27

53. Bell, J.C., Delargy, K.M., Seeney, A.M. *Proc. 18th Leeds-Lyon Symposium on Tribol.*, sept. 3-6, 1991 (Ed. Dowson, D., et al., Elsevier, New York, 1992), p387

54. Cao, L.L., Sun, Y.M., Zheng, L.Q., *Wear*, 1990, 140, 345

55. Vipper, A.B., Karaulov, A.K., Mischuk, O.A. *Lubrication Sci.*, 1994, 7, 93

56. Lindsay, N.E., Carter III, R.O., Schmitz, P.J., Haack, L.P., Chase, R.E., deVries, J.E., Willermet, P.A. *Spectrochimica Acta*, 1993, 49A, 2057

57. Jahanmir, S. *J. Tribol.*, 1987, 109, 577

58. Sieber, I., Meyer, K., Kloss, H., Schöpke., A. *Wear.*, 1983, 85, 43

59. Willermet, P.A., Kandah, S.K., Siegl, W.O., Chase, R.E. *ASLE Trans.*, 1983, 26, 523

60. Glaeser, W.A., Baer, D., Engelhardt, M. *Wear*, 1993, 162-164, 132

61. Georges, J.M., Martin, J.M., Mathia, T., Kapsa, Ph., Meille, G., Montes, H. *Wear*, 1979, 53, 9

62. Rounds, F. *Tribol. Trans.*, 1993, 36, 297

63. Rounds, F. *ASLE Trans.*, 1985, 28, 475

64. Rounds, F. *Tribol. Trans.*, 1993, 36, 297

65. Habeeb, J.J., Stover, W.H. *ASLE Trans.*, 1987, 30, 419

66. Smolenski, D.J., Kabel, R.H. *SAE Paper* No. 831760, presented at Fuels and Lubricants Meeting, San Francisco, CA, 1983

CHAPTER 6

THERMALLY DECOMPOSED PRODUCTS AND THERMALLY PREPARED FILMS

6.1 Introduction

Thermal decomposition has been considered as the major mechanism for the ZDDP decomposition to give antiwear films. Different methods have been employed to examine the thermal properties of ZDDP. The hot-wire method is one of the most popular methods used in such studies. It involves electrically heating a metal wire which is immersed in oil containing additives. Using this method, Barcroft et al. have studied a ZDDP containing both primary and secondary alkyl groups[1], a primary ZDDP and interaction of ZDDP with other additives[2]. They found that with increasing temperature, S, C and H content on the wire surface were reduced compared with the original ZDDP. The decomposition rate for different ZDDPs with the same number of C in the alkyl group is secondary-ZDDP > normal-ZDDP > Iso-ZDDP[1]. Other additives such as detergent and dispersant may interfere with ZDDP to increase ZDDP's decomposition temperature[2]. Coy and Jones[3,4] heated several small vials containing a known weight of ZDDP solution in a closed oven for 1, 2, 4, 8 and 16 hours at 180 ^{0}C in air. They reported a decomposition rate of ZDDP in the same order as found by Barcroft et al[1].

However, not all experimental results are consistent. In Harrison and Brown's study[5], they immersed a stainless steel disc in an oil containing n-butyl-, iso-butyl-, n-nonyl- and n-decyl-ZDDP at temperatures of 100, 150, 200 and 260 ^{0}C. According to their chemical analysis, several decomposition intermediates were suggested. Their experimental results showed that isobutyl ZDDP decomposed faster than n-butyl ZDDP, which contradicts the findings of other investigators[1,3,4]. Another interesting experiment was reported by Rounds[6]. In his experiment, 100 ml of the test oil plus fifteen 7.9 mm steel balls were placed in a glass test tube within a stainless bomb and 130 ml of the base oil was used as a heat transfer medium between the test tube and the bomb wall. He found that temperature only affected ZDDP decomposition rate but not the nature of the

degradation products. He also concluded that different ZDDP followed different pathways. Spedding and Watkins[7] used a boiling bath to heat a ZDDP to 160 ^{0}C, and 200 ^{0}C in nitrogen atmosphere. Various compounds have been found, but the main products related to AW effectiveness were believed to be zinc polyphosphates and mixed alkyl sulphides.

An oven decomposition test was conducted by Molina[8]. About 50 g of a commercial secondary ZDDP was placed in a test tube and heated in an oven at 200 ^{0}C in air for 1 hour. The residue was used for chemical analysis and an antiwear test. He reported that zinc pyrophosphate was one of the decomposition product and the residue provided better antiwear performance than ZDDP itself.

In this thesis, decomposition experiments in both solid state and in oil were performed. The additives used were: a synthesized secondary isopropyl-ZDDP (IP-ZDDP), a commercial secondary ZDDP (ZDDP-1), a commercial primary ZDDP (ZDDP-3), and ZDDP-1 in conjunction with a calcium sulphonate detergent (DET-1) or a succinic type dispersant (DISP). In order to find the effect of oxygen in the ZDDP decomposition mechanism, the oil decomposition experiments were conducted both in air and nitrogen atmosphere.

6.2 Thermally decomposed products of IP-ZDDP

IP-ZDDP was heated in an oven at 135 ^{0}C and 185 ^{0}C, respectively. During the heating at 135 ^{0}C, the sample colour turned to light brown with release of H_2S. At 185 ^{0}C, the powder first melted and then boiled which was accompanied by a very strong odour. The final product was a brown glassy residue that was collected for further analysis without purification. The elemental analysis results are listed in Table 6.2.1 and will be discussed later.

In Figure 6.2.1, P L-edge spectra of an AW film formed in 5 minutes (A), two thermally decomposed products at 185 ^{0}C (spectrum B) and 135 ^{0}C (spectrum C), a simulated spectrum (D) and the pure IP-ZDDP (spectrum E) are compared. The peak positions of these spectra are documented in Table 6.2.2. The spectrum (B) of the residue from the 185 ^{0}C heat treatment is very similar with that of the tribochemical film formed in five minutes (A) using the same ZDDP. The features in spectrum (B) are

Table 6.2.1 Elemental analysis of thermal decomposition products

Samples	C%	H%	P%	S%	Zn%
IP-ZDDP	29.31 (30.05)	5.80 (5.84)	12.75 (12.92)	26.25 (26.73)	(13.63)
IP-ZDDP in oven, 185 °C, 30 min	10.46	2.42	18.07	22.21	
IP-ZDDP in oil, 200 °C, 1 hr	10.25	2.49	17.79	20.07	
ZDDP-1 in oil, 200 °C, 1hr	12.42	2.79	18.26	19.37	19.34
ZDDP-1 in oil, 200 °C, 1hr, N_2	14.23	2.51	16.42	19.30	21.32

* Calculated values are in parenthesis.

Table 6.2.2 Peak positions of P L-edge spectra from IP-ZDDP thermal films

Samples	a	b	c	d	e
IP-ZDDP	133.7	134.6	135.4	-	140.2
AW film formed in 5 min	135.7	137.1	138.3	-	145.9
Decomposed in oven, 185 °C, 30 min	135.8	136.9	138.2	-	146.0
Decomposed in oven, 135 °C	133.8	134.7	135.4	139.7	145.5

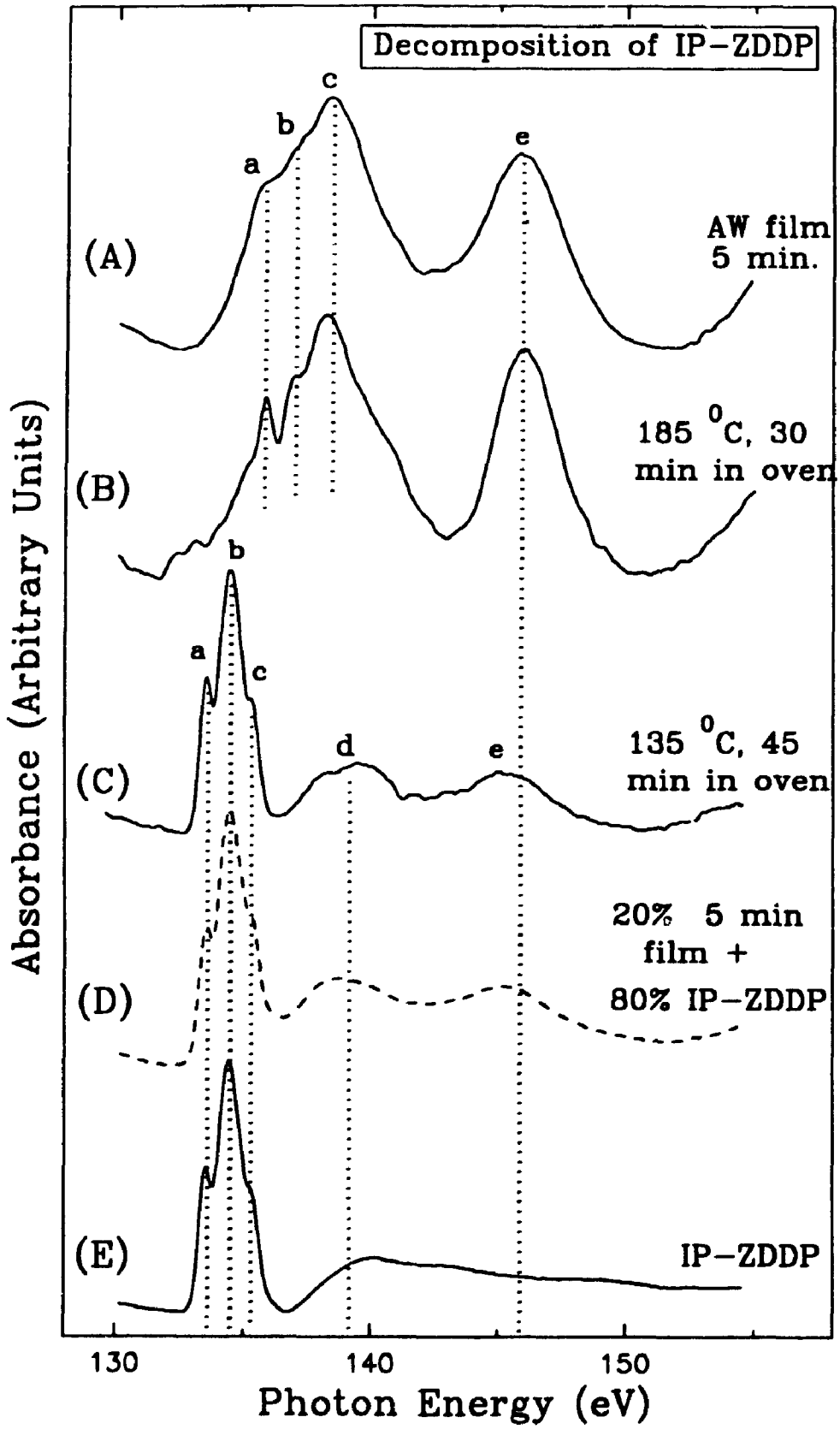

Figure 6.2.1 P L-edge spectra of IP-ZDDP decomposition products from solid state experiments

better resolved and are closer to that of the linear long chain phosphate discussed in section 3.1. The features are less resolved in spectrum (A) due to the intermediates formed in the rubbing process. On the other hand, the spectrum of the 135 ^{0}C residue (C) suggests that only a small portion of the additive has undergone decomposition. Features *a*, *b* and *c* and their positions (Table 6.2.2) are very close to the original ZDDP (Table 6.2.2 and spectrum E). However, the presence of feature *d* and *e*, which are aligned well with peaks *c* and *e* in spectra (A) and (B), indicates the formation of a small amount of phosphate. Indeed, the spectrum (C) can be simulated by digitally combining 80% pure ZDDP (spectrum E) and 20% AW film (spectrum A). This method has been described in Chapter 4 and 5. The simulated spectrum (D) matches spectrum (C) very closely confirming the partial decomposition of ZDDP and formation of phosphates. This result is in agreement with So et al's research[9]. They reported that secondary ZDDP began to chemisorb on a steel surface at temperature below 140 ^{0}C. Hastie et al.[10] in an experiment employing EXAFS spectroscopy also found that a commercial ZDDP decomposed at 135 ^{0}C.

The S L-edge spectra of those residues are compared with pure ZDDP spectrum in Figure 6.2.2. The similarity of spectrum (A) and (B) implies that at 135 ^{0}C most of the ZDDP has not decomposed, which supports the results of the P L-edge spectrum analysis (Figure 6.2.1).

6.3 Thermally prepared films on steel

6.3.1 IP-ZDDP

The thermal decomposition of IP-ZDDP has also been examined in base oil at 150 ^{0}C and 200 ^{0}C. At 150 ^{0}C, the oil remained clear with a yellow colour both in air and in N_2. At 200 ^{0}C, the oil turned dark brown and a buff-coloured precipitate formed in air, which was collected for elemental analysis. But at the same temperature, it turned only a little cloudy when the experiment was carried in N_2. The P L-edge spectra of the films generated in air (left) and in N_2 (right) are compared in Figure 6.3.1. The peak positions of these spectra are listed in Table 6.3.1. Spectra (A) and (B) in Figure 6.3.1 correspond to thermal films formed at 150 ^{0}C, measured in TEY mode and FY modes,

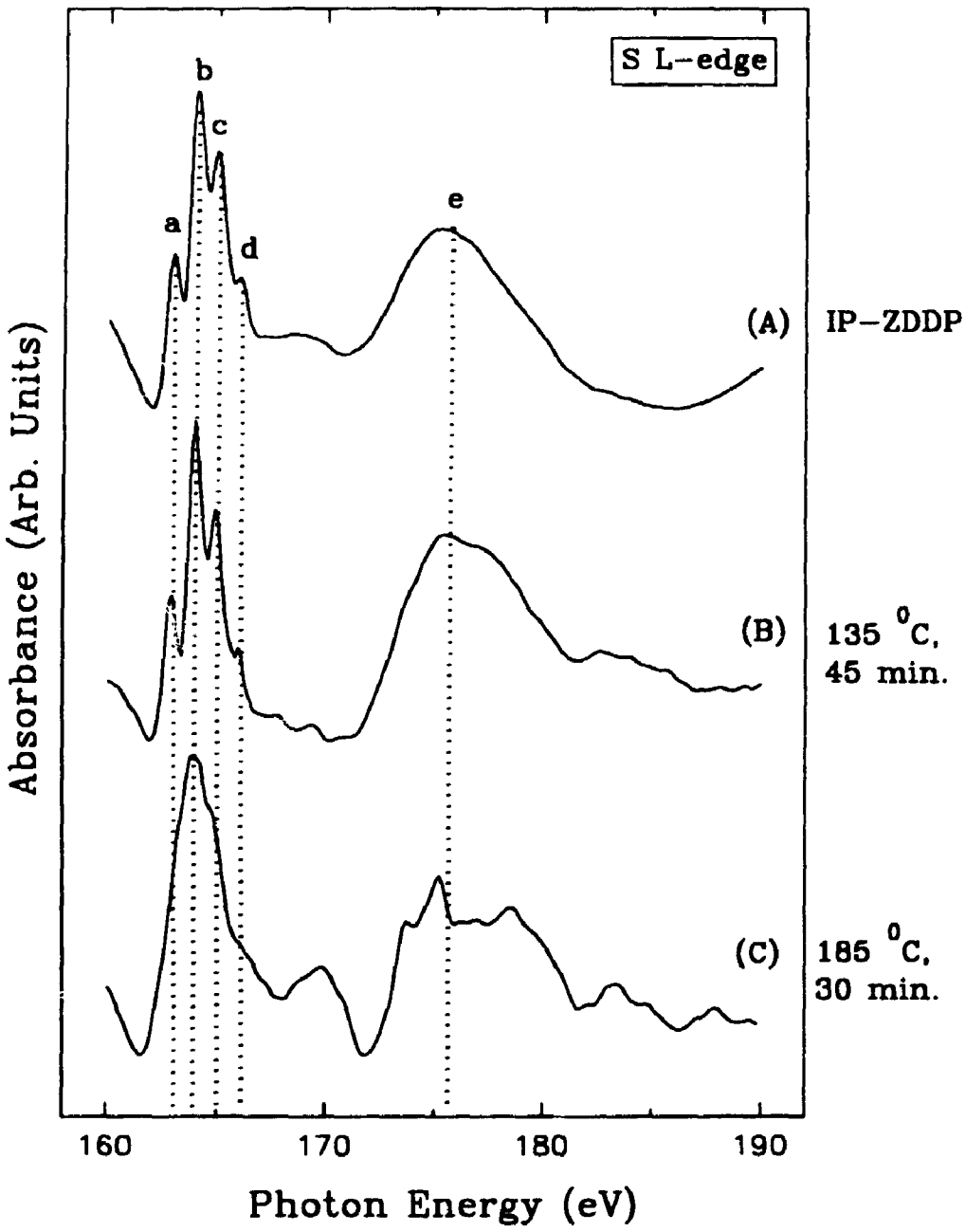

Figure 6.2.2 S L-edge spectra of IP-ZDDP decomposition products from solid state experiments

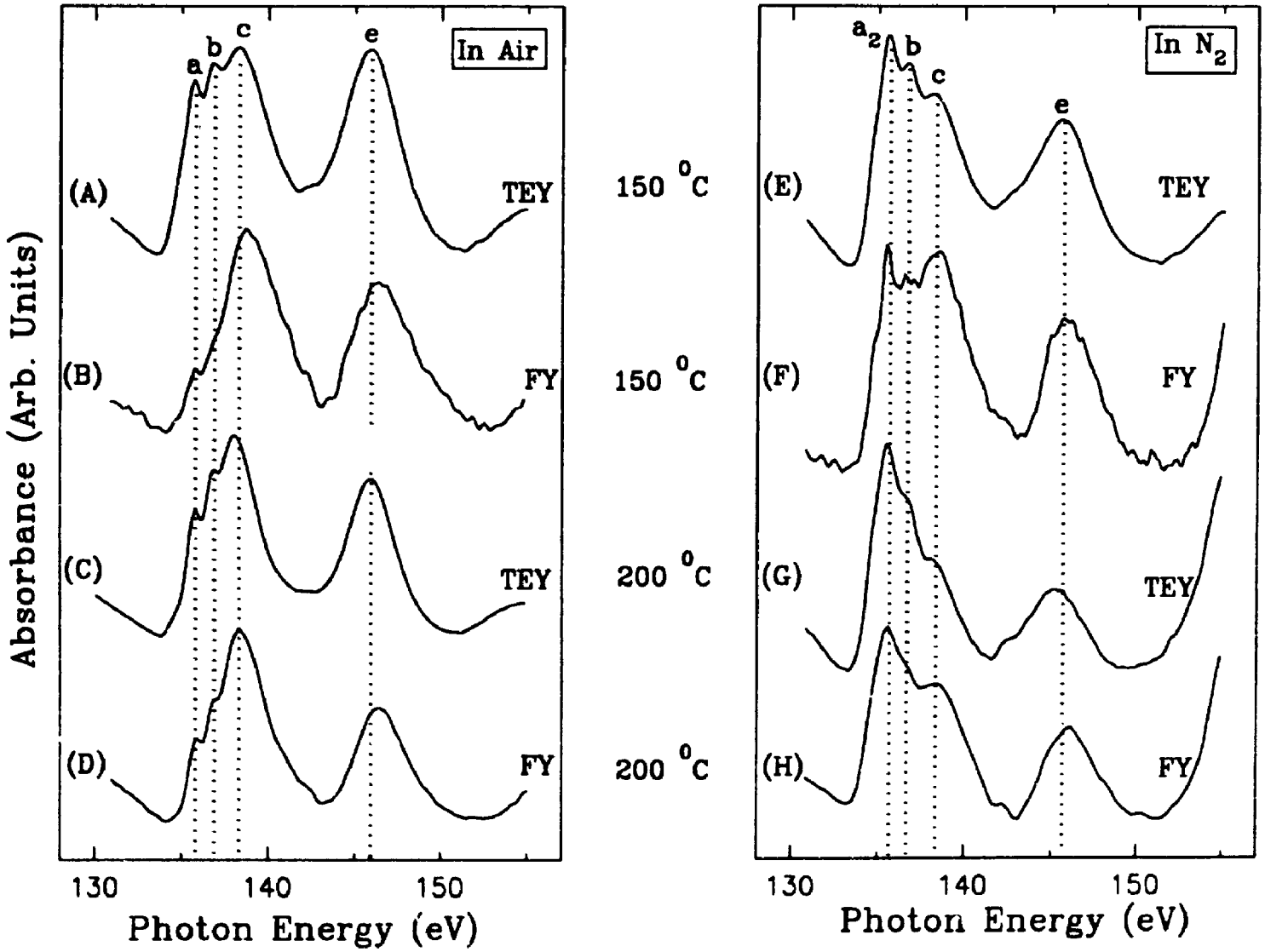

Figure 6.3.1 P L-edge spectra of IP-ZDDP thermal films

Table 6.3.1 Peak positions of P L-edge spectra of thermally prepared films

Films	Peak positions (±0.1 eV)					
	a_2	a	b	c	d	e
IP-ZDDP: 150 °C, TEY		135.6	136.6	138.2		145.8
150 °C, FY		135.8	136.8	138.7		146.3
150 °C, N_2, TEY	135.5		136.7	138.2		145.6
150 °C, N_2, FY	135.5		136.8	138.4		145.9
200 °C, TEY		135.8	136.8	138.0		145.9
200 °C, FY		135.9	136.9	138.3		146.4
200 °C, N_2, TEY	135.5		136.6	138.1		145.2
200 °C, N_2, FY	135.6		136.8	138.4		146.1
ZDDP-1, as is		133.6	134.5	135.3	139.9	
ZDDP-1, 150 °C, TEY	135.3		136.5	138.2		145.6
150 °C, N_2, TEY	134.6				138.6	143.0
200 °C, TEY		135.6	136.5	138.1		145.7
200 °C, N_2, TEY	135.0					143.2
ZDDP-3, 150 °C, TEY		135.8	136.8	138.4		145.7
150 °C, FY					140.0	146.4
150 °C, N_2, TEY	135.3			139.1		145.3
150 °C, N_2, FY	135.6				139.8	146.3
200 °C, TEY		135.8	136.7	138.2		145.9
200 °C, FY		135.2	136.2	138.2		145.9
200 °C, N_2, TEY		135.7	136.7	138.1		145.7
200 °C, N_2, FY		135.9	136.9	138.9		146.5
ZDDP-1 + DET-1						
150 °C, TEY	135.2			138.4		145.8
150 °C, N_2, TEY	135.1			139.2		145.6
200 °C, TEY		136.0	136.9	138.3		146.1
200 °C, FY		136.0	137.0	138.8		146.4
200 °C, N_2, TEY	135.7		136.9	138.0		145.8
ZDDP-1 + DISP						
150 °C, TEY	135.5			138.6		145.8
150 °C, N_2, TEY		135.6	136.7	138.3		145.8
200 °C, TEY		136.1	137.0	138.6		145.9
200 °C, FY					140.1	147.8
200 °C, N_2, TEY		135.9	136.9	138.5		145.7
200 °C, N_2, FY					139.9	146.4

respectively. Similar to the antiwear films discussed in Chapter 4, the film on the steel surface has a layer structure. On the topmost surface as shown in the TEY mode (A), the film is a long chain polyphosphate. Close to the steel surface, a short chain phosphate identified in FY mode is formed (B). A similar situation has been found at 200 ^{0}C, which are demonstrated in spectra (C) and (D), although the difference between surface and bulk composition is not that large.

Comparing these results with those films generated in N_2, it is clear that O_2 plays an important role in ZDDP decomposition. A strong peak a_2 in all spectra (E)-(H) indicates that a good portion of the ZDDP is protected from decomposition in the absence of O_2. Peak a_2 originates at least partly from unreacted ZDDP. Meanwhile peaks *c* and *e*, which correspond to a polyphosphate, indicate that some of ZDDP has been decomposed. No significant change can be observed when the temperature increased. This may imply that when the temperature remains above the ZDDP decomposition temperature, temperature no longer plays an important role in ZDDP decomposition mechanism. Other factors such as O_2 mainly affect the ZDDP's degradation. In general, spectra (E), (G) and (H) are similar. The relative intensities of peaks a_2 and *b* are higher than peak *c*. This kind of spectra are only seen for thermal films. Digital combination of ZDDP and linear polyphosphate failed to simulate these spectra. There are three possible explanations for these observations. First, a network structure of polyphosphates has formed. Zinc metaphosphate is believed to have such a structure[11]. Second, the polyphosphate contains alkyl group as cations. Several organic phosphates were measured as model compounds, which indicated this possibility. However, no similar spectrum has been found. Finally, it is a mixture of polyphosphate and unreacted ZDDP. Although peak a_2 position (135.5 eV) in the Table 6.3.1 is about 0.9 eV higher than peak *b* (134.6 eV) of ZDDP in the Table, it has been demonstrated in AW films (Chapter 4) that mixing of two spectra changed the peak position slightly. This species is not found in AW films. Thus the last assumption seems favoured.

In the S L-edge spectra, the influence of O_2 is more prominent, as is shown in Figure 6.3.2 and Table 6.3.2. In air at 150 ^{0}C, both TEY (spectrum A) and FY (spectrum B) spectra show that the S species is mainly a sulphate. The small peak *b* in spectrum (A) indicates a small amount of sulphide on the top surface. However, when

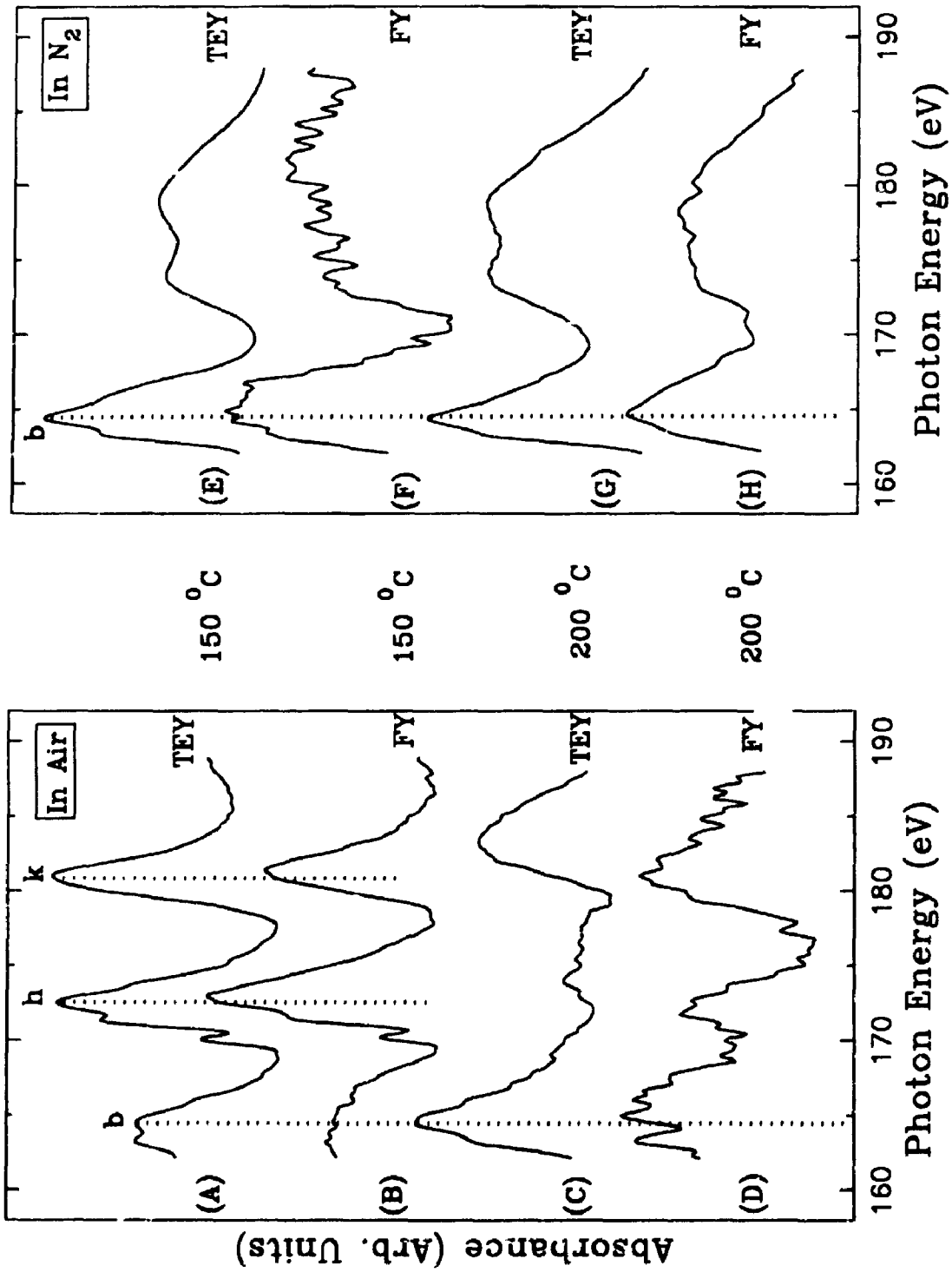

Figure 6.3.2 S L-edge spectra of IP-ZDDP thermal films

Table 6.3.2 Peak Positions of S L-edge Spectra of Thermally Prepared Films

Films	Peak positions (±0.1 eV)								
	a	b	c	f	g	h	i	j	k
IP-ZDDP, 150 °C, TEY		164.4				172.5			180.9
150 °C, FY						172.8			181.2
150 °C, N_2, TEY		164.4					173.9	178.9	
150 °C, N_2, FY		164.5							
200 °C, TEY		164.6							
200 °C, FY		165.0				172.1			181.1
200 °C, N_2, TEY		164.4					174.2	178.9	
200 °C, N_2, FY		164.7							
$ZnSO_4$				170.9	172.0	173.3	174.2		181.7
$FeSO_4$				170.9	172.1	173.3			181.2
ZDDP-1, 150 °C, TEY	163.2	164.6				172.8			181.1
150 °C, N_2, TEY	163.3	164.6					173.9	178.2	
200 °C, TEY	163.5	164.7	166.1				175.4	179.4	
200 °C, N_2, TEY	163.1	164.3							

(Continued in Next page)

(Table 6.3.2 contd.)

ZDDP-3, 150 °C, TEY		170.1	171.5	172.4	180.5
150 °C, FY		170.1	171.5	172.6	180.7
150 °C, N_2, TEY	164.0				
150 °C, N_2, FY	164.1				
200 °C, TEY	164.4				
200 °C, FY	163.8				
200 °C, N_2, TEY	164.4				
200 °C, N_2, FY	164.3				
ZDDP-1 + DET-1, 150 °C, TEY	164.0			171.3	180.1
150 °C, N_2, TEY	164.0			171.2	181.1
200 °C, TEY	165.0			171.2	180.4
200 °C, N_2, TEY	164.3			171.2	182.0
DET-1, 200 °C, TEY				171.1	181.1
ZDDP-1 + DISP, 150 °C, TEY	163.4			171.9	181.3
150 °C, N_2, TEY	163.8				

the temperature increases to 200 ^{0}C, sulphate on the surface was replaced by sulphide as shown in spectra (C) and (D). From a heating test of base oil without additive at 150 ^{0}C, it has been found that the sulphate signal is from the oxidation of sulphur present in base oil. There may be a competition of adsorption site between sulphate from the oil and sulphide from ZDDP. At 150 ^{0}C, sulphate dominates the surface. During the ZDDP decomposition, sulphate may form at first on the surface, and undergoes migration to the oil phase. The high temperature may increase the migration speed. Finally, sulphide replaces sulphate and dominates the steel surface. If this deduction is right, reducing O_2 supply in the system should retard the formation of sulphate. When the system was protected by N_2, as demonstrated on the right side of the Figure 6.3.2, only sulphide species are present at both 150 ^{0}C and 200 ^{0}C. Therefore, the O_2 function is that first, it provides oxygen for the formation of phosphates. Second, it oxidizes sulphur and/or sulphide to sulphate.

The influence of O_2 in the ZDDP decomposition has been studied by Willermet et al[12]. They found that oxygen participated in the ZDDP chemical reactions which lead to the formation of a highly wear-resistant surface film. From the tribology point of view, the wear rate in air was lower than that in N_2. The decomposition products of ZDDP were phosphates when air was present and phosphides under N_2 protection. Their conclusion is generally consistent with this work. O_2 helps the formation of polyphosphates which are responsible for the "wear-resistant" film. It shows that when the system is protected by N_2, the rate of phosphate formation is reduced. However, the decomposition product is not a phosphide, because phosphide can be easily distinguished from phosphates[13]. The formation of sulphate on the surface at lower temperature may cause corrosive wear. But it will not affect the AW effectiveness when the temperature is higher.

As can be seen in Table 6.2.1, elemental analysis of the precipitate from oil at 200 ^{0}C is similar to that from the oven test at 185 ^{0}C. The P L-edge spectrum of the precipitate (not show here) is similar to that of the film formed at the same temperature. Comparing the elemental analysis of the decomposition products from the oven and the oil test with the original ZDDP, C, H and S content have decreased while P content has increased. This implies that during the decomposition, C, H and S have partially left the

compound. Detailed discussion will be addressed later.

6.3.2 ZDDP-1

The nature and the mechanism of ZDDP adsorption on a steel surface are temperature dependent. At lower temperatures, ZDDP is reversibly physisorbed on a steel surface. At higher temperature, chemisorption take place which is also dependent on the experimental conditions[9,14]. Thermally prepared ZDDP-1 films were generated at different temperatures starting from room temperature to 200 ^{0}C. Except at 200 ^{0}C, no precipitate was formed in the oil. When the temperature of the oil was lower, such as 50 ^{0}C, or 100 ^{0}C, no film could be detected by XANES spectroscopy. This does not rule out the possibility of the adsorption of a few monolayers of ZDDP on the surface at lower temperatures, which has been suggested by previous investigators[9,14].

When the temperature was equal to or higher than 150 ^{0}C, thermal films were developed on the surface which could be characterized by the XANES spectroscopy. Figure 6.3.3 shows the P L-edge XANES spectra of the thermal films. The peak positions are also documented in Table 6.3.1. Due to an instrumental problem, no FY spectra could be recorded for these samples. Spectrum (A) is P L-edge spectrum of ZDDP-1 in base oil, which is similar to the IP-ZDDP (spectrum E in Figure 6.2.1). Spectra (B) and (C) are thermal films generated with N_2 bubbling at 150 ^{0}C and 200 ^{0}C, respectively. The general features of these two spectra are similar to ZDDP-1 (spectrum A) indicating that most of the ZDDP remain unreacted. When the temperature increases from 150 ^{0}C to 200 ^{0}C, peak *a* shifts to higher energy by about 0.8 eV.

When the decomposition was carried in air, the presence of peaks *c* and *e* in spectra (D) and (E) suggest the formation of a polyphosphate. At 150 ^{0}C (spectrum D), except for the polyphosphate formed, a strong peak a_2 and a clear shoulder on the left of peak a_2 imply the existence of a certain amount of unreacted ZDDP. In contrast, the spectrum of the film prepared at 200 ^{0}C (spectrum E) is different from the spectrum at 150 ^{0}C (D). The features are resolved better and peak intensities of *a* and *b* are even higher. On the other hand, the spectra of the thermal film formed at 200 ^{0}C and the precipitate collected at the same temperature (not shown here) are very similar which suggests that film originate from the same material. It is noticed that the relative

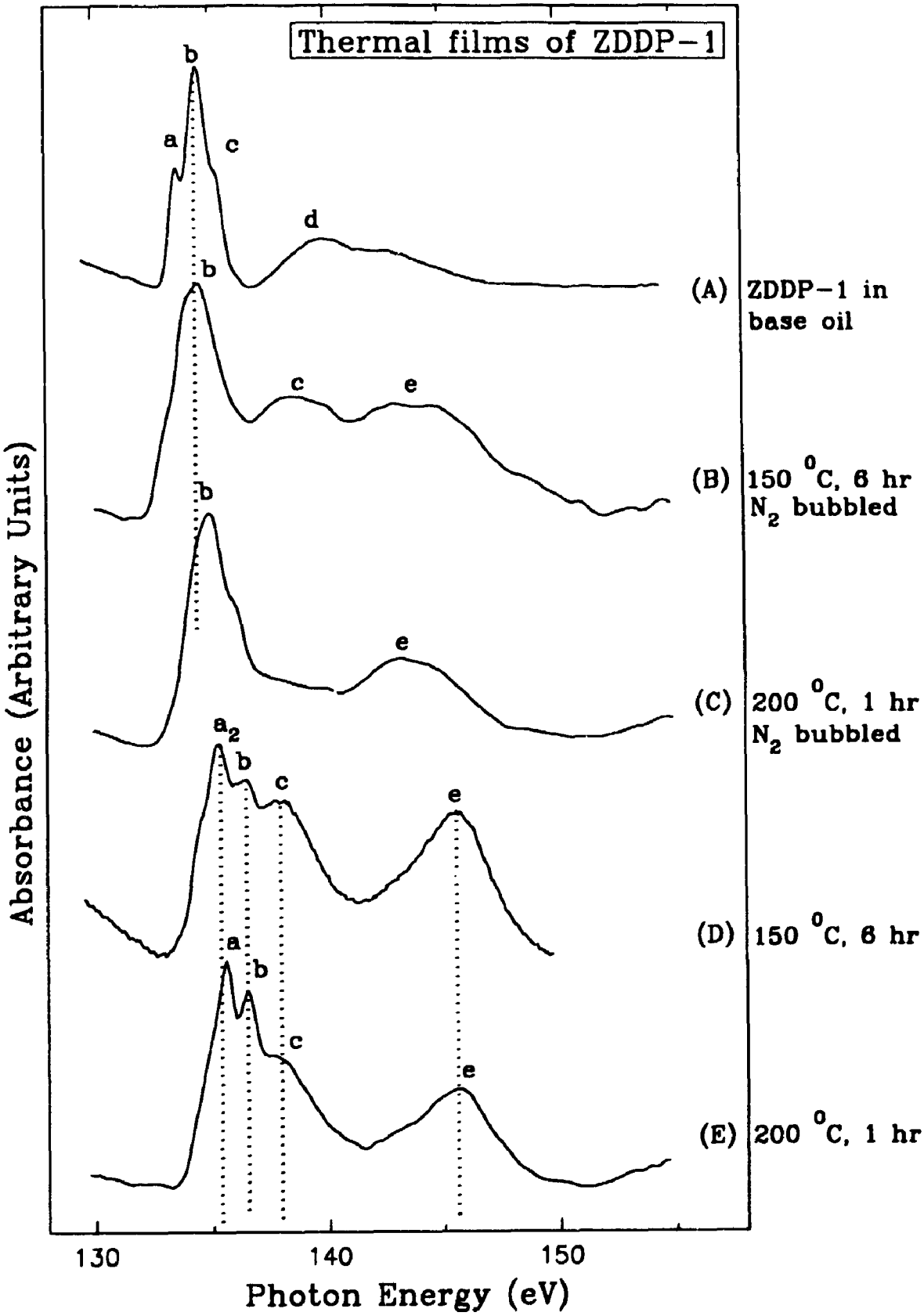

Figure 6.3.3 P L-edge spectra of ZDDP-1 thermal films

intensities of peaks *a* and *b* are higher than peak *c*, which has previously been discussed for IP-ZDDP films.

The S L-edge XANES spectra of the thermal films and decomposition products are presented in Figure 6.3.4 and their peak positions are also listed in Table 6.3.2. Spectra (A) and (B) correspond to two model compounds, $ZnSO_4$ and $FeSO_4$. The features are resolved better in the spectrum of $ZnSO_4$ (A). At 150 ^{0}C, spectrum (C) shows two well resolved regions. Peaks *a* and *b* belong to the reduced form of sulphur while *h* and *k* belong to the oxidized form of sulphur. The reduced part is different from pure ZDDP and resembles the triplet spectra one usually observed for alkyl sulphides[15]. The oxidized form of sulphur is similar to a metal sulphate (spectrum A and B). However, when the same experiment was carried in N_2, as demonstrated in spectrum (D), there is no sulphate formed. Therefore, the sulphate can still be attributed to sulphur from the base oil. At 200 ^{0}C, whether in air or in N_2 atmosphere, only sulphide was found in the films. The conversion of sulphide to sulphate and sulphate to sulphide has been suggested by Rhodes and Stair[16,17]. In air, the formation of iron sulphate was favoured thermodynamically. An iron sulphate surface layer could be sacrificially reduced to iron sulphide by radical intermediates formed in the oxidation process. They also found that when the temperature increased to more than 300 ^{0}C, the sulphate left on steel surface decreased dramatically and sulphide, on the other hand, still increased. Based on the results of this work, conversion of sulphate to sulphide cannot be supported. The migration of sulphate from surface to base oil seems to be a reasonable pathway[6,7].

Figure 6.3.5 compares the fluorescence yield (FY) and partial electron yield (PEY) of Fe L-edge spectra of ZDDP-1 thermally prepared films at 200 ^{0}C, in air and N_2 atmosphere. As discussed in Chapter 2, FY provides bulk information while PEY provides the topmost surface information. The PEY signal (spectra A and C) is much lower than the FY signal indicating the good coverage of thermal film over the steel surface. Meanwhile it shows that there is a little iron present in the film. Comparing peak *a* positions, the iron species on the topmost surface (A, C) is different from that in the substrate (B, D). The peak position of species on the surface shifted to high energy about 1 eV, which suggests the oxidation of iron after heating in base oil.

The elemental analysis results of the precipitate formed at 200 ^{0}C in oil with and

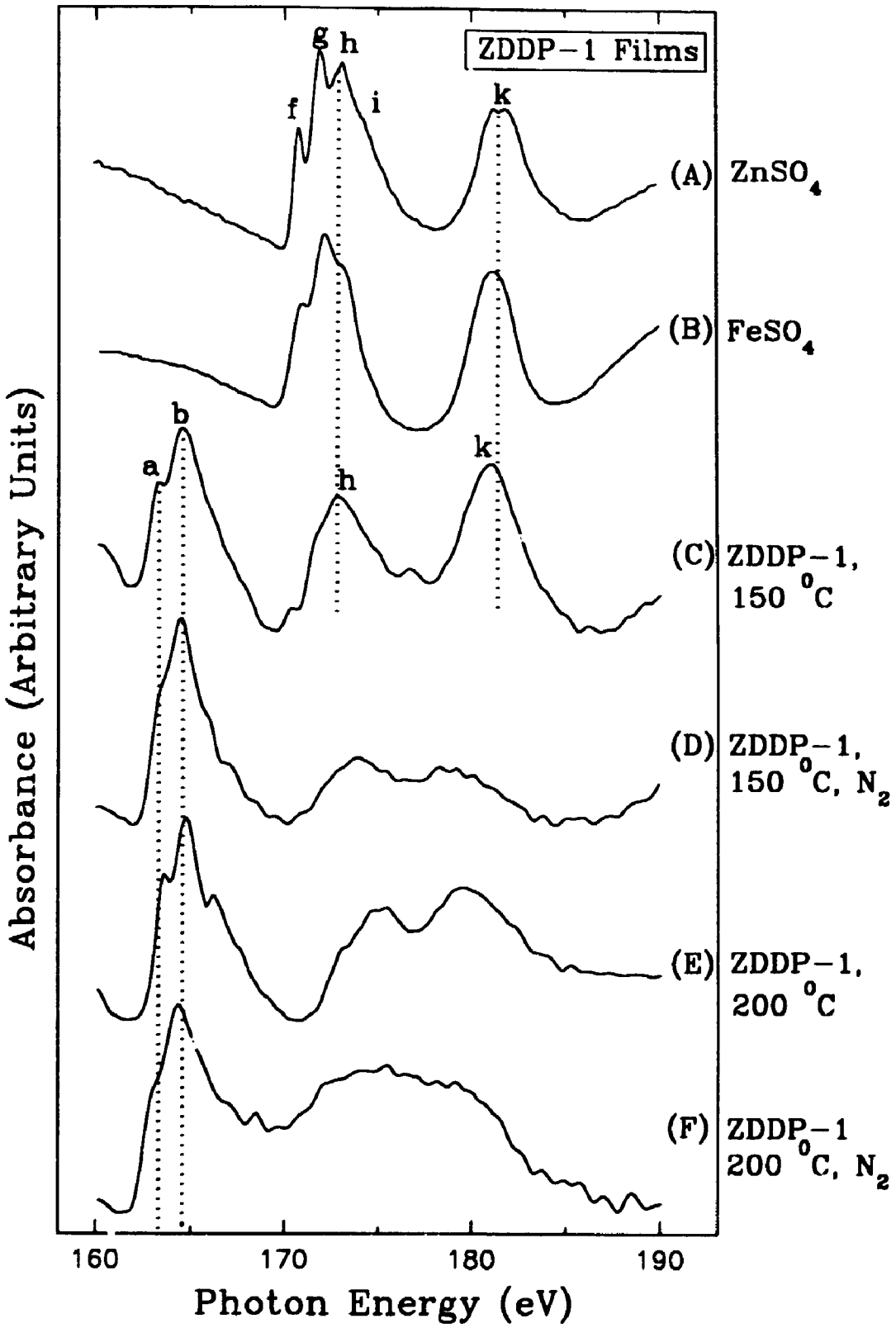

Figure 6.3.4 S L-edge spectra of ZDDP-1 thermal films

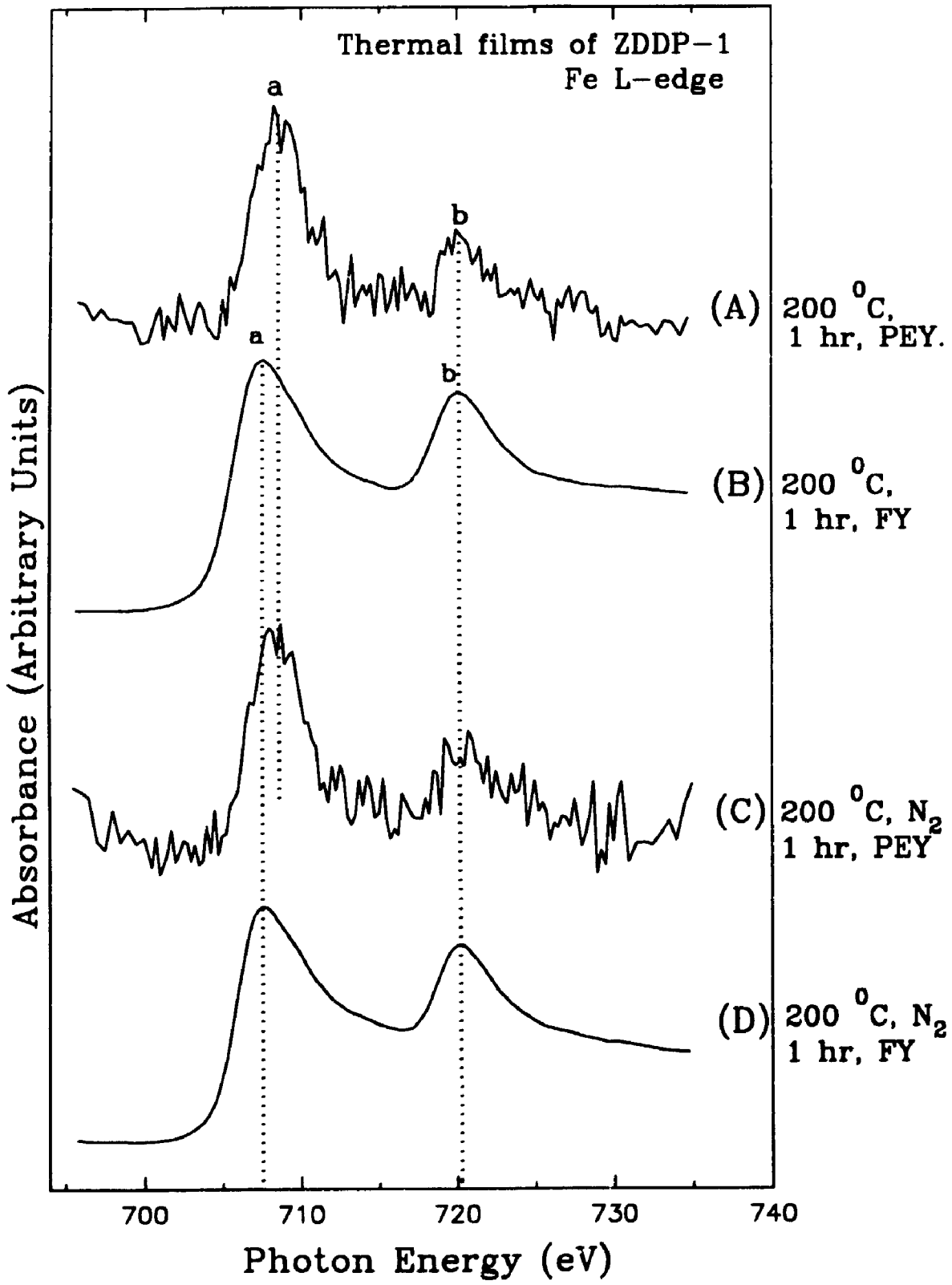

Figure 6.3.5 Fe L-edge spectra of ZDDP-1 thermal films

without N_2 bubbling are also presented in Table 6.2.1. As indicated in the table, all decomposition products, including those from IP-ZDDP decomposition, both in air and in oil, are depleted of carbon, hydrogen and sulphur compared to the original ZDDP but are enriched in phosphorus and Zn. This is in agreement with previous findings. Barcroft et al.[1] reported that ZDDP reacted with the iron surface. The reaction rate increased with increasing temperature. At 200 ^{0}C, the precipitate isolated from solution had the formula $Zn_{1.0}P_{1.87}S_{1.36}C_{2.03}H_{4.34}O_{3.12}$ compared with original: $Zn_1P_2S_4C_{20}H_{44}O_4$. It is obvious that C, H and S content is decreased. In this work using ZDDP-1 as additive, the formula for the precipitate is $Zn_{1.0}P_{1.97}S_{2.0}C_{3.5}H_{9.3}$ compared with the original: $Zn_1P_2S_4C_{18.4}H_{40.8}O_4$. S has been reduced to half and C, H decreased by 80% and 77%, respectively. The depletion of S, C and H has also been found by other researchers[5,6]. It is most likely that part of the decomposition products containing S, C and H migrate into the base oil[6,7].

The results show that temperature has a major influence on many aspects of tribological behaviour on the contact[18]. When temperature increases, first, the chemical reactivity of the system will be increased. Secondly, the fluid-film thickness will be decreased owing to a decrease of fluid viscosity. Finally, the chemical composition and properties of the boundary film will be changed. In an immersion test using secondary ZDDP as additive, Rounds[6] reported that reducing the O_2 supply to the system had almost no effect on the composition of precipitate but altered the composition of the steel surface a great deal. This observation is consistent with this work. Comparing the elemental analysis results in Table 6.2.1, the composition of precipitate from oil under air and under N_2 didn't change very much. However, the spectra of the film on the steel surface show remarkable difference at different conditions. Another investigation made by Rhodes and Stair[19] showed that O_2 affected the oxidation of sulphide to sulphate. They found sulphate only formed when O_2 was present. In this work, no sulphate was found on the steel surface when N_2 protection was used. The results presented above shows that both oxygen and temperature affect the decomposition results. Taking decomposition of ZDDP-1 as an example (Figure 6.2.3), when there is N_2 bubbling, the difference between 150 ^{0}C (spectrum B) and 200 ^{0}C (spectrum C) is small. The only difference is for peak *b* which is shifted to higher energy at higher temperature. When

there is no N_2 protection, the decomposition is really temperature dependent. At 150 ^{0}C (spectrum D), there are substantial amount of ZDDP present on the steel surface. When temperature increased to 200 ^{0}C (spectrum F), there is no clear indication of the presence of ZDDP, because ZDDP decomposes at such a high temperature. At the same temperature, the O_2 effect is significant. Under the N_2 protection, most of the ZDDP remains unreacted. The general shape of the spectra is much closer to that of pure ZDDP (spectrum A).

6.3.3 ZDDP-3

The observations for ZDDP-3 (a primary ZDDP) are similar to those for ZDDP-1. At 150 ^{0}C, the oil was yellow both in air and in N_2. At 200 ^{0}C, the oil turned to dark brown and a precipitate, developed when it was run in air. When the experiment was carried out in N_2, the oil turned a little cloudy.

Figure 6.3.6 shows P L-edge spectra of thermal films generated from ZDDP-3 both in air (left) and in N_2 (right). The peak positions are summarized in Table 6.3.1. It is noticed that at 150 ^{0}C, the films formed are thin both in air and in N_2 because the signal from FY mode, which probes the bulk, are very weak (spectra B and F). In air, the P species is a polyphosphate having relatively long chain (A). But in the N_2 test, ZDDP is protected from degradation as evidenced by the strong peak a_2 (E). Peaks *c* and *e* in spectrum (E), which correspond to phosphate, suggest that a small part of ZDDP-3 has been decomposed. At 200 ^{0}C, N_2 bubbling does not affect the decomposition products because the spectra of films formed in air (C and D) are similar to those formed in N_2 (G and H). The layer structure is similar to that found in IP-ZDDP films, the bulk has a much lower chain length polyphosphate than the surface. These spectra in O_2 are remarkably similar to some of the spectra from AW films.

From the S L-edge spectra, as shown in Figure 6.3.7, spectra (A) and (B) corresponding to the films formed at 150 ^{0}C show that there is absolutely no sulphide on steel surface. The sulphur species in the films is dominated by sulphate. When the temperature increases to 200 ^{0}C, sulphate migrates to the base oil and the surface is covered by sulphide from ZDDP decomposition. Under N_2 protection, no sulphate formed because of the shortage of O_2.

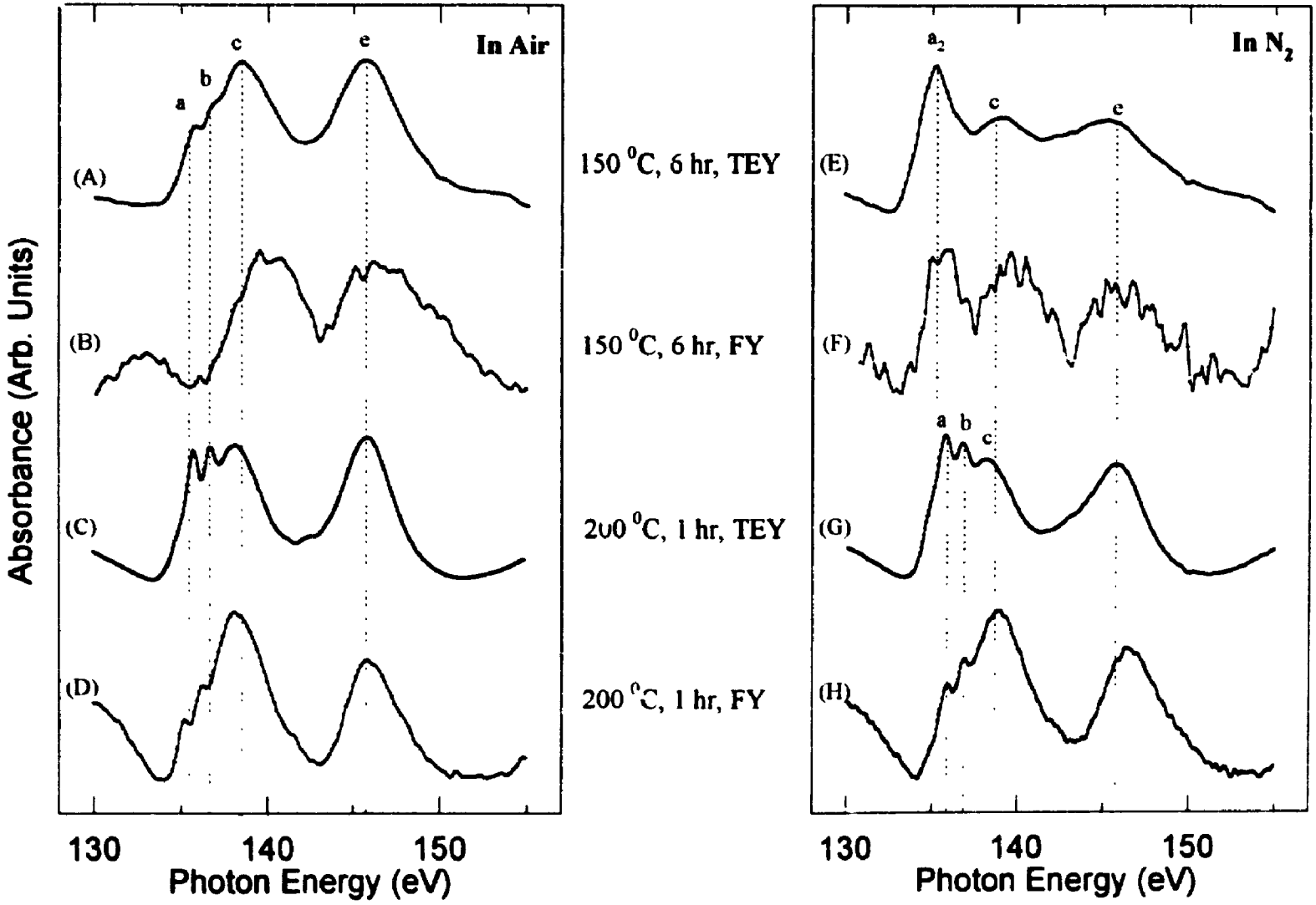

Figure 6.3.6 P L-edge spectra of ZDDP-3 thermal films

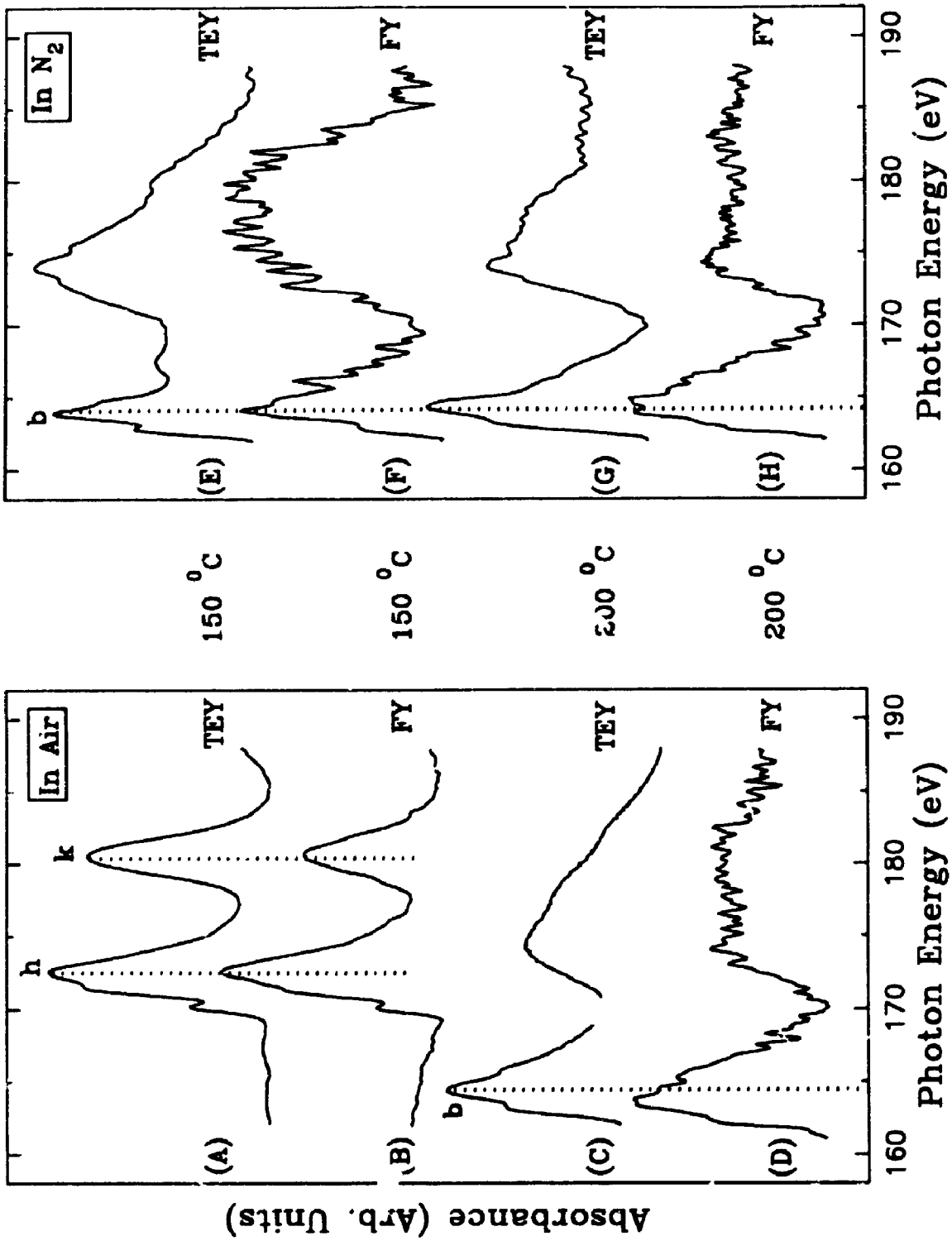

Figure 6.3.7 S L-edge spectra of ZDDP-3 thermal films

According to previous investigations, ZDDP-3, a primary ZDDP, should decompose more slowly than secondary ZDDP such as IP-ZDDP and ZDDP-1[1,3,4]. On the other hand, the AW film analysis for different ZDDP showed that polyphospnate chain length is different between primary ZDDP film and secondary ZDDP film.

The results of the thermally formed films from three ZDDPs are summarized in Table 6.3.3. Detailed composition of the ZDDPs have been listed in Table 2.1.2. The main components are: isopropyl ZDDP (100%) in IP-ZDDP; secondary butyl ZDDP (85%) in ZDDP-1 and primary butyl ZDDP (65%) in ZDDP-3. The composition of the films was derived semi-quantitatively using the procedure described in Chapter 4. From Table 6.3.3, it is obvious that alkyl groups bonded to ZDDPs have a significant effects on the nature of polyphosphate formation. Secondary ZDDP tends to produce longer chain length polyphosphate at 150 ^{0}C than primary ZDDP on the surface. This phenomenon seems to be related to the rate of the adsorption and the decomposition of the ZDDP on the surface. At higher temperature (200 ^{0}C), practically all ZDDPs produce long chain polyphosphates. In contrast, polyphosphate formed in the bulk is a shorter chain polyphosphate. At 150 ^{0}C, N_2 protection is more effective for primary ZDDP than secondary ZDDP for phosphate formation. It should be pointed out that N_2 bubbling removes O_2 from oil but oxygen is still present in the form of oxide on the substrate. Certainly at higher temperature this source of oxygen, when the reaction rate is much higher, can play an important role. This probably explains why at 200 ^{0}C, even with N_2 protection, primary ZDDP forms polyphosphate. Certainly further studies are required to understand fully the mechanisms of polyphosphate formation.

6.3.4 ZDDP-1 and DET-1

When ZDDP interferes with other additives such as detergent, its thermal property will be changed. ZDDP-1 and DET-1 (Calcium sulphonate) were heated in base oil at 150 ^{0}C (6 hours), 200 ^{0}C (1 hour) and 235 ^{0}C (1 hour). Even when the temperature reaches 235 ^{0}C, there is still no precipitate formed as previously found using ZDDP-1 alone. The colour of the solution changed from yellow to brown.

The P L-edge spectra of the films from ZDDP-1 plus DET-1 are demonstrated in Figure 6.3.8 and their peak positions are listed in Table 6.3.1. At 150 ^{0}C, ZDDP is

Table 6.3.3 Summary of thermally prepared films from different ZDDPs

ZDDPs		Film compositions at 150 °C		Film compositions at 200 °C	
		Air	N_2	Air	N_2
IP-ZDDP	TEY	Polyphosphate (very long chain), a little ZDDP*	Polyphosphate (long chain), some ZDDP	Polyphosphate (long chain), no ZDDP	Some polyphosphate; mostly ZDDP, or an intermediate
	FY	Polyphosphate (short chain), no ZDDP	Polyphosphate (short chain), lots of ZDDP	Polyphosphate (long chain), no ZDDP	Some polyphosphate; mostly ZDDP, or an intermediate
ZDDP-1 (85% secondary butyl ZDDP)	TEY	Polyphosphate (long chain); lots of ZDDP, or an intermediate	Little phosphate, mostly ZDDP	Polyphosphate (very long chain); or an intermediate	Mostly ZDDP
	FY	-	-	-	-
ZDDP-3 (65% primary butyl ZDDP	TEY	Polyphosphate (medium chain), no ZDDP	Little phosphate, mostly ZDDP	Polyphosphate (very long chain), no ZDDP	Polyphosphate (very long chain), some ZDDP or intermediate
	FY	Weak signal, polyphosphate (short chain ?)	Weak signal	Polyphosphate (short chain), no ZDDP	Polyphosphate (medium chain), a little ZDDP

* Based on Figure 4.2.2, the composition of ZDDP in the thermal films are estimated as: no: <5%; a little: ~5-10%; some: 10-20%; lots: 20-50%; mostly: >50%.

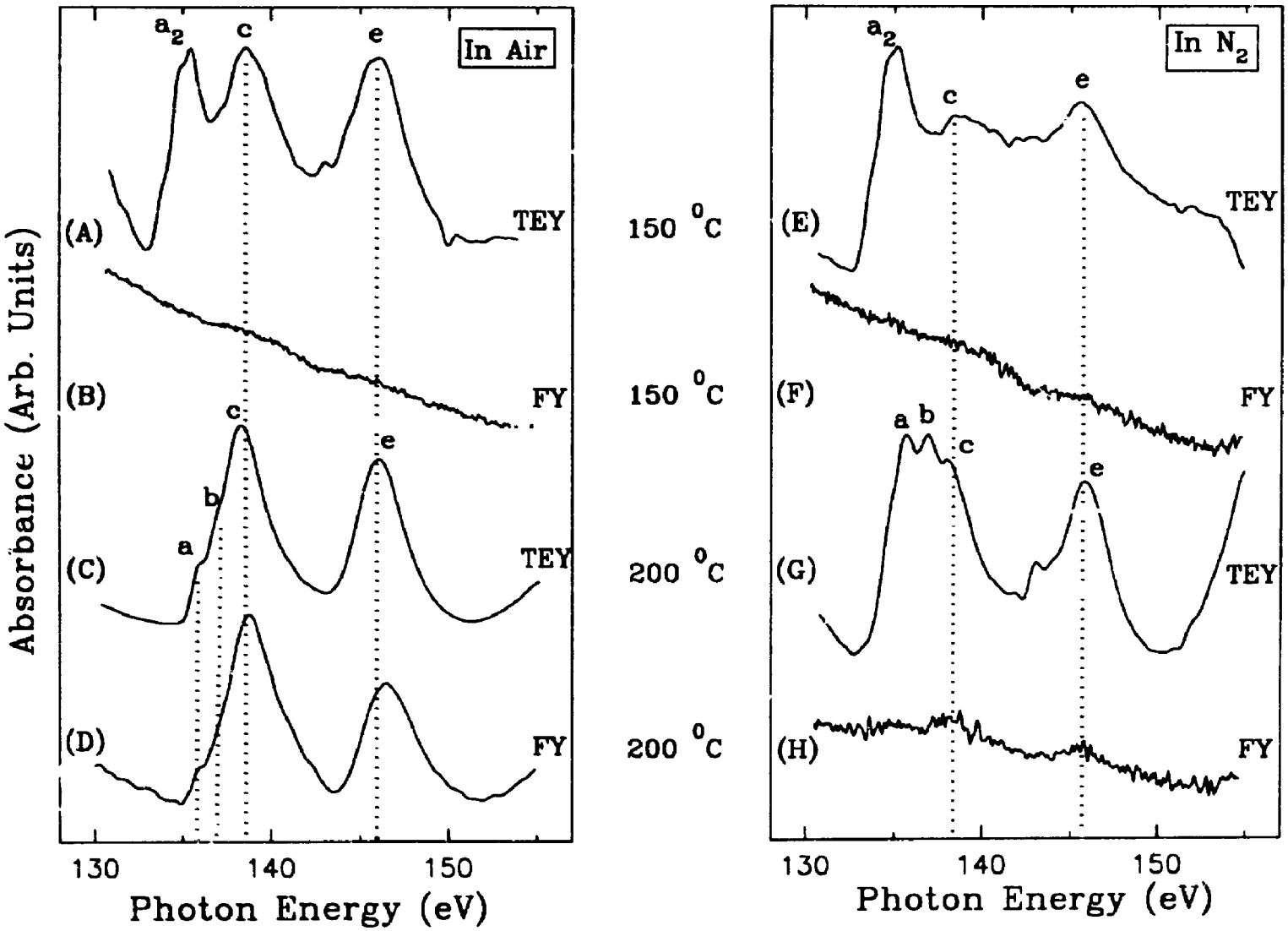

Figure 6.3.8 P L-edge spectra of the thermal films from ZDDP-1plus DET-1

partially decomposed as shown in spectrum (A). Peak a_2 represents the ZDDP contribution and peak *c* and *e* represent a phosphate. The film is very thin because almost no FY signal could be detected (spectrum B). Comparing this spectrum with spectrum (A) in Figure 6.3.3, it may be concluded that the ZDDP decomposition rate has been reduced by the addition of DET-1. Under N_2 protection, the intensities of peaks *c* and *e* in spectrum (E) decreased dramatically comparing with spectrum (A), which suggests that the rate of ZDDP decomposition, once again, is reduced by N_2 bubbling. When the temperature increases to 200 ^{0}C, most of the ZDDP is decomposed when the experiment is carried out in air. The spectrum (C) shows that a short chain phosphate is formed on the surface. This film is thicker than other three films as evidenced by the strong FY spectrum (D). When the same experiment is carried in N_2 (spectrum G), a strong peak *a* and a shoulder on the left of *a* indicate that some of the ZDDP has not reacted. The spectra of the films formed at 235 ^{0}C is similar to those at 200 ^{0}C, therefore they will not be shown here.

The S L-edge spectra in Figure 6.3.9 and their peak positions in Table 6.3.2 indicate that sulphide is present in the films. The low intensity of sulphide peak *b* in spectrum (A) implies that only a small percentage of S is in the sulphide form and the rest is in the sulphate form, which originates from the base oil. This is similar to the film from IP-ZDDP (Spectrum A of Figure 6.3.2). Peaks *k* and *h* are similar to the sulphate peaks, as discussed when ZDDP was used alone. However, in this case it is most likely that peaks *k* and *h* originate from the calcium sulphonate (DET-1) used here. The reason for this assignment is that N_2 do not affect sulphate formation as it did when ZDDP was used without detergent. A heating test using only DET-1 was performed and the S L-edge spectrum (E) confirm the above deduction. However, since the resolution is not high enough, it is impossible to exclude the presence of sulphate from the base oil. Actually, the peak positions of sulphate and sulphonate are very close. Lack of FY signal in spectra (B), (G) and (I) suggests formation of thin films on the steel surface. Spectrum (D) is interesting. From the P L-edge spectra (Figure 6.3.8), it was found that the film was thick enough to show the FY signal. Since no S signal could be detected in the S L-edge from FY mode, it means that sulphur species are only present on the topmost surface of the film.

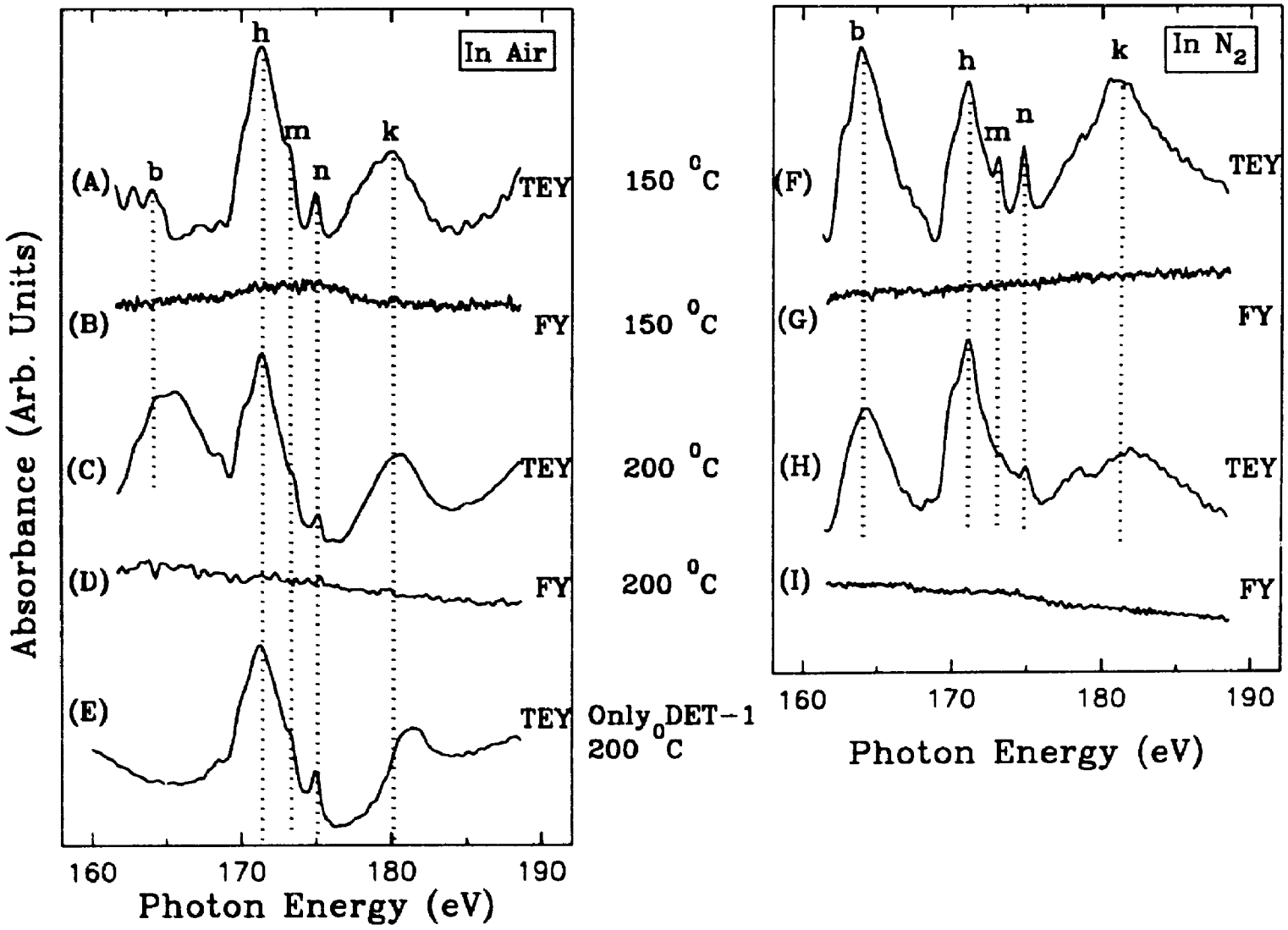

Figure 6.3.9 S L-edge spectra of the thermal films from ZDDP-1plus DET-1

It should be pointed out that peaks *m* and *n* are not related to sulphur species, they are the second order harmonics of Ca 2p signal. Calcium is from the calcium sulphonate detergent used. Ca first order spectra are shown in Figure 6.3.10. At 150 ^{0}C, both TEY and FY (not shown) signals can be detected while at 200 ^{0}C, only TEY signals present. It implies that Ca only contributes to the topmost surface of the films.

6.3.5 ZDDP-1 and DISP

Heating ZDDP-1 plus DISP resulted in a dark brown solution similar to what was found for ZDDP-1 and DET-1. Figure 6.3.11 shows P L-edge spectra from films generated from ZDDP-1 plus dispersant. Table 6.3.1 also collects the peak positions of these films. At 150^{0}C, the film produced in air (spectrum A) has peak a_2 which indicates a small amount of unreacted ZDDP. Meanwhile, the absence of peak *b* implies that the chain length of phosphate is short. Under N_2 protection, spectrum (E) shows that a longer chain polyphosphate is formed. Both in air and in N_2, the films are thin, because no FY signal is observed (spectra B and F). At 200 ^{0}C, spectra (C) and (G) show that short chain phosphates are formed on steel surface both in air and in N_2. In the FY spectra (D and H), peaks *c* and *e* have shifted to higher energy by about 1.5 eV. Since the signal is weak and the spectra are noisy, no assignment can be made.

S L-edge spectra of two films formed in 150 ^{0}C are shown in Figure 6.3.12. The peak positions are also collected in Table 6.3.2. No sulphur signal could be detected both in TEY and FY modes from the films formed at 200^{0}C. It means that the presence of dispersant at high temperature has washed out sulphur from the steel surface. This is consistent with the studies on AW films (Chapter 5), where depletion of sulphur has been discussed. In the air, sulphide is in a competition with sulphate coming from the base oil (spectrum A). While in N_2, the sulphate signal disappears and spectrum (C) is dominated by the sulphide signal. Both in air and N_2 atmosphere, films are very thin since no FY signal could be detected.

It has been reported by several groups that addition of a second additive like a detergent or dispersant affects the thermal stability of ZDDP. The presence of detergent and dispersant in the system will increase the ZDDP decomposition temperature[2,20,21]. This is in agreement with this work since no precipitate was found even at 235 ^{0}C in the

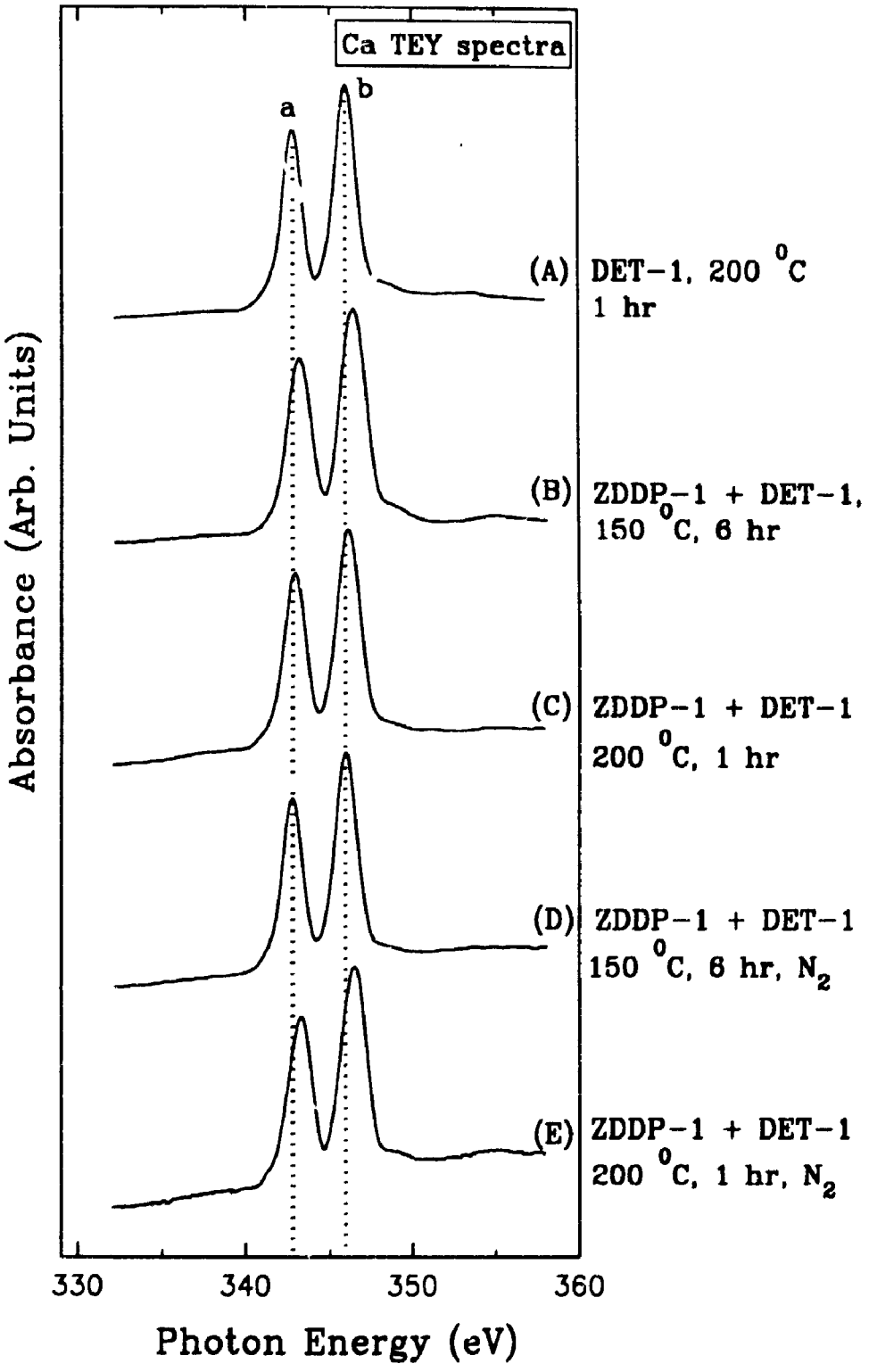

Figure 6.3.10 Ca L-edge spectra of the thermal films from ZDDP-1 plus DET-1

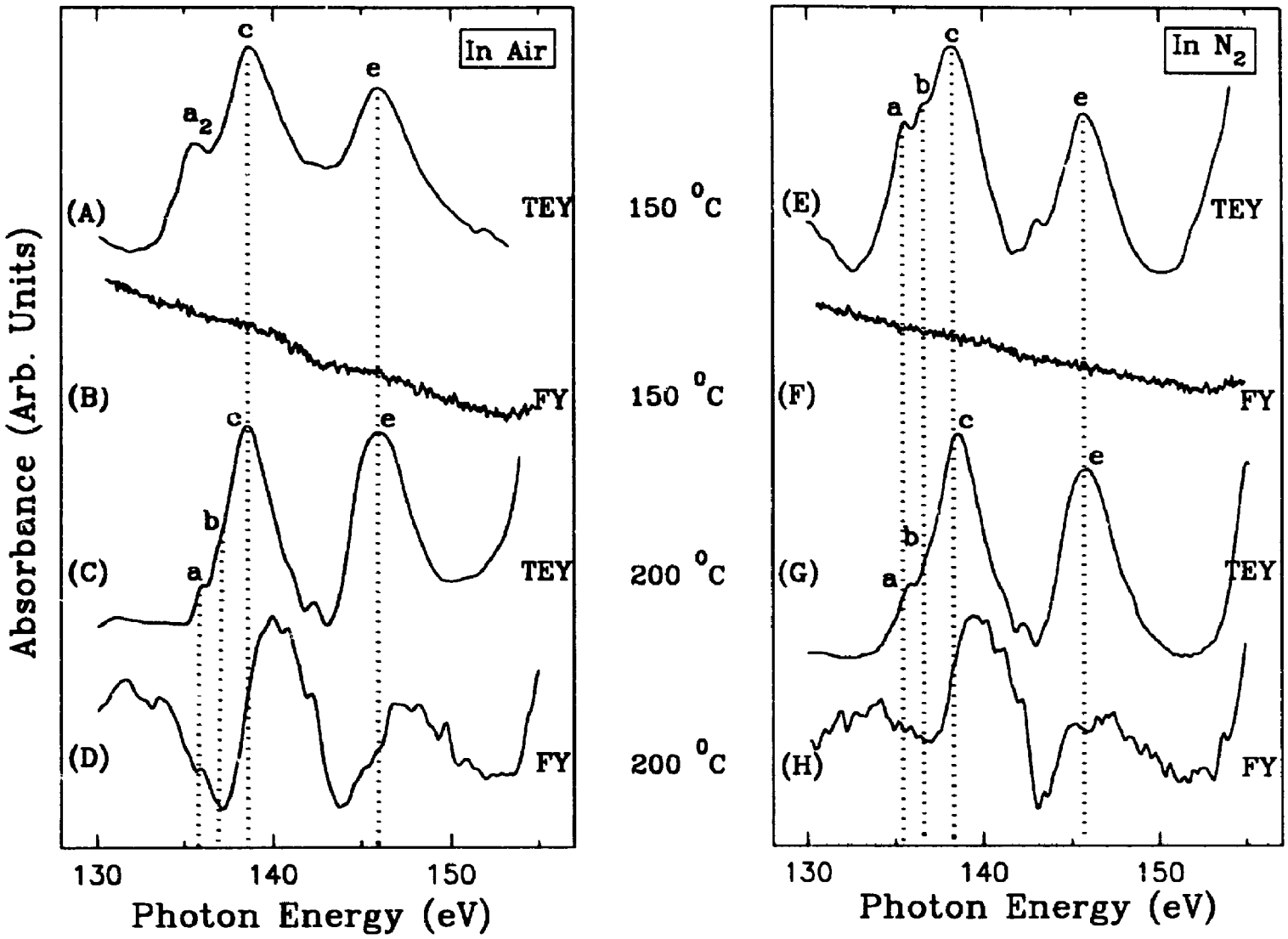

Figure 6.3.11 P L-edge spectra of the thermal films from ZDDP-1plus DISP

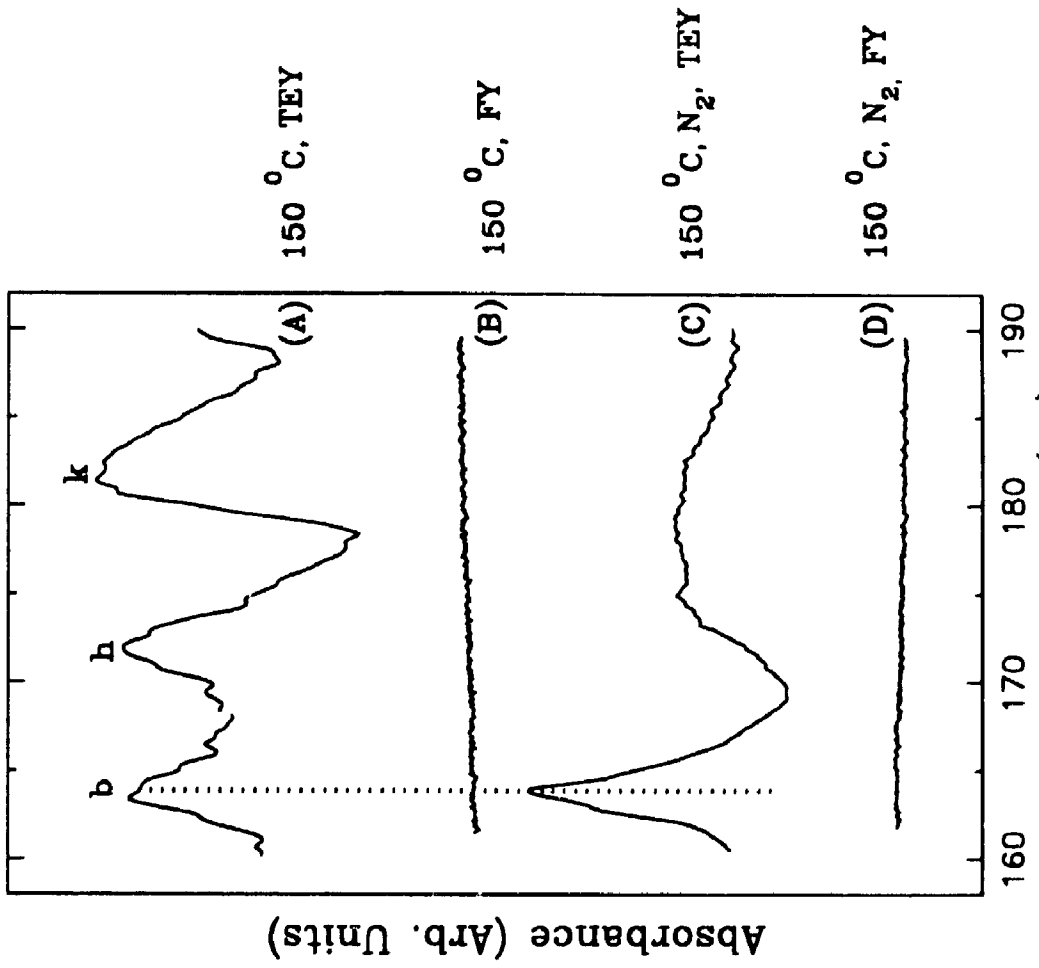

Figure 6.3.12 S L-edge spectra of the thermal films from ZDDP-1plus DISP

system containing DET-1 or DISP. Furthermore, at 150 ^{0}C, a certain amount of unreacted ZDDP was found as shown in spectrum (A) of Figure 6.3.8 and Figure 6.3.11.

Over the years, three possible mechanism have been proposed to explain how other additives interact with the ZDDP AW additive[22]. First, additives interact in the bulk oil before the surface active additive components contact the rubbing surface. This includes the neutralization of acidic decomposition products such as acid phosphate[23], complex formation with micelles[24] or amines[25,26], which may reduce ZDDP effectiveness. Secondly, the additive actively competes for the rubbing surfaces. The resulting AW or friction performance is the net result of this competition. In friction studies, even the sequence in which additives were added to a blend was found important[27]. Thirdly, the overbasing metallic detergents precipitate (usually as the carbonate) in the contact area to form a paste[28]. This paste could reduce wear by forming a grease-like material in the contact region. On the other hand, the precipitate may restrict the oil inlet leading to oil starvation in the contact region and will increase wear[29]. In the results presented above, all the three mechanisms can be operative. Further work is required to elucidate the situation.

6.4 Conclusions

Thermal decomposition of ZDDP has been tested both in the solid state and in oil. In the solid state, it is concluded that IP-ZDDP starts to decompose at 135 ^{0}C. At higher temperature such as 185 ^{0}C, the decomposed residue is mainly a long chain polyphosphate and sulphides.

Thermally prepared films were formed in base oil at temperatures of 150 ^{0}C and 200 ^{0}C both in air and in N_2 atmosphere. When using ZDDP alone, or IP-ZDDP, ZDDP-1 and ZDDP-3, they all decompose at 150 ^{0}C to form polyphosphates, which are similar to those found for the AW films. The layer structure is also similar to the AW films. On the top surface, the phosphate formed in both thermal and AW films has a long chain while the bulk has a short chain polyphosphate. O_2 plays an important role in ZDDP thermal decomposition. First, O_2 helps the decomposition of ZDDP to form phosphates. Second, O_2 oxidizes sulphur species to sulphate. Sulphur is present in base oil as an impurity. The sulphate formed in the films migrates to the oil at higher temperature.

Addition of DET-1 and DISP retard the decomposition rate of ZDDP. The films formed in the presence of DET-1 or DISP are much thinner than those just with ZDDP.

6.5 References

1. Barcroft, F.T., Bird, R.J., Hutton, J.F., Park, D. *Wear*, 1982, 77, 355

2. Barcroft, F.T., Park, D. *Wear*, 1986, 108, 213

3. Coy, R.C., Jones, R.B. *ASLE Trans*, 1981, 24, 77

4. Jones, R.B., Coy, R.C. *ASLE Trans.*, 1981, 24, 91

5. Harrison, P.G., Brown, P., *Wear*, 1991, 148, 123

6. Rounds, F.G. *ASLE Trans.*, 1975, 18, 79

7. Spedding, H., Watkins, R.C., *Tribol. Int.*, 1982, 15, 9

8. Molina, A. *ASLE Trans.*, 1987, 30, 479

9. So, H., Lin, Y.C., Huang, G.G.S. and Chang, S.T., *Wear*, 1993, 166, 17

10. Hastie, G.P., Roberts, K.J., Adams, D., Fischer, D., Meitzner, G., *Proc. 7th. Int. Conf. X-ray Absorption Fine Structure*, Kobe, Japan, 1992. *Jpn. J. Appl. Phys.*, Vol. 32, 1993, Suppl. 32-2, p407

11. Kasrai, M., Fuller, M., Scaini, M., Yin, Z., Brunner, R.W., Bancroft, G.M., Fleet, M.E., Fyfe, K., Tan, K.H. *Proceedings of the 21st Leeds-Lyon Symposium on Tribology*, Ed. Dowson, D. et al., Leeds, September, Elsevier, Amsterdam, 1995

12. Willermet, P.A., Kandah, S.K. *Lubrication Science*, 1993, 5, 129

13. Kasrai, M., Yin, Z., Bancroft G.M., Tan, K.H. *J. Vac. Sci. Technol.* A 1993, 11,2694

14. Plaza, S. *ASLE Trans.*, 1987, 30, 233

15. Brown, J.R., Kasrai, M., Bancroft, G.M., Tan, K.H., Chen, J.M. *Fuel*, 1992, 71, 649

16. Rhodes, K.L., Stair, P.C. *J. Vac. Sci. Technol. A.* 1988, 6, 971

17. Rhodes, K.L., Stair, P.C. *Tribol. Trans.*, 1993, 36, 27

18. Chao, S.-H, Ludema, K.C., Potter, G.E., DeKoven, B.M., Morgan T.A., Kar., K.K. *Wear*, 1994, 177, 33

19. Rhodes, K.L, Stair, P.C. *Tribology Transactions*, 1993, 36, 27

20. Rounds, F.G. *ASLE Trans.*, 1978, 21, 91

21. Shirahama, S., Hirata, M., *Proc. 5th. Int. Colloq. on Additive for Lubricants and Operating Fluids*, January, 1986

22. Rounds, F.G. *Lubrication Engineering*, 1989, 45, 761

23. Rounds, F.G. *ASLE Trans.*, 1985, 28, 475

24. Kaufman, S., Singleterry, C.R. *J. Colloid Sci.*, 1957, 12, 465

25. Rounds, F.G., *ASLE Trans.*, 1981, 24, 434

26. Shoimi, M., Tomizawa, H., Kuribayashi, T., Tokashiki, M. *Additives for Lubricants and Operating Fluids*, 5th International Colloquium, Esslingen, Germany, January 1986, P3.7-1

27. Rounds, F.G. *Additives for Lubricants and Operating Fluids*, 5th International Colloquium, Esslingen, Germany, January 1986, P4.8-1

28. Kapsa, Ph., Martin, J.M., Blanc, C., Georges, J.M. *ASME JOLT*, 1981, 103, 481

29. Yoshida, K., Sakurai, T. *STLE* preprint 87-TC-3B-1, presented at STLE/ASME joint Lubrication Conference, Oct. 1987

CHAPTER 7

GENERAL DISCUSSION

7.1 Review of previous mechanism studies

The mechanism of antiwear film formation has long been a subject in tribology studies. Using different experimental methods, several mechanisms have been proposed. In general, they are: thermal degradation[1,2,3,4,5,6], surface adsorption[7,8,9,10,11], hydrolysis[12], chemical reaction through FeO[13], oxidation by hydroperoxide[14,15,16,17,18], radicals[19,20,21,22], and oxygen in air[20,23,24], or a combination of the above[25,26,27,28].

It is believed that the antiwear effectiveness of ZDDPs is related to their rate of thermal decomposition. In an isolated system, Dickert and Rowe[1] suggested the following reaction:

$$\text{ZDDP} \rightarrow \text{G} + \text{L} + \text{S} \qquad (1)$$

where G (gas phase): olefin, H_2S

L (liquid phase): RSH, RSR

S (Solid phase):

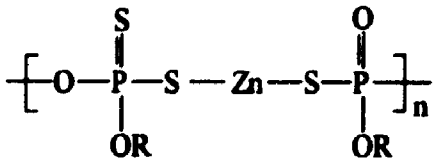

I

They found that the reaction speed is affected by the nature of the alkyl group. For example, secondary ZDDP is easier to decompose than primary ZDDP. Coy and Jones[2] heated several oil samples with a high concentration of ZDDP over 180 ^{0}C in an oven. Their findings supported Dickert and Rowe's conclusion. They also reported that for the same ZDDP, the rate of decomposition increased with increasing temperature and concentration. Molina[5] heated a commercial ZDDP in an oven at 200 ^{0}C in the presence of air for 1 hour. The decomposition products provided equal antiwear effectiveness to

that of the ZDDP. His results indicated that the precipitate formed during the thermal decomposition of ZDDP contained the relevant compounds necessary for good antiwear performance. He suggested that zinc pyrophosphate, which was one of the constituents of the thermal degradation of a secondary-alkyl ZDDP at 200 ^{0}C, was the chemical agent that gave the ZDDP's their known antiwear properties. But for good antiwear performance, it appeared that zinc pyrophosphate needed to be in an amorphous/microcrystalline state. In Harrison and Brown's[6] study, they reported that the thermal stability of the ZDDPs followed the order n-nonyl > n-decyl > n-butyl > iso-butyl. They proposed two possible structures (II and III) of solid residue based on their experimental data.

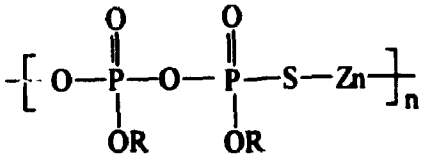

II

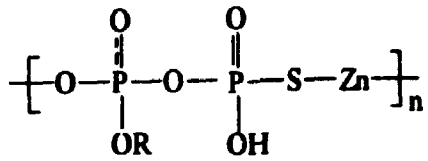

III

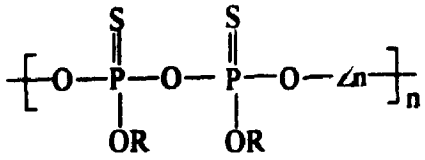

IV

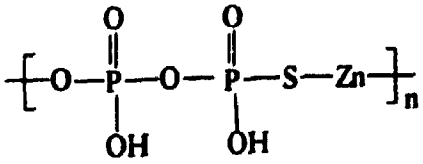

V